Etude de la dégradation par photolyse directe de pesticides - Caractérisation structurale et toxicité potentielle des photoproduits

Ahmad Rifai

THÈSE

Présentée et soutenue publiquement par

Ahmad RIFAI

pour l'obtention du titre de

DOCTEUR DE L'ÉCOLE POLYTECHNIQUE

Etude de la dégradation par photolyse directe de pesticides - Caractérisation structurale et toxicité potentielle des photoproduits

---

Soutenue le 09 Septembre 2013 devant le jury constitué de :

Dr. Nathalie KARPEL	Université de poitiers, CNRS	Rapporteur
Pr. Bruno LE BIZEC	LABERCA, Nantes	Rapporteur
Dr Corinne GOSMINI	Ecole Polytechnique, CNRS	Examinateur
Dr. Stéphane BOUCHONNET	Ecole Polytechnique, CNRS	Directeur de thèse
Pr. Farouk JABER	LAPPO, CLEA, CNRSL	Co-directeur de thèse

Laboratoire des Mécanismes Réactionnels (DCMR)

UMR N°7651 CNRS-Ecole Polytechnique

À ma mère, je dédie cette thèse

Merci Maman

Remerciement

Tout d'abord, je tiens à remercier dieu qui m'a donné l'occasion de continuer mes étude. Puis, je remercie l'Ecole doctorale de l'Ecole polytechnique qui m'a permis de réaliser ma thèse dans cette prestigieuse Ecole. Merci, pour le Centre National de Recherches Scientifique Libanais (CNRSL) qui a financé cette thèse. La Commission Libanaise de l'Energie Atomique (CLEA) qui m'ont recueilli au saine de leur Laboratoire d'Analyse de Pesticides et des Polluants Organiques (LAPPO) pour réaliser les recherches de cette thèse.

Je tiens à remercier vivement Dr. Stephane BOUCHONNET, mon directeur de thèse, pour la confiance qu'il m'a accordé en acceptant d'encadrer ce travail doctoral, pour ces multiples conseils et pour toutes les heurs qu'il a consacré à diriger cette recherche. J'aimerais également lui dire à quel point j'ai apprécié sa grande disponibilité et son respect sans faille des délais serrés de relecture des documents que je lui ai adressés. Enfin, j'ai été extrêmement sensible à ses qualités humaines d'écoute et de compréhension tout au long de ce travail doctoral.

Je tiens de remercier Pr. Farouk JABER, mon co-directeur de thèse. Des simples remerciement ne seront pas suffisants, sans vous la vie d'un étudiant puis un thésard n'aurait pas été ce qu'elle fut. Merci pour votre soutien à toute épreuve. Merci pour votre aide académique si précieuse. A la fin, mon père était décédé depuis longtemps mais avec votre soutien je me sens qu'il est tout le temps ici. Tous les mots ne suffisent pas pour dire merci.

Je remercie les membres du jury: Dr. Nathalie KARPEL et Dr. Bruno LE-BIZEC qui ont accepté d'être rapporteurs et de juger ce travail. Dr. Corine GOSMINI qui a accepté d'être examinatrice de ce travail.

Au DCMR:

Je souhaiterai remercier Dr. Gille OHANESSIAN, notre directeur de laboratoire, pour m'avoir accueillir au sein de son laboratoire des Mécanismes Réactionnels.

Je remercie Dr. Sophie BOURCIER pour tout le temps que tu m'a consacré et pour ta patience durant les expériences. Dr. Guy BOUCHOUX pour ton soutien durant le stage de master 2 et durant ma thèse. Dr. Carine CLAVAGERA pour la collaboration pour les calculs théoriques. Dr. Gille FRISON, Nicole EDITH, Thérèse MERIME pour votre soutien durant mes séjours au laboratoire. Merci pour les thésards et les stagiaires et pour vous tous ma famille française.

Au LAPPO:

Je souhaiterai remercier Dr. Bilal NSOULI, directeur du CLEA, pour m'avoir accueillir au sein de la commission et pour toutes les facilitées que vous m'avez offert.

Merci pour Dr Mohammad ISKANDARANI pour tous les conseils que vous m'avez donné durant mon travail. Pour Khaled HAWARI, Samia MOKH et Radwan SIDAWI pour votre soutien. Merci spéciale pour mes deux sœurs Dr. Abir KOUZAIHA et Aisha ASHI. Merci pour les thésards et les stagiaires. Merci ma deuxième famille.

Pour ma famille:

Je tiens remercier mon épouse, Bouthaina HOUSSARI, pour ton soutien durant mon travail. Tu as toujours été à ma côté pour les moments de déception que d'espoir. Merci, mes deux sœurs Nisrine et Arwa RIFAI pour votre aide et vous êtes les deux jolies fleurs dans ma vie. Merci Yehya BAADARANI, mon beau frère, pour tous les bons moments. Merci ma tante Hala RIFAI, pour ton aide académique durant mon enfance.

En France:

je remercie la famille de M. Mohammad KASSAB et la famille de M. Jean Claude BACCOMO pour leurs soutiens et pour les jolies vacances à Marmande. Merci beaucoup.

Merci à tout les gens qui m'ont soutenu durant ma vie.

Table des matières

Abréviations utilisées dans ce document

CLEA	Commission Libanaise d'Énergies Atomiques
CNRSL	Centre National de Recherches Scientifiques Libanais
DCMR	Laboratoire des Mécanismes Reactionnels
LAPPO	Laboratoire d'Analyse des Pesticides et des Polluants Organiques
REACH	Registration, Evaluation, Autorisation et Restriction des Produits Chimiques
MS	Spectrométrie de Masse
MS^n	Spectrométrie de Masse Multidimentionnelle
QSAR	Quantitative Structure Activity Relationship
FAO	Food and Agriculture Organisation
OMS	Organisation Mondiale de la Santé
CE	Commission Européenne
PM	Poids Moléculaire
INERIS	Institue National de l'Environnement Industriel et des Risques
EPA	United States Environmental Protection Agency
UV	Ultra Violet
GC	Chromatographie en phase gazeuse
LC / HPLC	Chromatographie en phase liquide à haute performence
MS/MS	Spectrométrie de masse en mode tandem
ESI	Source d'ionisation d'elecrtonébulisation
Q	Analyseur quadripôlaire
TOF	Analyseur temps de vol
FT-ICR	Analyseur cyclotronique
MRM	Mode *"Multiple Reaction Monitoring"*
SIM	Mode *"Selected Ion Monitoring"*
m/z	Masse / charge
TQ	Analyseur triple quadripôle
T.E.S.T.	Toxicity Estimation Software Tools
LMR	Limite Maximale Résiduelle
SPE	Extraction sur phase solide
HR	Mode de haute résolution en Q-TOF
EI	Source d'ionisation électronique

CI	Source d'ionisation chimique
$M^{+\cdot}$	Ion moléculaire
MH^{+}	Ion pseudo-moléculaire
LD	Dose létale
A.U.	Unité arbitraire
CID	Cellule de collision
DCA	Dichloroaniline
TD-DFT	Méthode de calculs
CC2	

Publications scientifiques

ARTICLES DE THESE

- **Characterization of the photodegradation products of metolachlor: structural elucidation, potential toxicity and persistence**

  Sarah Coffinet, Ahmad Rifai, Christophe Genty, Yasmine Souissi, Sophie Bourcier, Michel Sablier and Stéphane Bouchonnet.

  J. Mass Spectrom. 2012, 47, 1582–1593

- **UV-visible photo degradation of procymidone - structural characterization and potential toxicity of photoproducts**

  Ahmad Rifai, Yasmine Souissi, Christophe Genty, Carine Clavaguera, Sophie Bourcier, Farouk Jaber and Stephane Bouchonnet.

  Rapid Commun Mass Spectrom. 2013 Jul 15;27(13):1505-16

- **Structural characterization of photoproducts of pyrimethanil**

  Aziz Kinani, Ahmad Rifai, Sophie Bourcier, Farouk Jaber and Stéphane Bouchonnet.

  J. Mass. Spectrom 48:8 2013 Aug pg 983-7

- **Photolysis of metolachlor: Structures elucidation of degradation products by LC-MS and computer aided toxicity prediction**

  Ahmad Rifai, Christophe Genty, Yasmine Souissi, Stéphane Bouchonnet & Sophie Bourcier

  Accepted for publication in Journal of Mass Spectrometry

- **Structural characterization of photoproducts of Boscalid - structural characterization and potential toxicity of photoproducts**

  Soumis pour publication dans *Rapid Communications in Mass Spectrometry*

TRAVAUX ASSOCIES

- **Fragmentation reactions of phenoxide anions: deprotonated Dinoterb and related structures.**

  Ahmad Rifai, Sophie Bourcier, Delphine Arquier, Yannick Charvet, Farouk Jaber and Guy Bouchoux.

  J. Mass. Spectrom. 2011, 46, 1079–1088

- **Structures and dissociation mechanisms of protonated and electron ionized methamidophos**

  Ahmad Rifai, Sophie Bourcier, Farouk Jaber, Guy Bouchoux.

  Int. J. Mass Spectrom.2013, 7, 339-340

AVANT-PROPOS

Ce travail de thèse a été réalisé dans le cadre d'une collaboration entre le Laboratoire des Mécanismes Réactionnels du Département de Chimie de l'Ecole Polytechnique de Palaiseau, France, et le Laboratoire d'Analyse de Pesticides et de Polluants Organiques (LAPPO) de la Commission Libanaise de l'Energie Atomique (CLEA-CNRSL), Liban. Il a été co-encadré par les Docteurs Stéphane BOUCHONNET et Farouk JABER.

Introduction générale

Le développement industriel et les activités humaines produisent une quantité très importante de polluants chimiques (colorants, intermédiaires de synthèse, produits phytosanitaires, médicaments…). Parmi eux, les pesticides constituent une classe à part car ils sont délibérément introduits dans l'environnement. Il s'agit de substances destinées à lutter contre les parasites des cultures au sens large, c'est-à-dire contre des organismes jugés indésirables. La diffusion des pesticides dans la nature engendre une pollution des différents compartiments de la biosphère (eau, sol et atmosphère) et peut induire des effets toxiques aigus sur les êtres vivants de la biomasse terrestre et aquatique. Il est aujourd'hui démontré que certains pesticides sont des perturbateurs endocriniens et présentent en particulier des effets cancérogènes et mutagènes chez l'être humain.

Les pesticides peuvent subir différents processus de transformation dans le cycle biologique naturel (biodégradation, volatilisation, irradiation solaire…) ou suite aux traitements appliqués dans les filières de potabilisation des eaux naturelles et dans les stations de retraitement des eaux usées. La présence de produits de dégradation de pesticides dans notre environnement est d'autant plus alarmante que leurs structures et leurs toxicités potentielles demeurent généralement inconnues. Les laboratoires de surveillance des aliments travaillent à l'amélioration des méthodes d'isolation, de caractérisation et de dosage des pesticides dans les matrices environnementales (eau, fruits, légumes, viandes, poissons, coquillages, lait, œufs…). Les méthodes en vigueur sont développées et validées de manière à répondre aux exigences de directives internationales (REACH [1], 76/768/CEE [2], 91/414/CEE [3]) en termes de justesse, de précision, de seuils de détection et de limites de quantification. Il s'agit de vérifier que les teneurs en pesticides n'excèdent pas les concentrations maximales fixées par ces directives. Les produits de dégradation des pesticides ne sont généralement pas pris en considération dans la mesure où ils demeurent méconnus donc indétectables aux concentrations auxquelles ils sont susceptibles de se trouver en milieu naturel. L'analyse de traces par couplage chromatographie-spectrométrie de masse impose en effet que les molécules ciblées soient connues.

Des études récentes ont montré que les produits de dégradation des pesticides sont susceptibles d'exercer une toxicité égale, voire même parfois supérieure, à celle des molécules mères [4]; ils sont désormais reconnus comme "polluants émergents" [5, 6]. En dépit de cette prise de conscience de la nécessité de se préoccuper de ces polluants émergents, la méconnaissance de ces composés rend très difficile, voire impossible l'évaluation des risques sanitaires et environnementaux associés et empêche l'intégration de ces molécules dans les réglementations en vigueur.

La littérature scientifique montre que les recherches actuelles sont focalisées sur l'optimisation et la maîtrise des procédés de dégradation des molécules polluantes (ozonation, photocatalyse, chloration…). Dans la majorité des études publiés, les structures et les effets biologiques des sous-produits formés ne sont peu ou pas considérés, les cinétiques et rendements des réactions de dégradation constituant les enjeux majeurs de ces recherches. Ainsi, la plupart des études consacrées à la dégradation par photolyse ou photocatalyse de polluants environnementaux ont porté sur l'optimisation des conditions expérimentales de photo-traitement et sur les cinétiques réactionnelles [7]. Très peu de travaux sont consacrés à la photolyse naturelle, celle qui est exercée par le rayonnement solaire directement en surface des fruits et légumes traités ou en surface de l'eau contaminée en pesticides suite aux phénomènes de ruissellement.

Dans le cadre de cette thèse, nous avons développé une stratégie analytique permettant de caractériser les structures de composés issus de la dégradation par photolyse de pesticides. La première des molécules retenues pour ces recherches est le métolachlore. L'étude de la photolyse de ce dernier s'inscrivait dans la suite logique des études en cours au DCMR lors de mon arrivée au laboratoire, études consacrées à la photolyse et à l'ozonolyse d'autres pesticides de la famille des chloroacétamides : alachlore et acétochlore. Les trois autres molécules étudiées sont la procymidone (composé organochloré), le boscalid (carboxamide) et le pyriméthanil (anilinopyrimidine). Il s'agit de fongicides détectés dans des fruits et/ou des légumes lors d'analyses de routine effectuées au LAPPO, parfois en quantité abondante. A titre d'exemple, le boscalid a été détecté dans des feuilles de vigne à des concentrations pouvant atteindre 4 mg/L).

Pour chacune des molécules étudiées, notre démarche a consisté à modéliser la photodégradation en laboratoire, à identifier les produits de dégradation formés, à évaluer leur toxicité et à établir si les photoproduits caractérisés étaient effectivement présents en matrices environnementales.

Les expériences de photolyse en laboratoire ont été conduites sur un photoréacteur prototype conçu et construit dans le cadre de la thèse de Yasmine Souissi (achevée en 2012). Les structures chimiques de photoproduits ont été caractérisées grâce à deux techniques complémentaires : la chromatographie en phase gazeuse couplée à la spectrométrie de masse pour l'analyse des composés apolaires et peu polaires et la chromatographie liquide couplée à la spectrométrie de masse pour la détection des produits polaires. En préalable à la caractérisation structurale des produits de dégradation, nous avons étudié les mécanismes de fragmentation des molécules mères afin d'identifier des dissociations spécifiques de certaines

parties de la molécule. Par la suite, des expériences de spectrométrie de masse multidimensionnelle (MS^n) et des mesures de masses exactes ont permis de caractériser de nombreux photoproduits. L'évolution des abondances relatives des produits et la persistance de ces derniers ont été étudiées. Les résultats obtenus ont permis de proposer des mécanismes pour les réactions de photolyse.

Les toxicités des produits de photolyse ont été estimées sur la base de tests *in silico*, tests QSAR (*Quantitative Structure Activity Relationship*) récemment développés pour tenter de prévoir la toxicité des molécules.

Finalement, la détection en matrices réelles de certains photo-produits caractérisés suite aux irradiations menées en laboratoire a permis de démontrer le bien-fondé de la démarche analytique suivie.

Réferences

[1] REACH - Enregistrement, évaluation, autorisation et restriction des produits chimiques**.** *Http://Ec.Europa.Eu/Enterprise/Sectors/Chemicals/Reach/Index_Fr.Htm*. **2007**.

[2] 76/768/CEE. Le rapprochement des législations des États membres relatives aux produits cosmétiques. *Conseil des Communautés Européennes*. **1976.**

[3] 91/414/CEE. La mise sur le marché des produits phytopharmaceutiques. *Conseil des Communautés Européennes.* **1991**.

[4] R. Mckinlay, J.A. Plant, J.N.B. Bell, N. Voulvoulis. Endocrine disrupting pesticides: Implications for risk assessment. *Environ. Int.* **2008,** 34, 2, 168.

[5] M.L. Hladik, E.J. Bouwer, A.L. Roberts. Neutral degradates of chloroacetamide herbicides: Occurrence in drinking water and removal during conventional water treatment. *Water Res.* **2008,** 42, 20, 4905.

[6] U.S. Environmental Protection Agency. Final Contaminant Candidate List 3 Chemicals: Identifying the Universe. *Available from: http://www.epa.gov/ safewater /ccl/ccl3. html#chemical***. 2009**.

[7] N.B. Parilti, D. Akten. Optimization of TiO_2/Fe (III)/solar UV conditions for the removal of organic contaminants in pulp mill effluents. *Desalination*. **2011**, 265, 37.

Chapitre I - Synthèse bibliographique

I-1. Les Pesticides

I-1-1. Définitions

De longue date, l'homme a utilisé des substances minérales (cuivre, arséniate de plomb…) ou végétales pour combattre les organismes vivants indésirables dans les champs, les jardins, etc. Les chimistes ont ensuite synthétisé des substances organiques pouvant jouer ce rôle. Le Codex alimentaire (FAO/OMS, 1994) et l'Organisation Mondiale de la Santé définissent comme pesticide toute substance destinée à prévenir, détruire, attirer, repousser tout élément nuisible : plante, champignon, insecte, mammifère… durant la production, l'entreposage, le transport, la distribution et la transformation de denrées alimentaires, de produits agricoles ou d'aliments pour animaux [1].

Les règlements européens répertorient les pesticides selon leurs usages : produits phytosanitaires, phytopharmaceutiques, agropharmaceutiques, produits de traitement pour la protection des bois et d'autres matériaux [2, 3, 4, 5]. Dans le langage courant, le terme "pesticide" englobe également des molécules d'usage vétérinaire, des molécules entrant dans la composition de certaines peintures, vernis, etc., le terme "produit phytosanitaire" étant réservé aux produits spécifiquement dédiés à la protection des plantes.

Dans la directive 91/414/CE du 15 juillet 1991, la Communauté Européenne définit les pesticides comme "préparations contenant une ou plusieurs substances actives qui sont présentées sous la forme dans laquelle elles sont livrées à l'utilisateur et qui sont destinées à protéger les végétaux ou produits végétaux contre tous les organismes nuisibles" [2]. Les pesticides assurent la conservation des produits végétaux, pour autant que les substances ou produits ne fassent pas l'objet de dispositions particulières du Conseil ou de la Commission concernant les agents conservateurs ; ils ralentissent ou préviennent la croissance de végétaux indésirables.

On peut ainsi considérer que le terme "pesticide" regroupe des substances de différentes familles de composés organiques et inorganiques, naturels ou synthétisés par l'industrie chimique, destinés à repousser ou détruire les ravageurs et les espèces indésirables de plantes, champignons et animaux causant des dommages aux produits agricoles, aux denrées alimentaires, aux produits ligneux, ou aux aliments pour animaux.

I-1-2. Usage des Pesticides en Europe et au Moyen Orient

L'usage des pesticides synthétiques s'est généralisé après la deuxième guerre mondiale avec le développement de l'agriculture intensive. La prise de conscience des effets de ces substances sur l'environnement et la santé humaine date de la même période. Les premières mesures législatives destinées à réglementer l'usage des pesticides agricoles remontent en effet à 1941.

Aujourd'hui, l'usage des pesticides est largement répandu, majoritairement dans l'agriculture mais aussi dans les espaces privés ou publics : jardins, maisons, espaces verts, aménagements extérieurs, soins vétérinaires, protection corporelle, conservation des aliments, etc. Les tonnages de pesticides fabriqués dans le monde ont constamment augmenté depuis soixante ans. Toutefois, la tendance semble s'inverser actuellement dans certains pays européens. Il faut également considérer qu'à quantité égale, les substances actives actuelles sont beaucoup plus efficaces qu'il y a plusieurs décennies.

Tableau I-1. Tonnages en pesticides utilisés par les pays européens en 2001 [4]

Quantité de pesticides utilisées en Europe en 2001 (en tonnes de substance active)

	Fongicides		Herbicides		Insecticides		Divers		Total	% (a)	Surface/Surface en Europe (b)	Rapport (a/b)
	Tons	%	Tons	%	Tons	%	Tons	%				
France	54130	54,3	32122	32,2	2487	2,5	10896	10,9	99635	34,3	21	1,6
Italie	23288	51,8	8191	18,2	9747	21,7	3741	8,3	44967	15,5	11	1,4
Espagne	13790	33,7	10374	25,4	11631	28,4	5099	12,5	40894	14,1	21,1	0,7
Allemagne	8418	32,1	13337	50,9	868	3,3	3601	13,7	26224	9	12,1	0,7
Portugal	13915	56	6399	25,7	2616	10,5	1926	7,7	24856	8,5	2,9	2,9
Royaume -Uni	3628	18	11817	58,6	857	4,2	3874	19,2	20176	6,9	12	0,6
Grèce	4860	43,7	2650	23,9	2638	23,7	963	8,7	11111	3,8	6	0,6
Pays-Bas	3628	46,1	2172	27,6	227	2,9	1840	23,4	7867	2,7	1,4	1,9
Belgique/Lux	1595	31,5	2345	46,3	560	11,1	566	11,2	5066	1,7	1,1	1,5
Autriche	1088	38,6	1317	46,7	94	3,3	322	11,4	2821	1	2,4	0,4
Danemark	511	19,5	1925	73,5	66	2,5	116	4,4	2618	0,9	1,9	0,5
Suède	339	18,2	1462	78,4	24	1,3	40	2,1	1865	0,6	2,2	0,3
Finlande	192	13,4	1120	78,2	42	2,9	78	5,4	1432	0,5	1,6	
Irlande	410	30,7	795	59,6	84	6,3	45	3,4	1334	0,5	3,1	
	129792	44,6	96026	33,0	31941	11,0	33107	11,4	290866	100	100	

En Europe, environ 300.000 tonnes de pesticides ont été consommées en 2001 (tableau I-1). La France est le premier consommateur de pesticides parmi les pays européens, devant l'Italie et l'Espagne (figure I-1). Elle compte également parmi les premiers consommateurs si l'on rapporte les quantités de pesticides utilisées à l'étendue des surfaces cultivées (tableau I-1). En 2006, la France demeurait le troisième plus gros consommateur de pesticides au monde derrière les Etats-Unis et le Japon, respectivement premier et second.

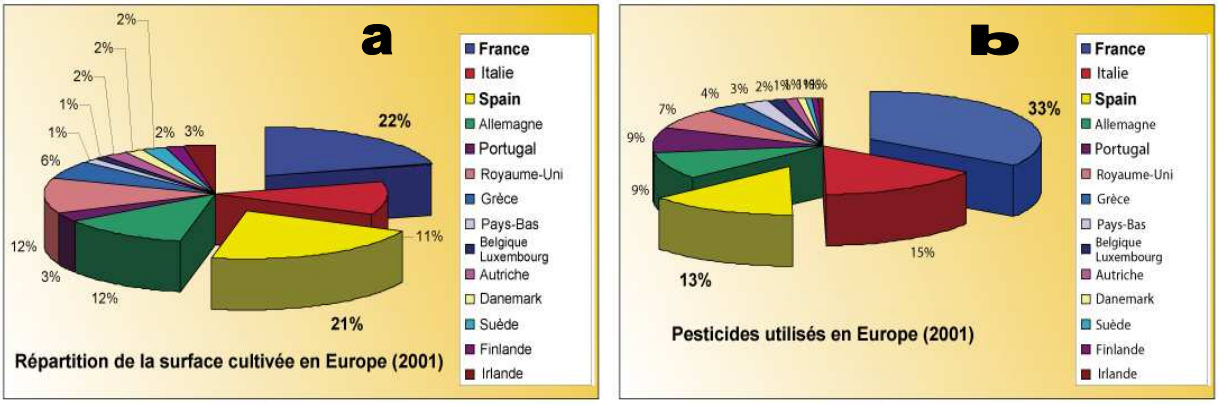

Figure I-1. Histogrammes représentant a) la répartition des surfaces cultivées en Europe, b) les pourcentages des quantités de pesticides utilisées dans les pays européens [4]

Au Moyen Orient, le Liban est un petit pays de 10.452 km^2 au bord de la Méditerranée. Les surfaces consacrées à l'agriculture représentent plus de 60% de sa superficie [5, 6] (figure I-2). Entre les années 1993 et 2002, le Liban était le premier consommateur de pesticides parmi les pays arabes avec une consommation moyenne de 5,5 kg/hectare ; il était suivi par le Koweït et le Qatar avec respectivement 4,5 et 3,2 kg/hectare (figure I-3) [7].

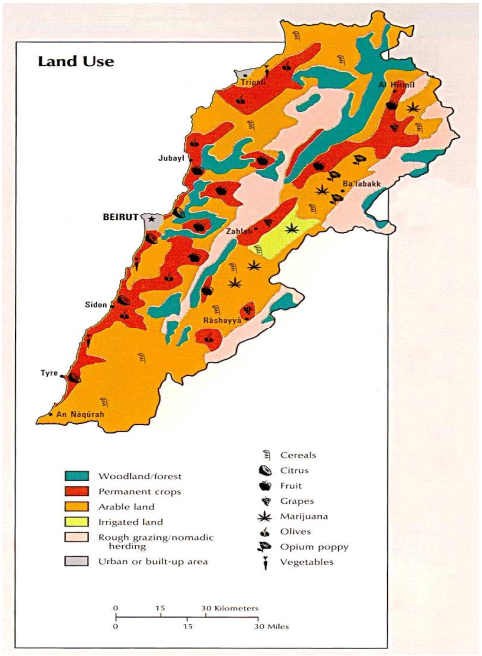

Figure I-2. Répartition des surfaces cultivées sur le territoire libanais

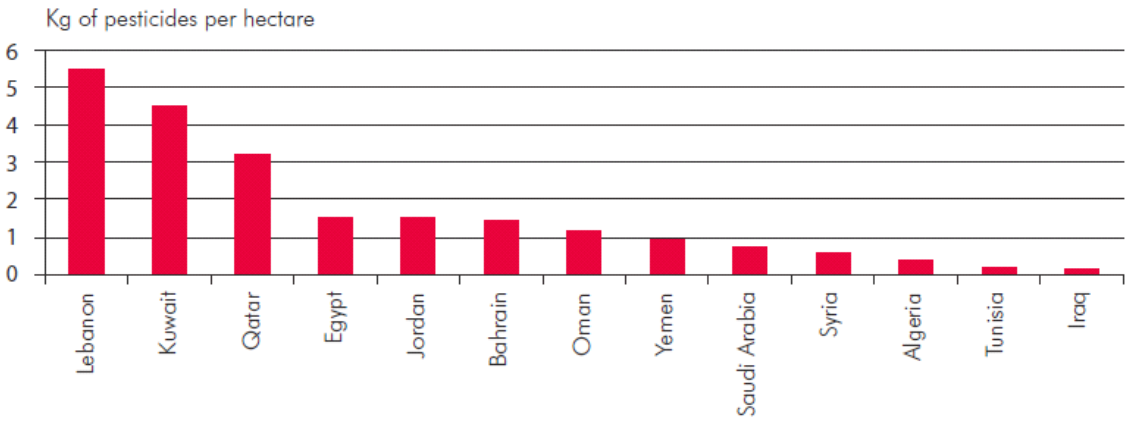

Figure I-3. Quantités de pesticides utilisées dans les pays arabes en kg/hectare

I-1-3. Classification des pesticides

Deux modes de classification sont utilisés pour répertorier les pesticides : selon leur nature chimique ou selon leur rôle fonctionnel attendu (tableau I-2) [3, 8].

Dans le premier cas, les pesticides sont classés selon la nature chimique de la substance active majoritaire et répartis en cinq groupes principaux :

- organochlorés (DDT, lindane, chlordane...),
- organophosphorés : esters phosphoriques, phosphoniques, phorothioniques (diazinon, dichlorovos, malathion...),
- carbamates formés par des sels ou esters d'acide carbamique (carbaryl, propoxur...),
- triazines (atrazine, propazine, simazine ...),
- urées substituées incluant plusieurs groupes fonctionnels : phényluréases, sulfonyluréases, etc. [3, 9].

La seconde classification, dite "fonctionnelle", consiste à répartir les pesticides en fonction du type de parasite à contrôler ou à éliminer. On définit ainsi les herbicides, insecticides, fongicides et rodenticides.

Les herbicides sont des substances (ou mélanges de substances) utilisées pour détruire ou empêcher la croissance de la végétation indésirable, des mauvaises herbes qui entrent en concurrence avec les cultures agricoles ou ornementales [6]. Les herbicides possèdent différents modes d'action sur les plantes, ce sont des perturbateurs de la régulation de l'auxine, principale hormone agissant sur la croissance des cellules. Ils sont également perturbateurs de la photosynthèse et inhibiteurs de la division cellulaire. Ils inhibent la

synthèse des lipides, de la cellulose ainsi que des acides aminés [8]. Les molécules actives des herbicides incluent diverses catégories de fonctions chimiques: acides carboxyliques, aliphatiques, amides, chloroacétanilides, benzonitriles, dinitrophénylamines, phénols, etc.

Les insecticides agissent contre les insectes qui parasitent les plantes en exerçant sur ces dernières des actions neurotoxiques, régulatrices de croissance et inhibitrices de la respiration. Les principes actifs des insecticides sont majoritairement des composés organochlorés qui, en raison de leur extrême toxicité, sont progressivement remplacés par des organophosphorés et des carbamates, moins nocifs pour les oiseaux et les mammifères mais plus dangereux pour la faune aquatique [10].

Les fongicides sont des substances permettant de lutter contre les maladies provoquées par les champignons et les moisissures [3, 11], ils peuvent agir comme inhibiteurs de la respiration et de la division cellulaire mais aussi comme perturbateurs de la biosynthèse des acides aminés ou des protéines et perturbateurs du métabolisme des glucides [3].

Les rodenticides agissent contre certains rongeurs nuisibles (rat, souris, mulot etc.). Ils peuvent avoir des compositions chimiques variées. La majorité d'entre eux appartient à deux familles : les anticoagulants et les convulsivants. Les premiers annulent l'effet de la vitamine K : les animaux meurent victimes d'hémorragies internes. Les convulsivants provoquent des spasmes musculaires entrainant le coma puis la mort [11].

Tableau I-2. Classification fonctionnelle et principaux principes actifs des pesticides [12]

Insecticides	**Herbicides**	**Fongicides**	**Rodenticides**
organophosphorés	composés chlorophénoxy	benzènes substitués	inorganiques
carbamates	pentachlorophénol	organochlorés	coumarines
pyréthrine et pyréthoïde	crésol, nitrophénols	carboximides	chlorécaciférols
dérivés de l'arsenic et autres composés	dérivés de l'arsenic et autres composés	anilinopyrimidine	convulsivants

Dans cette étude, nous nous sommes particulièrement intéressés à des fongicides largement utilisés au Liban dans la mesure où nous pouvions disposer d'échantillons réels

contaminés par ces molécules, échantillons procurés par le Laboratoire d'Analyse de Pesticides et de Polluants Organiques (LAPPO) de la Commission Libanaise de l'Energie Atomique. Dans le monde, les fongicides en question sont utilisés sur des cultures aussi diverses que la vigne, le riz [13], l'oignon [14], la tomate [15], la pomme [16], le raisin [17] ou la banane [18].

I-2. Les fongicides

I-2-1. Historique de l'utilisation des fongicides

Dès le XVIII^{ème} siècle, les fongicides sont utilisés pour lutter contre les maladies des plantes provoquées par des champignons. A l'époque, les techniques, bien qu'efficaces, étaient quelque peu rudimentaires. En 1761, Schulthess a préconisé l'utilisation de sulfate de cuivre contre l'oïdium qui affectait notamment les vignes. En 1800, Proust a mis en évidence l'effet anti-cryptogamique lié à l'épandage sur les feuilles de vert de gris ou de sels de cuivre mélangés à la chaux [19]. Le mélange de cuivre et de chaux a été baptisé "bouillie bordelaise". Ces deux produits sont toujours largement utilisés en agriculture. Suite à la seconde guerre mondiale, d'importantes évolutions ont concerné les produits chimiques utilisés, leur fréquence d'utilisation ainsi que leurs conditions d'application. Depuis trente ans, de nombreux fongicides dits "entre deux âges" (phthalimides, dithiocarbamates, dinitrophénols, chlorophényls) intègrent le marché des produits phytosanitaires. Ces produits présentent une activité systémique qui était inexistante chez leurs prédécesseurs. Aujourd'hui, le marché des fongicides est très large mais le nombre de fongicides homologués commence à diminuer sous la pression d'organismes publics, de plus en plus conscients de l'importance de sécuriser leur utilisation. Au cours des dix dernières années, 35% des pesticides enregistrés ont été rappelés, réexaminés et/ou retirés du marché. Les recherches portant sur l'écotoxicité et la santé humaine se sont multipliées [20].

I-2-2. Définition et mobilité des fongicides

Le terme "fongicide" signifie littéralement tuer (du latin *caedo*) le champignon (f*ungus*) [19]. Les fongicides tuent ou inhibent les champignons responsables de maladies aux répercussions économiques importantes, tant au niveau du rendement que de la qualité du produit. L'usage des fongicides durant la période de culture permet de réduire les pertes en entrepôt.

Les fongicides sont utilisés dans le cadre d'un programme de lutte intégrée qui doit prendre en considération la rotation des cultures et le choix des variétés tolérantes. Les dates de semis, de récolte, la fertilisation adéquate et la densité de semis doivent être précisées, ainsi que le mode de gestion des débris de culture et l'utilisation d'indicateurs de risque.

Si les fongicides restent à la surface de la plante et ne pénètrent pas dans les feuilles, on parle de "fongicides de surface". Les feuilles qui émergent après application ne sont pas protégées et les fongicides peuvent être lessivés par la pluie et désactivés par le soleil. Si les fongicides pénètrent dans la plante, on parle de "fongicides pénétrants".

Il existe trois types de pénétration, décrits ci-dessous.

Dans le premier cas, les gouttelettes restent sur la feuille : les pesticides pénètrent sous la cuticule au niveau du point de contact entre la plante et la gouttelette de solution phytosanitaire mais ne sont pas véhiculés par la sève de la plante. On parle alors de pénétration "translaminaire". Le fongicide n'entrant que localement dans la plante, les feuilles qui émergent après application ne sont pas protégées. Dans ce cas, le fongicide n'est pas lessivé par la pluie après avoir pénétré dans la plante.

Lorsque les fongicides sont principalement appliqués sur le sol, les molécules pénètrent dans la plante *via* les racines. Une faible proportion peut également pénétrer *via* le feuillage par absorption foliaire. Les fongicides migrent vers le haut de la plante avec la sève montante. On parle alors de "pénétration systémique à diffusion ascendante". Ainsi, les feuilles qui émergent après l'application sont protégées et le fongicide n'est pas lessivé par la pluie.

Lorsque les fongicides, appliqués sur les feuillages et le sol, migrent à la fois vers le haut (apex) et le bas (racine) de la plante avec les sèves montante et descendante, on parle de pénétration "complètement systémique". Comme dans le cas précédent, les feuilles émergeant après application sont protégées et le fongicide n'est pas lessivé par la pluie [14].

I-2-3. Fongicides retenus pour cette étude

I-2-3-1. Structures et propriétés physico-chimiques

Nous avons choisi pour cette étude trois fongicides parfois détectés dans des fruits ou des légumes lors d'analyses de routine au LAPPO - CNRSL. Il s'agit de la procymidone (organochloré), du boscalid (carboxamide) et du pyriméthanil (anilinopyrimidine). Leurs formules brutes, structures, masses moléculaires et solubilités dans l'eau sont données dans le tableau I-3.

Tableau I-3. Formules brutes, structures chimiques, poids moléculaires (PM) et solubilités dans l'eau des fongicides étudiés

Composé	Formule brute	Structure chimique	PM (g/mol)	Solubilité (mg/L)	Références
Procymidone	$C_{13}H_{11}Cl_2NO_2$	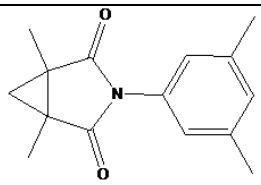	284	2,46	[21, 22]
Boscalid	$C_{18}H_{12}Cl_2N_2O$	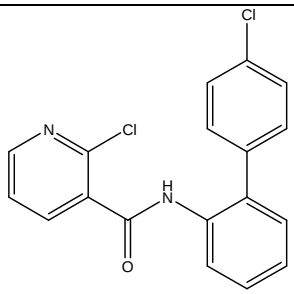	343	4,6	[23, 24, 25]
Pyriméthanil	$C_{12}H_{13}N_2$	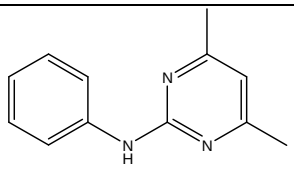	199	121,0	[26, 27]

La procymidone est un fongicide organochloré appartenant à la famille chimique des dicarboximides. Elle agit principalement sur les pourritures grises causées par *Botrytis cinerea Persoon*, aussi bien sur les fruits (raisin, pomme, fraise…) que sur les végétaux. Elle possède également une action vis-à-vis des sclérotinioses (*Sclerotinia minor et S. scerotiorum*) et des monilioses (*Monilia laxa et M. fructigena*) [28, 29].

Le pyriméthanil est un fongicide appartenant à la famille chimique des anilino-pyrimidines. Il agit principalement sur les pourritures grises causées par *Botrytis cinerea Persoon* sur le raisin mais possède également une action sur *Venturia inaequalis et Brotrytis spp.* qui contaminent les pois et les pommes. Ce pesticide présente un mode d'action différent

de celui des autres anti-botrytis : il inhibe la sécrétion par le pathogène des enzymes nécessaires au processus d'infection [26, 30].

Le boscalid appartient à la famille chimique des carboximides. Il agit contre la pourriture sclérotique sur le canola, la moisissure blanche sur les haricots, la brûlure aschochytique, la moisissure blanche et la moisissure grise (*Botrytis cinerea Persoon*) sur les pois chiches, les lentilles, les haricots et les fraises. Il combat également l'affaissement sclérotique (répression), la brûlure hâtive de la pomme de terre, la pourriture brune et la brûlure des fleurs des fruits suivants : abricot, cerise douce ou acide, nectarine et pêche. Enfin, il permet de lutter contre le blanc de la vigne [24, 31].

I-2-3-2. Toxicité des fongicides étudiés

La plupart des fongicides sont perturbateurs du système endocrinien de l'être humain et présentent en particulier des effets cancérogènes et mutagènes [32].

Concernant les fongicides étudiés, la procymidone est un antagoniste compétitif des androgènes à leur récepteur, provoquant ainsi des retards de développement chez les descendants mâles [33]. Elle a également été incriminée quant à des effets sur la reproduction et l'induction de tumeurs testiculaires dans une étude menée sur le long terme chez le rat [34]. Par ailleurs, il a récemment été rapporté que cette dicarboximide réduit le poids de la prostate et des vésicules séminales [35].

Selon le rapport rendu en 2006 par l'INERIS, le pyrimethanil présente des effets de toxicité chronique chez le rat : il induit un retard de croissance avec augmentation du cholestérol plasmatique. Une augmentation du poids du foie et des lésions histopathologiques au niveau du foie et de la thyroïde ont également été rapportées [30, 27].

Selon l'EPA, Le boscalid ne présenterait pas d'effets toxiques à cours terme. A long terme en revanche, les études menées sur des animaux de laboratoire ont démontré que le foie et la thyroïde constituaient les organes cibles d'une toxicité chronique. Le rat serait une espèce plus sensible. Chez celui-ci, le boscalid peut provoquer une augmentation du poids de la glande thyroïde accompagnée de changements histopathologiques: hypertrophie cellulaire diffuse au niveau des vésicules thyroïdiennes et hyperplasie en foyer de cellules des vésicules thyroïdiennes, baisse des concentrations en T3 et T4, hausse de la concentration en thyrotropine. Ces effets seraient néanmoins réversibles après interruption de l'exposition au

boscalid. Il est postulé comme très probable que les effets sur la thyroïde résulteraient de l'induction chronique d'enzymes microsomiales de type II dans le foie. Ces effets n'ont pas été notés chez le chien ni la souris. Le produit a été classé par l'EPA comme ayant une évidence suggestive de cancérogénicité chez le rat en raison de la présence d'adénomes au niveau des cellules des vésicules thyroïdiennes. Dans des études portant sur la reproduction et le développement des animaux de laboratoire, les petits n'ont pas démontré de sensibilité accrue, comparativement aux adultes, après exposition *in utero* et/ou postnatale au boscalid. Le produit n'est ni génotoxique ni neurotoxique [29, 36].

I-3. Réactions photochimiques

I-3-1. Principe de la photolyse et réactions mises en jeu

Différentes méthodes de traitements chimiques, en particulier les procédés d'oxydation tels que la chloration et l'ozonation, ont montré leur efficacité pour la réduction des concentrations en pesticides. L'efficacité du traitement dépend naturellement de la structure de la molécule traitée ainsi que de la nature et de la dose d'agent oxydant. D'autres traitements chimiques basés sur des procédés photochimiques tels que la photo-oxydation par les rayonnements UV, la photo-catalyse ou encore le traitement par photo-fenton ont également été rapportés dans la littérature [37, 38].

L'irradiation UV est utilisée dans le traitement des eaux plus souvent à des fins de désinfection que de décontamination. Dans ce dernier cas, elle peut impliquer deux processus différents: la photolyse directe et la photolyse indirecte. La photolyse directe implique l'absorption des radiations UV par la molécule à détruire, qui passe ainsi par un état excité favorisant sa décomposition. La présence d'au moins un groupement chromophore est nécessaire. Dans ce cas, la transformation du composé chimique est une conséquence directe de l'absorption d'un photon. La photolyse indirecte, quant à elle, implique l'absorption de la lumière par une molécule autre que les produits chimiques à traiter, engendrant ainsi la formation d'intermédiaires excités. On parle de photo-transformation indirecte lorsque d'autres espèces excitées transfèrent de l'énergie, des électrons ou des atomes d'hydrogène au produit chimique pour induire la transformation. Ces intermédiaires excités réagissent avec la molécule à traiter pour entrainer sa dégradation. On parle également de photolyse sensibilisée.

Dans le cadre de ce travail de thèse, nous nous sommes intéressés à la photolyse directe. Cette dernière est régie par deux principaux paramètres : le coefficient d'absorption molaire

de la molécule et le rendement quantique. Ces deux paramètres sont spécifiques du composé chimique et conditionnent l'interaction entre la molécule et la lumière. Le coefficient d'absorption molaire traduit le taux de radiation qu'un composé en solution peut absorber à une longueur d'onde donnée. La première loi de la photochimie établit que seule la lumière absorbée peut produire un effet photochimique. De ce fait, le traitement des contaminants par UV n'est efficace que si l'irradiation UV émise par la lampe est absorbée par le contaminant [39].

Les réactions (1) à (6) sont initiées par l'absorption de lumière par le substrat (R) à dégrader. Les molécules absorbant l'énergie lumineuse sont soit activées (R*) (réaction (1)), soit dissociées (réaction (4)), le mécanisme induit dépendant du type de substrat étudié [40]. En présence de dioxygène, la molécule excitée va produire un radical $R^{\cdot}$ (réaction (2)) ou $RO_2^{\cdot}$ (réaction (5)), selon sa nature. Ce sont ces espèces radicalaires qui se dissocient pour conduire aux photoproduits (réactions (3) et (6)). Par la suite, les photoproduits peuvent être partiellement minéralisés par des réactions d'oxydation.

$$R + h\nu \rightarrow R^{*} \qquad \text{réaction (1)}$$

$$R^{*} + O_2 \rightarrow R^{\cdot} + O_2^{*} \qquad \text{réaction (2)}$$

$$R^{\cdot} \rightarrow \text{Produits} \qquad \text{réaction (3)}$$

$$RX + h\nu \rightarrow R^{\cdot} + X^{\cdot} \qquad \text{réaction (4)}$$

$$R^{\cdot} + O_2 \rightarrow RO_2^{\cdot} \qquad \text{réaction (5)}$$

$$RO_2^{\cdot} \rightarrow \text{Produits} \qquad \text{réaction (6)}$$

L'absorption d'un photon dans le cas de la photolyse en phase aqueuse est une condition nécessaire mais non suffisante pour qu'une molécule subisse une transformation par photolyse directe [41]. L'énergie absorbée doit être suffisante pour provoquer le clivage de liaisons, des réarrangements, des réactions d'oxydation ou de réduction. La photo-transformation entre en compétition avec d'autres processus de désactivation tels que l'extinction, et d'autres processus radiatifs ou non. En conséquence, la fraction des molécules excitées qui subissent

réellement une photo-transformation (i.e. le rendement quantique) est généralement bien inférieure à 1 (habituellement < 0.1 et parfois < 0.01) [42, 43].

I-3-2- Le photo-traitement des pesticides

Dans la grande famille des pesticides, nombreuses sont les molécules dont la structure permet l'absorption de l'énergie lumineuse dans le domaine de l'ultraviolet et du visible [19]. De ce fait, ces composés sont susceptibles de subir une photolyse directe. En milieu naturel, les pesticides en aérosols, dissous ou absorbés peuvent subir des réactions photochimiques lorsqu'ils sont exposés à la lumière solaire [44]. Plusieurs articles de synthèse ont été consacrés à la photodégradation des pesticides [37, 45, 46].

Comme évoqué précédemment, l'absorption de photons est possible grâce à la présence de chromophores ; elle donne lieu à une modification de la structure électronique des molécules entrainant un passage de l'état fondamental à l'état excité. Le tableau I-4 présente des exemples de groupements chromophores présents chez certains pesticides.

Tableau I-4. Exemples de groupes chromophores présents chez certains pesticides [47]

Groupe chromophore	Longueur d'onde maximale d'absorption (nm)	Valeur approximative du coefficient d'extinction molaire ($m^2.mol^{-1}$)
C=C	180	10000
C=N	< 220	20
Benzène	260	200
C=O	280	20
Ar-NO_2	280	7000
N=N	350	5
N=O	300	100

L'irradiation directe des pesticides les conduit dans un état singulet excité qui peut ensuite évoluer vers un état triplet [43]. Ces états d'excitation peuvent induire des phénomènes d'homolyse, d'hétérolyse ou de photo-ionisation, comme représenté figure I-4.

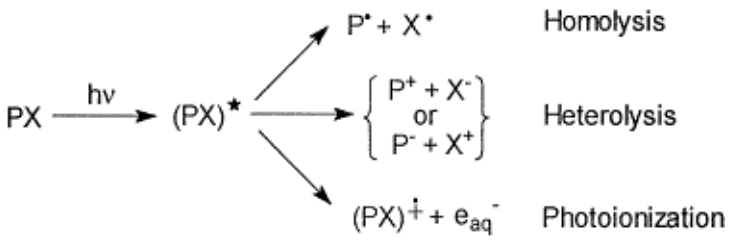

Figure I-4. Événements chimiques possibles lors de la photolyse directe d'un pesticide [43].

I-4. Réference

[1] D.Jawich. Etude de la toxicité de pesticides vis-à-vis de deux genres de levures : approche cinétique et moléculaire. *L'Institue National Polytechnique de Toulouse. and Université Saint Joseph de Beyrouth*. **2005**.

[2] 91/414/CEE. la mise sur le marché des produits phytopharmaceutiques. *Conseil des Communautés Européennes.* 1991.

[3] K. El Mrabet. Les pesticides. *Rapport de Laboratoire National De Metrologie et D'essaie - Paris*. **2008.**

[4] US Environmental Protection Agency. Pesticides. *Http://Www.Era-Orleans.Org /Afip /Fr/Pesticides.Html.* **2012.**

[5] Trading economics. Agricultural land in Lebanon. *Http://Www.Tradingeconomics. Com/Lebanon/Agricultur al-Land-Sq-Km-Wb.Data.Html*. **2012.**

[6] P.R. Salameh, M. Waked, I. Baldi, P. Brochard, B. Abi Saleh. Chronic bronchitis and pesticide exposure: a case–control study in Lebanon. *Eur. J. Epidemio.* **2006**, 21, 681.

[7] I. Bashour. CHAPTER 10 - Pesticides, Fertilizers and Food Safety. *Report of the arab forum for environment and development - Arab Environment: future challenges.* **2007**, 137.

[8] W.M.A. Niessen. Group-specific fragmentation of pesticides and related compounds in liquid chromatography-tandem mass spectrometry. *J. Chromatogr. A.* **2009**, 1217, 25, 4061.

[9] Y. Pico, C. Blasco, G. Font. Environmental and food applications of LC-tandem mass spectrometry in pesticide-residue analysis: An overview. *Mass Spectrom. Rev.* **2004**. 23, 1, 45.

[10] Http://Environnement.Doctissimo.Fr/Proteger-La-Terre/Pesticides/Qui-Sont-Les-Pesticides-.Html.

[11] National Pesticides Information Center. Rodenticides Topic Fact Sheet. **2011**.

[12] A. Fait, B. Iversen, M. Tiramani, S. Visentin, M. Maroni. Prevention des risques pour la santé liés à l'utilisation des pesticides dans l'agriculture. Fengsheng HeEditor, Occupational Medcine, Chinese Academy of Preventive Medcine. **2004**.

[13] S. Serghat, A. Mouria, A. Ouazzani Touhami, A. Badoc, A. Douira. Effet de quelques fongicides sur le développement *in vitro* de pyricularia grisea et helminthosporium oryzae. *Bull. Soc. Pharm. Bordeaux* . **2004**, 143, 7.

[14] C. Odile. Comment bien utiliser ses fongicides – systémiques, translaminaires et cie – dans l'oignon. *Agriculture et agroalimentaire- CANADA.*

[15] K. Hibar, M. Daami-Remadi, M. El Mahjoub. Effets de certains fongicides de synthèse et biologiques sur la croissance mycélienne et l'agressivité de Fusarium oxysporum f. sp. radicis-lycopersici. *Tropicultura.* **2007**, 25, 3, 146.

[16] K. Attrassi, R. Benkirane, B. Attarassi, A. Badoc, A. Douira. Efficacité de deux fongicides benzimidazolés et de l'anilinopyrimidine sur la pourriture des pommes en conservation. *Bull. Soc. Pharm. Bordeaux* . **2007**, 146, 195.

[17] M.R. González-Rodríguez, B. Cancho-Grande, J. Simal-Gándara. Multiresidue determination of 11 new fungicides in grapes and wines by liquid–liquid extraction/clean-up and programmable temperature vaporization injection with analyte protectants/gas chromatography/ion trap mass spectrometry. *J. Chromatogr. A.* **2009,** 1216, 32, 6033.

[18] D. Koné, J.B . Odjochoumou, L.B. Edson, C. Brahima, A. Séverin. Activités in vitro de différents fongicides sur la croissance chez mycosphaerella fijiensis var. difformis stover et dickson, cladosporium musae morelet et deightoniella torulosa (Syd.) ellis, parasites isolés de la phyllosphère des bananiers en Côte-d'Ivoire. *C. R. Biol.* **2009**, 332, 5, 448.

[19] J. Lhoste. Les Fongicides. *Office de la Recherche Scientifique et Technique Outre-Mer*. **1960**.

[20] G. Gilbert. La resistance des champignons aux fongicides. *Rapport de ministère de l'agriculture des pêcheries et de l'alimentation, Qébec.* **1999**.

[21] Environnemental INERIS : Normes de Qualité. Procymidone - (Ed.: 32809-16-8 CAS). **2011**.

[22] Unit Agriculture and Environment - REACH. Procymidone. **2012**.

[23] Chemnet CAS. Boscalid. *http://www.chemnet.com/cas/fr/188425-85-6/Boscalid.html.*

[24] European Commission - Health and Consumer Protection - General Directorate. Boscalid - Ed.: chain Safety of the food. **2008**, 3919.

[25] REACH. Boscalid. **2007.**

[26] European Commission Health and Consumer Protection Directorate-General. Pyrimethanil - Safety of the food chain. 2010, 10019.

[27] INERIS. Pyrimethanil - N° CAS 53112-28-0. *Normes de Qualité Environnementale*. 2011.

[28] C. Ferreira. Effets des perturbateurs endocriniens sur la fertilité male. *École National Veterinaire d'Alfort.* 2010.

[29] Institut Française de La Vigne et du Vin. Le Botrytis ou Pourriture Grise. *http:// www.vignevin-sudouest.com/publications/fiches-pratiques/botrytis-pourriture-grise. p hp.* **2005**.

[30] EFSA. Conclusion on the peer review of pyrimethanil. *http://www.efsa.eu.int.* **2006**.

[31] T. Veloukas, M. Leroch, M. Hahn, G. S. Karaoglanidis. Detection and Molecular Characterization of Boscalid-Resistant Botrytis cinerea Isolates from Strawberry. *Plant disease*. **2011**, 95.

[32] W. Mnif, A. Ibn Hadj Hassine , A. Bouaziz, A. Bartegi, O. Thomas, B. Roig. Effect of Endocrine Disruptor Pesticides: A Review. *Int. J. Environ. Res. Publ. Health.* **2011,** 8, 2265.

[33] K.W. Ostby, J. Lambright, C. Wolf, P. Mann, J. Gray. The fungicide procymidone alters sexual differentiation in the male rat by acting as an androgen-receptor antagonist *in vivo* and *in vitro*. *Toxicol. Ind. Health.* **1999**, 15, 80.

[34] M.F. Cengiz, M. Certel, B. Karakaş, H. Göçmen. Residue contents of captan and procymidone applied on tomatoes grown in greenhouses and their reduction by duration of a pre-harvestinterval and post-harvest culinary applications. *Food Chem.* **2007**, 100.

[35] P.R. Jacobsen, M. Axelstad, J. Boberg, L.K. Isling, S. Christiansen, K.R. Mandrup, L.O. Berthelsen, A.M. Vinggaard, U. Hass. Persistent developmental toxicity in rat offspring after low dose exposure to a mixture of endocrine disrupting pesticides. *Reprod. Toxicol.* **2012**, 34, 237.

[36] U. S. Environmental Protection Agency. Boscalid. *Ed.: Office of Prevention Pesticides and Toxic substances.* 2003, 85.

[37] C. Hyun-Shik, C. Kwang-Ho, L. Byungwhan, C. Sang-June. The methods of identification, analysis, and removal of endocrine disrupting compounds (EDCs) in water. *J. Hazard. Mat.* **2009**, 172, 1.

[38] T. Katagi. Photodegradation of pesticides on plant and soil surfaces. *Rev. Environ. Contam. Toxicol.* **2004**, 182, 1.

[39] A.D. Vallero. Environmental contaminants: assessment and control. Elsevier Academic Press. **2004**, 410.

[40] P.M. Badot, G. Crini. Traitement et épuration des eaux industrielles polluées: Procédés membranaires, bioadsorption et oxydation chimique. Presses Université Franche - Comté. **2007,** 339.

[41] Organisation for Economic Co-operation and Development. Phototransformation de produits chimiques dans l'eau – Photolyse directe. Ligne Directrice de l'OCDE pour les essais de produits chimiques. **2008**.

[42] J. Harris. Rates of Direct Aqueous Photolysis. *Handbook of Chemical Property Estimation Methods .Environmental Behavior of Organic Compounds*. McGraw-Hill Publishers, New York, U.S. **1982**.

[43] M. Theodore. Predicting photoreaction rates in surface waters. *Chemosphere*. **1999**, 38, 1379.

[44] R. Calvet, E. Barriuso, C. Bedos, P. Benoit, M.-P. Charnay, Y. Coquet. *Les pesticides dans le sol: Conséquences agronomiques et environnementales*. Edition France Agricole, France. **2005**.

[45] H.D. Burrows, M. Canle, J.A. Santaballa, S. Steenken. Reaction pathways and mechanisms of photodegradation of pesticides. *Journal of Photochemistry and Photobiology B-Biology*. **2002**, 67, 71.

[46] A. Kiss and D. Virag. Interpretation and modelling of environmental behaviour of diverse pesticides by revealing photodecomposition mechanisms. *Microchem. J.* **2009**, 92, 119.

[47] R.A. Larson, E.J. Weber. Reaction Mechanisms in Environmental Organic Chemistry. CRC Press, Boca Raton. **1994**, 181.

Chapitre II - Techniques expérimentales

Ce chapitre présente l'ensemble des matériels et méthodes utilisés dans le cadre de cette thèse ; il est divisé en quatre parties. La première présente le photoréacteur et la lampe de mercure utilisés pour les expériences de photolyse. La seconde partie décrit les étapes de préparation des échantillons. La troisième partie est consacrée aux techniques de chromatographie et de spectrométrie de masse utilisées dans cette étude. Enfin, la quatrième partie présente les tests *in silico* mis en œuvre pour estimer la toxicité des photoproduits caractérisés.

II-1. Photolyse

II-1-1. Mise en œuvre expérimentale de l'irradiation UV-visible

Les paramètres expérimentaux utilisés pour ces recherches ont été préalablement optimisés lors d'une précédente étude effectuée dans notre laboratoire dans le cadre de la thèse de Yasmine Souissi (soutenue en 2012).

II-1-1-1. Le Photoréacteur

Le réacteur utilisé (figure II-1) permet l'irradiation simultanée de six solutions. La température est régulée à 25 ± 2 °C par des ajouts réguliers d'eau glacée. La solution irradiée est homogénéisée par ultrasons. Pour chaque expérience, des essais témoins sont réalisés afin de vérifier que les ultrasons ont pour seul effet d'assurer l'homogénéisation de la solution, sans conséquence sur la dégradation du pesticide étudié.

Figure II-1 Photographie du photoréacteur utilisé

II-1-1-2. La lampe à vapeur de mercure

Dans la lampe à vapeur de mercure, une décharge électrique entre deux électrodes initie l'excitation des atomes de mercure qui émettent des radiations en retournant à leur état fondamental. Les intensités relatives des différentes raies d'émission dépendent de la pression de mercure dans la lampe. La lampe que nous utilisons est une lampe à haute pression (HPL-N 125W/542 E27 SG, Philips, 94856 Ivry sur Seine, France). La distribution spectrale de cette lampe est représentée figure II-2a. Les lampes à vapeur de mercure moyenne et haute pression fonctionnent dans des conditions de température plus élevées que celles des lampes à basse pression. Par conséquent, les atomes de mercure sont excités à différents niveaux d'énergie et émettent de nombreuses raies de forte intensité dans l'ultraviolet et le visible. Le spectre UV de la lampe utilisée a été mesuré grâce à un spectromètre à fibre optique (vaSpec-2048, Avantes) [1]. Les raies émises par la lampe polychromatique s'étendent entre 200 et 1100 nm. Les spectres d'émission de la lampe sont représentés figure II-2- (a et b).

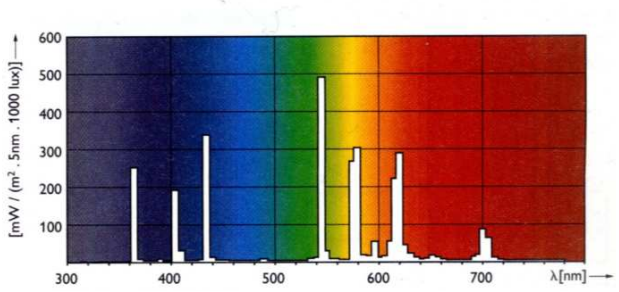

2a

2b

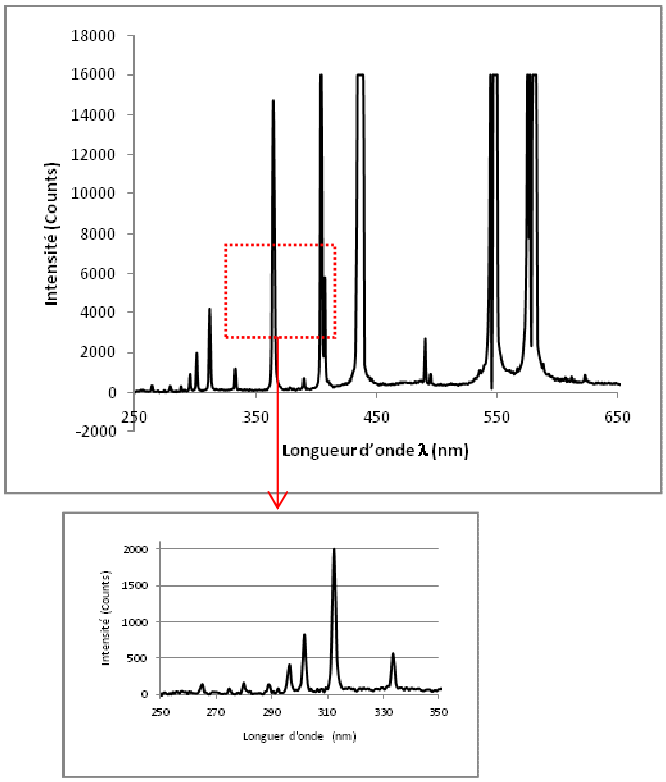

Figure II-2 : a- Distribution spectrale de la lampe HPL-N et b- Spectre UV-Visible de la lampe HPL-N mesuré par un spectrophotomètre à fibre optique.

II-2. Méthodes de préparation des échantillons

La préparation d'échantillon constitue une partie clé du protocole analytique car elle influe directement sur les quantités d'analytes collectées dans l'échantillon à analyser. Dans la mesure où nous sommes confrontés à l'analyse de composés inconnus, nous avons utilisé des méthodes d'extraction peu sélectives afin de récupérer le maximum de photoproduits. Ces méthodes présentent par ailleurs le double avantage d'être simples à mettre en œuvre et relativement rapides.

La méthode d'extraction liquide-liquide a été choisie en amont des analyses par GC-MS car elle permet d'extraire une grande variété de solutés. Elle repose sur la différence de solubilité des constituants d'un mélange entre deux phases non totalement miscibles, l'une aqueuse et l'autre organique. Dans nos études, la solution photolysée est extraite à deux reprises par le dichlorométhane (volume/volume) à l'aide d'une ampoule à décanter. La phase organique est récupérée et évaporée sous flux d'azote à 50 °C. L'extrait sec est repris par le solvant d'injection en GC-MS.

Dans le cas du Pyriméthanil, l'étape de chauffage sous flux d'azote a été supprimée, des expériences préliminaires ayant montré que les produits de photolyse étaient évaporés durant la préparation d'échantillon. Ceci nous a conduits à diminuer les volumes de dichlorométhane utilisés pour l'extraction liquide-liquide et à analyser l'extrait organique par GC-MS sans reconcentration préalable.

Au début de ces travaux de thèse, l'équipe de chimie analytique et environnementale du DCMR utilisait l'extraction sur phase solide SPE (*Solid Phase Extraction*) préalablement à l'analyse par couplage LC-MS/MS des produits de photolyse. Des cartouches Oasis HLB de marque WATERS (6 ml/200 mg, diamètre des particules : 30µm) ont été utilisées pour l'extraction des produits de photolyse de l'estrone. Des cartouches Atoll 30 ATH de marque INTERCHIM (3 ml/200 mg, diamètre des particules : X) ont été utilisées pour l'extraction des produits de photolyse des chloroanilines. Les résultats obtenus ont montré que la somme des abondances des produits de photolyse était souvent inférieure à la quantité initiale de pesticide photolysé, témoignant du fait que tous les produits n'étaient pas extraits par SPE.

Nous avons décidé en conséquence de supprimer toute étape d'extraction, de manière à être certains de collecter le maximum de photoproduits à l'issue de la réaction. Nous avons prélevé quelques microlitres de la solution photolysée auxquels nous avons ajouté quelques

microlitres de méthanol additionné de 0,1% d'acide formique avant d'analyser directement la solution *par LC-MS/MS.*

II-3. Méthodes d'analyses physico-chimiques utilisées

Les fongicides et leurs produits de dégradation sont présents à l'état de traces dans les matrices environnementales. Pour les analyser, il est nécessaire d'utiliser des méthodes de séparation et de détection à la fois spécifiques et sensibles. La séparation des pesticides est généralement réalisée par chromatographie en phase gazeuse (abrégée GC pour *Gas Chromatography*) [2, 3], ou en phase liquide (HPLC pour *High pressure Liquid Chromatography*) [4]. Parce qu'elle est sensible, sélective et spécifique, la spectrométrie de masse, simple (MS pour *Mass Spectrometry*) [5] ou en tandem (MS/MS) [6, 7], s'est aujourd'hui imposée comme principale technique de détection. Le recours au couplage GC-MS ou au couplage LC-MS dépend essentiellement de la volatilité et de la stabilité thermique des analytes considérés. La volatilité d'un composé dépend principalement de son poids moléculaire et de sa polarité : plus il est lourd et polaire et moins il est volatil. En règle générale, les composés apolaires et peu polaires sont analysés par GC-MS alors que les composés plus polaires sont analysés par LC-MS.

II-3-1. Techniques de séparation

II-3-1-1. La chromatographie en phase gazeuse

La chromatographie en phase gazeuse est une technique permettant la séparation de molécules relativement volatiles et thermiquement stables [8]. Les molécules sont évaporées dans l'injecteur où elles sont mélangées à un gaz dit "gaz vecteur" qui véhicule les analytes à l'intérieur d'une colonne capillaire dont la paroi interne est recouverte d'un film chimique nommé "phase stationnaire". Les composés migrent dans la colonne à des vitesses différentes. La vitesse de migration d'un analyte dépend de sa volatilité et des interactions qui s'exercent avec la phase stationnaire [9]. Les molécules sont ainsi séparées dans le temps : chaque molécule est caractérisée par un temps de rétention correspondant au temps écoulé entre l'injection et la détection de cette dernière. La colonne capillaire sort du chromatographe et entre dans le spectromètre de masse *via* une "ligne de transfert", il s'agit d'un cylindre chauffé à haute température (environ 300 °C) de manière à éviter la recondensation des molécules éluées avant leur arrivée au détecteur.

Dans le cadre de cette étude, les méthodes chromatographiques ont été développées sur un chromatographe "Varian 450GC" équipé d'un passeur automatique d'échantillons "Varian CP-8400". Les séparations chromatographiques ont été réalisées sur une colonne capillaire Varian "*Factor Four* VF-XMS" de phase stationnaire peu polaire (10% diphényl / 90% diméthylpolysiloxane) aux caractéristiques physiques suivantes : longueur : 60 m, diamètre interne : 0,25 mm, épaisseur de film : 0,25 µm.

II-3-1-2. La chromatographie en phase liquide (LC)

La chromatographie en phase liquide est une technique de séparation utilisée principalement pour la séparation de molécules présentant une polarité moyenne ou élevée. Les molécules sont injectées en solution dans la phase dite « mobile », phase liquide formée d'un solvant ou d'un mélange de solvants dont la polarité dépend de celles des molécules qui constituent le mélange à séparer. La colonne chromatographique est également choisie selon la nature des analytes. On distingue deux sortes de chromatographie liquide : la LC dite en "phase normale" où la phase stationnaire est polaire et la LC dite en "phase inverse" où la phase stationnaire est apolaire. Lorsque l'élution dans la colonne se fait avec un mélange dont la composition n'évolue pas au cours du temps on parle de "mode isocratique". Lorsque, au contraire, la constitution de la phase mobile varie au cours du temps, on parle de "mode gradient" : les proportions relatives de solvants de polarités différentes sont modifiées au cours de l'élution pour améliorer la qualité de la séparation chromatographique [1].

Dans cette étude, les séparations chromatographiques ont été réalisées en phase inverse sur un chromatographe en phase liquide à haute performance (HPLC) (Alliance 2690, Waters) équipé d'un injecteur automatique d'échantillons. Nous avons utilisé des colonnes de type C18 2.1 x 150 mm (Atlantis, France).

II-3-2. Techniques d'analyses

Dans le cadre de cette thèse, les méthodes de spectrométrie de masse utilisées en couplage GC-MS ont été développées sur une trappe ionique "Varian 240-MS" configurée en ionisation interne qui permet la production des ions par l'ionisation électronique (à une énergie de 70 eV) ou par l'ionisation chimique positive. Les ions formés sont analysés sur une gamme de rapports masse sur charge (m/z) allant de 10 à 650 u.m.a. Les rapports m/z sont balayés à une vitesse de 6000 m/z par seconde. Tandis que, les méthodes de LC-MS ont été

développées sur deux spectromètres de masse, tous deux munis d'une source d'électronébulisation : un triple- quadripôle (TQ) (MS 6410- Agilent Technologies) et un quadripôle associé à un temps de vol (Q-TOF Premier- Waters).

II-3-2-1. La source d'électronébulisation

L'électronébulisation (ou ESI pour "*ElectroSpray Ionization*") a été mise au point par John Bennet Fenn en 1988 et lui a valu le prix Nobel de chimie en 2002. Il s'agit d'une technique d'ionisation à pression atmosphérique qui permet de former des ions en phase gazeuse par des mécanismes de désolvatation de faible énergie induisant généralement peu de fragmentation. L'ESI est considérée comme une technique d'ionisation douce par opposition à d'autres techniques comme l'ionisation électronique.

La figure II-4a illustre le principe de l'électronébulisation. La première étape consiste en la formation de gouttelettes chargées à l'extrémité d'un capillaire métallisé porté à un potentiel électrique de plusieurs kilovolts. La polarité du potentiel appliqué (positif ou négatif) détermine la détection soit des ions positifs, soit des ions négatifs. La deuxième étape consiste en la fission des gouttelettes qui résulte de la répulsion coulombienne induite par l'évaporation du solvant. Cette évaporation est accélérée par séchage au diazote, à une température de 80 à 120 °C. La dernière étape est la désolvatation totale à l'issue de laquelle on obtient des ions désolvatés prêts à être analysés en phase gazeuse. Une photographie de nébulisat est présentée sur la figure II-4b. La source ESI utilisée pour cette étude présente une géométrie orthogonale particulièrement adaptée à l'utilisation de hauts débits en couplage LC-MS. Cette géométrie limite l'introduction de molécules neutres dans le spectromètre de masse.

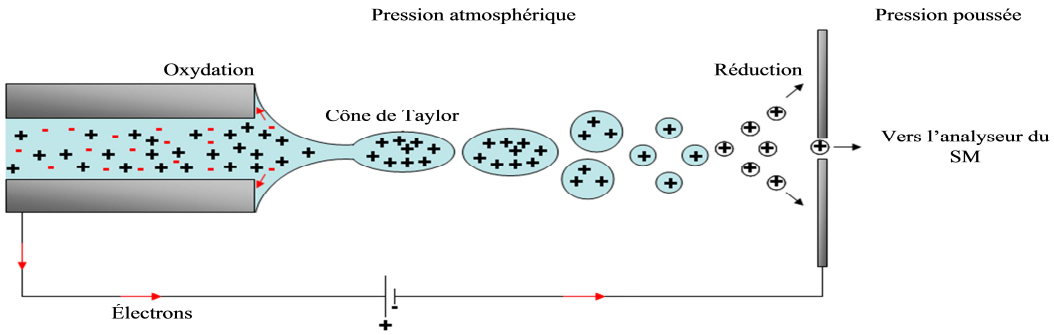

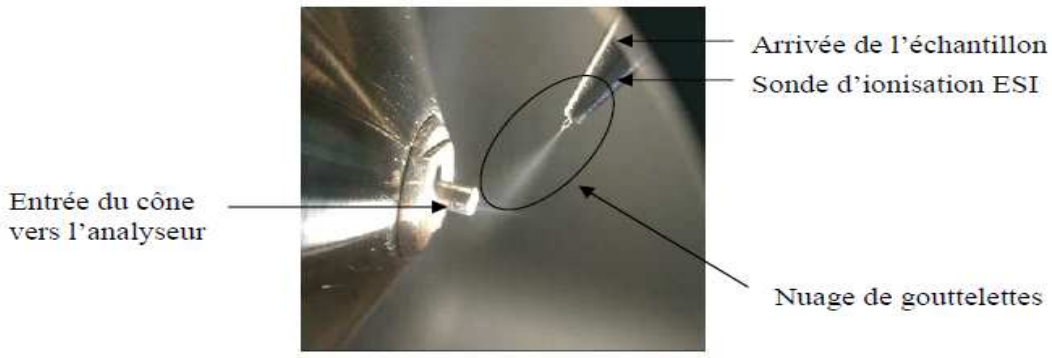

Figure II-4 Source d'électronébulisation (a) principe de fonctionnement (d'après Kebarle, 2000 [10]) (b) photographie de la source ESI

Le transfert et l'accélération des ions vers l'analyseur du spectromètre de masse sont assurés par un champ électrique.

II-3-2-2. Analyseur utilisés dans cette étude

a- Le quadripole (Q)

Comme le montre la figure II-5, un quadripôle est systématiquement associé à un système d'extraction et de focalisation des ions produits en source. Il s'agit le plus souvent d'un hexapôle ou d'une lentille électrostatique (analogue électrique d'une lentille optique). Le quadripôle est constitué de quatre électrodes métalliques parallèles raccordées électriquement deux à deux, de section idéalement hyperbolique. Ces électrodes sont cylindriques et longues de douze à vingt centimètres selon les modèles. L'application d'un potentiel de type $U+V\cos\omega t$ crée un champ quadripolaire entre les électrodes.

Deux électrodes symétriques par rapport à l'axe central du quadripôle sont portées à un potentiel de type $U+V\cos\omega t$, les deux autres au même potentiel mais de signe opposé ($-U-V\cos\omega t$). U et $V\cos\omega t$ sont, respectivement, les composantes de tension continue et de tension alternative du potentiel de radiofréquence. V et ω sont, respectivement, l'amplitude et la pulsation de la tension alternative. La valeur de ω est fixée par le constructeur. Les polarités des électrodes sont rapidement inversées, ce qui confère aux ions un mouvement "en tire-bouchon" dont l'amplitude radiale dépend des paramètres U et V. Pour qu'un ion de rapport m/z donné ait une trajectoire stable dans le quadripôle et qu'il puisse ainsi atteindre le détecteur, il faut que les paramètres U et V soient tels que l'amplitude radiale de la trajectoire de l'ion soit inférieure à la distance séparant les électrodes. Dans la pratique, le quadripôle

fonctionne comme un filtre à ions : on fait varier simultanément les valeurs de U et de V de manière à ce que les ions produits par la source soient stables à tour de rôle. A un instant t donné, ne sont détectés que les ions d'un m/z donné. Les autres ions vont heurter les électrodes ou les parois internes du spectromètre; ils se déchargent et sont entraînés par le système de pompage [11, 12, 13].

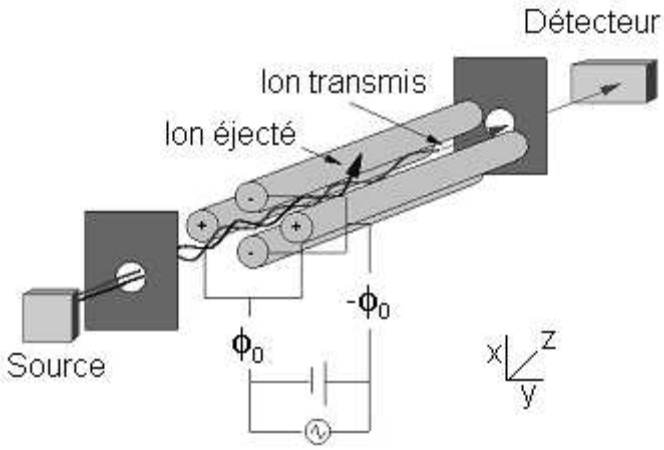

Figure II-5 Schéma d'un analyseur quadripolaire

b- La trappe ionique

La trappe ionique est constituée de 3 électrodes : une électrode annulaire au centre, une électrode d'entrée et une électrode de sortie dites "électrodes chapeaux" (figure II-3). Une radiofréquence de type $V\cos\omega t$ est appliquée sur l'électrode annulaire, V et ω étant respectivement l'amplitude et la pulsation ou fréquence angulaire de la radiofréquence. Il en résulte un champ quadripolaire au sein duquel chaque ion acquiert un mouvement oscillant dont l'amplitude et la fréquence dépendent du rapport m/z de l'ion et de la valeur de V. Des "*spacers*" en quartz en forme d'anneau jouent le rôle d'isolants électriques entre les électrodes. Les deux électrodes chapeaux sont percées en leur centre, l'une pour permettre l'introduction séquentielle d'électrons et l'autre pour permettre l'éjection des ions vers le détecteur. L'éjection des ions est assurée par l'augmentation progressive de la valeur de V, associée à l'application d'une radiofréquence $V_2\cos\omega_2 t$, dite "modulation axiale", entre les électrodes chapeaux. Le balayage de V amène les ions, tour à tour et par m/z croissant, en résonance avec la modulation axiale, ce qui a pour effet de les éjecter en direction du détecteur [9].

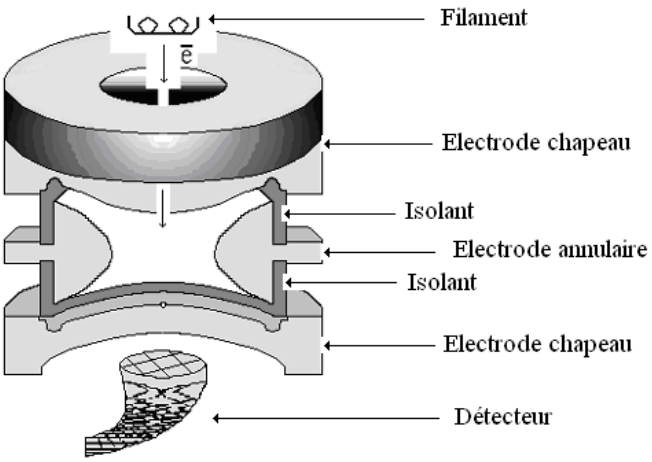

Figure II-3. Schéma d'une trappe ionique à ionisation interne

c- Temps de vol (TOF)

A leur sortie de la source, les ions sont focalisés par des lentilles électrostatiques. Ils entrent dans l'analyseur à temps de vol (TOF) (voir figure II-6). Le "*pusher*" situé à l'entrée du TOF permet d'envoyer les ions par paquets dans un tube de vol (horizontal ou vertical selon les appareils) dans une direction perpendiculaire à leur trajectoire initiale. Les ions sont accélérés par une différence de potentiel V appliquée entre deux grilles. Sous l'effet de V, chaque ion acquiert une énergie cinétique (E_{cin}) égale à zeV, ze correspondant à la charge de l'ion. Les ions parcourent ensuite le tube de vol avec la vitesse acquise lors de leur accélération. Le tube de vol est une région sous vide et libre de champ. L'énergie cinétique d'un ion est égale à $\frac{1}{2}$ mv^2 où m et v sont respectivement sa masse et sa vitesse. Les ions sont séparés selon l'équation :

$$\frac{1}{2}\, mv^2 = zeV$$

Si L est la longueur du tube de vol, la vitesse v d'un ion correspond à la longueur L divisée par le temps t mis par l'ion à parcourir celle-ci. Par conséquent, il existe entre le rapport m/z d'un ion et son temps de vol t la relation suivante:

$$m/z = 2eV/(L/t)^2$$

Il est ainsi possible d'accéder au rapport m/z d'un ion directement par la mesure de son temps de vol. En raison de turbulences dans la zone d'accélération (collisions avec des neutres, répulsion coulombienne entre les ions, etc.), des ions de même rapport m/z peuvent

acquérir des énergies cinétiques initiales sensiblement différentes ; ils auront, par conséquent, des vitesses et des temps de vol différents. Ceci se traduit par une augmentation de la dispersion des temps de vol et donc par une baisse de la résolution. Pour pallier à ce problème, les ions traversent un réflecteur électrostatique qui permet de les refocaliser en énergie cinétique et donc en temps de vol avant leur détection. Les spectromètres de masse utilisant un TOF sont généralement équipés d'un détecteur constitué de galettes de microcanaux, ce type de détecteur offrant une large surface de collection des ions [14].

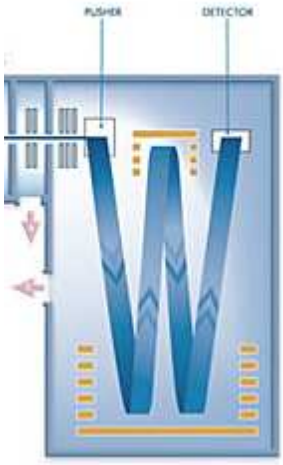

Figure II- 6 Analyseur à temps de vol.

II-3-2-3. Modes d'acquisitions utilisés dans cette étude

a- Analyses en balayage ou "fullscan"

Le mode d'acquisition *en balayage* (*fullscan*) est utilisé lorsque l'on souhaite enregistrer des spectres de source, c'est-à-dire des spectres où sont présents tous les ions produits dans la source. Travailler en balayage revient à enregistrer les ions sur une large gamme de rapports m/z. Celle-ci débute en général à 45 ou 50 Th en raison des ions résultants de l'ionisation de l'atmosphère résiduelle dans la source : m/z 18 ($H_2O^{+\cdot}$), m/z 28 ($N_2^{+\cdot}$ et $CO^{+\cdot}$), m/z 32 ($O_2^{+\cdot}$) et m/z 44 ($CO_2^{+\cdot}$) et couvrent plusieurs dizaines ou centaines de Thomson en fonction des analytes d'intérêt.

Ce mode est utilisé lorsque l'on est confronté à l'analyse d'analytes inconnus et que l'on souhaite caractériser ces derniers, mais il est très rarement utilisé en quantification. Il est le mode d'acquisition le plus spécifique mais le moins sélectif et également celui qui fournit les seuils de détection les plus élevés.

b- Analyses en tandem (MS/MS)

La MS/MS est la méthode la plus approprié pour les analyses environnementales car elle est sélective, sensible et spécifique puisqu'elle fournit généralement des spectres de masse suffisamment riches en ions pour caractériser un analyte sans ambiguïté. La MS/MS est également utilisée pour l'identification structurale de molécules inconnues. La détermination des fils, petits fils, arrière petits fils, etc d'un ion permet d'établir un « arbre généalogique des ions » [15]. La connaissance des transitions facilite grandement l'interprétation du spectre de masse.

- Mise en œuvre de la MS/MS en trappe ionique

La figure II-7 montre les trois étapes d'une séquence d'acquisition MS/MS en trappe ionique. La première étape consiste en l'isolation de l'ion précurseur. L'ionisation est réalisée à une certaine valeur de V, amplitude de la radiofréquence appliquée à l'électrode annulaire (1). Cette valeur correspond à une valeur de rapport m/z en deçà de laquelle les ions ne sont pas piégés. L'ionisation étant terminée, la valeur de V est augmentée pour éjecter de la trappe ionique les ions de m/z inférieurs au rapport m/z de l'ion précurseur (x). Le balayage de V est ralenti lorsque l'on approche de la valeur correspondant à m/z = x, de manière à ce que l'isolation des ions précurseurs soit précise (2). L'éjection des ions de rapports m/z supérieurs à x résulte de l'application entre les électrodes chapeaux d'une combinaison de fréquences faisant entrer tous ces ions en résonance (3). La phase d'isolation des ions précurseurs étant achevée, l'amplitude V de la radiofréquence de piégeage des ions est ramenée à une valeur correspondant à m/z = x', de manière à ce que soient piégés dans la trappe ionique, durant la phase d'activation pas collisions, tous les ions de rapports m/z supérieurs à x' (4). Un balayage de l'amplitude de la radiofréquence permet la détection des ions formés par CID (*Collision Induced Dissociation*) (5).

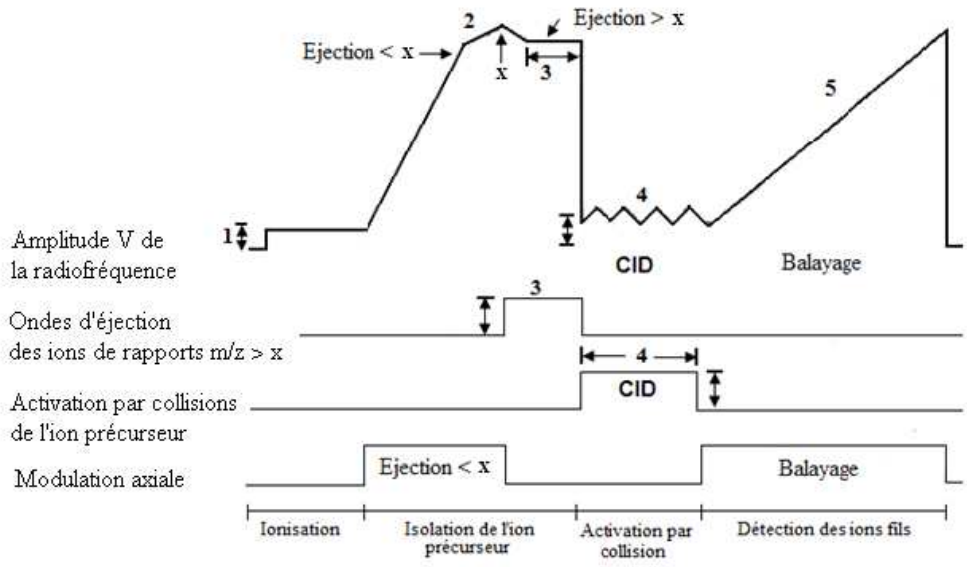

Figure II-7. Séquence de MS/MS en trappe ionique

- Mise en œuvre de la MS/MS avec un TQ ou un Q-TOF

Dans les instruments de type TQ (figure II-8) et Q-TOF (figure II-9), plusieurs modes d'acquisition peuvent être utilisés en MS/MS. Le premier est la détermination des fils d'un ion : l'ion d'intérêt est sélectionné dans le premier quadripôle (Q1). L'ion est accéléré à une énergie cinétique comprise entre 0 et 300 eV et activé par collision avec un gaz inerte dans le deuxième quadripôle (Q2). Les ions fragments résultants sont analysés à l'aide d'un troisième analyseur (Q3 ou TOF) en balayage. Le deuxième est la recherche des précurseurs d'un ion : le premier quadripôle est en balayage et le troisième analyseur en SIM ("*selected ion monitoring*) sur l'ion dont on cherche les ions précurseurs. Le troisième mode est le balayage en perte de neutre : les analyseurs Q1 et Q3 (ou Q1 et TOF) sont en balayage avec un écart de m/z correspondant à la perte de neutre recherchée.

Les trois modes d'acquisition en MS/MS cités ci-dessus, sont communs au TQ et au Q-TOF. Le mode *Multiple Reaction Monitoring* (MRM) est spécifique du TQ. Il est utilisé pour des analyses quantitatives, les trois modes précédents étant peu adaptés à la quantification car peu sensibles en raison des phases de balayage. En MRM, les quadripôles Q1 et Q3 sont en mode SIM ; l'absence de balayage permet d'atteindre des seuils de détection compatibles avec l'analyse de traces.

Avec le temps de vol, le mode de haute résolution permet d'atteindre une précision en masse de quatre chiffres après la virgule. Il permet de distinguer des ions dits "isobares", c'est

à dire des ions qui possèdent le même rapport m/z nominal alors que leurs formules chimiques différents.

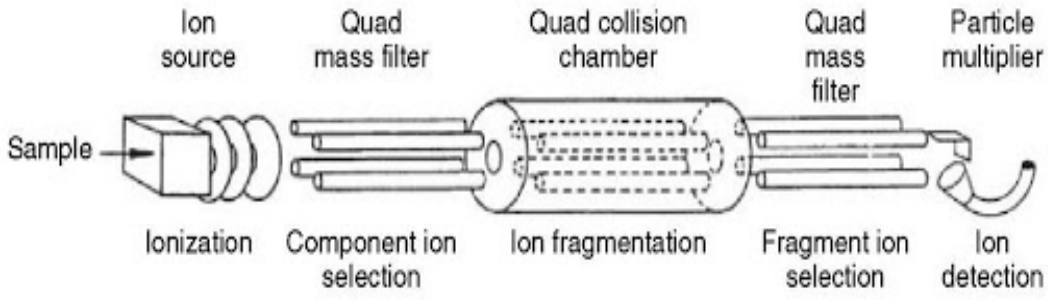

Figure II-8. Schéma d'un spectromètre à triple quadripôle (TQ)

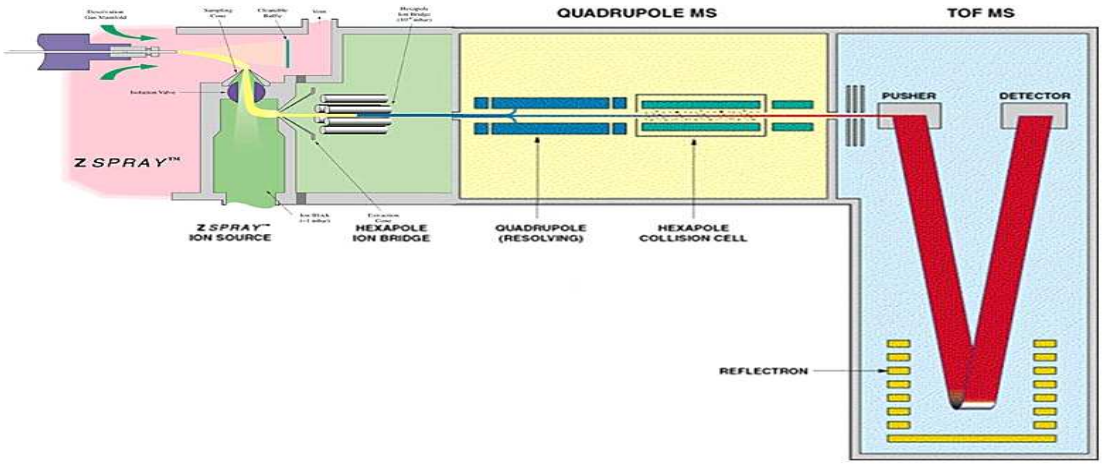

Figure II-9. Schéma d'un spectromètre de masse tandem quadripôle-temps de vol (Q-TOF)

II-4. Tests de prédiction toxicologique *in silico*

II-4-1. Principe

La recherche de méthodes alternatives à l'expérimentation animale est aujourd'hui une nécessité pour obtenir des résultats rapides et fiables quant aux propriétés toxiques et écotoxiques des substances chimiques. Ces méthodes sont également nécessaires pour répondre aux préoccupations sociétales relatives à une démarche éthique en expérimentation animale. La règlementation REACH et les directives sur la protection des animaux (76/768/CEE, 86/609/CEE, 2010/63/UE) préconisent la diminution de l'utilisation d'animaux pour les tests de bio-toxicité et d'écotoxicité. Les méthodes alternatives utilisées doivent répondre à un ou plusieurs principes des "3R" :

- ***Remplacement***: dans cette catégorie, on trouve les méthodes qui remplacent l'animal, soit de manière absolue (aucune utilisation d'animaux) soit de manière relative (utilisation de tissus ou de cellules animales).

- ***Réduction:*** quand le remplacement n'est pas possible, ou du moins pas encore, les scientifiques essaient de trouver des moyens pour réduire le nombre d'animaux utilisés. Il s'agit en fait d'optimiser les résultats obtenus au moyen de statistiques.

- ***Raffinement :*** cette voie vise en quelque sorte à améliorer la vie des animaux de laboratoire. On cherche autant que possible à diminuer ou éliminer la douleur et le stress infligés. On peut également recourir à des organismes dits « inférieurs » (plantes, microorganismes, invertébrés).

La modélisation bio-informatique dite "*in silico*" supprime totalement l'utilisation des animaux. Elle contribue à l'évolution rapide de nouveaux tests de toxicité où l'information structurale est compil de grandes bases de donnés chimiques dans le but de classifier ou élaborer des modèles prédictifs [15, 16].

Dans cette étude, la toxicité des pesticides étudiés et de leurs produits de dégradation a été estimée par le logiciel T.E.S.T. ("*Toxicity Estimation Software Tool*"). Il s'agit d'un logiciel développé par l'Agence de Protection Environnementale des États Unis et librement accessible sur internet [43]. Les utilisateurs peuvent dessiner la structure du produit chimique d'intérêt ou l'importer à partir d'une base de données. La toxicité est estimée par plusieurs méthodes dites « QSAR » (*Quantitative Structure Activity Relationship*). Le QSAR est un modèle mathématique utilisé pour prédire différents types de toxicité de produits chimiques à partir de leurs caractéristiques physiques et de leur structure (poids moléculaire, nombre des cycles dans la structure, etc.) appelés descripteurs moléculaires. Les modèles QSAR simples permettent d'estimer la toxicité de produits chimiques en utilisant une simple fonction linéaire de descripteurs moléculaires [17]:

$$Toxicité = ax_1 + bx_2 + c$$

où x_1 et x_2 sont les variables de descripteurs indépendants et a, b et c sont des paramètres ajustés. Le poids moléculaire et le coefficient de partage octanol-eau sont des exemples de descripteurs moléculaires. Lorsque les conditions ne permettent pas de bio-essais

traditionnels, les tests QSAR constituent une alternative aux essais biologiques. Les résultats obtenus doivent être impérativement comparés à des données expérimentales de la littérature.

II-4-2. Les différents types de tests de toxicité prédictive

Le tableau II-3 répertorie les différents tests de toxicité prédictive réalisables avec le logiciel T.E.S.T. Les principes des différents tests y sont brièvement discutés.

Tableau II-3. Listes des tests réalisables avec le logiciel T.E.S.T.

Test	**Réglem-entation**	**Principe du test**	**Réfé-rences**
Fathead minnow (tête de boule) LC50	SPE 1/ RM/ 22 2ème éd.	Estimation de la dose décimant 50% d'une population de tête-de-boule	[18, 19, 20, 21]
Daphnia magna (daphnie de Magna) LC50	ISO 6341	Estimation de la dose décimant 50% d'une population de daphnies, ainsi que des effets sur la reproduction et la mobilité	[22, 23, 24]
Tetrahymena pyriformis IGC50		Estimation de la dose inhibant la croissance de 50% d'une population de *Tetrahymena pyriformis*.	[25]
Oral rat LD50		Estimation de la dose décimant 50% d'une population de rat ou souris, des effets sur les changements de poids corporel, sur la consommation alimentaire	[26, 27]
Developmental toxicity (toxicité sur le plan du développement)		Estimation des effets sur le développement de l'embryon pendant la grossesse : mort de l'organisme, anomalies structurelles, altération de la croissance et déficiences fonctionnelles.	[28]
Mutagenicity (Mutagénicité)	REACH	Estimation de la mutagénicité cellulaire	[29]

II-5. Réferences

[1] R.R. Chowdhury, P. Charpentier, M.B. Ray. Photodegradation of Estrone in Solar Irradiation. *Ind. Eng. Chem. Res.* **2010**, 49, 6923.

[2] S.M. Martan, L.E. Silvia, I.T. Montti. Method development and validation for boscalid in blueberries by solid-phase microextraction gas chromatography, and their degradation kinetics. *Food Chem.* **2013,** 136, 1399.

[3] E. Pose-Juan, B. Cancho-Grande, R. Rial-Otero, J. Simal-Gandara. The dissipation rates of cyprodinil, fludioxonil, procymidone and vinclozoline during storage of grape juice. *Food Control.* **2006**, 17, 1012.

[4] W. Lohmann, R. Datzer, G. Gatter, M.V. Leeuwen Suze, U. Karst. On-Line Electrochemistry/Liquid Chromatography/Mass Spectrometry for the Simulation of Pesticide Metabolism. *J. Am. Soc. Mass Spectrom*. **2009**, 20, 138.

[5] Y. Li, M.R. Kim, L.K. Bong, S. Kim In, H. Shim Jae. Determination of procymidone residues in ginseng by GC-ECD and GC-MS equipped with a solvent-free solid injector. *Food Control*. 2007, 18, 364.

[6] S.K. Cho, A.M. Abd El-Aty, H.P. Ki, J.H. Park, M. E. Assayed, Y.M. Jeong, Y.S. Park, J.H. Shim. Simple multiresidue extraction method for the determination of fungicides and plant growth regulator in bean sprouts using low temperature partitioning and tandem mass spectrometry. *Food Chem.* **2013**, 136, 1414.

[7] T. Rodri-guez-Cabo, I. Rodri-guez, M. Ramil and R. Cela. Dispersive liquid-liquid microextraction using non-chlorinated, lighter than water solvents for gas chromatography-mass spectrometry determination of fungicides in wine. *J. Chromatogr. A.* **2011**, 1218, 6603.

[8] D. Libong, S. Bouchonnet. Le couplage chromatographie en phase gazeuse-spectrométrie de masse. *Recherche et développement.* **2005**, 7.

[9] S. Bouchonnet. *Interprétation des spectres de masse en couplage GC-MS*, Lavoisier, France, **2012**.

[10] P. Kebarle, M. Peschke. On the mechanisms by which the charged droplets produced by electrospray lead to gas phase ions. *Anal. Chim. Acta.* **2000**, 406, 11.

[11] P.H. Dawson. *Quadrupole Mass Spectrometry and its Application*. **1977**, 81.

[12] E. Schenell. A. Constantin. *Mass Spectrometry.* Ellis Horwood Series in Analytical Chemistry, Ellis Horwood Limited, London. **1990**, 184.

[13] S. Bouchonnet, D. Libong. Le couplage chromatographie en phase gazeuse-spectrométrie de masse. *http://www.dcmr.polytechnique. fr/moyens /cou plage.pdf*.

[14] E.W. Schlag. *Time of Flight Mass Spectrometry and its Applications*, Ed. Elsevier, France. **1994**.

[15] H. J. Scott, C.E. Cowan-Ellsberry, T. Gareth. Use of quantitative structural analysis to predict fish bloconcentration factors for pesticides. *Agric. Food Chem.* **2009**, 57, 958.

[16] E. Zvinavashe, J.M. Albertinka, M. Rietjens, C.M. Ivonne. On the number of EINECS compounds that can be covered by (Q)SAR models for acute toxicity. *Toxicology Letter*. **2009**, 184, 67.

[17] U.S. Environmental Protection Agency (www.epa.gov/nrmrl/std/qsar/qsar.html). *User's Guide for T.E.S.T. (version 4.1) (Toxicity Estimation Software Tool)*. **2012**.

[18] S. Beggel, I. Werner, R. E. Connon and J. P. Geist. Impacts of the phenylpyrazole insecticide fipronil on larval fish: Time-series gene transcription responses in fathead minnow (Pimephales promelas) following short-term exposure. Sci. Total Envi**. 2012**, 426, 160.

[19] Canada Environnement. Méthode d'essai biologique: essai de croissance et de survie des larves de tet-de-boule. **2011**.

[20] J. Crago, R. Klaper. A mixture of an environmentally realistic concentration of a phthalate and herbicide reduces testosterone in male fathead minnow (Pimephales promelas) through a novel mechanism of action. *Aquat. Toxicol.* **2012**, 74, 110.

[21] L.T. Yonkos, D.J. Fisher, R. Reimschuessel. Atlas of feathed minnow normal histology. *An online publication of the University of Maryland Aquatic Pathobiology Center (http://aquaticpath.umd.edu/ fhm).* **2000**.

[22] S. Grimme, J. Antony, S. Ehrlich, H. Krieg. A consistent and accurate *ab initio* parametrization of density functional dispersion correction (DFT-D) for the 94 elements H-Pu. *J. Chem. Phys*. **2010**, 132.

[23] Institute Austrian Standards. ISO 6341- Water quality-Determination of the inhibition of the mobility of daphnia magna Straus (Cladocera, Crustacea) - Acute toxicity test. **2010**.

[24] S. Santiago, K.B. van Slooten, N. Bennibghoff, M. Dumas. Guide pour l'utilisation des tests ecotoxicologiques. Institue forel - Ecole polytechnique fédèrale de laussane. **2002**.

[25] F. Quiniou, G. Cueff, X. Caisey. Etude de la toxicité des eaux et des sédiments de la Seine. **2003.**

[26] C. Clavaguera, F. Piuzzi, J.-P. Dognon. Electronic spectrum of tryptophan-phenylalanine. A correlated *Ab Initio* and time-dependent density functional theory study. *J. Phys. Chem. B.* **2009**, 113, 16443.

[27] European Union. 3600/92/EU. *Official Journal of the European Union*. **1992**, 4.

[28] Economique Organisation Cooperation Developpement. Ligne directrice de l'OCDE pour les éssais de produits chimiques - Etude de la toxicité pour le développement prénatal. **2001**.

[29] REACH. Enregistrement, évaluation, autorisation et restriction des produits chimiques. *http://ec.europa.eu/enterprise/sectors/chemicals/reach/index_fr.htm.* **2007**.

Chapitre III. Photo-transformation du métolachlore

III-1. Introduction

Lors de mon arrivée au laboratoire DCMR, les études de l'équipe « Chimie analytique et environnementale » étaient principalement consacrées à la photolyse et à l'ozonolyse de pesticides de la famille des chloroacétamides comme l'alachlore et l'acétochlore (thèse de Yasmine Souissi). J'ai ainsi débuté mes travux de recherche par l'étude de la photodégradation du métolachlore. Cette première étude m'a permis d'assimiler la stratégie analytique utilisée au DCMR pour caractériser les structures de photoproduits.

Avec une grande solubilité dans l'eau (500 mg/L), le métolachlore est utilisé pour lutter contre les mauvaises herbes comme les graminées annuelles et certaines dicotylédones dans les cultures de maïs, de soja, de pommes de terre, de haricots, de sorgho, de betteraves à sucre et de rutabagas. Il s'agit d'un herbicide sélectif qui inhibe la germination et est absorbé par les hypocotyles et les pousses des plantes.

La Directive 2000/60/EC de l'Union Européenne répertorie le métolachlore parmi les trente-trois polluants à surveiller prioritairement dans les eaux européennes. Depuis 2011, ce pesticide est classé comme perturbateur endocrinien. Il influe sur plusieurs étapes de l'homoéostasie de l'axe hypothalamo-hypophyso-thyroïdien (HPT) et perturbe le système thyoridien chez le médaka (poisson de la famille des Adrianichthyidae). Il présente des effets toxiques sur le développement des animaux avant et après la naissance et exerce des effets cytotoxiques et génotoxiques dans les lymphocytes humains ainsi que des dommages chromosomiques. En conséquence, la directive 600/2010/EU de l'Union Européenne a fixé à 0,05 mg/kg la limite maximale résiduelle (LMR) du métolachlore dans les cultures.

L'étude de la photolyse du métolachlore par irradiation UV-visible présente un intérêt certain, d'une part pour caractériser les photoproduits susceptibles de se former dans l'environnement sous l'influence du rayonnement solaire, d'autre part pour établir si la photochimie peut constituer un traitement de choix pour dépolluer l'eau contaminée par des herbicides de type chloroacétamide. Un tel traitement ne conduit jamais la minéralisation complète des polluants ;des sous-produits sont libérés en quantités significatives dans l'eau après photolyse. Il est d'ailleurs plus pertinent de parler de « phototransformation ». Il est donc important d'établir les structures chimiques et toxicités potentielles des photoproduits formés avant d'envisager un traitement par photochimie.

Dans notre étude, des solutions de métolachlore ont été préparées à une concentration de 50 mg/L pour les expériences d'identification structurale. Les solutions utilisées pour les études cinétiques ont été préparées à une concentration de 2 mg/L. Le réacteur utilisé dans les expériences de photodégradation est décrit au chapitre 2. L'extraction liquide-liquide a été utilisée pour les solutions analysées par couplage GC-MS. L'extraction sur phase solide (SPE) a été utilisée pour les solutions analysées par couplage LC-MS, . Pour s'assurer des structures proposées la dégradation du produit marqué, avec 6 deutériums à la place de 6 hydrogènes dans la molécule du métolachlore, est étudiée dans les mêmes conditions expérimentales (figure 1 de l'article 1). Cette étude de dégradation permet de préciser la partie de la molécule affectée par l'irradiation ce qui facilite l'identification structurale des sous produits.

La polarité des sous produits peut varier du très polaire au non polaire. Pour couvrir la gamme de polarité, deux techniques de séparations ont été utilisés : GC/MS et LC/MS. La séparation sur la GC est favorable pour les molécules non polaires, tandis que sur la LC, la séparation est favorable pour des molécules qui possèdent une polarité moyenne ou élevée. Les deux appareils sont couplés à la spectrométrie de masse comme détecteur. Le GC est couplé à un spectromètre de masse trappe ionique muni d'une source capable de passer facilement de l'ionisation électronique à l'ionisation chimique. Cette trappe ionique est utilisée en mode MS^n qui permet l'identification des parents des ions fragments d'une manière continue. La LC est couplé à un spectromètre de masse tandem quadripôle – temps de vol (Q-TOF) muni d'une source electrospray (ESI). Le TOF est utilisé en haute résolution mode W en proposant des formules brutes pour les masses exactes.

Pour établir l'ordre de formation des produits de dégradation du métolachlore et leur rémanence dans la solution, une étude cinétique est faite en GC/MS (en mode d'ionisation chimique CI et en mode d'analyse scan de m/z 50 vers m/z 290). Cette étude est divisée en deux parties : la première sert à évaluer la formation et la disparition des produits en fonction du temps d'irradiation et la deuxième permet de savoir si la réaction de dégradation continu son évolution après l'arrêt de la lampe. Pour cela, nous avons irradié 1 litre de solution de métolachlore durant 30 minutes en prélevant 70 ml à des temps précis. Puis, chaque prélèvement est divisé en 7 tubes de 10 ml et les solutions restes à température ambiante et à l'abri de la lumière pendant 32 heures. L'analyse de solutions irradiées qui viennent du premier prélèvement répond à la première partie et l'analyse de chaque solution des tubes à différent temps répond à deuxième partie. Le Benzophenone est ajouté à chaque solution avant l'analyse comme étant un étalon interne.

Les toxicités des sous produits détectés en GC/MS et en LC/MS ont été estimées à l'aide du programme de calcul de toxicité *in silico* T.E.S.T. (voire chapitre 2).

III-2. Characterization of the photodegradation products of metolachlor: structural elucidation, potential toxicity and persistence

Sarah Coffinet, Ahmad Rifai, Christophe Genty, Yasmine Souissi, Sophie Bourcier, Michel Sablier and Stéphane Bouchonnet

J. Mass Spectrom. 2012, **47**, 1582–1593

Aqueous solutions of metolachlor and metolachlor-d_6 were photolyzed with UV-visible radiations. The structures of 15 by-products of metolachlor were determined through gas chromatography-mass spectrometry analyses using electron and chemical ionization combined with multistage mass spectrometry. The photolysis by-products of metolachlor resulted mainly from dehalogenation and hydroxylation, in some cases accompanied by cyclization. In silico tests for toxicity prediction showed that the toxicity of some photolysis products is expected to be greater than that of metolachlor. Persistence studies showed that the by-product relative abundances vary in large amounts with the irradiation time. The post-photolysis evolution of the solution was also studied, in order to determine the persistence of the main by-products. It allowed to establish that most of the by-products can be found more than 12h after the end of the photolysis, which is of a great concern as treated water is generally available for consumption only a few hours after treatment in most of industrial processes.

Keywords: water treatment; metolachlor; photodegradation; by-products; toxicity; persistence

Introduction

Among the European countries, France is the first consumer of pesticides: more than 76.100 tons of active species were sold there in 2004.[1] This situation is becoming of a great concern as these pesticides are very frequently detected in large amounts in soil and freshwater.[2,3] Indeed, a study from the French water agency found traces of pesticides in 91% of collecting stations in 2007.[4] In the meantime, every year, more and more publications are issued pointing out the potential risks of these substances on the environment,

the biodiversity and the human health.[5,6] As a consequence of this awareness raising, the processes currently used to treat water are put into questions, and new processes are in constant development.[7,8] Photolysis is more and more investigated as a means to remove micropollutants.[9] UV photolysis is already commonly used as an alternative of disinfection with chlorine. In 2004, PWN, national water supplier of the Netherlands, conjointly to the company Trojan UV, opened a pilot plant in Andijk (Netherlands) using photolysis for disinfection as well as for micro-pollutant decontamination.[10,11] In this plant, photolysis is not used as a replacement of conventional techniques such as ozonation but rather as an additional technique based upon the idea that multiplying the ways of degradation would target a larger range of pollutants. This study focuses on the photolysis by-products of a widely used herbicide, metolachlor. This pesticide, from the chloroacetanilide family also including alachlor and acetochlor, is mainly used to treat corn and was classified by the European Union as one of the 33 priority pollutants in the European Water Framework Directive 2000/60/EC.[12] Of priority concern is the high solubility of metolachlor in water ($530 mg l^{-1}$ at 20 °C) and thus its likely presence in natural waters, as pointed out by Rivard.[13] Hence, its removal by innovative techniques such as UV photolysis is of a particular importance. However, as noticed by Sanchez *et al.*, such a treatment does not necessarily result on the complete mineralization of the pollutants and by-products are usually released in significant amounts in the water after photodegradation.[14] It is thus particularly important to establish their chemical structures and their potential toxicity before generalizing the use of these new plants. In 2007, Wu *et al.* reported a study devoted to photodegradation of metolachlor applying UV and UV/H_2O_2. Their researches, mainly devoted to kinetics measurements, led to suggest chemical structures for six photoproducts among the 14 detected by gas chromatography coupled with mass spectrometry.[15] The present work is devoted to the structural elucidation of 15 photodegradation products of metolachlor and the evaluation of their toxicity. Kinetic studies on irradiation time as well as on post-photolysis evolution were carried out to better understand the way byproducts are formed and their potential persistence in water.

Materials and methods

Chemicals Metolachlor and methylene chloride - chromatographic grade - were purchased from Sigma-Aldrich (St Quentin Fallavier, France), while metolachlor-d_6 was

purchased from Cluzeau Info Labo (Ste- Foy-la-Grande, France). Chemical structures of metolachlor and metolachlor-d_6 are displayed in Fig. 1. Stock aqueous solutions of metolachlor were prepared by dissolving metolachlor in deionized water. Structural investigations were carried out with a solution at 50mg.l^{-1} while a solution at 2mg.l^{-1} was used for the kinetic measurements. Additional experiments were performed irradiating a solution at 50mgl^{-1} of metolachlor in a real water matrix: water collected from the Ecole Polytechnique lake at Palaiseau – France. Benzophenone (internal standard for the kinetic experiments) and high purity methanol (> 99.99) for chemical ionization (CI) were purchased from Fluka Chemie AG (Buchs, Switzerland).

Photolysis experiments

Photolysis was performed in a self-made reactor consisting in six 120 ml quartz tubes immerged into a sonicator (AL04-12, Advantage-Lab, Switzerland). UV irradiation was delivered by a high-pressure mercury lamp (HPL-N 125 W/542 E27 SG; Philips, Ivry-sur-Seine, France). Radiation was produced at wavelengths ranging from 200 nm to 650 nm. Metolachlor presents a significant absorbance in the 240–280 nm range.[9] According to manufacturer data, the incident radiation flux was 6200 lm. The photoreactor was filled with deionized water and regularly cooled by ice addition to maintain the temperature at 20±4 °C.

Sample preparation

Liquid-liquid extractions were carried out using a separating funnel. Each sample was extracted twice with 20 ml of methylene chloride. The organic phase was dried under a gentle nitrogen stream, and the dry residue was solubilized in 100 ml of methylene chloride containing benzophenone at 1 µg.ml^{-1} to serve as an internal standard for gas chromatography-mass spectrometry (GC-MS) analysis. Five aqueous solutions at 50mg.l^{-1} of metolachlor were extracted as previously described. Metolachlor-d_6 was added into each tube after extraction, at the same concentration. Extraction recoveries were evaluated comparing the chromatographic peaks integrations of metolachlor and metolachlor-d_6 on the MH^+ ionic currents. The recovery yield was estimated at 92% (CV=9% for n=5).

Gas chromatography and mass spectrometry operating conditions

Analyses were carried out on a VARIAN 450GC gas chromatograph equipped with a CP 8400 autosampler and coupled with a VARIAN 240MS ion-trap mass spectrometer

switched into the internal mode. Separation was performed on a 60-m-long 'VF-Xms' capillary column (VARIAN) with an internal diameter of 0.25 mm and a film thickness of 0.25 mm. All experiments were performed automatically injecting 1.0 ml of sample in the splitless mode at a rate of 50 ml s^{-1}. The injector temperature was set at 280 ºC, and high purity (99.999 %) helium was used as carrier gas at a constant flow of 1.4 ml min_1. Oven was programmed as follows: 50 ºC held during 30 s, up to 150 ºC at a rate of 15 ºC min^{-1}, up to 180 ºC at a rate of 6 ºC min^{-1}, up to 230 ºC at a rate of 3 ºC min^{-1} and finally up to 300 ºC at a rate of 20ºC min^{-1}. The total analysis duration was 33 min. The mass spectrometer was calibrated with the ions resulting from electron ionization (EI) of perfluorotributylamine. The manifold, the ion-trap electrodes and the transfer line temperatures were respectively held at 100 ºC, 200 ºC and 280 ºC. Positive CI was performed using methanol as reagent. Spectra were recorded using the automatic gain control function with target values fixed at 20.000 and 5.000 for EI and CI, respectively. The filament emission current was set at 10 mA in EI and 50 mA in CI. The electron multiplier voltage was automatically optimized at 2200 V. Full scan spectra were acquired recording ions from m/z 50 to m/z 500 at a frequency of 3 spectra/s. During multiple stage mass spectrometry experiments, precursor ions were isolated with a 1 m/z window, stored with a Paul stability parameter (qz) of 0.30 and fragmented by collision-induced dissociation (CID) during 20 ms with helium playing the role of target gas. Activation energies ranging from 0.45 V to 0.60 V were used in the resonant excitation mode.

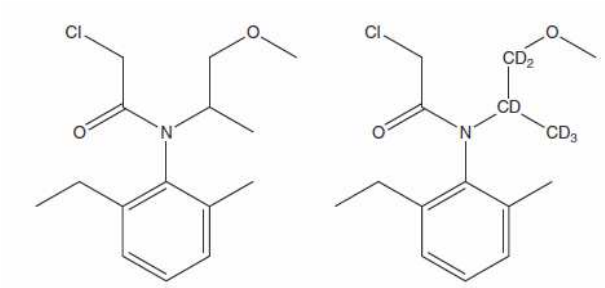

Figure 1. Chemical structures of metolachlor (left hand) and metolachlor-d_6 (right hand).

Results and discussion

Characterization of degradation products of metolachlor

The chromatogram of a solution of metolachlor irradiated for thirty minutes is displayed in Fig. 2; peaks labeled with an 'X' correspond to impurities present in the reference solution of metolachlor. The comparison with the results obtained irradiating an aqueous solution of metolachlor-d_6 almost pure (99.9%) permitted to discard by-products issued from impurities and not from metolachlor itself. Given the complexity of the chromatogram of the photolyzed solution, only compounds providing a peak with a signal to noise ratio greater than 10 were investigated. A total of 15 compounds were identified as photodegradation products. They are numbered as a function of their retention time and listed in Table 1. Two products, 4 and 5, were taken into consideration although they were already present in the non photolyzed solution because of a noticeable increase of their relative abundance after photolysis. The use of CI with methanol as reagent gas permitted to determine the molecular weights of all compounds of interest (see Table 1) as this technique provides abundant MH^+ ions. It is to be noted that the absence of characteristic isotopomer MH^+ ions indicates that the chlorine atom of metolachlor was eliminated during the photolysis process in all cases. Elimination of the chlorine atom during mass spectrometry analysis rather than photolysis experiments was taken into consideration, but this hypothesis was finally discarded according to the following reasons. First, if the loss of HCl following protonation of a chlorinated molecule is a well-established mechanism in CI, it rather occurs with reagents with low proton affinity such as methane. To our knowledge, loss of HCl using methanol as reagent gas has never been reported. Furthermore, if such a mechanism should occur here, it would be certainly observed with protonated metolachlor. We previously studied the CI of metolachlor using different reagents under various conditions of temperature and pressure and never observed HCl loss from MH^+ ions.[17]

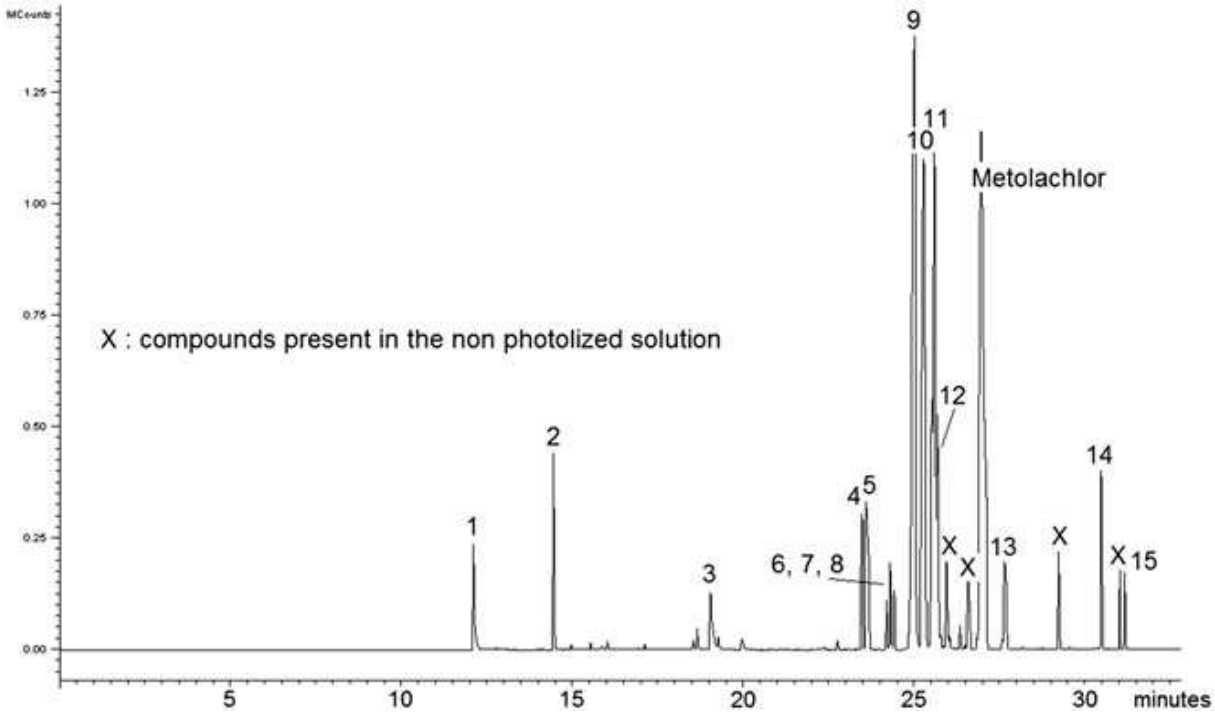

Figure 2. Chromatogram of an aqueous solution of metolachlor irradiated for 30 min.

None of the compounds could be identified based on the NIST nor WILEY EI mass spectra data base so that their structures had to be elucidated by mass spectrometry investigations.[18,19] The ion-trap mass analyzer allowed to carry out multi stage mass spectrometry on MH^+ ions of photolysis products from both metolachlor and deuterated metolachlor. Data collected are given in Table 1; they were used to establish the structures displayed. According to previous experiments and literature data, we postulated that C–C bonds constituting the skeleton of the aromatic ring and its alkyl chains do not break during photolysis.[20]

The m/z ratios of MH^+ ions of compounds 1 and 3 (133 and 177 Th corresponding to molecular weights of 132 and 176, respectively) are not shifted when comparing the corresponding mass spectra of the photolyzed solutions of metolachlor and metolachlor-d_6. It indicates that the $–(CH_3)CH–CH_2–$ chain was lost during the formation of these compounds. Moreover, according to the nitrogen rule, the even molecular weights of 1 and 3 (132 and 176 a.m.u., respectively) show that the nitrogen atom of metolachlor was lost during the formation of both compounds. The chemical structure of 1 was proposed on the basis of a chemical formula of C_9H_8O, also considering the short elution time of 1 (indicating a low polarity). Product 1 could result from hydroxylation of the ethyl group (see below) followed by a nucleophilic attack of the oxygen atom onto the aromatic ring. The loss of 28 a.m.u. from m/z

133 (MH^+ ion) in CID experiments can be rationalized by the mechanism 3-1 in Fig. 3 providing a stable carbocation at m/z 105.

In MS/MS, the pseudo-molecular ion of 3 losses 18 a.m.u. (H_2O), which, combined with the tailing shape of the corresponding chromatographic peak, indicates a quite polar structure likely including at least two oxygen atoms. The structure proposed is reported in Table 1; the corresponding dissociation pathways leading to ions at m/z 159 and m/z 131 are displayed in Fig. 3 (mechanism 3-2). A lactone structure has been first considered for 3, but its formation from metolachlor through a photolysis process was much harder to rationalize than for the structure retained (see below).

At the exception of 1 and 3, all the photolysis products of deuterated metolachlor provided mass spectra in which MH^+ ions are shifted by 6 a.m.u. comparing with those of the unlabelled molecules. This led to the conclusion that the N-(CH_3)$CHCH_2$-O chain (see Fig. 1) was not affected by the photolysis process for these compounds. In CID experiments, the pseudo molecular ions of 12 among the 15 by-products (all except 1, 3 and 14) first underwent an abundant loss of 32 a.m.u. corresponding to CH_3OH elimination after direct protonation of the ether functionality, as depicted on mechanism 3-3 (Fig. 3) in the case of 2. As the oxygen atom is not the most basic site of the molecule, initial protonation on the nitrogen atom followed by proton transfer from the protonated amino group onto the oxygen atom of the ether functionality through a five center transition state can also be considered. Methanol elimination allows to establish that the ether functionality was not affected by photolysis.

Compound 2 provided an abundant pseudo-molecular MH^+ ion at m/z 206. Formation of 2 from metolachlor thus involved a loss of 78 a.m.u.; it was assumed to result from the removal of the Cl–CH_2–C(O) chain followed by cyclization with the ethyl group. The analysis of the main dissociation pathways (mechanism 3-3) confirmed this hypothesis, and the structure in Table 1 was finally proposed. The transitions observed when performing MS^3 on the MH^+ ion of the deuterated analogous of 2 (m/z 212→m/z 180→m/z 132 and m/z 212→m/z 180→m/z 152) are in good agreement with the fragmentation mechanisms.

Table 1. Molecular weight, retention time, relative abundance, chemical structure and main MS^n transitions recorded in GC-MS with CI ionization mode for photolysis products of metolachlor

	Molecular weight	Retention time (min)	Relative abundance[a]	Shift for metolachlor-d_6	Main transitions in CI-MS^n (m/z)	Chemical structure proposed
1	132	12.15	2.8	0	133 → 105 (−28) 105 → 103 (−2)	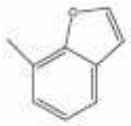
2	205	14.47	3.4	6	206 → 174 (−32) 174 → 146 (−28) 174 → 132 (−42)	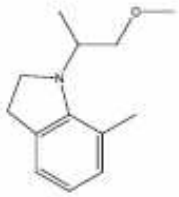
3	176	19.06	1.8	0	177 → 159 (−18) 159 → 131 (−28)	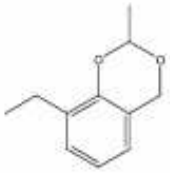
4	247	23.48	2.8	6	248 → 216 (−32) 248 → 176 (−72)	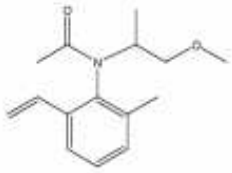
5	233	23.59	6.1	6	234 → 202 (−32) 234 → 206 (−28) 206 → 176 (−30) 176 → 148 (−28) 148 → 146 (−2)	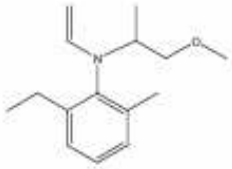
6	247	24.21	0.9	6	248 → 216 (−32) 248 → 176 (−72) 216 → 174 (−42) 216 → 188 (−28)	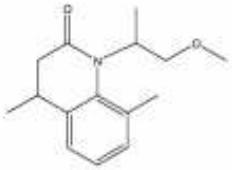
7	247	24.30	1.3	6	248 → 216 (−32) 248 → 176 (−72) 216 → 174 (−42) 216 → 188 (−28)	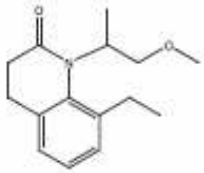

(Continues)

Table 1. (Continued)

	Molecular weight	Retention time (min)	Relative abundance[a]	Shift for metolachlor-d_6	Main transitions in CI-MS^n (m/z)	Chemical structure proposed
8	247	24.40	0.1	6	248 → 216 (−32) 248 → 176 (−72) 216 → 174 (−42) 216 → 188 (−28) 188 → 160 (−28)	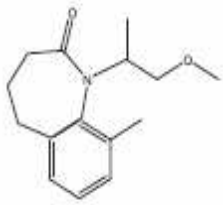
9	265	25.00	30.1	6	266 → 250 (−16) 266 → 248 (−18) 266 → 234 (−32) 248 → 216 (−32)	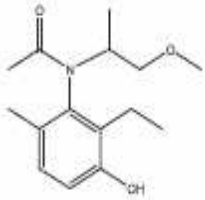
10	265	25.24	22.6	6	266 → 248 (−18) 266 → 234 (−32) 248 → 216 (−32) 248 → 206 (−42) 216 → 174 (−42)	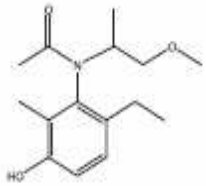
11	265	25.48	6.1	6	266 → 248 (−18) 266 → 234 (−32) 248 → 216 (−32) 248 → 206 (−42)	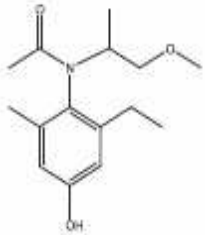
12	265	25.59	16.2	6	266 → 248 (−18) 266 → 238 (−28) 266 → 234 (−32) 248 → 216 (−32) 248 → 206 (−42)	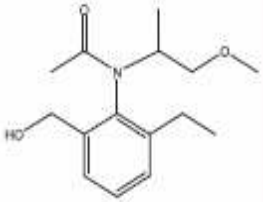
13	265	25.88	1.2	6	266 → 248 (−18) 248 → 216 (−32) 248 → 206 (−42) 206 → 176 (−30) 206 → 149 (−57)	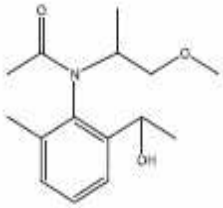

(Continues)

Table 1. (Continued)

	Molecular weight	Retention time (min)	Relative abundance*	Shift for metolachlor-d_6	Main transitions in Cl-MS^n (m/z)	Chemical structure proposed
14	265	27.70	3.3	6	266 → 218 (−48) 266 → 206 (−60)	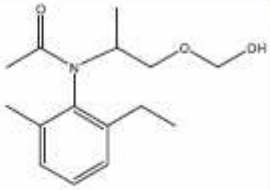
15	265	31.15	1.1	6	266 → 234 (−32) 266 → 208 (−58) 206 → 149 (−57)	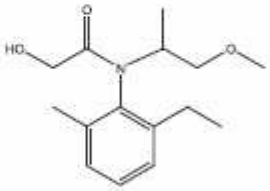

*% of the total of all the product abundances.

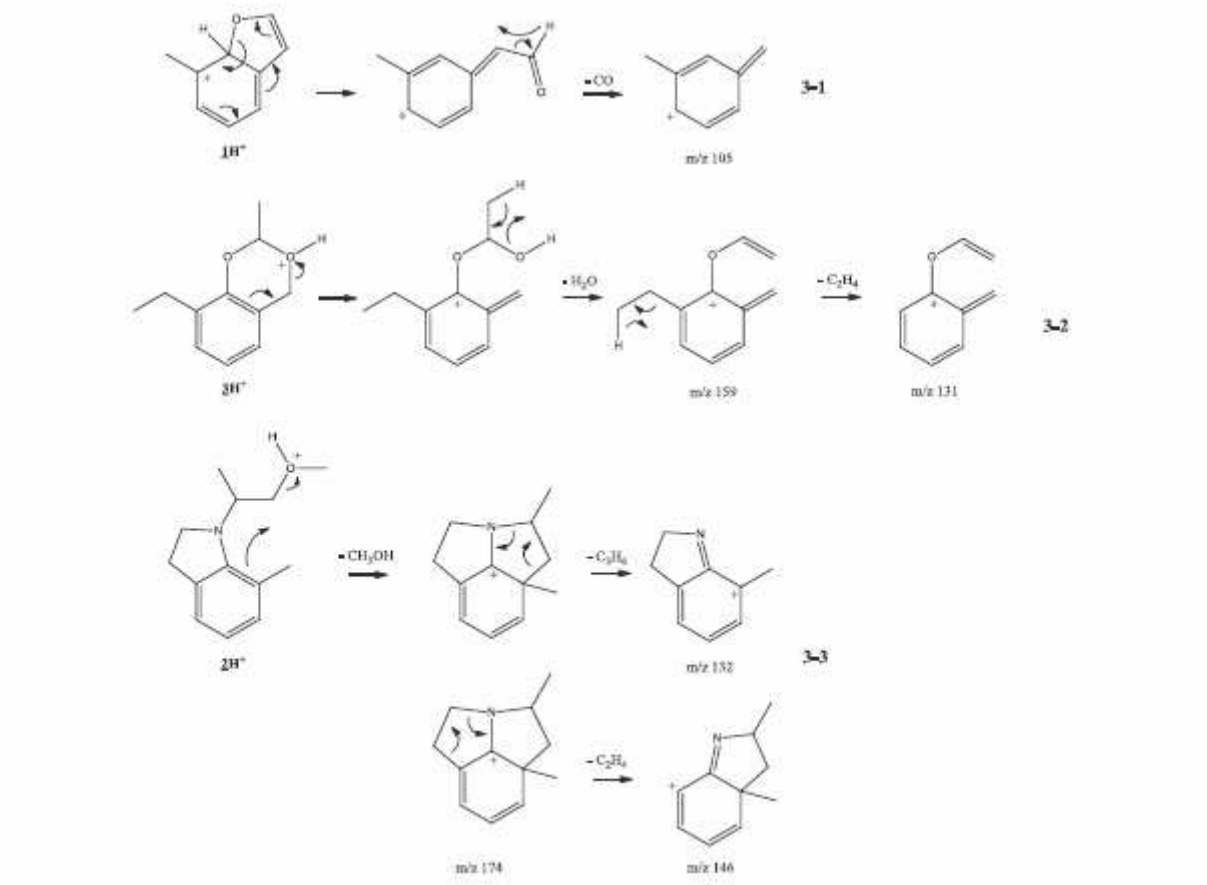

Figure 3. Dissociation pathways of the pseudo-molecular ions of compounds 1, 2 and 3

Among the 15 main photolysis products, seven compounds were found with a molecular weight of 265 a.m.u.: 9, 10, 11, 12, 13, 14 and 15. They were assumed to be isomers resulting from chlorine elimination from metolachlor and hydroxyl addition onto the latter. The pseudo-molecular ions of all these compounds lose 32 a.m.u. (CH_3OH), in agreement with the remaining of the ether functionality and 18 a.m.u. (H_2O), in agreement with the addition of a hydroxyl group, with the exception of 15 for which only the loss of CH_3OH is observed. Discarding the alkyl chain between the amide and ether functionalities (based on experiments on metolachlor-d_6), OH addition can occur onto eight sites. Distinguishing the different isomers was difficult as they provided almost identical mass spectra. However, the search for specific ions led us to the classification used in Table 1. Compound 14 is the only one which directly loses 48 a.m.u. and not 32 a.m.u. from MH^+ under CID experiments. This loss corresponds to $CH_2(OH)_2$ elimination and indicates that the hydroxyl is located in alpha position of the ether group in the case of compound 14. In the same way, compound 15 is the only one which loses 58 a.m.u. (HOCHCO) straight from MH^+; thus it was identified as resulting from a hydroxyl attack onto the primary methyl carbon of the amide functionality. It is to be remarked that compound 15 was identified by *Wu et al.* in a previous work.[15] Considering the similarity between their mass spectra and their close retention times, compounds 9, 10 and 11 were assumed to correspond to the three phenol-containing isomers.

Among them, compound 9 is the only one for which a loss of 16 a.m.u. (CH_4) is observed from MH^+, indicating an ortho effect as displayed in scheme 4-1 (Fig. 4). Consequently, compound 9 was identified as the compound bearing an OH group in ortho position of the ethyl group. Both other compounds were distinguished considering the boiling points of two molecules with phenolic structures close to those proposed for 10 and 11: 225 °C for 3-ethyl-1-methylphenol and 233 °C for 4-ethyl-2-methylphenol.[21] According to these data, compound 10 was identified as the easier compound to vaporize and thus the first to elute on a low polarity capillary column. Compounds 12 and 13 are thus expected to result from hydroxyl addition onto the alkyl groups carried by the aromatic ring. As compound 12 is the only one to lose 28 a.m.u. (ethylene elimination according to the mechanism 4-2 in Fig. 4) from MH^+, it was logically identified as the isomer with the hydroxyl on the methyl group. Compound 13 was assumed to result from the hydroxyl attack on the alpha site of the ethyl group considering the very easy water elimination from MH^+ (abundant peak at m/z 248 in its mass spectrum) through a classical four-center mechanism comparable to the water

elimination from the pseudo-molecular ion of 3 in scheme 3-2 (Fig. 3). Furthermore, this hypothesis is in good agreement with the one above, according to which compound 1 could result from the non-observed isomer which would have resulted from hydroxyl addition onto the beta position of the ethyl group.

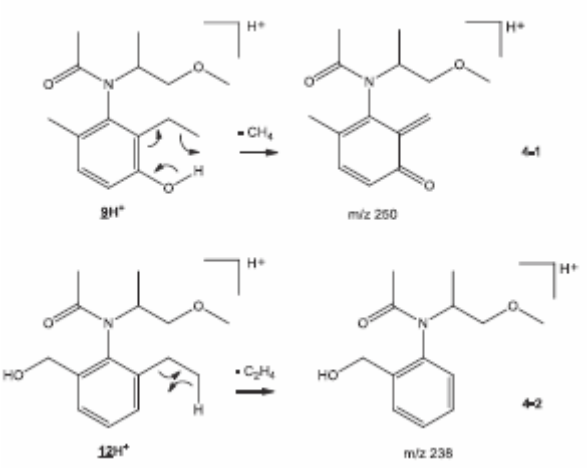

Figure 4. Ortho effect from the pseudo molecular ion of 9 and ethylene elimination from the pseudo molecular ion of 12

Compounds 4, 6, 7 and 8 feature almost identical mass spectra and a molecular weight of 247; they only differ by 18 a.m.u. with the isomers treated in the previous paragraph and could be considered as resulting from water loss from some of the latter. Since three of the four chemical structures considered elute with very close retention times and provide very similar CID mass spectra, it was postulated that they correspond to the cyclic compounds 6, 7 and 8 (Table 1). 8 corresponds to a structure suggested by Wu *et al.* in a previous work devoted to metolachlor photolysis.[15] The pseudo-molecular ions of the three compounds consecutively loss CH_3OH and $H_2C{=}CO$ to provide m/z 174 ions, according to the schemes 5-1 and 5-2 in Fig. 5. MS^3 experiments performed on the three compounds with the same activation energies at each step showed the following transitions for 8: $MH^+ \rightarrow$m/z 216$\rightarrow$m/z 188$\rightarrow$m/z 160. The last one is not observed for 6 and 7. The formation mechanism of the ion at m/z 160 is given in scheme 5-2 in the case of 8. It would lead to much less stable ions (non conjugated vinylic ions) at m/z 146 and at m/z 160 in the cases of 6 and 7, respectively. The scheme 5-3 displays the dissociation pathway proposed to explain the direct loss of 72 a.m.u. from the pseudo-molecular ions of 6, 7 and 8. The isomeric structures displayed in Table 1 were proposed in accordance with the dissociation pathways proposed in Fig. 5 for the formation of ions at m/z 216, m/z 188 and m/z 160 shifted to m/z 222, m/z 194 and m/z 166,

respectively, in the case of metolachlor-d_6. Ions at m/z 176 are not shifted with metolachlor-d_6, in agreement with the dissociation pathway 5-3. The structures 6 and 7 could not be differentiated neither on the basis of their mass spectra nor on that of their retention times so that two similar structures were suggested without the possibility of specifying the elution order.

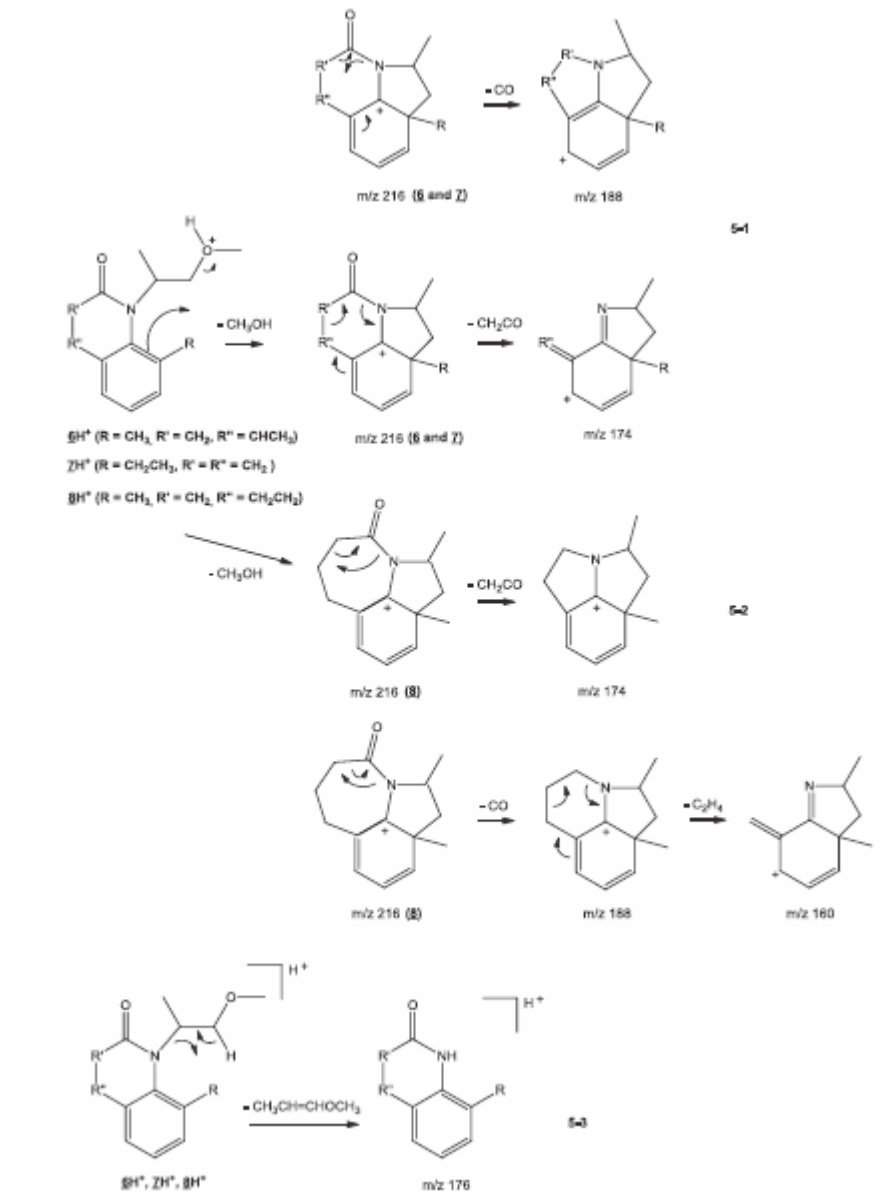

Figure 5. Main dissociation pathways of the protonated ions of isomers 6, 7 and 8.

The structure proposed for compound 4 corresponds to the only non-cyclized isomer with a molecular weight of 246. CIDs carried out on MH^+ ions in CI (losses of methanol and

of CH_3–CH = CH–OCH_3) are in good agreement with the chemical structure proposed for 4. The MH^+ ion in the mass spectrum of the deuterated equivalent of 5 is shifted by 6 a.m.u., showing evidence that 5 has kept the –(CH_3)CH–CH_2– chain. It differs by 14 a.m.u. from the compounds studied in the previous paragraph, i.e. 5 includes one CH2 group less than them. The structure in Table 1 was proposed on the basis of the dissociation pathways displayed in Fig. 6, in agreement with the fact that m/z 206, m/z 176 and m/z 148 ions are shifted by 6 Th in the case of metolachlor-d_6. Some m/z 146 ions are shifted to m/z 151 while a part of them are shifted to m/z 150 in the CID mass spectra of the deuterated analogous of 5. This led us to suggest that H_2 elimination from m/z 148 ions can occur in two ways, as depicted in Fig. 6. The chemical structures proposed for 4 and 6 were previously suggested by *Wu et al.* [15].

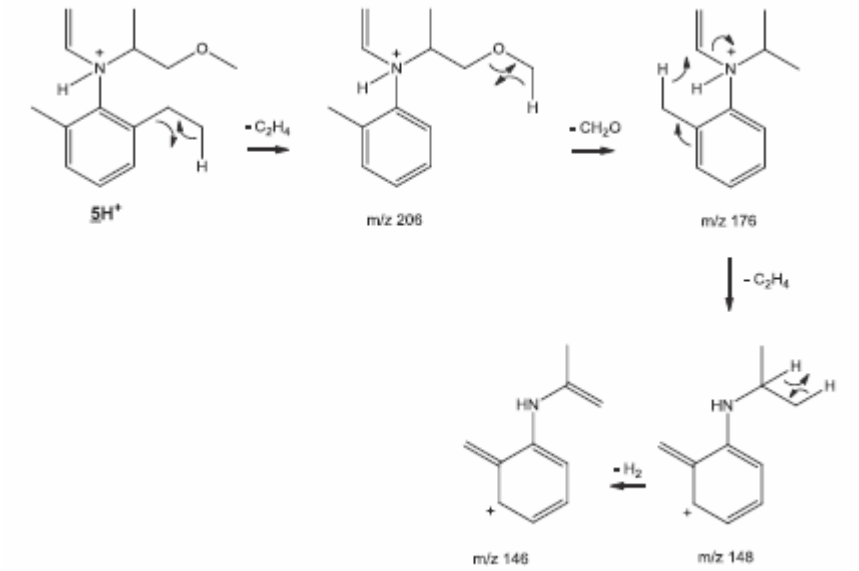

Figure 6. Dissociation pathways of the pseudo-molecular ions of 5.

Persistence studies

With the aim of following the evolution of the photolysis byproducts as a function of the irradiation time, as well as their persistence in the solution, photolysis of a 1 L solution of metolachlor was performed during 30 min. 70 ml was taken of the solution every 5 min until 20 min and at the end of the experiment and aliquoted in 10 ml lots. Each aliquot was then frozen at -80 °C after having been let at ambient atmosphere for times ranging from 0 to 32 h (0, 1 h, 2 h, 4 h, 7 h, 12 h, 25 h and 32 h). Eventually, a relative empirical quantitation (no response function could be plotted as no standards were available for photolysis products) was performed based on the GC-MS chromatograms recorded in the CI mode, scanning ions from

m/z 50 to m/z 290. Benzophenone at 1 $mg.ml^{-1}$ in methylene chloride was added to each sample before analysis to serve as an internal standard. For each sample, the amounts of compounds were estimated integrating the chromatographic peak area of each molecule on the ionic currents of MH^+ ions and dividing it by the chromatographic peak area of benzophenone integrated on the ionic current of the pseudo-molecular ion at m/z 183.

Concerning the evolution of the products abundances as a function of the time of irradiation, three major trends were highlighted. Products 4, 5, 6, 7, 8, 12, 13 and 15 display the same behaviour. Their concentrations increase with the time of irradiation to reach a maximum after 20 to 30 min of photolysis. An example of this is shown in Fig. 7, which displays the kinetics of evolution for compound 6 for this series. On the contrary, products 9, 10 and 11 are mainly formed at the beginning of the photolysis, i.e. during the first 10 min of irradiation, as shown in Fig. 7 in the case of compound 10. The best explanation for the decrease in abundance of these phenolic compounds after 10 min is that their irradiation probably led to bi- or tri-phenols too polar to be detected by GC-MS, as reported, for instance, in a recent study devoted to estrone photolysis.[22] The last trend is followed by products 2 and 3, for which no significant evolution can be drawn since their concentrations remain roughly the same whatever the irradiation duration. Unfortunately, evolution of compounds 1 and 14 could not be followed because of their too low concentrations even in the first measurements. It is interesting to have a special focus on the evolution of the two families of isomers determined in the structural study, which constitute by far the main by-products of metolachlor. The four compounds with a molecular weight of 247 a.m.u. follow the same trend. This is also the case of phenolic isomers 9, 10 and 11 with a molecular weight of 265 a.m.u.

The highest concentrations for most of the products were measured between 4 and 12 h after the photolysis and were followed by a rather sharp decrease. At these times, the phenolic compounds represented more than 50% of the total amount of the photolysis products (relative abundances are given in Table 1). Moreover, it is to be noted that 11 among the 15 products (2, 3, 4, 5, 6, 7, 8, 9, 10, 11 and 12) are still present in the solution 32 h after the end of photolysis.

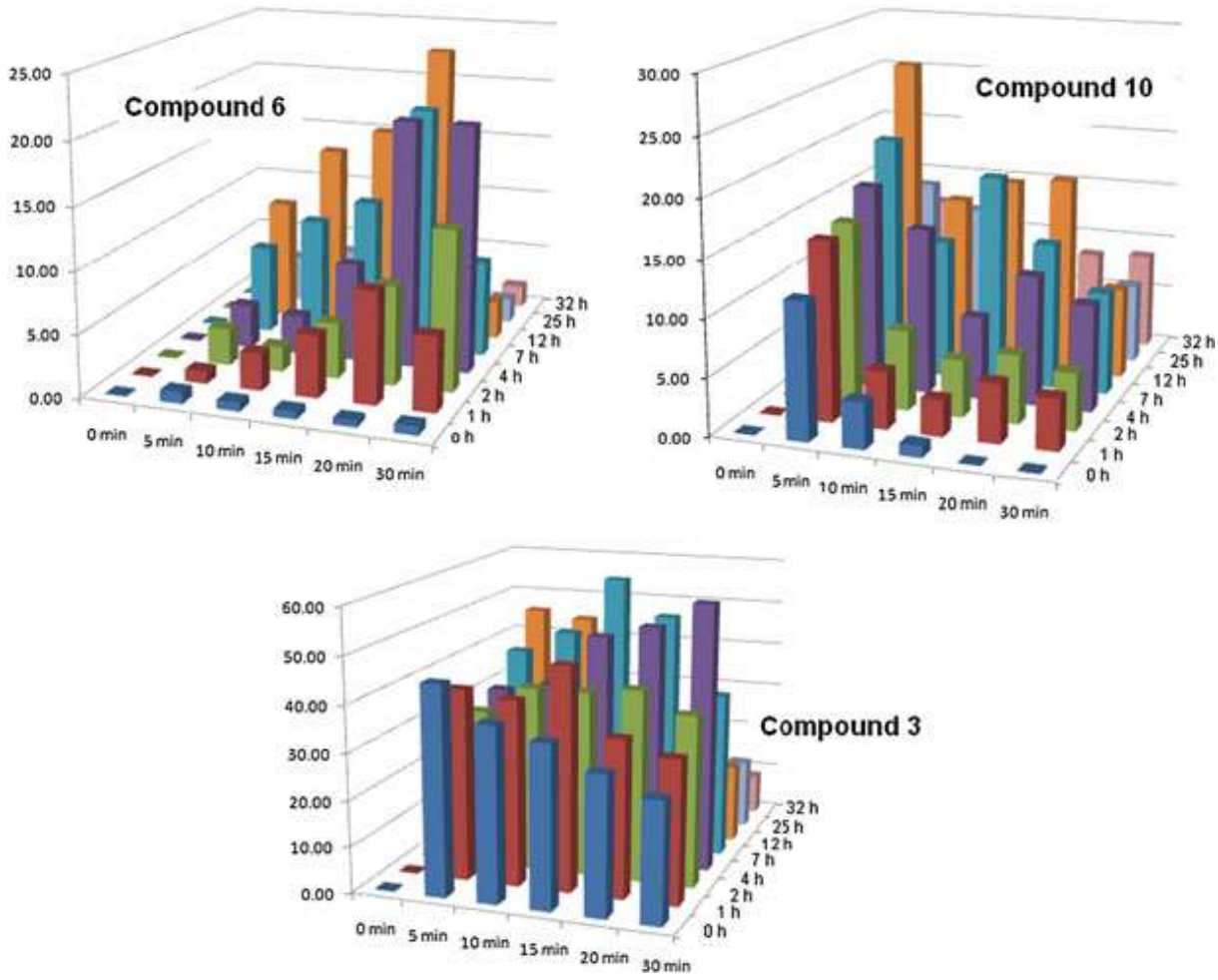

Figure 7. Evolution as a function of irradiation time and post-photolysis evolution of compounds 6, 10 and 3

Photolysis pathways

Attempts to correlate the formation of these by-products were made on the basis of the chemical structures that we proposed. Since the chlorine atom has been removed for all the photolysis products, the cleavage of the C–Cl bond has been assumed to be the first step of the photolytic process. As depicted in Fig. 8, the resulting radical can undergo $HO^{\cdot}$ or $H^{\cdot}$ addition from water. Direct addition of $HO^{\cdot}$ provides 15 while that of $H^{\cdot}$ leads to a molecule (left hand of Fig. 8), which submitted to irradiation, give the phenolic structures 9 to 11. The radical issued from $Cl^{\cdot}$ Loss can also quickly rearrange via $H^{\cdot}$ transfer before hydroxyl addition from water. The formation of photolysis products 12, 13 and 14 can be easily explained on this assumption. H_2O losses through concerted mechanisms involving the added hydroxy group lead to the formation of 6 from 12, 4 and 7 from 13. On the right hand on Fig. 8, a structure referenced as X (not observed in the chromatogram) is displayed, corresponding

to the addition of a hydroxy group in beta position onto the ethyl group carried by the aromatic ring. X could lead to 8 through H_2O loss. No mechanism has been found to rationalize the formation of the compound 5.

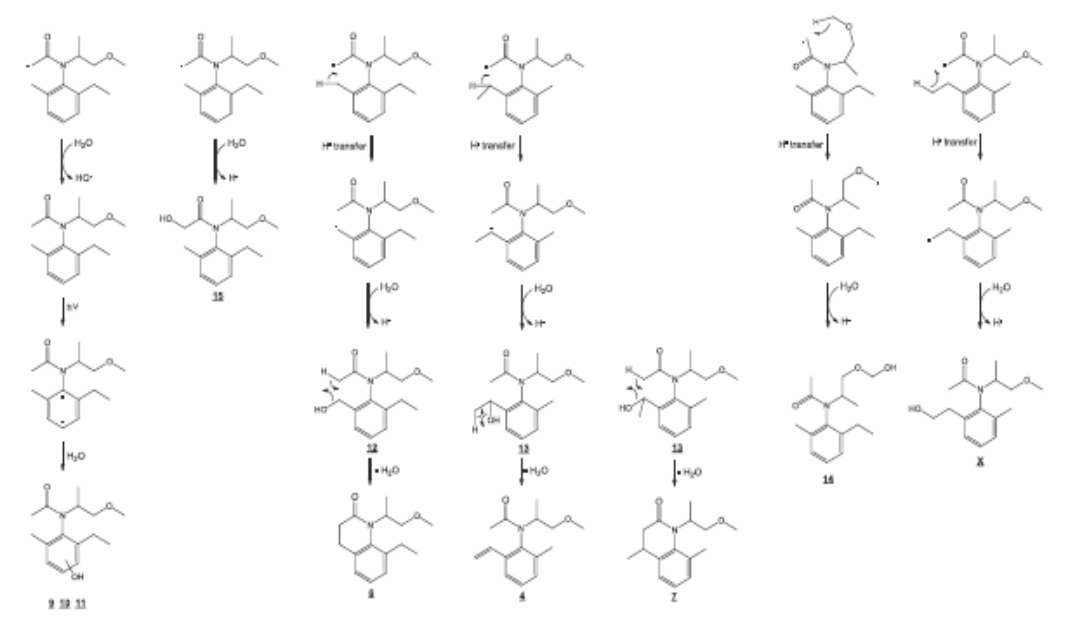

Figure 8. Suggested formation pathways for the photolysis products 4, 6, 7 and 9 to 15

In silico toxicity prediction for metolachlor and its photoproducts

Metolachlor and its photodegradation products may affect a population through the consumption of contaminated food or drinking water. Thus, the occurrence of health damages should be investigated. As a first step for toxicity investigation, we chose to use a computer-based predictive model. The different endpoints of the used predictive model related to human health disturbance were tested with the parent molecule and its degradates. Rat lethal dose (LD50), developmental toxicity and Ames mutagenicity were predicted for metolachlor and its 15 phototransformation products. No mutagenicity was observed for metolachlor and its degradation products though the software simulation. This observation is in agreement with the literature data which indicates that metolachlor does not induce gene mutation.[23]

However, the metolachlor molecule and its transformation products all exhibited a developmental toxicity effect. Developmental toxicity includes any effect interfering with

normal development, both before or after birth. All the photoproducts have a developmental toxicity estimated around 0.5 to 1.19 A.U (Fig. 9 (a)). The photoproduct 15 corresponding to hydroxylated dechlorinated metolachlor seemed to be the most toxic for development. The effect of the majority of the other metolachlor degradates was shown to be as toxic as the parent molecule. The developmental toxicity of metolachlor and its photoproducts predicted by the software announce potential embryotoxic, foetotoxic or teratogenic effects including growth and developmental retardation, organ toxicity, structural defects as well as peri- and postnatal defects. Some studies in the literature reported developmental effects concerning metolachlor and its degradation products enhancing the relevance of this predictive software as a prospective tool for the establishment of in vitro and/or in vivo assays to investigate the real occurrence of those compounds. A previous study devoted to risks associated with the use of metolachlor showed that its teratogenicity after breakdown was highlighted.[24] It was also reported that metolachlor exhibited cytotoxic and genotoxic effect in human lymphocytes as well as chromosome damage.[25] Moreover, *Hill and co-workers* reported that the chloroacethyl group lower the genotoxicity of the dialkylquinoneimines (diethyl, ethylene methyl and dimethyl).[26] This may explain the fact that the photoproducts, which have lost the chlorine atom, exhibited a predicted developmental toxicity potential.

Oral rat LD50 endpoint indicates the amount of chemical in mg/Kg body weight in that would cause 50% of rats to die after oral ingestion of a test population. The oral rat LD50 predicted values for metolachlor, and its photoproducts are displayed in Fig. 9 (b). According to the toxicity scale classification of Hodge and Sterner, among all the compounds, three of them (2, 5 and 10) seem to be slightly toxic, and all the others including metolachlor are moderately toxic.[27] We can also notice that the photolysis of metolachlor engenders the production of compounds for which the oral rat LD50 is not reduced compared to the parent molecule. It is to be noticed that an increase in rat liver tumors in females and few nasal tumors in males have been observed for metolachlor.[28] In vivo and/or in vitro biological assays should be achieved in order to confirm the *in silico* toxicity prediction. The products mixtures should also be tested in order to investigate whether a synergic effect of the by-products exists or not.

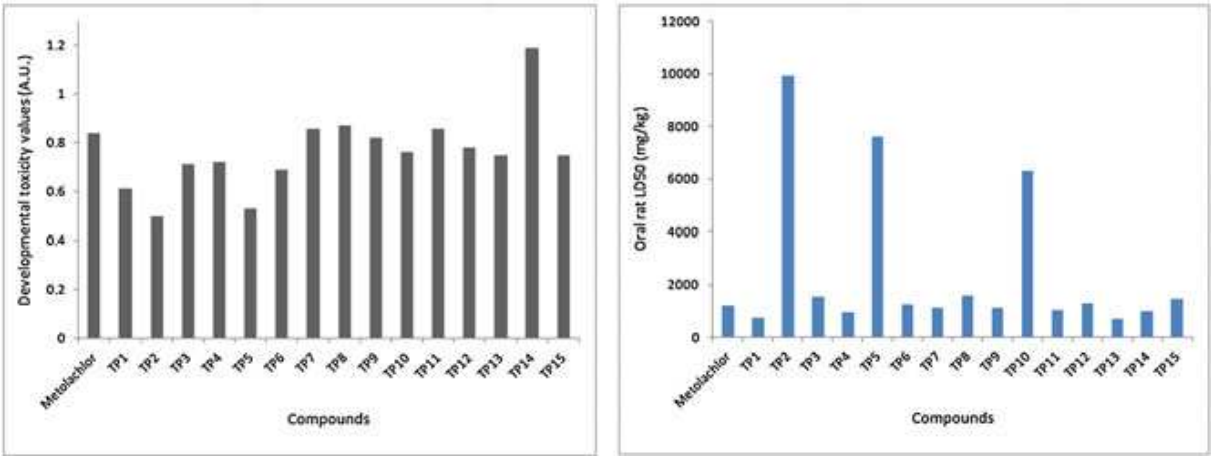

Figure 9. *In silico* predicted developmental toxicity (a) and rat lethal dose 50 (b) for metolachlor and its photoproducts Toxicity Estimation Software Tool ©2011 U.S. Environmental Protection Agency.

Conclusion

Fifteen products resulting from the photolysis of metolachlor were characterized based on GC-MS^n analyses. This study complements the results found by *Wu et al.* in a study mainly devoted to the optimization of photolysis processes.[15] The present work confirms the postulated structures of four by-products and allowed differentiation of isomeric compounds. In all the products, the chlorine atom was eliminated, which constitutes an interesting result in terms of ecotoxicology. In comparison, recent works conducted in our laboratory have shown that ozonation of chlorinated herbicides mainly provide by-products which had kept the chlorine atom.[29] However, the main photolysis by-products characterized here include phenolic species whose biological activity should be investigated since phenols and alkyl phenols are well known to act as endocrine disruptors.[30] The evolution of the products as a function of the time of irradiation showed that most of the products are already present after 5 min of photolysis. Therefore, shortening the time of exposure does not seem a solution to limit the number of by-products, although the concentrations of some of them decrease with a longer exposure. Post photolysis kinetic studies showed that most of byproducts have a long persistence time in water. This is of particular interest when one considers that, in some houses, treated water is available for consumption only 3 h after the end of water treatment. The fate of these by-products must be considered since they are demonstrated here as potential persistent compounds into drinking water. This study is therefore another demonstration that photolysis of micro-pollutants may not lead to their complete

mineralization. It shows the importance to develop more research on the by-products resulting from the photolysis treatment on different identified micro pollutants (other pesticides but also drugs residues and metabolites).

References

[1] J.N. Aubertot, J.M. Barbier, A. Carpentier, J.J. Gril, L. Guichard, P. Lucas, S. Savary, I. Savini, M. Voltz. Pesticides, agriculture et environnement. Réduire l'utilisation des pesticides et limiter leurs impacts environnementaux. Rapport d'Expertise scientifique collective, INRA et Cemagref, I.a. Cemagref Editor. 2005.

[2] J.D. Byer, J. Struger, E. Sverko, P. Klawunn, A. Todd. Spatial and seasonal variations in atrazine and metolachlor surface water concentrations in Ontario (Canada) using ELISA. Chemosphere 2011, 82(8), 1155.

[3] D. Whitall, W.D. Hively, A.K. Leight, C.J. Hapeman, L.L. McConnell, T. Fisher, C.P. Rice, E. Codling, G.W.McCarty, A.M. Sadeghi, A. Gustafson, K. Bialek. Pollutant fate and spatio-temporal variability in the choptank river estuary: factors influencing water quality. Sci. Total Environ. 2010, 408(9), 2096.

[4] Stratégie Nationale pour la Biodiversité - Rapport d'activité 2009 in www.developpement-durable.gouv.fr, d.l.E. Ministère de l'Ecologie, du Développement durable et de la Mer - France Editor.

[5] V.M. Kale, S.R. Miranda, M.S. Wilbanks, S.A. Meyer. Comparative cytotoxicity of alachlor, acetochlor, and metolachlor herbicides in isolated rat and cryopreserved human hepatocytes. J. Biochem. Mol. Toxicol. 2008, 22(1), 41.

[6] P. Krajcsi, B. Oosterhuis, K. Vukman, E. Vagi, H. Glavinas, I. Jablonkai. Specific interactions of chloroacetanilide herbicides with human ABC transporter proteins. Toxicology 2008, 248(1), 45.

[7] M. Petrovic, S. Gonzalez, D. Barcelo. Analysis and removal of emerging contaminants in wastewater and drinking water. TrAC, Trends in Anal. Chem. 2003, 22(10), 685.

[8] A.L. Roberts, M.L. Hladik, E.J. Bouwer. Neutral degradates of chloroacetamide herbicides: Occurrence in drinking water and removal during conventional water treatment. Water Res. 2008, 42(20), 4905.

[9] V. Feigenbrugel, C. Loew, S. Le Calve, P. Mirabel. Near-UV molar absorptivities of acetone, alachlor, metolachlor, diazinon and dichlorvos in aqueous solution. J. Photochem. Photobiol. A 2005, 174(1), 76.

[10] Trojan ECT case study PWN installed in http://www.trojanuv.com

[11] J.A.M.H. Hofman, G.F. Ijpelaar, S.G.J. Heijman, J.S. Vrouwenvelder, J.C. Kruithof, W.G.J. Van der Meer. Drinking water treatment in The Netherlands: outstanding and still ambitious. Water Sci. Technol. Water Supply 2004, 4(5-6), 253.

[12] Directive 2000/60/EC of the European Parliament and of the Council of 23 October 2000 establishing a framework for Community action in the field of water policy, O. 327.

[13] L. Rivard. Environmental fate of metolachlor in http://pestreg.cdpr. ca.gov/docs/emon/pubs/fatememo/metolachlor.pdf 2003.

[14] V.J. Pereira, S. Sanches, M.T.B. Crespo. Drinking water treatment of priority pesticides using low pressure UV photolysis and advanced oxidation processes. Water Res. 2010, 44(6), 1809.

[15] C. Wu, H. Shemer, K.G. Linden,. Photodegradation of metolachlor applying UV and UV/H2O2. J. Agric. Food Chem. 2007, 55(10), 4059.

[16] http://www.epa.gov/nrmrl/std/qsar/qsar.html

[17] P.H. Goulden, S. Coffinet, C. Genty, S. Bourcier, M. Sablier, S. Bouchonnet. Investigation of the Unusual Behavior of Metolachlor under Chemical Ionization in a Hybrid 3D Ion Trap Mass Spectrometer. Anal. Chem. 2011, 83(20), 7587.

[18] NIST/EPA/NIH, NIST mass spectral library, National Institute of Standards and Technology, US Secretary of Commerce, Washington, DC, USA, 2005.

[19] Wiley. Wiley Registry of Mass Spectral Data. 7th Edition. Wiley: New York, USA, 2005.

[20] S. Bouchonnet, S. Kinani, Y. Souissi, S. Bourcier, M. Sablier, P. Roche, V. Boireau, V. Ingrand. Investigation of the dissociation pathways of metolachlor, acetochlor and alachlor under electron ionization - application to the identification of ozonation products. Rapid Commun. Mass Spectrom. 2011, 25(1), 93.

[21] Reference standard database NIST n_ 69 in http://webbook.nist.gov/ chemistry/

[22] Y. Souissi, S. Bourcier, S. Bouchonnet, C. Genty, M. Sablier. Estrone direct photolysis: By-product identification using LC-Q-TOF. Chemosphere 2012, 87(2), 185.

[23] C.K. Grisolia, I. Ferrari. *In vitro* and *in vivo* studies demonstrate nonmutagenicity of the herbicide metolachlor. Braz. J. Genet. 1997, 20 (3), 411.

[24] O. Osano, W. Admiraal, D. Otieno. Developmental disorders in embryos of the frog Xenopus laevis induced by chloroacetanilide herbicides and their degradation products. Environ. Toxicol. Chem. 2002, 21(2), 375.

[25] B. Roloff, D. Belluck, M. Lorraine. Cytogenetic effects of cyanazine and metolachlor on human lymphocytes exposed in vitro. Mutat. Res. Lett. 1992, 281(4), 295.

[26] A.B. Hill, P.R. Jefferies, G.B. Quistad, J.E. Casida. Dialkylquinoneimine metabolites of chloroacetanilide herbicides induce sister chromatid exchanges in cultured human lymphocytes. Mutat. Res-Gen. Tox. En. 1997, 395(2-3), 159.

[27] H.C. Hodge, J.H. Sterner. Tabulation of Toxicity Classes. Am. Ind. Hyg. Assoc. J. 1949, 10(4), 93.

[28] WHO. W.H.O. Guidelines for Drinking-water Quality: Recommendations. WHO Library cataloguing in publication data 2004. (3rd edition).

[29] S. Bouchonnet, S. Bourcier, Y. Souissi, C. Genty, M. Sablier, P. Roche, V. Boireau, V. Ingrand. GC-MS^n and LC-MS/MS couplings for the identification of degradation products resulting from the ozonation treatment of Acetochlor. J. Mass Spectrom. 2012, 47(4), 439.

[30] A. Soares, B. Guieysse, B. Jefferson, E. Cartmell, J.N. Lester. Nonylphenol in the environment: a critical review on occurrence, fate, toxicity and treatment in wastewaters. Environ. Int. 2008, 34(7), 1033.

III-3. Conclusion

Caractérisation structurale

L'analyse des solutions de métolachlore photolysé par GC-MS a montré quinze produits de dégradation. Deux produits sont détectés dans les solutions non photolysées mais leurs abondances relatives augmentent considérablement suite à l'irradiation. Les structures proposées pour les photo-produits ont été confirmées par l'analyse de la solution de métolachlore-d_6 photolysée. Deux photo-produits n'incluent aucun atome de deutérium, cela implique que la partie « éther » des molécules (figure 1) de métolachlore et de métolachlore-d_6 a été affectée par l'irradiation. Les autres photo-produits du métolachlore-$d_6$incluent les 6 deutériums, ce qui signifie qu'ils ont conservé la partie « éther » de la molécule. Les structures ont été validées en rationalisant la formation des ions fragments des ions obtenus par dissociation dans la cellule de collision (CID) sous différentes énergies pour chaque produit.

Aspects cinétiques

L'étude cinétique a montré que les abondances des produits 4, 5, 6, 7, 8, 12, 13 et 15 augmentent et passent par un maximum après 20 à 30 min d'irradiation. Les composés 9, 10 et 11 se forment durant les 10 premières minutes. Les abondances des produits 2 et 3 restent élevées quelque soit le temps d'irradiation. Les abondances relatives des produits évoluent après l'irradiation. La plupart d'entre eux présentent une abondance maximale entre 4 et 12 h après la fin de l'irradiation. Les produits phénoliques représentent plusde 50% de l'abondance relative totale. Onze photo-produits, parmi les quinze produits de transformation, sont toujours détectés 32 h après l'irradiation.

Toxicité prédictive

L'estimation de la toxicité du métolachlore et des produits de dégradation détectés en GC/MS a montré qu'ils ne présentent pas de mutagénicité. Cependant, ils ont des effets toxiques sur le développement du fœtus avant la naissance et sur la taille de l'animal après la naissance. L'estimation de l'oral rat LD50 montre que trois photo produits (2, 5 et 10) semblent être légèrement toxique, et tous les autres, y compris le métolachlore sont modérément toxiques.

Chapitre IV

Etude de la photo-transformation de la procymidone

IV-1. Introduction

La procymidone est un fongicide appartenant à la famille chimique des organochlorés. Généralement, elle est utilisée pour lutter contre les pourritures grises qui attaquent les raisins. Les normes internationales et la littérature indiquent que ce pesticide ne se dégrade pas sous irradiation UV sans ajout de catalyseur mais des tests au laboratoire ont montré le contraire. L'objectif de cette étude est d'identifier les photoproduits de la procymidone sous irradiation UV de manière à tenter de prédire le devenir de ce fongicide sous irradiation solaire.

À cause de la faible solubilité de la procymidone dans l'eau (4.5 mg L^{-1} à 25 °C), des solutions mères ont été préparées dans l'acetonitrile avant dilution dans l'eau. Des solutions de procymidone ont été préparées à 5 $mg.L^{-1}$ pour les expériences d'identification structurale et à 0,5 $mg.L^{-1}$ pour les études cinétiques. Le réacteur utilisé pour les expériences de photodégradation est décrit au chapitre 2. L'extraction liquide-liquide a été utilisée et les solutions analysées par couplage GC-MS.

Dans la littérature, quelques articles rapportent l'analyse de la procymidone par LC/MS avec une source ESI. Dans notre étude, nous n'avons pas réussi à détecter la procymidone en LC-MS quel que soit le dispositif utilisé: HPLC-Q-TOF, nano LC-FT-ICR et LC-TQ. Néanmoins, les courants ioniques totaux des photoproduits dans les chromatogrammes de GC-MS des solutions irradiées comparé à celui de la procymidone dans la solution de référence suggèrent que plus de 90% des produits sont détectés par GC-MS. Le mode MS^n a été utilisé pour identifier les ions parents et ions fils de la procymidone et des photoproduits.

La molécule de procymidone contient plusieurs sites susceptibles d'être ionisés. La structure de l'ion le plus probable a été déterminée grâce à des calculs de chimie quantique avec des méthodes TD-DFT et CC2.

Les études cinétiques ont permis d'établir des corrélations entre la formation et la disparition de certains produits et ainsi de proposer des mécanismes de photochimie.

La toxicité des photoproduits de la procymidone a été estimée à l'aide du programme T.E.S.T (voir chapitre 2).

IV-2. UV-visible photo degradation of procymidone - structural characterization and potential toxicity of photoproducts

Ahmad Rifai, Yasmine Souissi, Christophe Genty, Carine Clavaguera, Sophie Bourcier, Farouk Jaber and Stephane Bouchonnet

RATIONALE: Procymidone is a dicarboximide fungicide mainly used for vineyard protection but also for different crops. The structural elucidation of by-products arising from the UV-visible photo degradation of procymidone has been investigated by gas chromatography coupled with mass spectrometry. The potential toxicities of photoproducts were estimated by in silico tests.

METHODS: Aqueous solutions of procymidone were irradiated up to ninety minutes in a self-made reactor equipped with a mercury lamp. Analyses were carried out on a gas chromatograph coupled with an ion trap mass spectrometer operated in electron ionization and methanol positive chemical ionization. Multiple stage collision induced experiments were performed to establish dissociation pathways of ions. Toxicities of byproducts were estimated using the QSAR T.E.S.T. program.

RESULTS: Sixteen photoproducts were investigated. Chemical structures were proposed mainly based on the interpretation of multistage collision induced dissociation experiments but also on their relative retention times and kinetics data. These structures led to suggest photo degradation pathways. Only three photoproducts remain present after ninety minutes of irradiation. Among them, 3,5-dichloroaniline presents a predicted rat LD50 toxicity about ten times greater than that of procymidone.

CONCLUSIONS: 3,5-dichloroaniline is the only photoproduct reported in previous articles. Eight by-products among the sixteen characterized might be as toxic, if not more, than procymidone itself considering the QSAR predicted rat LD50.

Keywords: procymidone, photolysis, degradation products, potential toxicity, quantum chemistry, GC-MS

1. Introduction

Procymidone is a dicarboximide fungicide mainly used for vineyard protection but also for strawberry, flowers and various ornamental cultivations [1, 2]. According to the European Commission directive 2006/132/EC, all Member States of the EU should amend or withdraw existing authorizations for plant protection products containing procymidone as an active substance. In 2010, the European Union set the Maximum Residue Level (MRL) of procymidone in crops at 0.02 mg/kg [3]. Procymidone presents anti-androgens toxicity and ability to induce developmental and/or reproductive dysfunctions by interfering with the endocrine system of exposed organisms [4-7] and is part of endocrine disruptor family [8]. The United States Environmental Protection Agency reported that procymidone and its main metabolite, the 3,5-Dichloroaniline (3,5-DCA) are carcinogenic products with dietary assessment [9]. Thus, the detection of this pesticide and its metabolites in the environmental samples is a priority in quality control. The transformation of pesticides in the environment is a highly complex process affected by many physical and chemical factors [10]. According to Burrows *et al.*, most pesticides are resistant to chemical and/or photochemical degradation under typical environmental conditions and very little information is available regarding their natural degradation processes, the quality, structure and biological impact of their degradation products [11]. Previous studies devoted to the degradation of procymidone have been focused on the photo catalytic degradation techniques. Hustert and Moza studied the photochemical degradation of procymidone and viniclozolin in water using a mercury lamp with $\lambda \geq 290$ nm. This study established that the addition of Fe_2O_3 and TiO_2 catalyzes the photo degradation of both compounds and that the presence of humic and fulvic acids (naturally extracted by the water from the soil constituents) increases the rate of photo degradation. Monodechlorination, didechlorination and isomerization are the major photo degradation pathways [12]. Schwack *et al.* studied the potential of procymidone to undergo photo induced processes in the presence of different organic groups. Their objectives were to find an explanation for the formation of bound residues in plant cuticles in the presence of polymer molecules, waxes and cutin. In isopropanol, cyclohexane and cyclohexene, photo degradation led to substitute a chlorine atom by a solvent molecule [13]. Vanni and co-workers studied the degradation of procymidone in agriculture land under various pH and temperature conditions. They reported that the total degradation of procymidone occurred at alkaline pH and at high temperature in few days; the main metabolite detected in their studies was 3,5-DCA [14]. The present study

aims to identify photo degradation products of procymidone in water and to assess their potential toxicity. It is now well admitted that sunlight absorbance in water may be significantly modified by the presence of dissolved organic matter but we consider here that photodegradation may start as soon as the aqueous solution of herbicide in sprayed on leaves and fruits, under intense sunlight irradiation. This study was first devoted to the structural elucidation of photoproducts using multiple-stage stage mass spectrometry coupled with gas chromatography (GC-MS^n). Structural elucidation of photoproducts was performed on the basis of the collision induced dissociations observed in both electron ionization and positive chemical ionization modes. Photolysis mechanisms were also suggested to explain the formation of the photoproducts formed from irradiated procymidone in water. An approach of quantitative structure–activity relationship (QSAR) was used to assess the potential toxicity effect of procymidone and of its photo degradation products. For that purpose we used a Toxicity Estimation Software Tool (T.E.S.T.), a U.S. Environmental Protection Agency developed program, to predict mutagenicity, oral rat lethal doses, developmental toxicity as well as growth inhibition concentrations and lethal doses of aquatic organisms.

2. Materials and methods

2.1. Chemicals and reagents

Procymidone (99% purity) was purchased from Sigma Aldrich (St Quentin Fallavier, France). The chemical structure of procymidone is displayed in Figure 1. Chromatographic grade solvents (99.99% purity), methylene chloride and acetonitrile, were also purchased from Sigma Aldrich. Considering the poor solubility of procymidone in water (4.5 mg/L at 25 °C), a solution of procymidone at 100 mg/L was first prepared in ACN. This solution was then used to prepare working solutions in water at 5.0 mg/L. This high concentration was used for structural investigations on photoproducts as multi stage mass spectrometry experiments require relatively high analyte concentrations. Aqueous solutions at 0.5 mg/L were used for kinetic measurements.

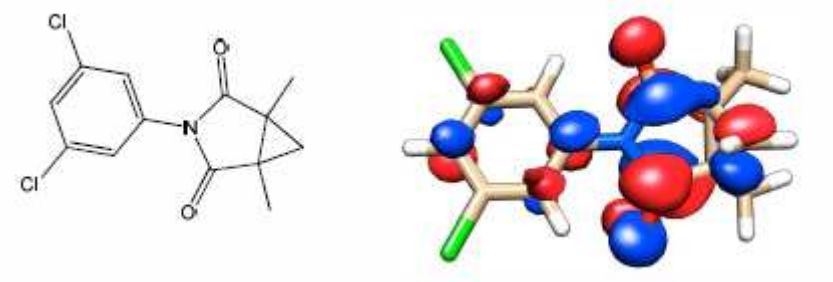

Figure 1. Chemical structure of procymidone and nature of the first excited state (CC2 level).

2.2. Photolysis experiments

Photolysis experiments were carried out in a self-made reactor equipped with a high-pressure mercury lamp (HPL-N 125W/542 E27 SC; Phillips, Ivry-sur-Seine, France) delivering radiation at wavelengths ranging from 200 nm to 650 nm. The absorbance spectrum of procymidone displays an absorption maximum between 200 and 208 nm [15]. According to manufacturer data, the incident radiation flux was 6200 lm. The reactor consists in six quartz tubes of 120 mL disposed in a circle around the lamp and immerged into a sonicator (AL04-12, Advantage-Lab, Switzerland) filled with deionized water. During experiments, the reactor was regularly cooled by ice addition to avoid uncontrolled heating of the irradiated solutions and to maintain a constant temperature of 25 ± 3 ºC. For each experiment, 50 mL of a solution of procymidone (see above) were used.

2.3. Sample preparation

After photolysis, 6 mL of solution were taken from the quartz tube and transferred into a separating funnel. 6 mL of methylene chloride were added to the solution which was then shaken and left to settle for ten minutes. The organic phase was collected and dried under a gentle nitrogen stream and the dry residue was dissolved into 200 µL of methylene chloride for GC-MS analysis.

2.4. Gas chromatography and mass spectrometry operating conditions

Analysis were carried out on a Varian 450GC gas chromatograph equipped with a CP8400 autosampler and coupled with a VARIAN 240MS ion trap mass spectrometer operated in the internal ionization mode. A 60 meter-long "VF-Xms" capillary column (VARIAN) with an internal diameter of 0.25 mm and a film thickness of 0.25 µm was used. For all analysis, 2 µl of solution were injected automatically in the splitless mode at a rate of 50 µL s^{-1}. The injector temperature was set to 280 ºC and high purity helium (99.999 %) was used as carrier gas at a constant flow of 1.4 mL min^{-1}. The column oven temperature was programmed from an initial temperature of 50 °C held during 1 min, increased to 280 °C at 15 °C/min, held 5 min at 280 °C, then increased at 10 °C/min to a final temperature of 300 °C, which was held for 20 min, for a total analysis duration of 43 minutes. The manifold, the ion-trap electrodes and the transfer line temperatures were respectively held at 100 °C, 200 °C and 280 °C. The mass spectrometer was calibrated with the ions resulting from electron ionization (EI) of perfluorotributylamine. Chemical ionization (CI) experiments were performed using methanol as the reagent. Spectra were recorded using the automatic gain control (AGC) function with target values fixed at 20,000 and 5,000 for electron ionization and chemical ionization (CI), respectively. The filament emission current was set at 10 µA in EI and 50 µA in CI. The electron multiplier voltage was automatically optimized at 2200 V for a gain value of 10^5. Full scan mass spectra were acquired recording ions from m/z 50 to m/z 500 at a scan rate of 0.33 sec/scan, each spectrum resulting from ion acquisitions on 5 microscans. In multiple stage mass spectrometry (MS^n) experiments, precursor ions were stored with a Paul stability parameter (qz) of 0.30 and fragmented by collision induced dissociation with activation energies ranging from 0.30 V to 0.80 V in the resonant excitation mode.

2.5. Quantum chemistry calculations

Geometry optimizations were performed at the DFT/B3LYP-D3 level, including the new implementation of dispersion corrections [16, 17] in the TURBOMOLE 6.4 package [18]. The minima were characterized by vibrational frequency calculations. All the calculations have been carried out with the polarized valence-triple-zeta TZVPP basis set. The most energetically stable geometry of the molecule (Figure 1) was used for the calculation of the electronic excited states by both the CC2 coupled cluster model and the time-dependent

density functional theory (TD-DFT) using the B3LYP-D3 functional. The CC2 equations are an approximation to the coupled cluster singles and doubles (CCSD) ones [19].This method is considered as an accurate tool for the investigation of the excited states of molecules [20]. Regarding the nature and the transition energies, both methods provide similar results that will be described in the result section (See supplementary material, part 1).

2.6. Computer aided toxicity prediction

Toxicity Estimation Software Tool (T.E.S.T.) is an Environmental Protection Agency online available computerized predictive system with Quantitative Structure Activity Relationships (QSAR) mathematical models [21]. T.E.S.T. has a variety of toxicity endpoints used to predict chemical toxicity values from their physical properties such as molecular structure. T.E.S.T. model uses a simple linear function of molecular descriptors such as the octanol-water partition coefficient, molecular weight or the number of benzene rings (see equation 1).

$$Toxicity = ax_1 + bx_2 + c \qquad (1)$$

x_1 and x_2 are independent descriptor variables and a, b, and c are fitted parameters. Models for assessing toxicity solely from molecular structure are based on information-rich structural descriptors that quantify transport, bulk, and electronic attributes of a chemical structure. Besides molecular weight, the QSAR model employs size-corrected E-values for quantification of molecular bulk. The size- corrected E-values are computed from a rescaled count of valence electrons [22]. Electrotopological state values (E-values), as numerical quantifiers of molecular structure, encode information about the electron content (valence, sigma, pi and lone-pair), topology, and environment of an atom, or a group of atoms, in a molecule [22]. The predicted toxicity is estimated by taking an average of the predicted toxicities from the above QSAR methods, provided the predictions are within the respective applicability domains.

3. Results and Discussion

3.1. Characterization of the photoproducts of procymidone

A series of experiments was performed with 8 irradiation times ranging from 0 to 90 min: 0, 5, 10, 15, 20, 40, 60 and 90 min. The comparison of the corresponding chromatograms, recorded in the EI mode, showed that the relative abundances of photoproducts vary significantly according to the irradiation time. The relative abundances of photoproducts are plotted as a function of the irradiation time in Figure 2. A precise quantitation of photo products was not possible given the lack of standards. Thus abundances were just estimated by integrating chromatographic peaks on the total ionic current (TIC); they are expressed in Figure 2 in an arbitrary unit proportional to the TIC. The abundance of procymidone was not plotted because it was out of scale. Disappearance of procymidone follows a pseudo exponential type curve. Only 5% of the initial amount of procymidone is still detected after 60 min of irradiation. Procymidone is no more detected after 90 min of irradiation. Among the sixteen photoproducts detected, thirteen are formed as soon as irradiation begins; their concentrations reach maximum values for photolysis times around 10 minutes before decreasing to reach trace amounts after 40 minutes of irradiation. The three other compounds referred as 1, 2 and 7 (see numbering in Table 1) are also detected as soon as irradiation begins; their concentrations rapidly increase during the first thirty minutes and go on increasing at a slower rate until the end of experiment; 1, 2 and 7 are the only by-products remaining in significant amounts in water after 90 minutes of irradiation of procymidone.

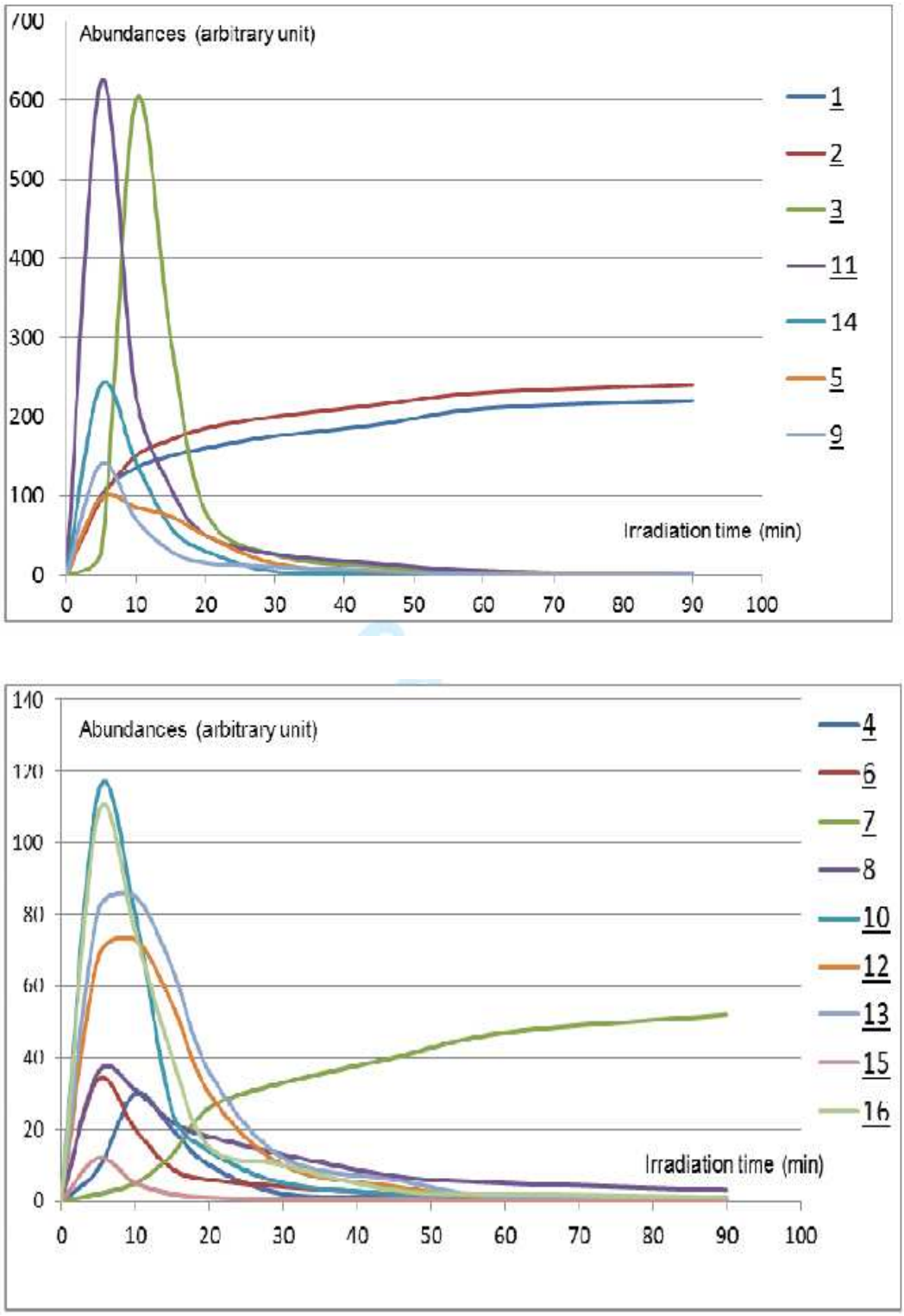

Figure 2. Abundances of photoproducts (arbitrary unit) as a function of the irradiation time (refer to Table 1 for the numbering of compounds). Major and minor abundances are plotted above and below, respectively.

All degradation products were detected with a significant abundance (≥ 2%) in the solution corresponding to an irradiation time of 15 min. This solution was then chosen to perform MS^n experiments on all the photoproducts. The corresponding chromatogram is displayed in Figure 3. Peaks that are not numbered correspond to compounds that are detected in the non-irradiated reference solution of procymidone (corresponding to t=0), which has undergone the same sample preparation process. Only the compounds detected with a signal to noise ratio higher than 10 were investigated. A few articles report the analysis of procymidone using LC-MS coupling with an ESI source in positive mode [14, 23, 24]. We did not succeed in detecting procymidone in LC-MS whatever the device used: HPLC-Q-TOF and nanoLC-FT-ICR. Nevertheless, the comparison of the total ionic currents of the photoproducts in the chromatograms of the irradiated solutions with that of procymidone in the reference solution suggests that more than 90% of products are detected by GC-MS.

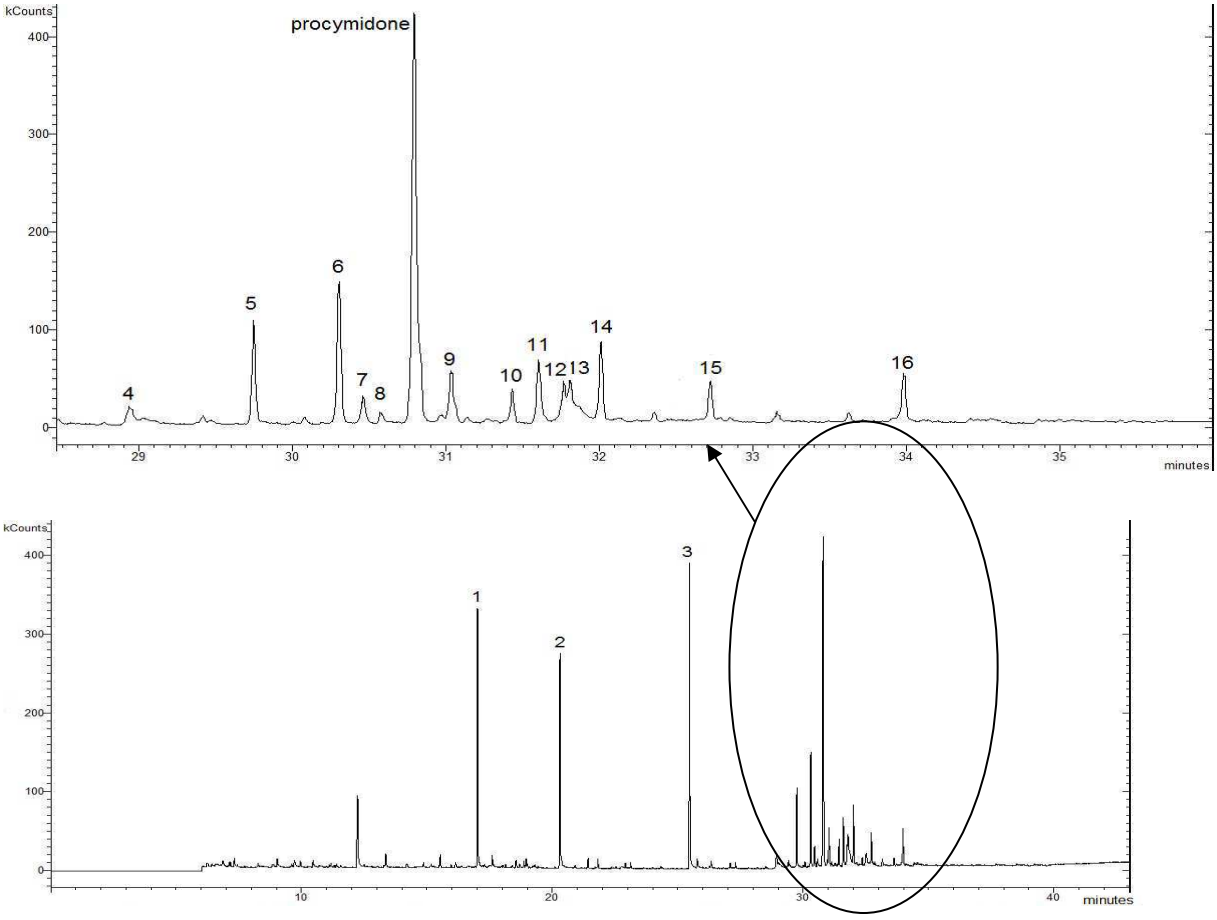

Figure 3. Chromatogram (EI mode) of an aqueous solution of procymidone at 5 mg L^{-1} irradiated for 15 min. Non-numbered peaks correspond to compounds also detected in the non-irradiated solution.

Molecular weights of the photoproducts of procymidone were easily determined. For each compound, the heavier ion (often also the most abundant one) in the CI mass spectrum was first assumed to correspond to the MH^+ pseudo molecular ion. This assumption was systematically confirmed by the presence of an ion at m/z = M (assumed to correspond to $M^{+\cdot}$) in significant abundance in the EI spectrum. Molecular weights are reported in Table 1.

According to literature data devoted to the photolysis of chlorinated compounds, the loss of the chlorine atom under irradiation often constitutes the first step of the degradation process [25-27]. In the case of procymidone, the isotopic distributions observed for $M^{\cdot+}$ and MH^+ ions of photoproducts show that chlorine atoms were not removed by photolysis in any case.

Compounds 1 and 2 were identified as 1,3-dichloro-5-isocyanatobenzene and 3,5-dichlorobenzenamine, respectively, with probabilities greater than 95% according to the NIST spectral database so that no particular structural investigation was carried out [28]. Compounds 6, 9, 11, 14 and 15 have the same nominal molecular weight (MW = 283 amu for the major isotopomer including two ^{35}Cl atoms) as procymidone and were assumed to be isomers of the latter. A mechanism has been suggested (see Figure 4) to rationalize isomerization of procymidone under irradiation. The TD-DFT and CC2 calculations reveal that the first excited state of procymidone corresponds to a triplet spin state with an excitation from the dichlorophenyl group to the two C=O groups (Figure 1). Consequently, it can be considered that the oxygen atoms constitute the most favorable ionization sites of procymidone. In the gas phase, electron ionization of a carbonyl function is followed by the heterolytic cleavage of the bond(s) in alpha; this is referred as alpha cleavage by mass spectrometrists [29]. We postulated that the same alpha cleavage occurs in aqueous solution and is accompanied by the aperture of the strained three-center ring. This leads to a distonic ion displayed in the form of three mesomeric structures referred as a, b and c at the left side of Figure 4. Like in mass spectrometry, we considered that the reactivity induced by the radical should be greater than that induced by the charge, the latter being furthermore stabilized by surrounding water molecules in the present experiment. In aqueous solution, the radical can react with a water molecule to abstract a hydrogen atom or a hydroxyl radical. Both cases were considered from each mesomeric form to provide six structures that may likely cyclize to lead to carbocations better stabilized by inductive and mesomeric effects. The cyclized structures are referred as a_1, a_2, b_1, b_2, c_1 and c_2 in Figure 4. In pure water, those six even

Table 1. Molecular weights, retention times, relative abundances after 15 min of irradiation and main MS^n transitions recorded in GC-MS with both CI and EI ionization modes for photolysis products of procymidone. Suggested structures based on mass spectra interpretation are given in the right hand column.

	Molecular weight	Retention time (min)	Relative abundance[a]	Main transitions in CI-MS^n (m/z)	Main transitions in EI-MS^n (m/z)	Chemical structure proposed
1	187	17.00	11.5	188 → 160 (-28) 188 → 153 (-35) 153 → 125 (-28) 125 → 90 (-35)	187 → 159 (-28) 159 → 124 (-35) 124 → 97 (-27)	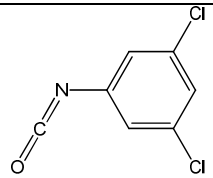
2	161	20.27	10.3	162 → 127 (-35) 127 → 126 (-1) 126 → 100 (-26)	161 → 134 (-27) 134 → 99 (-35) 161 → 126 (-35)	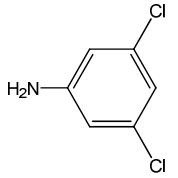
3	231	25.45	12.6	232 → 162 (-70) 162 → 127 (-35)	231 → 187 (-44) 187 → 152 (-35) 231 → 161 (-70) 161 → 126 (-35)	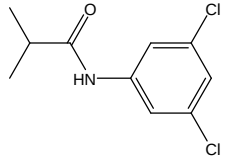
4	285	28.80	1.7	286 → 258 (-28) 258 → 230 (-28) 230 → 202 (-28)	285 → 257 (-28) 257 → 187 (-70) 187 → 152 (-35) 187 → 145 (-42) 145 → 110 (-35)	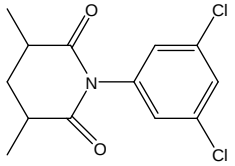

5	273	29.71	5.9	274 → 256 (-18) 256 → 228 (-28) 274 → 246 (-28) 246 → 218 (-28)	273 → 245 (-28) 245 → 161 (-84) 161 → 126 (-35)	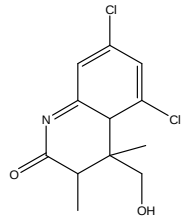
6	283	30.26	2.3	284 → 186 (-98) 284 → 256 (-28) 256 → 238 (-18) 238 → 221 (-28) 221 → 181 (-40) 181 → 165 (-18)	283 → 255 (-28) 255 → 254 (-1) 254 → 226 (-28) 226 → 191 (-35)	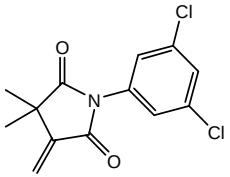
7	287	30.42	1.4	288 → 270 (-18) 270 → 242 (-28) 242 → 240 (-2)	287 → 259 (-28) 259 → 189 (-70) 189 → 161 (-28) 161 → 126 (-35)	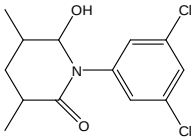
8	271	30.54	1.9	272 → 256 (-16) 272 → 244 (-28)	271 → 256 (-15) 256 → 228 (-28) 228 → 200 (-28) 200 → 265 (-35)	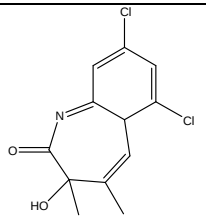
9	283	30.99	5.6	284 → 256 (-28) 256 → 241 (-15) 241 → 203 (-38) 203 → 185 (-18) 203 → 158 (-45) 158 → 130 (-28)	283 → 268 (-15) 268 → 240 (-28) 240 → 205 (-35) 283 → 241 (-42) 241 → 213 (-28) 213 → 178 (-35)	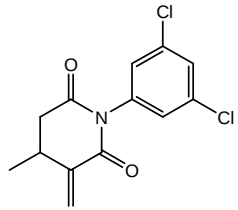

10	299	31.39	5.5	300 → 258 (-42) 258 → 240 (-18) 258 → 230 (-28) 230 → 186 (-44)	299 → 282 (-17) 299 → 257 (-42) 257 → 256 (-1) 256 → 221 (-35)	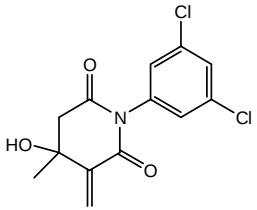
11	283	31.57	15.3	284 → 256 (-28) 256 → 238 (-18) 256 → 228 (-28) 228 → 193 (-35) 193 → 178 (-15) 193 → 158 (-35)	283 → 268 (-15) 268 → 240 (-28) 240 → 205 (-35)	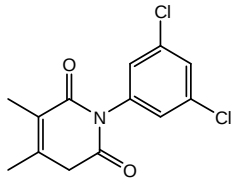
12	315	31.73	5.3	316 → 298 (-18) 298 → 270 (-28) 270 → 242 (-28)	315 → 300 (-15) 300 → 272 (-28) 272 → 244 (-28) 315 → 298 (-17) 298 → 270 (-28) 270 → 242 (-28)	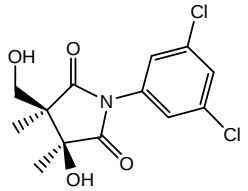
13	315	31.77	5.3	316 → 298 (-18) 298 → 270 (-28) 270 → 242 (-28)	315 → 300 (-15) 300 → 272 (-28) 272 → 244 (-28) 315 → 298 (-17) 298 → 270 (-28) 270 → 242 (-28)	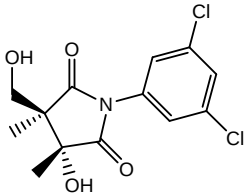

14	283	31.97	9.7	284 → 256 (-28) 256 → 238 (-18) 238 → 203 (-35) 203 → 167 (-36)	283 → 268 (-15) 268 → 240 (-28) 240 → 205 (-35) 283 → 256 (-27) 256 → 228 (-28) 228 → 193 (-35)	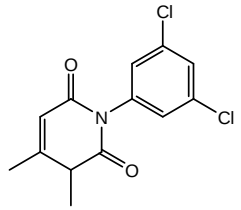
15	283	32.46	0.5	284 → 256 (-28) 256 → 238 (-18) 238 → 223 (-15) 238 → 200 (-38) 200 → 169 (-31) 200 → 154 (-46)	283 → 256 (-27) 256 → 228 (-28) 228 → 193 (-35)	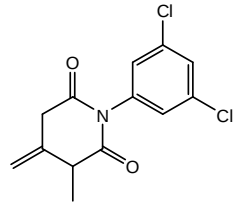
16	281	33.90	5.2	282 → 264 (-18) 264 → 229 (-35)	281 → 253 (-28) 253 → 252 (-1) 252 → 217 (-35) 281 → 229 (-52) 229 → 201 (-28) 201 → 200 (-1) 200 → 165 (-35)	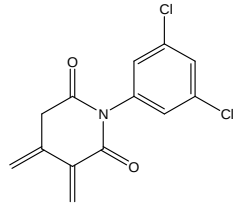

[a] % of the total of all the product abundances

number electrons cations may react each other with a water molecule by capturing either a hydride H^- or a hydroxyl anion OH^-. Considering both hypothesis leads to the twelve structures displayed at the right side of Figure 4. a_{11} and a_{12} result respectively from capture by a_1 of H^- and of OH^-. The same notation is used for structures b_{11}, b_{12}, c_{11}, etc.

They are six photoproducts detected with the same nominal molecular weight (283 amu) than procymidone and with close retention times (ranging from 30.26 to 32.46 min) around that of procymidone (30.8 min). Figure 4 shows that six compounds with the same nominal mass (283) as procymidone (and thus assumed to be isomers of the later) can be formed according to the mechanisms suggested: water loss from a_{12} leads to three isomers, water loss from a_{21} provides two isomers (one of which common with one issued from a_{12}), water loss from b_{12} gives the only five membered ring isomer and water loss from c_{12} leads to two tautomeric forms of isomers issued from a_{12}. Compounds 6, 9, 11, 14 and 15 were assumed to correspond to these five isomers. Their chemical structures were elucidated on the basis of the MS^n experiments performed in the EI mode. For the molecular ion of each structure, the charge has been assumed to be carried by one of the oxygen atoms according to the results of quantum chemistry calculations (see above). As shown in Figure 5, alpha cleavage leads to distonic ions whose reactivity is largely driven by the radical. 6 is the only structure for which the alpha cleavage from $M^{\cdot+}$ leads to a tertiary radical stable enough to permit monoxide elimination prior to radical elimination. 9 corresponds to the only structure that can eliminate $CH_3^{\cdot}$ and CH_2=CH-CH_3 following electron ionization (transitions m/z 283 → m/z 268 and m/z 283 → m/z 241 in Table 1). 11 corresponds to the structure that can only eliminate $CH_3^{\cdot}$ from $M^{\cdot+}$ (transition m/z 283 → m/z 268 in Table 1). 14 corresponds to the structure that can eliminate $CH_3^{\cdot}$ and CH_2=$CH^{\cdot}$ from $M^{\cdot+}$ (transitions m/z 283 → m/z 268 and m/z 283 → m/z 256 in Table 1). Finally, 15 corresponds to the structure that can only eliminate CH_2=$CH^{\cdot}$ from $M^{\cdot+}$ (transition m/z 283 → m/z 256 in Table 1). It is to be noted that $Cl^{\cdot}$ losses are not displayed in Figure 4 because they result from homolytic cleavages under high activation energies that do not contribute to distinguish isomers in the present case.

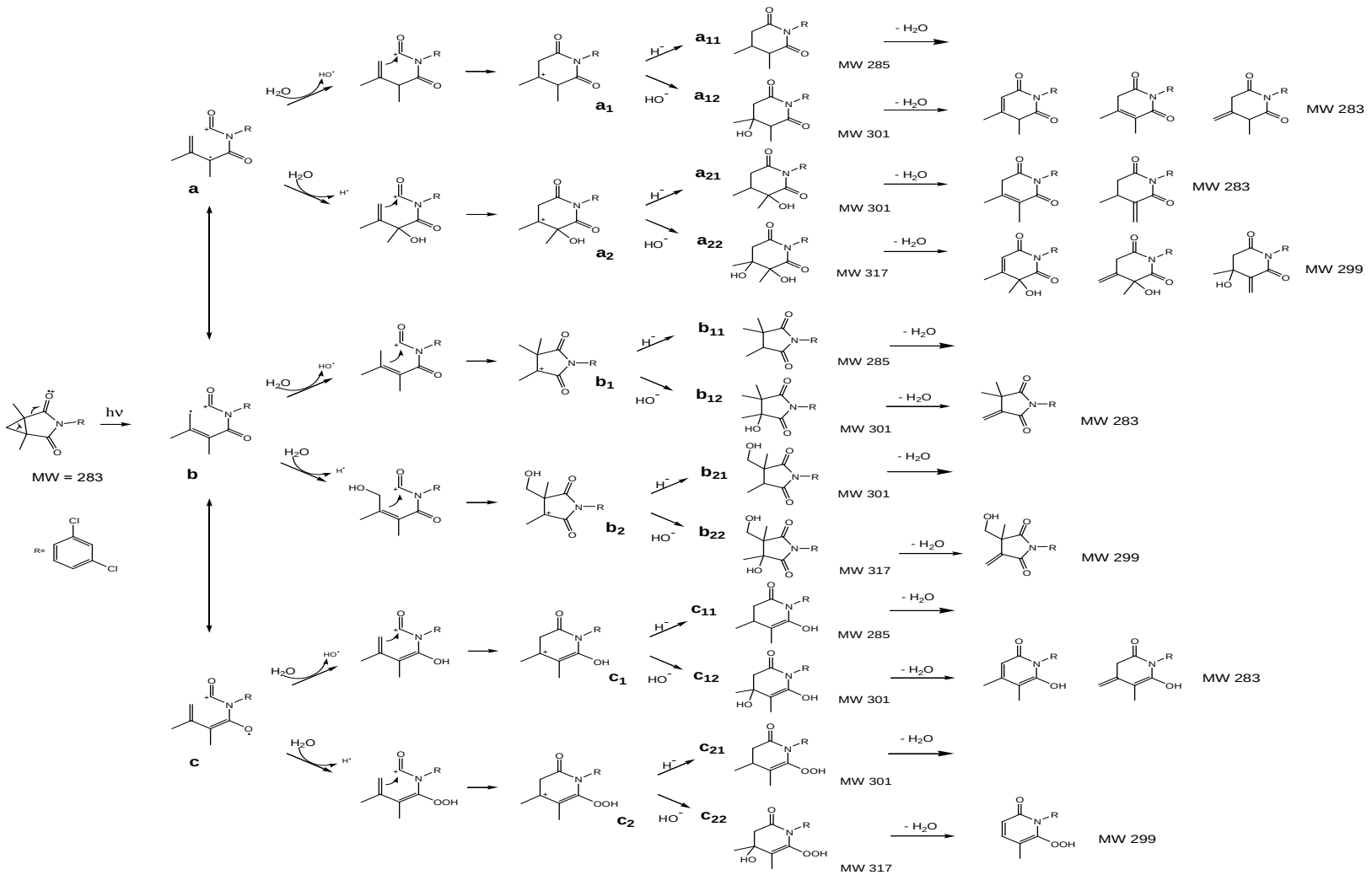

Figure 4. Mechanisms proposed to explain the isomerization of procymidone under irradiation in water

Compound 4 (285 amu, see Table 1) could correspond to one of the structures a_{11}, b_{11} or c_{11}, the latest corresponding to the enolic form of a_{11}, in Figure 4. The fact that only one isomer is detected rather suggests the symmetrical structure displayed in Table 1 whose formation is easily explained by consecutive captures of a hydrogen atom and a hydride ion by ionized procymidone, according to the mechanism detailed in Figure 6. This hypothesis is supported by the fact that the symmetrical structure proposed for 4 is the only one allowing the transitions observed in CI-MS^n (m/z 286 → m/z 258 → m/z 230 → m/z 202); the corresponding mechanisms are given in the supplementary information file, figure SI-2. These three consecutive losses of 28 amu in CI-MS^n are not possible from a_{11}, b_{11} nor c_{11}.

The formation of compound 7 (287 amu, see Table 1) can be rationalized by consecutive additions of a hydrogen atom and a hydride ion on 4 after ionization of the later, by a mechanism analogous to that proposed for the formation of 4 from ionized procymidone (Figure 5). EI-MS^n and CI-MS^n transitions recorded for 7 are rationalized in the figure SI-3. Concerning compound 3 (MW 231, eluted at 25.45 min), the losses of 70 amu in CI-MS^2 and 44 amu in EI-MS^2 suggest that a C_3H_7CO group is bound to the nitrogen atom. The chemical structure including an isopropyl group displayed in Table 1 for 3 may be formed after photoionization of 4, as proposed in Figure 6. Kinetics data show that the formation of 7 and 3 is accompanied by the disappearance of 4 (see above); it strongly supports the hypothesis according which 3 and 7 would result from photo-ionization of 4. EI-MS^n and CI-MS^n transitions recorded for 3 are rationalized in the figure SI-3. The dissociation pathways of 3 in EI-MS^n lead to ions at m/z 187 and m/z 161 which correspond respectively to the compounds 2 and 1 ionized.

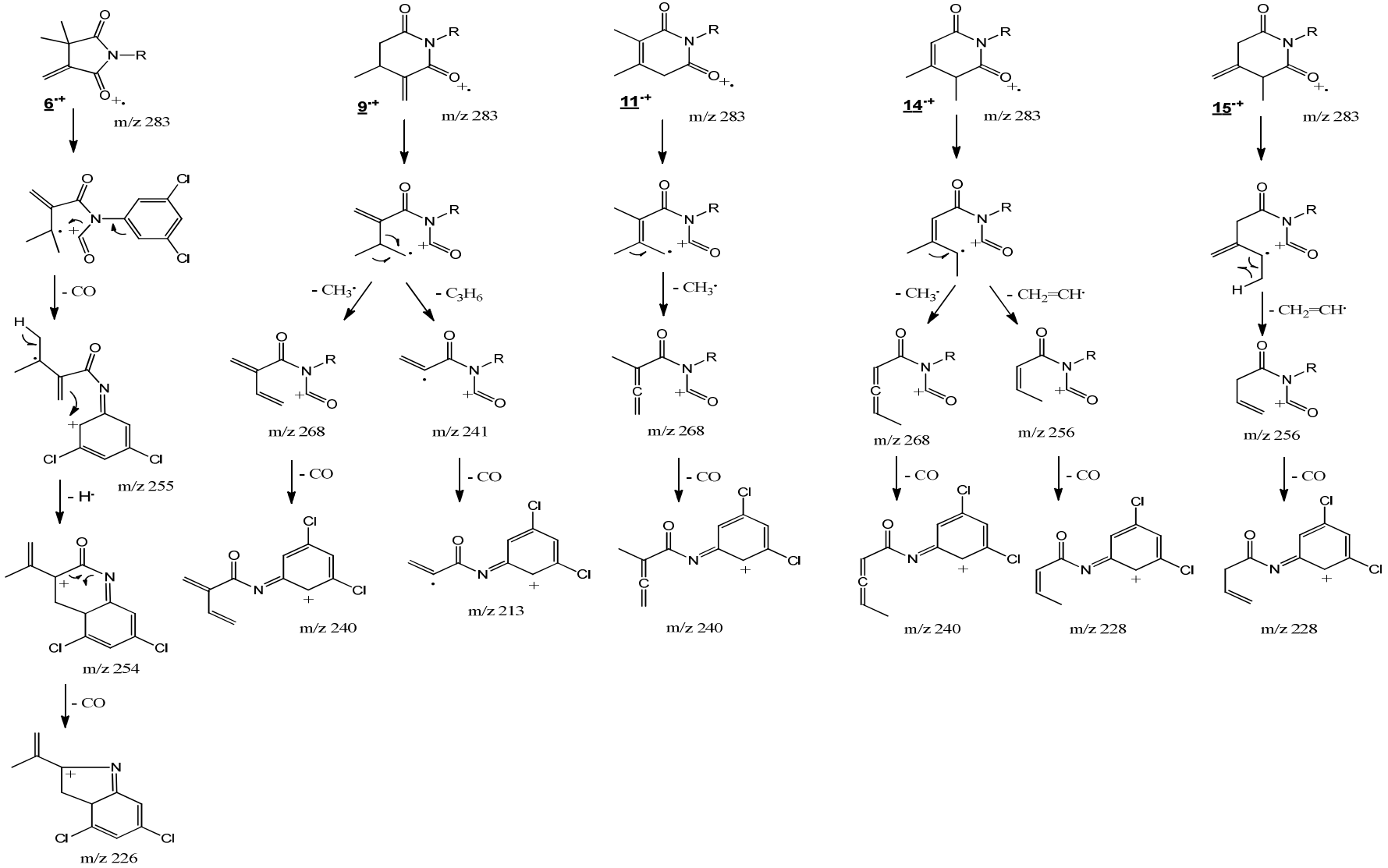

Figure 5. Dissociation pathways in EI-MS^n of compounds 6, 9, 11, 14 and 15.

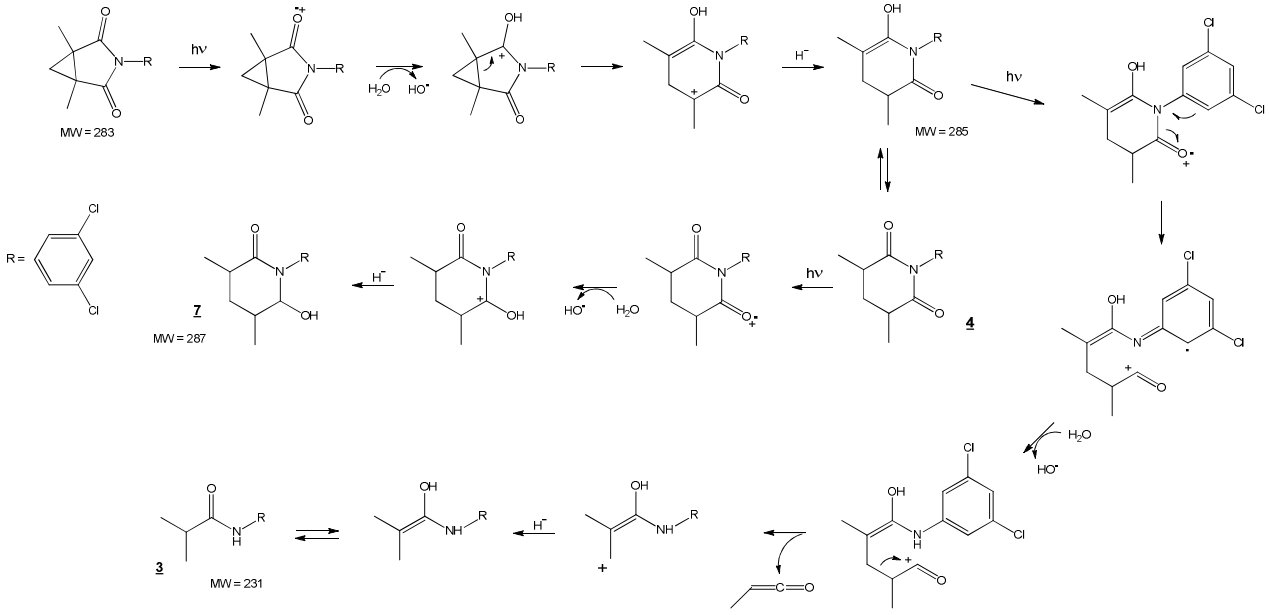

Figure 6. Mechanisms proposed to explain the formation of compounds 3, 4 and 7 from irradiated procymidone in water

Compound 5 weights 273 amu; its formation likely results from HO· addition on ionized procymidone followed by CO elimination and hydride addition, as displayed in Figure 7. Figure 6 shows that three isomers weighting 273 amu can be formed from structures a, b and c (see Figure 4) according to such a mechanism. The consecutive transitions m/z 273 → m/z 245 → m/z 161 in CI-MS^3 suggest that the detected isomer is that issued from structure b in Figure 7, based on the dissociation pathways proposed in the supplementary information file, figure SI-4. Compound 8 weights 271 amu; its formation likely results from HO· addition on ionized procymidone followed by CO elimination and proton elimination, as displayed in Figure 7. Five isomers with a nominal mass of 271 can be formed from structures a, b and c according to such a mechanism. The only isomer allowing consecutive losses of a radical methyl and two carbon monoxide molecules in EI-MS^4 (m/z 271 → m/z 256 → m/z 228 → m/z 200) is one of those issued from structure a in Figure 7 (see Table 1). Dissociation pathways suggested to explain the recorded EI-MS^n and CI-MS^n transitions for 8 are given in the supplementary information file, figure SI-5.

Compound 10 (MW 299 amu) was detected at 31.39 min. Based on the reactions in Figure 4, five isomers weighting 299 amu can be easily formed from photo ionized procymidone. The CI-MS^n transitions, especially m/z 300 → m/z 258 and m/z 258 → m/z 240 (consecutive losses of CH_2=CO and H_2O) allowed to conclude in favor of the structure proposed in Table 1 (one of the structures issued from a_{22} in Figure 4), according to the dissociation pathways provided in the supplementary information file, figure SI-6. Compounds 12 and 13 have the same weight of 315 amu, a weight which, compared with that of procymidone (MW 283), may likely correspond to the addition of two hydroxyl groups and the loss of H_2. Figure 4 displays three isomers weighting 317 amu resulting from the addition of two hydroxyl groups on procymidone: a_{22}, b_{22} and c_{22}. Among them, only b_{22} can easily eliminate H_2 through oxidation of an alcohol function into an aldehyde one. Compounds 12 and 13 provide exactly the same transitions in EI-MS^n and CI-MS^n experiments (see Table 1) and have very close retention times (31.73 and 31.77 minute, respectively). This led us to consider 12 and 13 as two diastereoisomers of b_{22} (see Figure 4) whose formation under irradiation would be explained by the mechanism suggested in Figure 8. The fact that both compounds are formed in equal ratios is in good agreement with this mechanism. The EI-MS^n and CI-MS^n transitions perfectly match the structures proposed in Table 1 for 12 and 13; the corresponding dissociation pathways are displayed in the supplementary information file, figure SI-7.

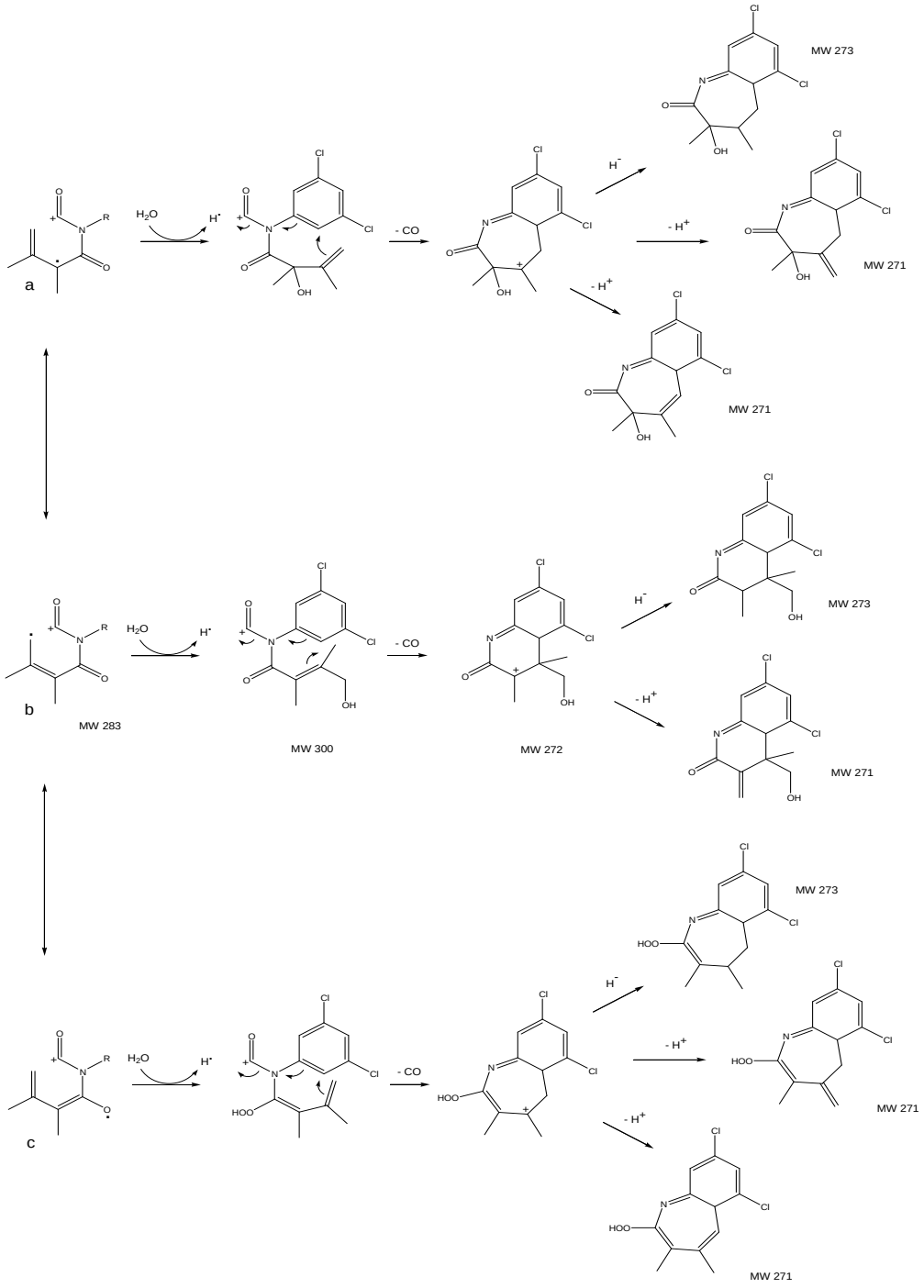

Figure 7. Mechanisms proposed for the formation of compounds weighting 271 and 273 amu from irradiated procymidone in water (structures **a**, **b** and **c** are mesomeric forms resulting from the aperture of the five-membered ring of ionized procymidone, see figure 4)

Compound 16 (281 amu) was assumed to result from dehydrogenation of procymidone. A mechanism involving consecutive losses of $H^{\cdot}$ and H^{+} from ionized procymidone has been proposed in Figure 8. Mechanisms corresponding to the EI-MS^n and CI-MS^n transitions observed for 16 are proposed in the supplementary information file, figure SI-8.

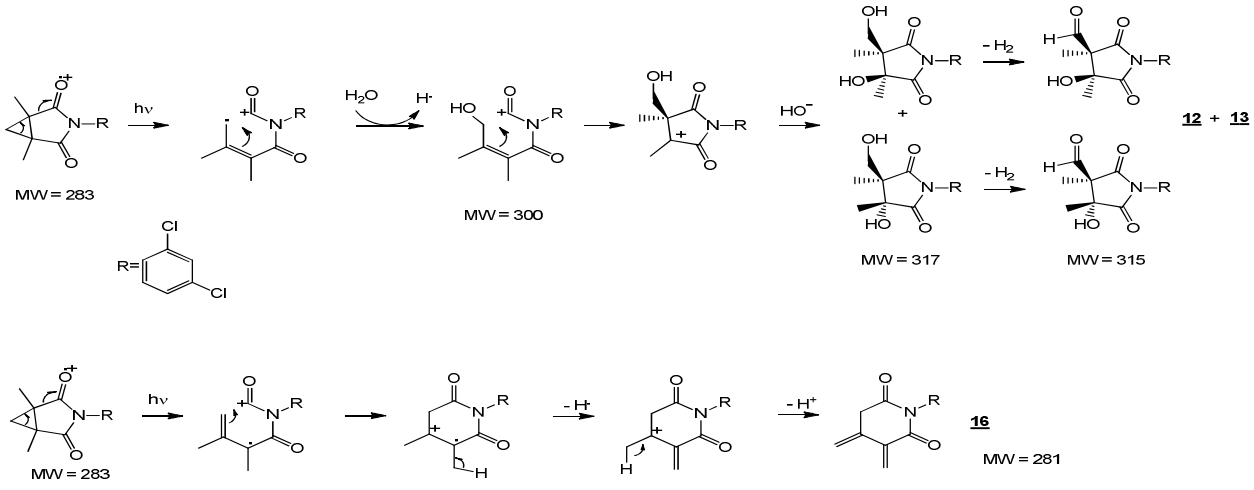

Figure 8. Mechanisms proposed to explain the formation of compounds 12, 13 and 16 from irradiated procymidone in water

3.2. Toxicity prediction

In order to evaluate the toxicity of procymidone and its photodegradation products, a toxicity simulation using *in silico* tools was performed. We chose in this study only to report the significant results, i.e. oral rat LD50 toxicity (Figure 9).

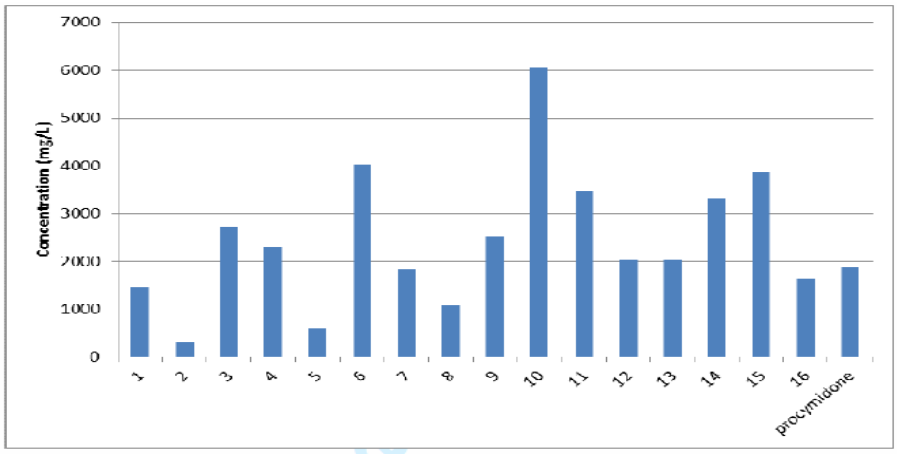

Figure 9. Oral rate LD50 toxicity (mg/L) of procymidone and photoproducts

We observed that the procymidone and all its identified photodegradation products exhibit a developmental toxicity. Procymidone was reported in the literature as being a competitive antagonist to the androgen binding to their receptor causing thereby development in male offspring [30]. The effects on reproduction and the induction of testicular tumors in a long term rat study can be explained by the effects of procymidone on the endocrine system [31]. A recent study stated that this dicarboximide fungicide reduces weights of the prostate and seminal vesicle [32]. Thus the procymidone developmental toxicity prediction through the QSAR simulation was coherent with the literature data. It is to be noticed that all degradation products generated through procymidone photolysis kept the 3,5-dichloroaniline (3,5-DCA) on the molecule skeleton. The U. S. Environmental protection agency treats 3,5-DCA as a cancer-causing chemical based on the carcinogenicity of the structurally related compound p-chloroaniline [33]. This metabolite was reported as the final product of the degradation metabolic pathway of dicarboximidic fungicides [14]. It also was assigned as more toxic and persistent than one of its parent: vinclozolin. In particular, toxicity of 3,5-DCA has been shown to be related to anti-androgenic activity [34]. The hypothesis of developmental toxicity potential related to the 3,5-DCA common part of all degradation products is then postulated.

Procymidone is of low acute toxicity by the oral route. Its rat and mice oral LD50 was reported in the literature to be >5000 mg/kg [31]. The displayed value of oral rat LD50 by the simulation software cannot be taken into consideration because the prediction does not represent an external prediction as procymidone was present in the training set. We observed a low acute toxicity as

this endpoint with values which varied for the several degradation products between 1000 and approximately 6000 mg/kg except for compounds 2 and 5 for which those values were estimated at 302 and 590 mg/kg, respectively, thus considered as moderately toxic. The compound 2, the 3,5-DCA, was reported also in the literature as of moderate acute toxicity in mice in coherence with the QSAR predicted Rat LD50 [35]. Based on the overall effects on renal function and morphology, Lo et al. [36] found that 3,5-DCA is the most nephrotoxic of the dichloroanilines and that it can cause acute kidney toxicity in rats which may justify the predicted LD50.

4. Conclusion

The UV-visible photo degradation of procymidone in water led to sixteen photoproducts of significant abundance, three of them remaining persistent after 90 minutes of irradiation. Chemical structures were proposed on the basis of multistage collision induced experiments. Structures were assigned also considering kinetics data and the likely evolution of irradiated species in aqueous phase. The results on toxicity estimation showed that possible developmental toxicity could be generated through the photolytic process of procymidone; 3,5-dichloroaniline, one of the persistent products might be responsible for this potential toxicity. *In vitro* bioassay should then be achieved to further investigate the toxicological behavior of those degradates.

5. References

[1] J. Martins, C. Esteves, A. Limpo-Faria, P. Barros, N. Ribeiro, T. Simoes, M. Correia, C. Delerue-Matos. Analysis of six fungicides and one acaricide in still and fortified wines using solid-phase microextraction-gas chromatography/tandem mass spectrometry. Food Chem. 2012, 132, 630.

[2] E. Pose-Juan, B. Cancho-Grande, R. Rial-Otero, J. Simal-Gandara. The dissipation rates of cyprodinil, fludioxonil, procymidone and vinclozoline during storage of grape juice. Food Control 2006, 17, 1012.

[3] E. COMMISSION. Vol. 9, Journal officiel de l'Union européenne, 2010.

[4] Y. Souissi, S. Bourcier, S. Bouchonnet, C. Genty, M. Sablier. Estrone direct photolysis: By-product identification using LC-Q-TOF. Chemosphere 2012, 87, 185.

[5] G. D. Charles, H. L. Kan, M. R. Schisler, B. Bhaskar Gollapudi, M. Sue Marty. A comparison of in vitro and in vivo EDSTAC test battery results for detecting antiandrogenic activity. Toxicol. Appl. Pharmacol. 2005, 202, 108.

[6] M. B. Rosen, V. S. Wilson, J. E. Schmid, L. E. Gray. Gene expression analysis in the ventral prostate of rats exposed to vinclozolin or procymidone. Reprod. Toxicol. 2005, 19, 367.

[7] E. Union. 3600/92DE. Official Journal of the European Union 1992, 4.

[8] K. Inawaka, M. Kawabe, S. Takahashi, Y. Doi, Y. Tomigahara, H. Tarui, J. Abe, S. Kawamura, T. Shirai. Maternal exposure to anti-androgenic compounds, vinclozolin, flutamide and procymidone, has no effects on spermatogenesis and DNA methylation in male rats of subsequent generations. Toxicol. Appl. Pharmacol. 2009, 237, 178.

[9] O. o. P. P. a. T. Substances. Report of the Food Quality Protection Act (FQPA) Tolerance Reassessment Progress and Risk Management Decision (TRED) for Procymidone. United States Environmental Protection Agency 2005.

[10] A. Kiss, S. Rapi, C. Csutoras. GC/MS studies on revealing products and reaction mechanism of photodegradation of pesticides. Microchem. J. 2007, 85, 13.

[11] H. D. Burrows, L. M. Canle, J. A. Santaballa, S. Steenken. Reaction pathways and mechanisms of photodegradation of pesticides. J. Photoch. Photobio. B 2002, 67, 71.

[12] K. Hustert, P. N. Moza. Photochemical degradation of dicarboximide fungicides in the presence of soil constituents. Chemosphere 1997, 35, 33, 17

[13] W. Schwack, B. Bourgeois, F. Walker. Fungicides and photochemistry photodegradation of the dicarboximide fungicide procymidone. Chemosphere 1995, 31, 4033.

[14] A. Vanni, R. Gamberini, A. Calabria, P. Nappi. Determination and identification of metabolites of the fungicides Iprodione and Procymidone in compost. Chemosphere 2000, 41, 1431.

[15] A. G. Frenich, J. L. M. Vidal, M. M. Galera. Use of the cross-section technique linkedwith multivariate calibration methods to resolve complex pesticide mixtures. Anal. Chem. 1999, 71, 4844.

[16] S. Grimme. Accurate description of van der Waals complexes by density functional theory including empirical corrections. J. Comput. Chem. 2004, 25, 1463.

[17] S. Grimme, J. Antony, S. Ehrlich, H. Krieg. A consistent and accurate ab initio parametrization of density functional dispersion correction (DFT-D) for the 94 elements HPu. J. Chem. Phys. 2010, 132.

[18] U. o. K. a. F. K. GmbH. in TURBOMOLE GmbH (Ed.: www.turbomole.com), 2012.

[19] C. Hattig, F. Weigend. CC2 excitation energy calculations on large molecules using the resolution of the identity approximation. J. Chem. Phys. 2000, 113, 5154.

[20] C. Clavaguera, F. Piuzzi, J.-P. Dognon. Electronic spectrum of tryptophanphenylalanine. A correlated ab Initio and time-dependent density functional theory study. J. Phys. Chem. B 2009, 113, 16443.

[21] U. S. E. P. Agency. in Risk Management Sustainable Technology (Ed.: http://www.epa.gov/ordntrnt/ORD/NRMRL/std/qsar/qsar.html), 2012.

[22] L. H. Hall, B. Mohney, L. B. Kier. The electrotopological state - structure information at the atomic level for molecular graphs. J. Chem. Inf. Comput. Sci. 1991, 31, 76.

[23] B. Gilbert-López, J. F. García-Reyes, A. R. Fernández-Alba, A. Molina-Díaz. Evaluation of two sample treatment methodologies for large-scale pesticide residue analysis in olive oil by fast liquid chromatography–electrospray mass spectrometry. J. Chromatogr. A 2010, 1217, 3736.

[24] T. Cajka, J. Hajslova, O. Lacina, K. Mastovska, S. J. Lehotay. Rapid analysis of multiple pesticide residues in fruit-based baby food using programmed temperature vaporiser injection–low-pressure gas chromatography–high-resolution time-of-flight mass spectrometry. J. Chromatogr. A 2008, 1186, 281, 18

[25] T. Alapi, K. Van Craeynest, H. Van Langenhoeve, J. Dewulf, A. Dombi. Direct VUV photolysis of chlorinated methanes and their mixtures in a nitrogen stream. Chemosphere 2007, 66, 139.

[26] T. Alapi, A. Dombi. Direct VUV photolysis of chlorinated methanes and their mixtures in an oxygen stream using an ozone producing low-pressure mercury vapour lamp. Chemosphere 2007, 67, 693.

[27] S. Coffinet, A. Rifai, C. Genty, Y. Souissi, S. Bourcier, M. Sablier, S. Bouchonnet. Characterization of the photodegradation products of metolachlor: structural elucidation, potential toxicity and persistence. J. Mass Spectrom. 2012, 47, 1582.

[28] NIST/EPA/NIH. NIST Mass Spectral Library. National Institute of Standard and Technology 2005, DC.

[29] F. W. McLafferty. Interpretation of Mass Spectra- 3rd edition, University Science Books - Mill Valley, California 1980.

[30] J. Ostby, W. Kelce, C. Lambright, C. Wolf, P. Mann, J. L. Gray. The fungicide procymidone alters sexual differentiation in the male rat by acting as an androgen-receptor antagonist in vivo and in vitro. Toxicol. Ind. Health 1999, 15, 80.

[31] M. F. Cengiz, M. Certel, B. Karakas, H. Göçmen. Residue contents of captan and procymidone applied on tomatoes grown in greenhouses and their reduction by duration of a pre-harvest interval and post-harvest culinary applications. Food Chem. 2007, 100, 1611.

[32] P. R. Jacobsen, M. Axelstad, J. Boberg, L. K. Isling, S. Christiansen, K. R. Mandrup, L. O. Berthelsen, A. M. Vinggaard, U. Hass. Persistent developmental toxicity in rat

offspring after low dose exposure to a mixture of endocrine disrupting pesticides. Reprod. Toxicol. 2012, 34, 237.

[33] USEPA. Reregistration Eligibility Decision (RED) Iprodione. Prevention, Pesticides and Toxic Substances. EPA738-R -98-019 1998, November 1998.

[34] J. B. Lee, H. Y. Sohn, K. S. Shin, J. S. Kim, M. S. Jo, C. P. Jeon, J. O. Jang, J. E. Kim, G. S. Kwon. Microbial biodegradation and toxicity of vinclozolin and its toxic metabolite 3,5- dichloroaniline. J. Microbiol. Biotechn. 2008, 18, 343.

[35] F. WHO. Pesticide Residues in Food 2007: Joint FAO-WHO Meeting on Pesticide Residues. WHO, Food and Agriculture Organization of the United Nation 2007.

[36] H.-H. Lo, P. I. Brown, G. O. Rankin. Acute nephrotoxicity induced by isomeric dichloroanilines in Fischer 344 rats. Toxicology 1990, 63, 215.

Supplementary information

Table SI-1. Nature of the first excited states of procymidone at CC2 and TD-DFT levels

State	CC2/TZVPP	TD-DFT B3LYP-D3/TZVPP	Nature / Molecular Orbitals
T1	4.103	3.508	dichlorophenyl → C=O
T2	4.703	4.218	dichlorophenyl → C=O
T3	4.744	4.294	dichlorophenyl → C=O

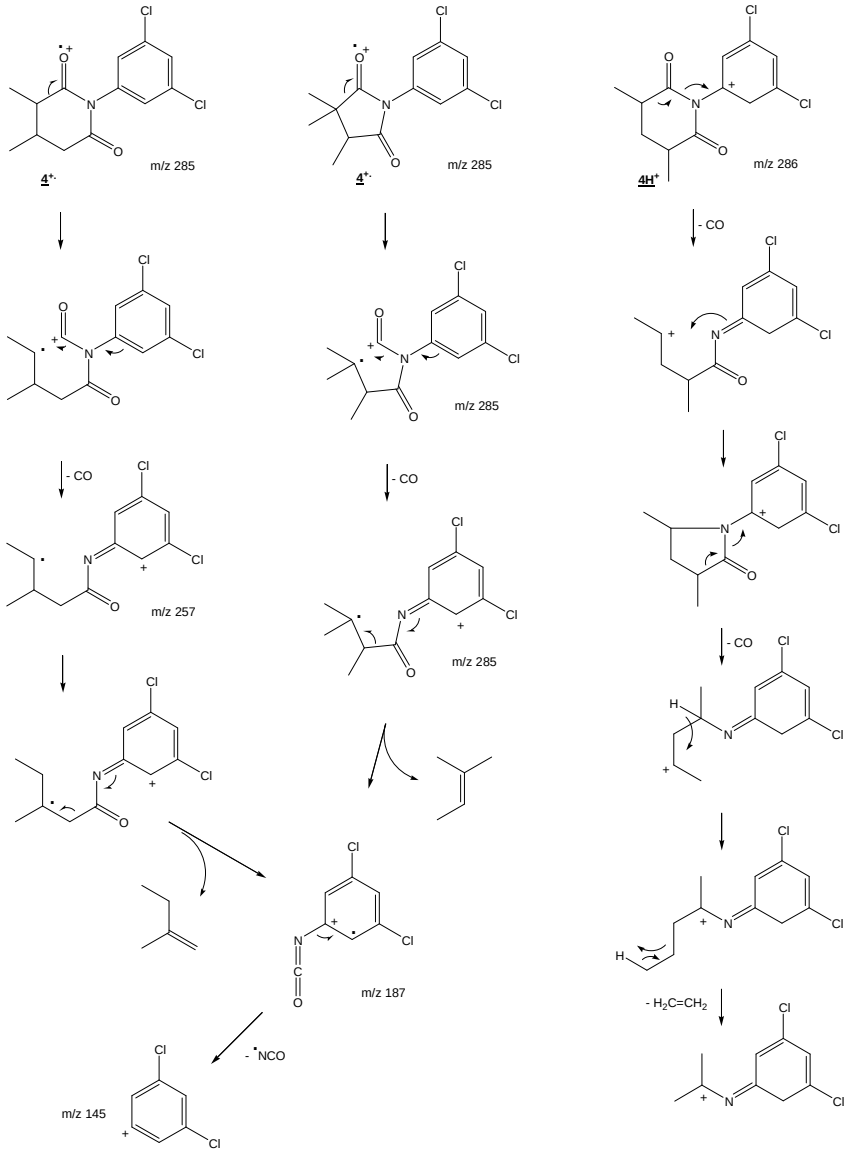

Figure SI-2. Dissociation pathways in EI-MS^n (left hand) and CI-MS^n (right hand) of compound 4

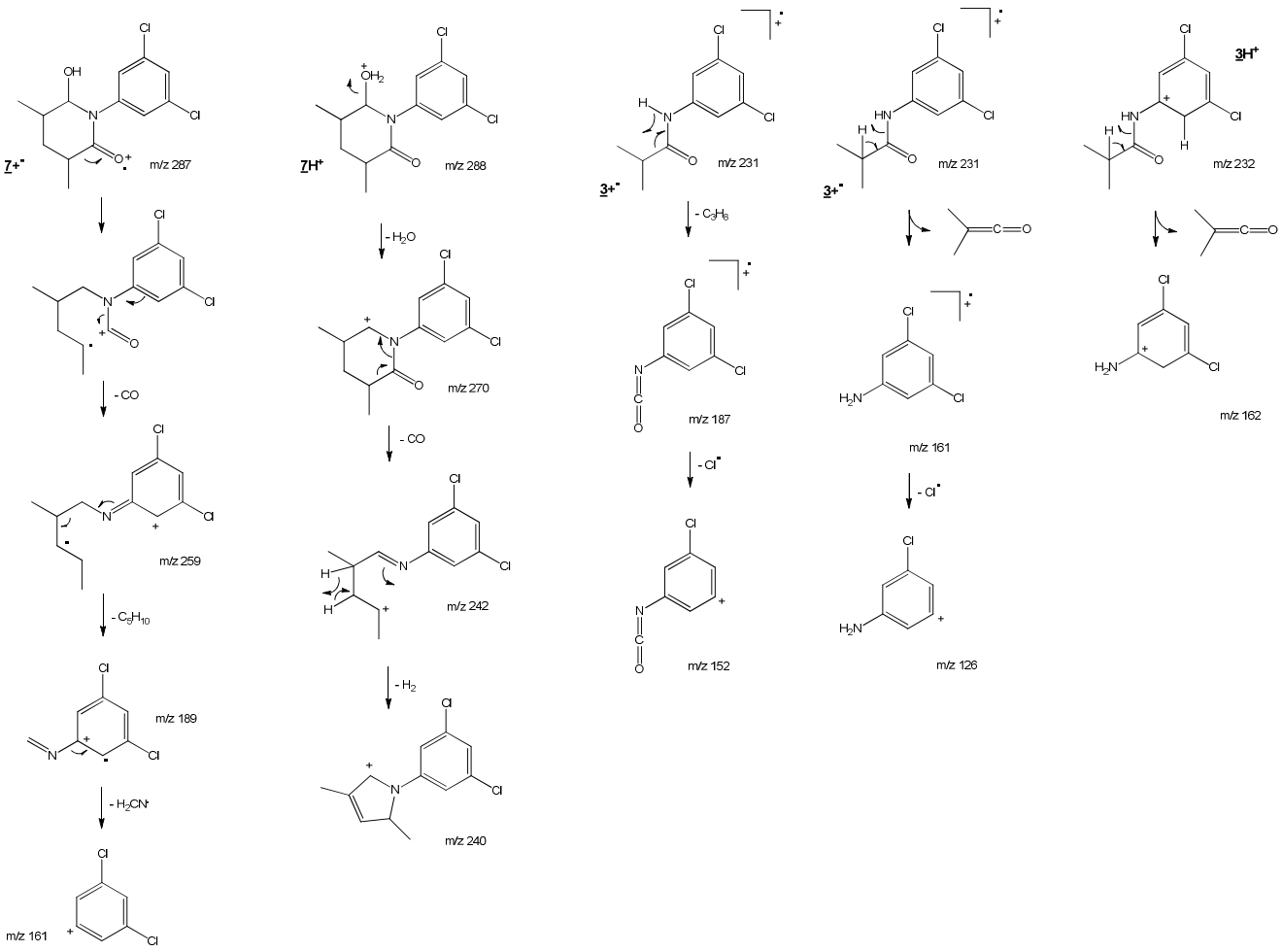

Figure SI-3. Dissociation pathways in EI-MS^n and CI-MS^n of compounds 7 (left hand) and 3 (right hand)

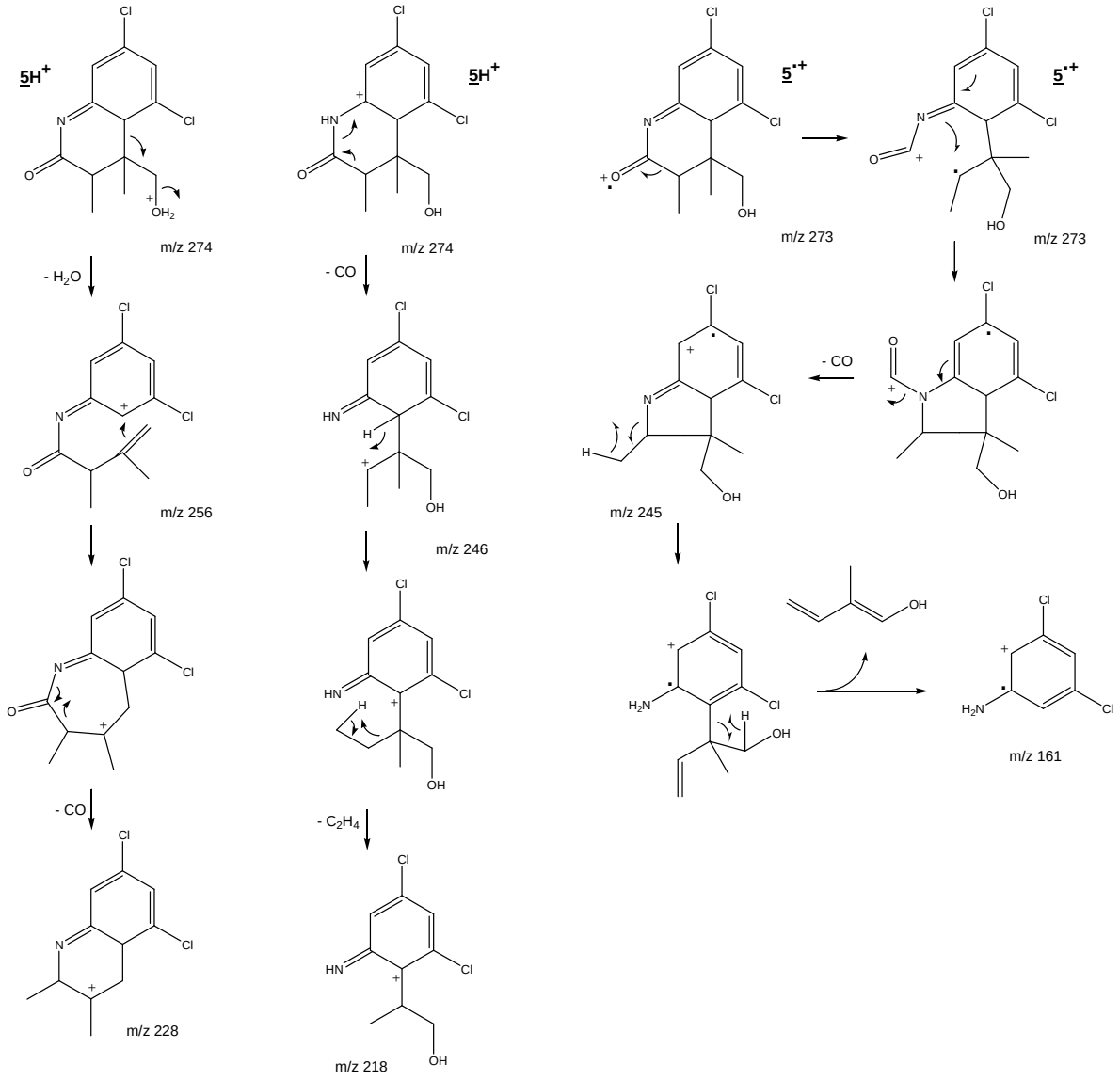

Figure SI-4. Dissociation pathways in CI-MS^n (left hand) and EI-MS^n (right hand) of compound 5

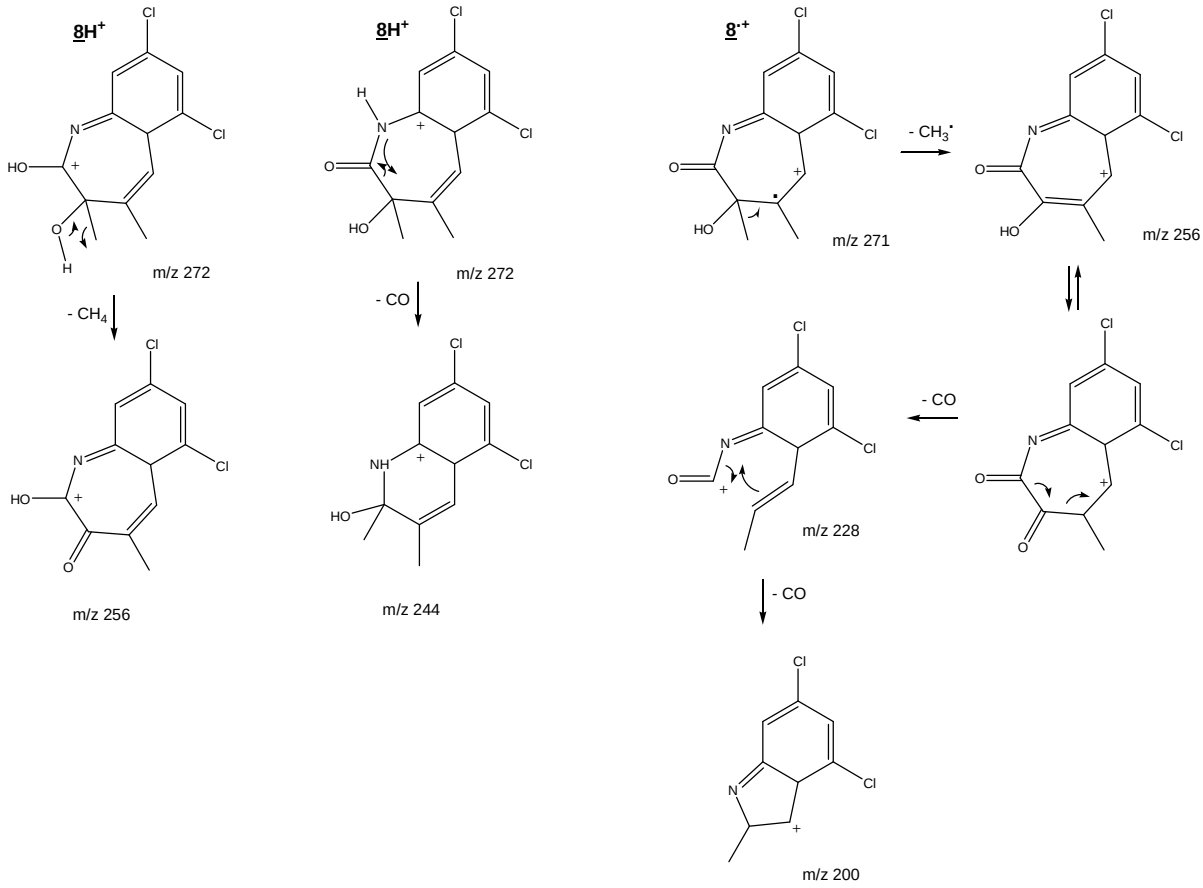

Figure SI-5. Dissociation pathways in CI-MS^n (left hand) and EI-MS^n (right hand) of compound 8

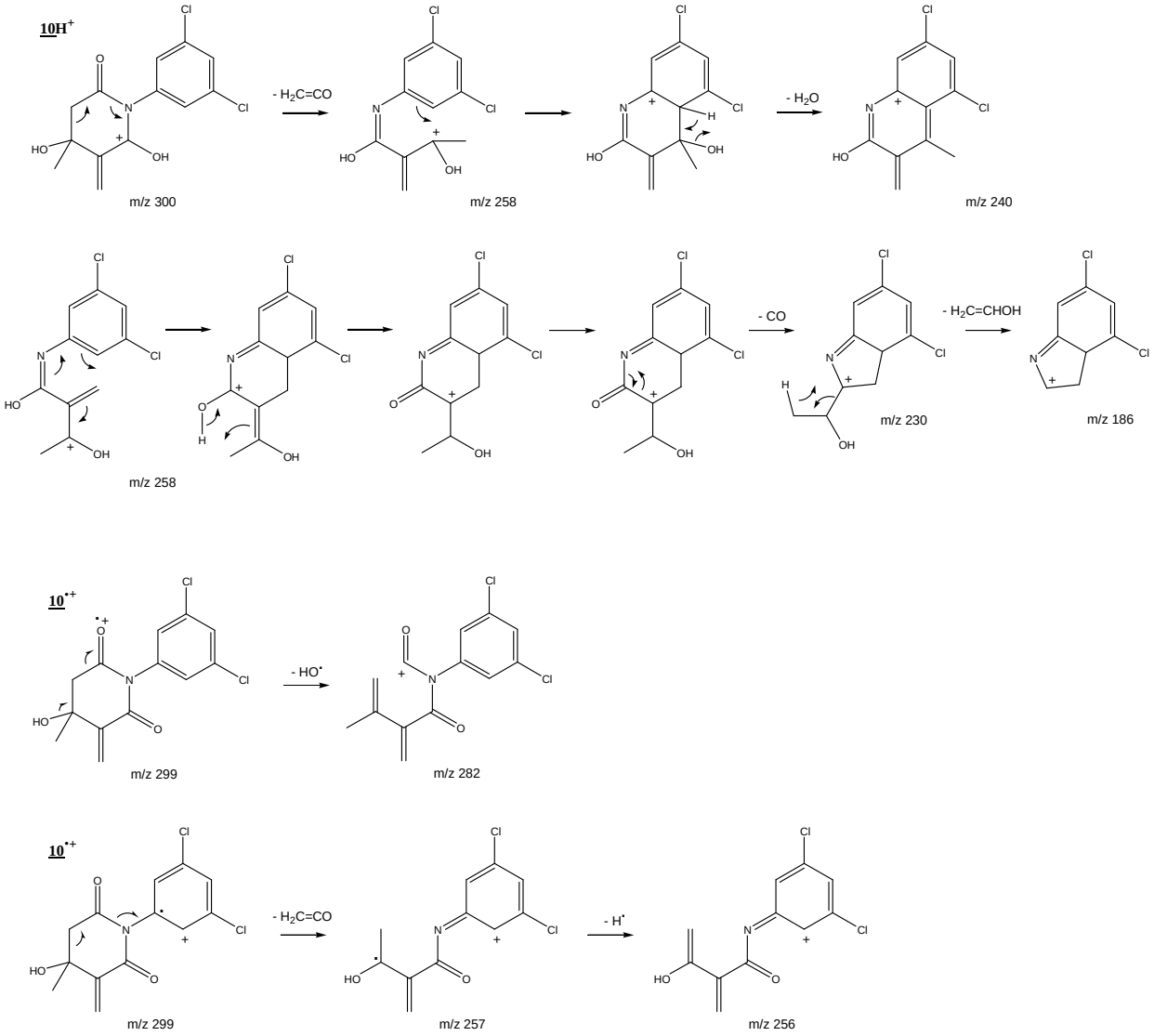

Figure SI-6. Dissociation pathways in CI-MS^n (top) and EI-MS^n (bottom) of compound 10

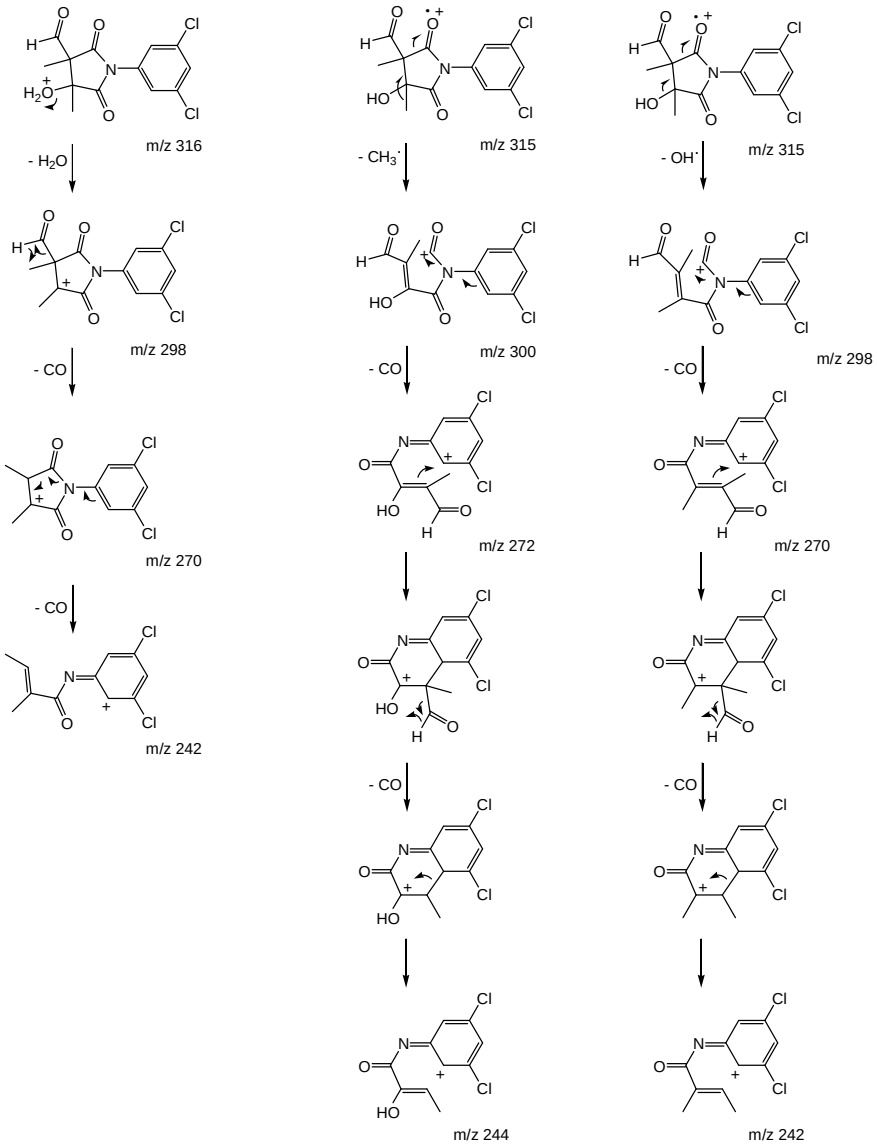

Figure SI-7. Dissociation pathways in CI-MS^n (left hand) and EI-MS^n (right hand) of compounds 12 and 13

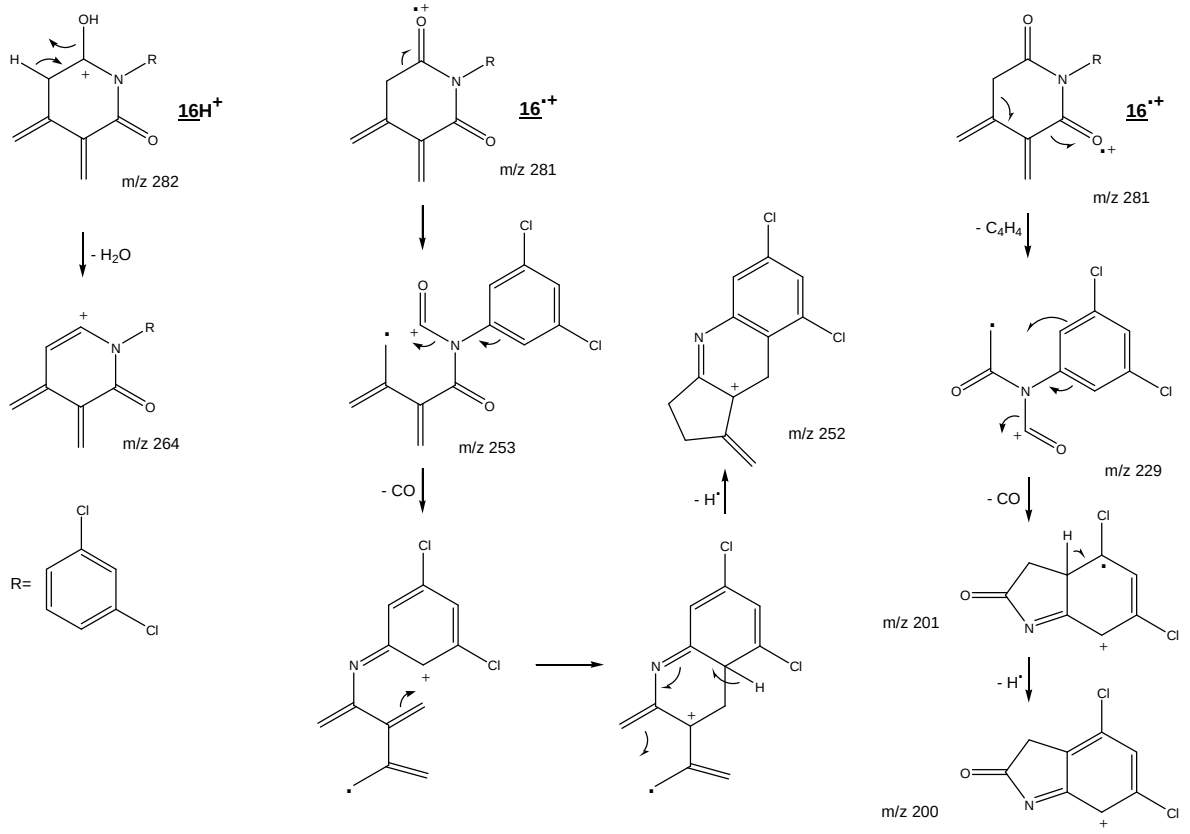

Figure SI-8. Dissociation pathways in CI-MS^n (left hand) and EI-MS^n (right hand) of compound 16

IV-3. Conclusion

Caractérisation structurale

La comparaison des chromatogrammes des solutions photolysées avec celui de la solution de référence de procymidone a montré la formation de seize photo produits. D'après les distributions isotopiques observées en spectrométrie de masse, tous les photoproduits ont conservé les deux atomes de chlores alors que la perte de l'atome de chlore sous irradiation était quasiment systématique dans le cas du métolachlore. Les résultats des calculs théoriques ont montré que la forme ionique la plus stable de la procymidone résulte de l'arrachement d'un électron libre de l'un des oxygènes des fonctions cétones. Depuis cette forme ionisée, trois structures distoniques ont été proposées; elles réagissent avec les molécules d'eau pour donner les structures de onze photoproduits. Les formes bi-cycliques dominent les structures des photoproduits de la procymidone. Seules les structures des trois premiers produits de dégradation incluent le cycle bi chloré avec une chaine alkyle. Parmi les photoproduits observés dans cette étude, seule la 3,5-dichloroaniline avait été préalablement dans la littérature. Les structures des photoproduits ont été établies par l'étude des mécanismes de dissociation des ions pseudo-moléculaires et moléculaires sous différentes énergies de collisions en spectrométrie de masse multi étapes (MS^n).

Aspects cinétiques

L'étude cinétique de la formation des photoproduits de la procymidone par rapport au temps d'irradiation a été réalisée jusqu'à 90 minutes. Après 60 min d'irradiation, la quantité de procymidone restante dans la solution correspond à 5% de la quantité initiale. Après 90 minutes d'irradiation, la procymidone n'est plus détectés mais trois produits de dégradation demeurent dans la solution. Les treize autres produits sont observés dès les premières minutes d'irradiation. Ils atteignent une abondance maximale après 10 minutes puis diminuent pour se trouver au niveau de traces après 40 minutes d'irradiation.

Toxicité prédictive

D'après l'agence de protection environnementale des États Unis, la 3,5-dichloroaniline présente des effets plus toxiques que celle de la molécule mère, en termes de cancérogénicité en particulier. Les résultats observés par QSAR donnent des valeurs proches de celles de la

littérature. L'estimation de la toxicité des autres photoproduits a montré que leur toxicité LD50 chez le rat est modérée mais tous présentent des effets toxiques potentiels sur le développement du fœtus.

Chapitre V - Photo-transformation du pyrimethanil

V-1. Introduction :

Ce chapitre présente l'étude de la dégradation du pyrimethanil sous irradiation UV-visible. Le pyrimethanil est un fongicide appartenant à la famille des anilino pyrimidines. Il est utilisé pour lutter contre la pourriture grise qui attaque plusieurs arbres fruitiers et la tavelure du poirier. Dans la littérature, plusieurs études rapportent la photocatalyse du pyrimethanil sous irradiation solaire et sous radiation UV avec des lampes de xénon ou de mercure.

Les solutions mères du pyrimethanil ont été préparées dans l'acétonitrile à 100 $mg.L^{-1}$. Cette solution a été diluée pour préparer les solutions utilisées à 5 $mg.L^{-1}$ dans cette étude. L'extraction liquide-liquide a été utilisée pour les solutions analysées par GC-MS. Contrairement au cas du métolachlore, la méthode SPE n'a pas utilisée pour l'extraction des photoproduits du pyriméthanil avant analyse par LC-MS. Un mélange ACN/acide formique (0.1%) a été ajouté à quelques microlitres de la solution irradiée dans le flacon d'injection. La simplification de l'extraction évite la perte de photoproduits inconnus durant cette étape. L'analyse des solutions irradiées a été faite par GC-MS en trappe ionique et en LC-QTOF.

Une étude cinétique a été réalisée pour visualiser l'apparition et la disparition des produits de dégradation durant la photolyse.

Structural characterization of photoproducts of pyrimethanil

Aziz Kinani, Ahmad Rifai, Sophie Bourcier, Farouk Jaber and Stéphane Bouchonnet

Introduction

Pyrimethanil is an anilino-pyrimidine fungicide particularly active against gray mold (*Botrytis cinerea*) and pear scab (*Venturia inaequalis* and *Venturia pirina*) on grapes, strawberries, tomatoes, fruits, vegetables and ornamental plants in greenhouses and open field situation [1-5]. According to the European Food Safety Authority (EFSA), pyrimethanil has no evident mutagenic, genotoxic or carcinogenic potential, but a short-term toxicity study on rats and mice has shown an increase in liver weight accompanied by changes in the histopathology of the liver and thyroid [6]. To avoid these side effects, the concentration of pyrimethanil has been limited by legislation. The European Commission set the Maximum Residue Level (MRL) of pyrimethanil at 10 mg/L in citrus fruits, 5 mg/L in pome fruits, strawberries, table and wine grapes and 0.05 mg/L in tree nuts (EC/600/2010) [7]. It is thus important to increase our knowledge regarding the concentration of pyrimethanil in environmental matrices, its degradability and the factors affecting it. One of these factors is the photo alteration by sunlight, which is known to play a significant role in the degradation of this compound, due to the prolonged half-life (77 days approximately) of pyrimethanil in the environment [8]. Previous studies on the degradation of pyrimethanil were carried out mainly in a waste water treatment context and focused on the photo catalytic degradation using various salts as catalysts. Agüera *et al* [9] used TiO_2, Vanni *et a.l* [10] and Anfossi *et al.* [11] added iron III, Navarro *et al.* [12] added ZnO and Gomis *et al.* [13] used thiopyrylium. Irradiation was carried out using a mercury or xenon lamp or direct sunlight. These studies have showed that a long irradiation time (between 150 and 1400 min, depending on the conditions and catalyst) is required for total disappearance of pyrimethanil. Degradation of pyrimethanil in water using the technique of photo-Fenton was investigated by Sirtori *et al*. They reported that the addition of sodium chloride accelerated the reaction and characterized four chlorinated photo-Fenton by-products [14]. The aim of the present study was the identification of UV-visible photo transformation products of pyrimethanil in water. Liquid chromatography coupled with tandem mass spectrometry (LC-MS/MS) and gas chromatography coupled with multi stage mass spectrometry ($GC\text{-}MS^n$) were used for analysis, with the aim of

covering a large range of polarities for the detection of the potential transformation products. Elucidation of the structures of photoproducts was carried out performing high resolution measurements and collision induced dissociation experiments. Photolysis mechanisms have also been proposed to explain the formation of photo products of pyrimethanil in water.

Material and methods

Pure pyrimethanil (99%) and chromatographic grade solvents (99.99% purity), methylene chloride (DCM), acetonitrile (ACN) and formic acid (FA) were purchased from Sigma Aldrich (St Quentin Fallavier, France). Taking into account the low solubility of pyrimethanil in water (121 mg L^{-1} at 25 °C), a first solution was prepared at 100 mg L^{-1} in ACN. This solution was then diluted to prepare working solutions in water at a concentration of 5.0 mg L^{-1} (i.e. 5% ACN/ 95% H_2O). This high concentration was necessary to allow multi stage mass spectrometry experiments on the photo products of low abundance. According to the ROMIL technical report, ACN does not absorb UV light since its transmission at 200 nm is about 100% [15]. Consequently, ACN is expected not to affect the nature of the photoproducts obtained during irradiation. This is the main reason why it has been currently used to dissolve pyrimethanil in previous studies devoted to photolysis. For instance, Gomis *et al.* studied photocatalytic degradation pathways of pyrimethanil in pure ACN [13]. Photolysis experiments were carried out in a self-made reactor equipped with a high-pressure mercury lamp (HPL-N 125W/542 E27 SC; Phillips, Ivry-sur-Seine, France) delivering radiation at wavelengths ranging from 200 nm to 650 nm. The absorbance spectrum of pyrimethanil shows an absorption maximum between 260 and 280 nm [16]. According to manufacturer data, the incident radiation flux was 6200 lm. The reactor consists in six quartz tubes of 120 mL disposed in a circle around the lamp and immerged into a sonicator (AL04-12, Advantage-Lab, Switzerland) filled with deionized water. The solution of pyrimethanil was degassed with a nitrogen stream prior to irradiation and was sonicated during irradiation so that free oxygen is not expected to be dissolved in water in significant amounts. During experiments, the reactor was cooled by water circulation to maintain a constant temperature of 25 ± 3 ºC. For each experiment, 30 mL of a solution of pyrimethanil were used.

LC-MS/MS analysis were performed on a 2690 series HPLC instrument coupled with a quadrupole time-of-flight “Premier” mass spectrometer equipped with a Z-spray electrospray ionization (ESI) source (Waters Technologies, Saint Quentin en Yvelines, France). Compounds

were separated on a T 3.3 µm analytical column C18 2.1 x 150 mm (Atlantis, France). The HPLC solvents were ACN with 0.1% FA (A) and water with 0.1% FA (B). 10 µL were injected with a mobile phase flow of 0.2 mL min^{-1}. The following program of linear gradient was applied: 30% of A for 11.0 min and 30-100% of A from 11.1 to 20.0 min. The column was reconditioned with 30% of A from 20.1 to 30.0 min. Ions were recorded in positive ion mode in the 50-750 domain. The ESI cone and capillary voltages were set at 20 V and 3 kV, respectively. Extraction cone and ion guide voltages were set at 3 V and 4 V, respectively. Source and desolvation temperature were fixed at 120 °C and 450 °C. Nebulization and desolvation were performed using nitrogen gas. The cone gas flow was 70 L h^{-1} and the desolvation gas flow was 700 L h^{-1}. For collision-induced dissociation (CID) experiments, Argon was used as collision gas with a flow of 0.28 mL min^{-1}. The electrostatic mirror was used in the W-mode for accurate m/z measurements. GC-MS analyses were carried out on a Varian 450GC gas chromatograph coupled with a Varian 240MS ion trap mass spectrometer; operating conditions were reported in a recent paper [17].

Results and discussion

This study is the first to report by-product structures obtained by UV-visible irradiation of pyrimethanil without added catalyst. Most of the previous studies devoted to pyrimethanil photolysis used solar irradiation [18], a neon lamp [19,20] or a xenon lamp with cut off of irradiation under 290 nm [21]. Thus, based on the UV-visible spectra of pyrimethanil (maximum absorption between 260 and 280 nm [16]), negligible photodegradation was expected. In the present study, the light has not been filtered, thus explaining why phototransformation products were observed.

The relative abundances of by-products were determined from times ranging from 15 minutes up to 8 hours of irradiation. All the photoproducts were detected in the solution irradiated for three hours; this solution was thus selected to carry out CID and high resolution experiments on photoproducts. At this time, the degradation yield of pyrimethanil, estimated on the basis of total ion currents, was about 60%. Eight photoproducts were detected in LC-MS. Retention times, exact m/z ratios of molecular ions and CID main fragment ions are reported in Table 1. Only compound 1 and aniline in trace amounts were detected in GC-MS; they were easily characterized owing to the NIST spectra data base with matching scores greater than 94% [22].

The first step of the transformation process was assumed to correspond to the formation of a radical cation by electron removal, as postulated in previous studies [17,21,23]. The secondary amine and all the double bonds of the system constitute likely ionization sites: electron removal leads in all cases to a highly delocalized radical cation. In aqueous solution, the radical cation can be captured by a water molecule. The resulting species can eliminate a proton to give a solvated free radical, which can in turn undergo subsequent photoionization to lead to a cation with an even number of electrons.

Three compounds referred as 6, 7 and 8 were detected with a molecular weight of 215 amu at retention times of 5.97, 17.70 and 18.06 min, respectively. They likely result from hydroxylation of pyrimethanil. Under CID, 7 and 8 provided an ion at m/z 77. This ion, also detected for pyrimethanil, corresponds to the benzene ring ionized $C_6H_5^+$. It suggests that the benzene part of the molecule was not affected in the formation of both compounds 7 and 8. H_2O addition on ionized pyrimethanil followed by proton elimination leads to the free radical referred as A in figure 2. Subsequent photoionization of A leads to a cation with an even number of electrons on which water addition followed by proton elimination leads to two isomeric structures with MW = 233 amu. These compounds were not detected in this work but they were reported in a previous study devoted to the photo catalytic degradation of pyrimethanil [11]. Water elimination from each of these structure leads to compounds 7 and 8 (figure 2). 7 corresponds to the only structure which can eliminate CO in mass spectrometry while 8 can eliminate $HO^{\cdot}$ and H_2O, leading to a stable final state in both cases, and also H_2CO (see Table 1). A cyclic structure has been postulated for 6 given its short elution time in comparison with 7, 8 and pyrimethanil. Indeed, Hamilton reported that the elution times in reverse-phase HPLC are correlated to the number and the size of the rings and that cyclic structures elute before their acyclic analogues [24]. In mass spectrometry, the pseudo molecular ion $6H^+$ eliminates CO, as $7H^+$ does. Furthermore, figure 1 shows that the formation of 6 follows the disappearance of 7, thus suggesting that 6 likely arises from degradation of 7. A mechanism involving photo ionization of 7 followed by cyclization and water molecule additions has been postulated for the formation of 6 (see figure 2, right hand). Dissociation pathways of pseudo molecular ions of 6, 7 and 8 are given in figure 3.

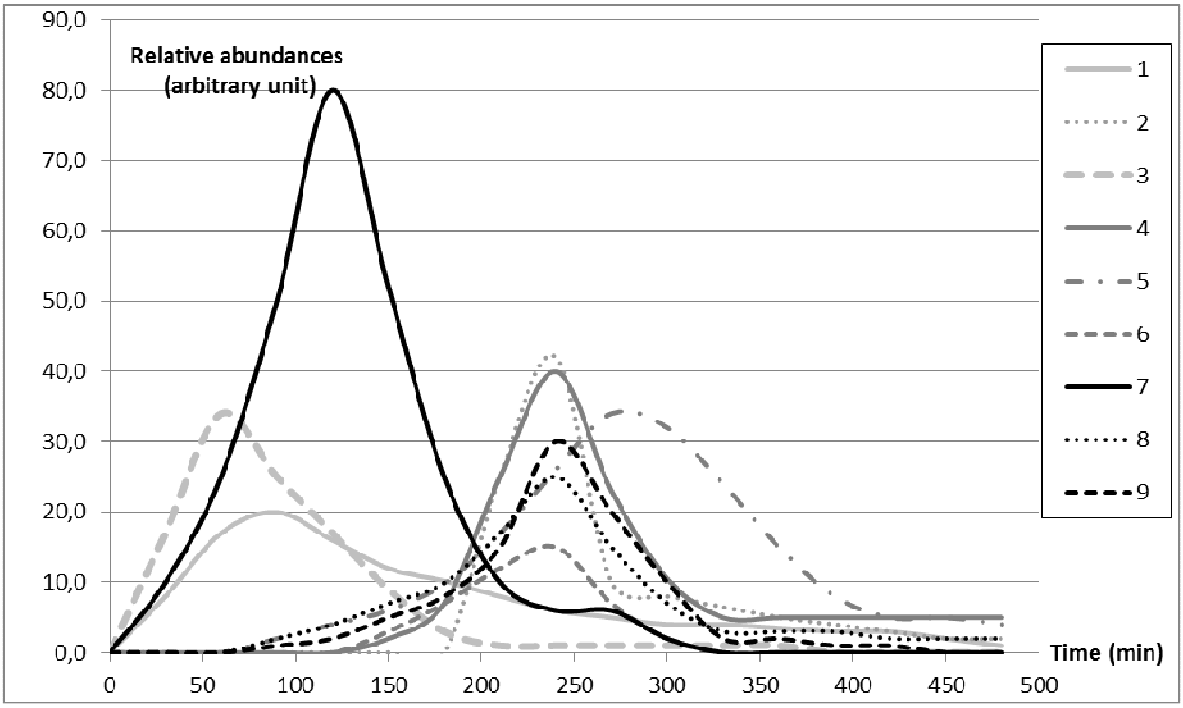

Figure 1. Relative abundances of photoproducts as a function of the irradiation time.

Table 1. Retention times, relative intensities, experimental m/z, CID transitions and proposed structures for the phototransformation products of pyrimethanil

Compound	Retention time (min)	Relative intensity[a]	Experimental m/z of MH^+	Error (ppm)	DBE[b]	Elemental composition	CID transitions (m/z)	Proposed structure	References[c]
1	2.12	10.2	124.0870	-4.0	3.5	$C_6H_{10}N_3$	124 → 83 (-41) 124 → 107 (-17) 107 → 67 (-40)	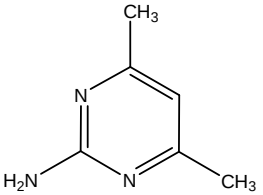	[9, 11, 13, 18, 19]
2	2.58	8.0	178.0964	3.4	5.5	$C_9H_{12}N_3O$	178 → 94 (-84) 178 → 136 (-42) 136 → 119 (-17)	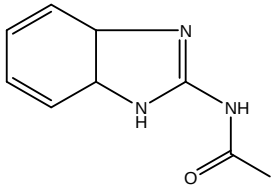	
3	3.30	3.0	200.1182	-3.0	7.5	$C_{12}H_{14}N_3$	200 → 159 (-41) 159 → 143 (-16) 143 → 117 (-26)	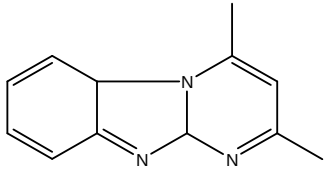	
4	3.30	17.5	214.0990	4.7	8.5	$C_{12}H_{12}N_3O$	214 → 171 (-43) 214 → 143 (-71) 214 → 186 (-28) 186 → 117 (-69) 186 → 159 (-27)	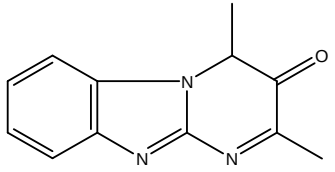	

5	3.34	9.8	198.1127	-1.5	9.0	$C_{12}H_{12}N_3$	198 → 182 (-19) 198 → 171 (-27) 198 → 157 (-41) 157 → 117 (-40)	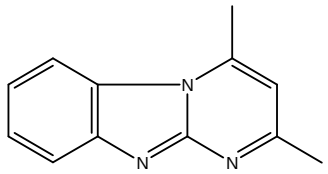	
6	5.97	9.0	216.1146	4.2	7.5	$C_{12}H_{14}N_3O$	216 → 198 (-18) 216 → 77 (-139) 216 → 188 (-28) 188 → 117 (-71)	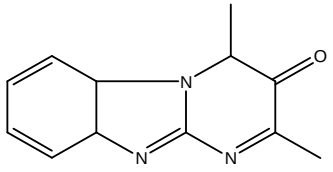	
7	17.70	25.0	216.1120	-7.9	7.5	$C_{12}H_{14}N_3O$	216 → 77 (-139) 216 → 123 (-93) 216 → 188 (-28) 188 → 172 (-16) 188 → 160 (-28)	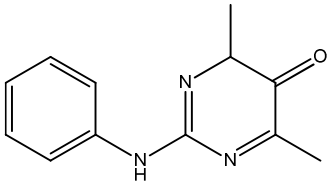	[9, 11, 14]
8	18.06	9.9	216.1147	4.6	7.5	$C_{12}H_{14}N_3O$	216 → 198 (-18) 216 → 199 (-17) 199 → 77 (-122) 199 → 122 (-77) 216 → 186 (-30) 186 → 160 (-26)	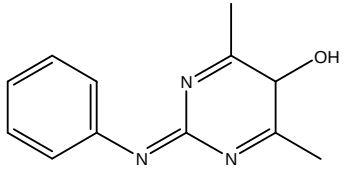	
Pyrimethanil	18.60	-	200.1184	0.1	7.5	$C_{12}H_{14}N_3$	200 → 77 (-123) 200 → 107 (-93) 200 → 143 (-57) 200 → 183 (-17)	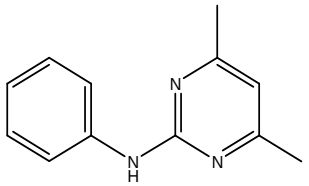	

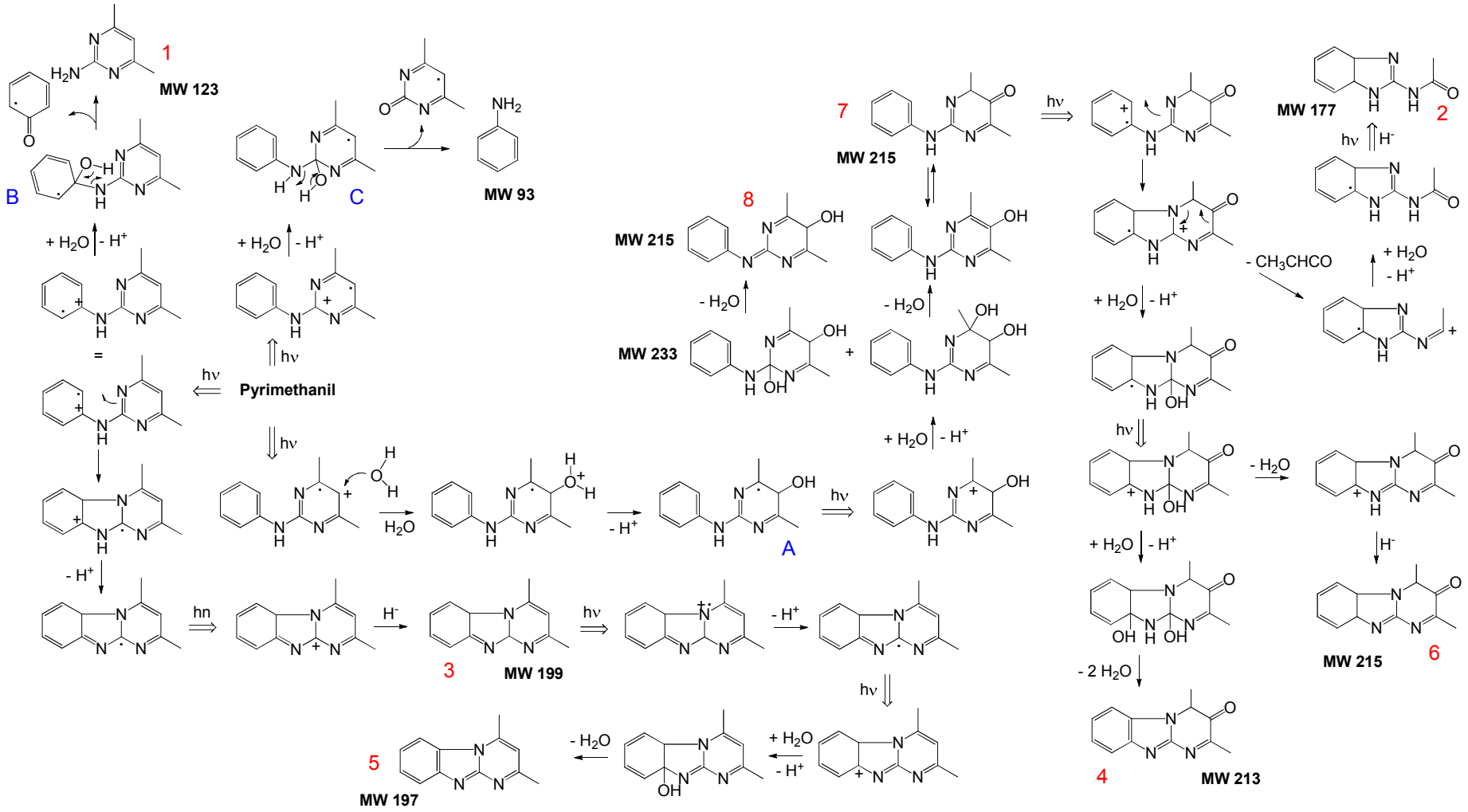

Figure 2. Mechanisms postulated for the formation of compounds 1 to 8 from irradiated pyrimethanil

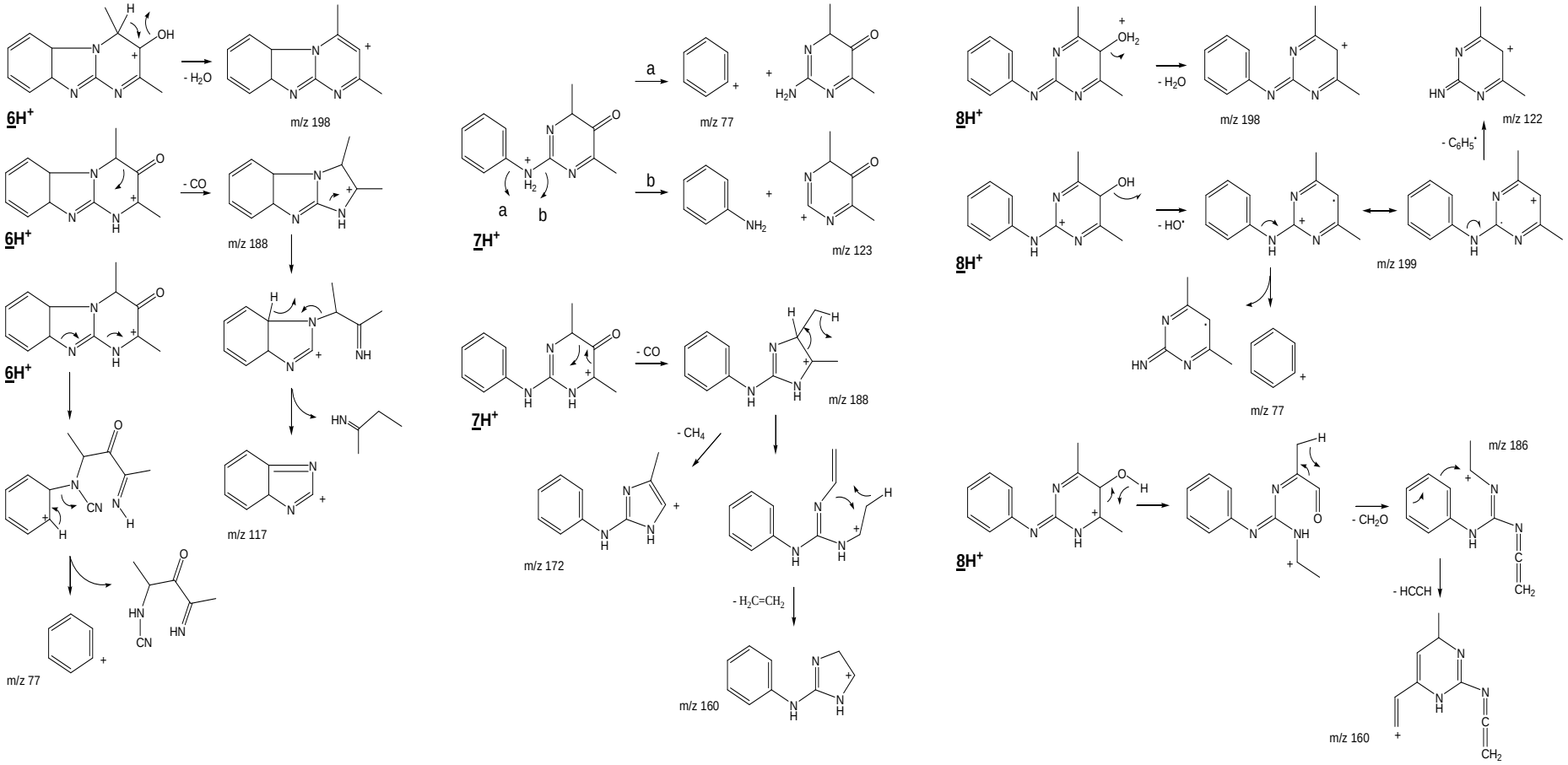

Figure 3. Dissociation pathways of pseudo molecular ions of 6, 7 and 8.

Given that kinetics data for compound 4 (213 amu) match those for 6 (see figure 1) and that $\underline{4}H^+$ also eliminates CO, 4 was assumed to result from dissociation of 7 by a mechanism analogous to that postulated for the formation of 6 (figure 2, right hand). The formation of compound 2 (MW 177) may be also rationalized by a mechanism following photoionization of 7, in competition with that postulated for the formation of 6 and involving a ring aperture induced by the positive charge (figure 2, right hand). Dissociation pathways of pseudo molecular ions of 2 and 4 are given in figure 4.

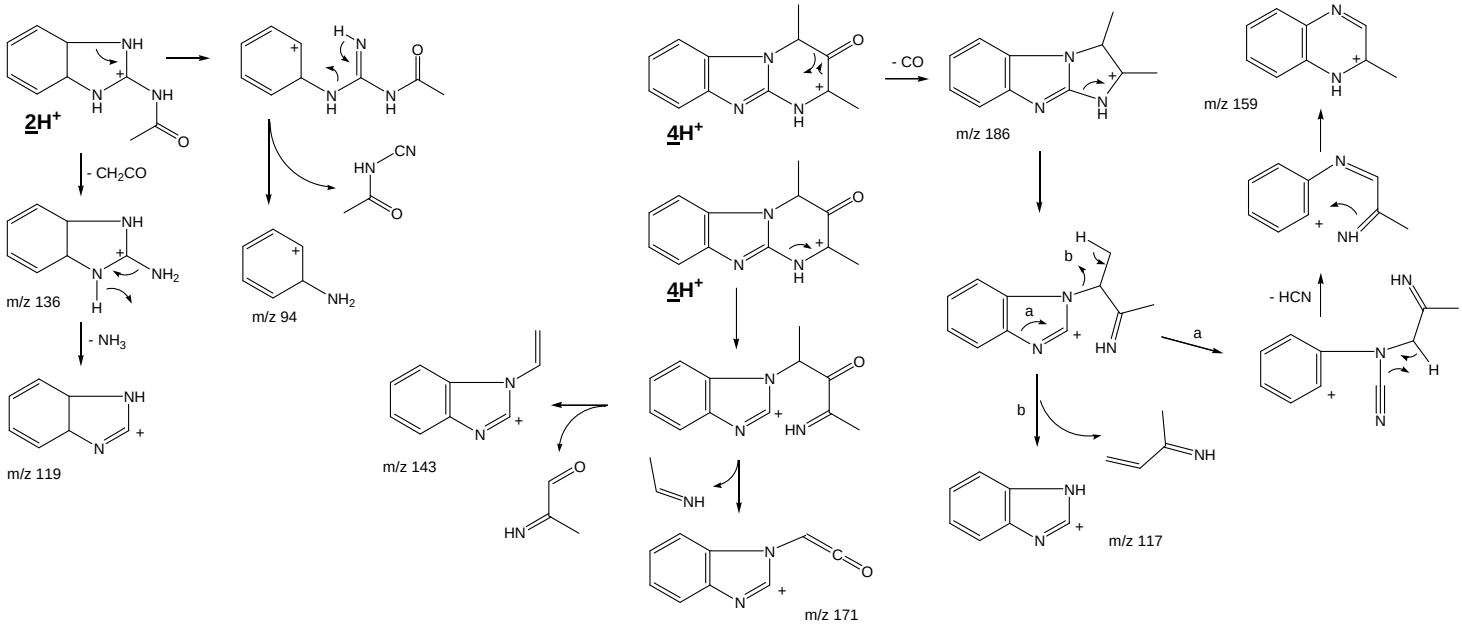

Figure 4. Dissociation pathways of pseudo molecular ions of 2 and 4.

Structures B and C in figure 2 result from a water molecule addition on ionized pyrimethanil followed by proton elimination. Compound 1, also characterized in GC-MS (see above), results from elimination of the cyclohexa-2,4-dienone radical from B while the loss of the radical pyrimidine radical from C leads to aniline; both compounds have been detected in a previous study [9]. Isomeric forms of B and C have also been considered; they are not displayed in figure 2 as they lead, according to the mechanisms postulated above, to molecules which are not detected.

Kinetics data show that 3 (eluted at 3.3 minute) is among the first compounds that are formed under irradiation. Cyclization of ionized pyrimethanil followed by proton elimination leads to a free radical, whose subsequent photoionization followed by hydride addition leads to **3**. The

structure postulated for 3 is in good agreement with the consecutive losses of CH_3CN, CH_4 and CN observed under collisional activation of the ion $3H^+$. Kinetics data (see figure 1) show that compound 5 seems to be produced from 3. Furthermore, given their very close retention times (3.30 min for 3 *vs.* 3.34 min for 5) and their difference of two mass units (MW = 199 for 3 *vs.* MW = 197 min for 5), 5 was postulated to result from dehydrogenation of 3 after photoionization of the later according to the mechanism depicted in figure 2. Dissociation pathways of pseudo molecular ions of 3 and 5 are given in figure 5.

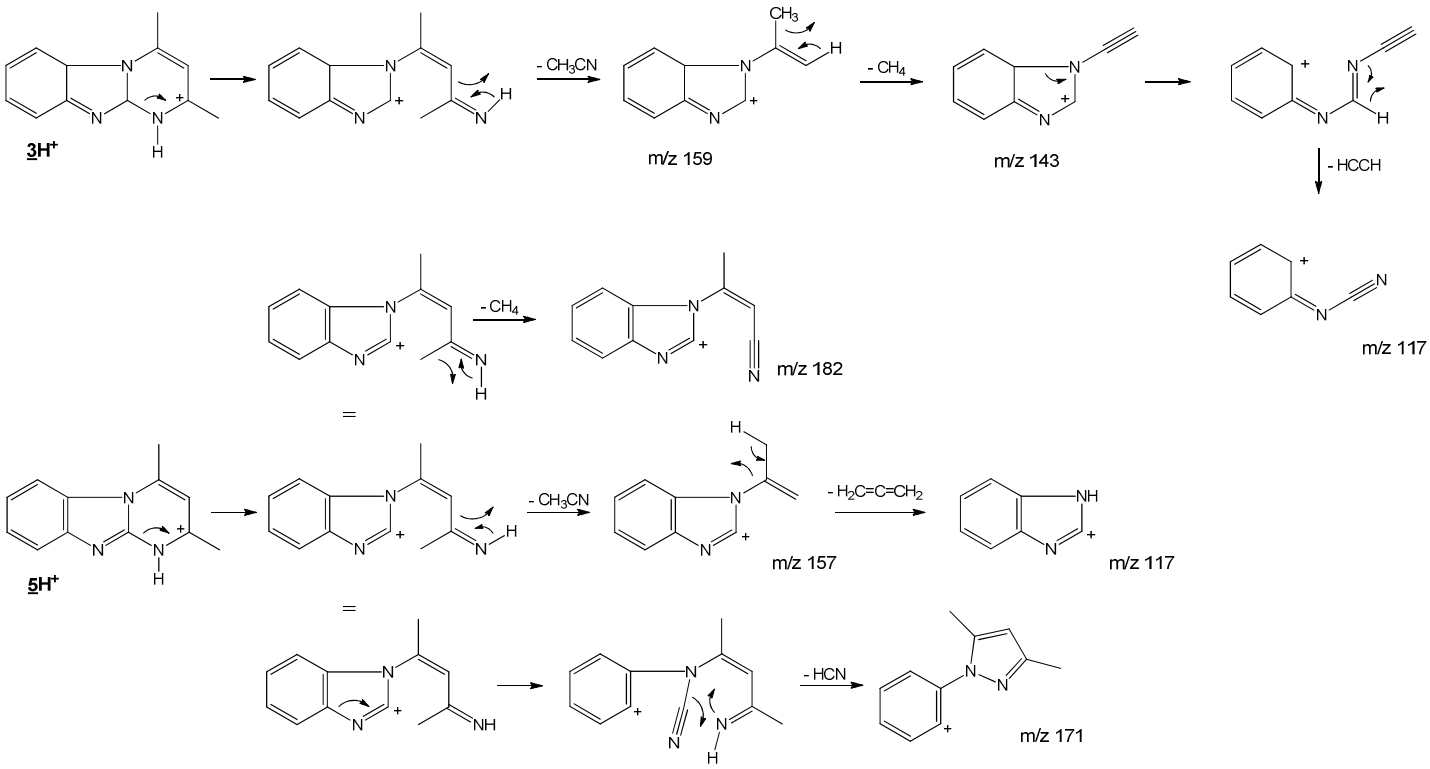

Figure 5. Dissociation pathways of pseudo molecular ions of 3 and 5.

Conclusion

In conclusion, eight photo products were identified by HPLC-MS/MS. Among them, compound 1 was the only one which was also detected by GC-MS, with traces amounts of aniline. With the exception of compounds 1 and 7, the structures proposed for photoproducts on the basis of mass spectra interpretation have not been reported in previous studies.

References

[1] V. L. Garau, A. Angioni, A. A. Del Real, M. Russo, P. Cabras. Disappearance of azoxystrobin, pyrimethanil, cyprodinil, and fludioxonil on tomatoes in a greenhouse. *J. Agri. Food Chem.* **2002**, *50*, 1929.

[2] A. Navalon, A. Prieto, L. Araujo, J. L. Vilchez. Determination of pyrimethanil and kresoxim-methyl in green groceries by headspace solid-phase microextraction and gas chromatography-mass spectrometry. *J. Chromatogr. A* 2002, *975*, 355.

[3] X. H. Sun, Y. F. Liu, Z. C. Tan, Y. Y. Di, H. F. Wang, M. H. Wang. Heat capacity and enthalpy of fusion of pyrimethanil laurate ($C_{24}H_{37}N_3O_2$). *J. Chem. Thermodyn.* **2004**, *36*, 895.

[4] X. Yu, L. Pan, G. Ying, R. S. Kookana. Enhanced and irreversible sorption of pesticide pyrimethanil by soil amended with biochars. *J. Environ. Sci.-China.* **2010**, *22*, 615.

[5] H. Zhao, Y. K. Kim, L. Huang, C. L. Xiao. Resistance to thiabendazole and baseline sensitivity to fludioxonil and pyrimethanil in Botrytis cinerea populations from apple and pear in Washington State. *Postharvest. Biol. Tec.* **2010**, *56*, 12.

[6] EFSA. http://www.efsa.eu.int, **2006**.

[7] E. COMMISSION. *Vol. 9*, Journal officiel de l'Union Européenne, **2010**.

[8] INERIS. Pyrimethanil - N° CAS 53112-28-0. *Normes de qualité environementale* **2011**.

[9] E. A. Ana Aguera, Ana Tejedor and Armando Fernandez-Alba. Photocatalytic pilot scale degradation study of pyrimethanil and its main degradation products in waters by means of solid-phase extraction followed by gaz and liquid chromatography with mass spectrometry detection. *Environ. Sci. Technol.* **2000**, *34*, 1563.

[10] A. Vanni, F. Fontana. Photodegradation of Pyrimethanil induced by iron(III) in aqueous solutions. *J. Environ. Monit.* **2003**, *5*, 635.

[11] L. Anfossi, P. Sales, A. Vanni. Degradation of anilinopyrimidine fungicides photoinduced by iron(III)-polycarboxylate complexes. *Pest Management Science* **2006**, *62*, 872.

[12] S. Navarro, J. Fenoll, N. Vela, E. Ruiz, G. Navarro. Photocatalytic degradation of eight pesticides in leaching water by use of ZnO under natural sunlight. *J. Hazard. Mater.* **2009**, *172*, 1303.

[13] J. Gomis, A. Arques, A. M. Amat, M. L. Marin, M. A. Miranda. A mechanistic study on photocatalysis by thiapyrylium salts. Photodegradation of dimethoate, alachlor and pyrimethanil under simulated sunlight. *Appl. Catal., B* **2012**, *123*, 208.

[14] C. Sirtori, A. Zapata, S. Malato, A. Agueera. Formation of chlorinated by-products during photo-Fenton degradation of pyrimethanil under saline conditions. Influence on toxicity and biodegradability. *J. Hazard. Mater.* **2012**, *217*, 217.

[15] M. Ashley. ROMIL technical report. *www.romil.com* **2006**, *Cambridge GB-CB5 9QT*.

[16] V. Feigenbrugel, S. Le Calve, P. Mirabel. Molar absorptivities of 2,4-D, cymoxanil, fenpropidin, isoproturon and pyrimethanil in aqueous solution in the near-UV. *Spectrochim Acta A* **2006**, *63*, 103.

[17] S. Coffinet, A. Rifai, C. Genty, Y. Souissi, S. Bourcier, M. Sablier, S. Bouchonnet. Characterization of the photodegradation products of metolachlor: structural elucidation, potential toxicity and persistence. *J. mass. spectrom.* **2012**, *47*, 1582.

[18] I. Oller, W. Gernjak, M. I. Maldonado, L. A. Perez-Estrada, J. A. Sanchez-Perez, S. Malato. Solar photocatalytic degradation of some hazardous water-soluble pesticides at pilot-plant scale. *J. Hazard. Mater.* **2006**, *138*, 507.

[19] A. Vanni, F. Fontana, A. Cignetti, M. Gennari. Behaviour of pyrimetranil in soil: Abiotic and biotic processes, *Pesticide in air, plant, soil & water system. Proceedings of the XII Symposium Pesticide Chemistry, Piacenza, Italy, 4-6 June 2003 pp. 233-238.*

[20] A. Vanni, L. Anfossi, A. Cignetti, A. Baglieri, M. Gennari. Degradation of pyrimethanil in soil: Influence of light, oxygen, and microbial activity. *J. Environ. Sci. Health. B* **2006**, *41*, 67.

[21] T. Katagi. Photodegradation of pesticides on plant and soil surfaces. *Rev. Environ. Contam. Toxicol., Vol 182* **2004**, *182*, 1.

[22] NIST/EPA/NIH. NIST Mass Spectral Library. *National Institute of Standard and Technology* **2005**, DC.

[23] D. O. J. S. Miller. Photolysis of polycyclic aromatic hydrocarbons in water. *Water Research* **2001**, *35*, 233.

[24] R. J. Hamilton. in *Blackie Academic and Professional* Thomson Science, New york, **1998**.

V.3- Conclusion

Caractérisation structurale

Huit photoproduits ont été détectés durant cette étude. Un seul composé a été détecté par GC-MS et par LC-MS. La structure de ce produit a été établie grâce à bibliothèque de spectres NIST en GC-MS et par l'analyse des ions fragments obtenus en LC-MS. Les sept autres produits ont été détectés par LC-MS. Des structures bi- et tricycliques ont été suggérées sur la base des spectres de masse mais également des temps de rétention des photoproduits.

Aspects cinétiques

Les expériences de photolyse ont montré que la dégradation du pyriméthanil n'est pas aussi intense que pour les autres molécules étudiées puisqu'il reste 60% de ce composé après huit heures d'irradiation. À l'exception de trois photoproduits, tous les composés disparaissent après six heures d'irradiation.

Chapitre VI – Photo-transformation du boscalid

VI-1. Introduction

Le boscalid est un fongicide organochloré. Cette étude est l'une des premières consacrées à la photo transformation du boscalid sans ajout du catalyseur.

En raison de la faible solubilité du boscalid dans l'eau (4,64 mg L^{-1} à 25 °C), les solutions mères ont été préparées dans l'ACN à 100 mg. L^{-1}. Les solutions irradiées utilisés pour les expériences d'identification structurale ont été diluées à 5 mg. L^{-1}. L'extraction liquide-liquide a été utilisée pour les solutions analysées par GC/MS. Les analyses LC/MS ont été menées après un simple ajout de mélange ACN/ acide formique (0.1 %) à la solution aqueuse.

Une étude cinétique a été conduite pour contrôler la formation et la disparition des photoproduits en fonction du temps d'irradiation. Cette étude a permis de déterminer les photoproduits issus directement de la molécule mère et ceux dont la formation passe par des structures intermédiaires.

La toxicité des produits de dégradation du pyrimethanil a été estimée à l’aide du programme T.E.S.T. (voir chapitre 2).

UV-visible degradation of boscalid - structural characterization of photoproducts and potential toxicity using *in silico* tests

Ahmad Rifai[1,2], Aziz Kinani[1], Yannick Lassalle[1], Yasmine Souissi[1], Carine Clavaguera[1], Sophie Bourcier[1], Farouk Jaber[2] and Stéphane Bouchonnet[1]

[1] Laboratoire des Mécanismes Réactionnels UMR-7651, École Polytechnique, 91128 Palaiseau Cedex, France.

[2] Laboratoire d'Analyse des Pesticides et des Polluants Organiques - Commission Libanaise de l'Énergie Atomique - Centre National de Recherches Scientifiques - Beyrouth, Lebanon

* Corresponding author, e-mail: stephane.bouchonnet@polytechnique.edu

Abstract

RATIONALE: Boscalid is a carboximide fungicide mainly used for vineyard protection as well as for tomato, apple, blueberry and various ornamental cultivations. The structural elucidation of by-products arising from the UV-visible photo degradation of boscalid has been investigated by GC-MS^n and LC-MS/MS couplings. The potential toxicities of transformation products were estimated by *in silico* calculations.

METHODS: Aqueous solutions of boscalid were irradiated up to 150 minutes in a self-made reactor equipped with a mercury lamp. Analyses were carried out on a gas chromatograph coupled with an ion trap mass spectrometer operated in both EI and CI modes and on a liquid chromatograph coupled with a Q-TOF mass spectrometer operated in ESI. Multiple stage collision induced experiments were performed to establish dissociation pathways of ions. The

QSAR (Quantitative Structure-Activity Relationship) T.E.S.T. program allowed to estimate the toxicities of by-products.

RESULTS: Eight photoproducts were investigated. Chemical structures were proposed on the interpretation of multistage collision induced dissociation experiments but also on kinetics data. These structures led to suggest photo degradation pathways. Three photoproducts were finally detected in Lebanon in a real grape leaves sample for which routine analysis had led to the detection of boscalid at 4 mg Kg^{-1}.

CONCLUSIONS: With the exception of one of them, the structures proposed for the photoproducts on the basis of mass spectra interpretation have not been reported in previous studies. *In silico* toxicity predictions showed that two photoproducts are potentially more toxic than the parent compound considering oral rat LD50 while five photoproducts may induce mutagenic toxicity. With the exception of one compound, all photoproducts may potentially induce developmental toxicity.

Keywords: boscalid, photolysis, quantum chemistry, GC-MS**,** LC-MS, transformation products, potential toxicity

Introduction

Pesticides are widely used throughout the world, especially in agriculture for crop protection. According to the World Health Organization (WHO), their use is still increasing worldwide and new pesticides are developed and introduced to the market every year [1]. Among them, boscalid is a relatively new pesticide belonging to the class of succinate dehydrogenase inhibitor (SDHI) carboximide fungicides. It was first synthesized in 2003 and introduced to the market by BASF in 2008[2]. It is mainly used for vineyard protection as well as for tomato, apple, blueberry and various ornamental cultivations[3,4,5,6]. This pesticide has different biological activities against different stages of fungal development; it inhibits spore germination and especially germ tubes extension. Its activity spectrum includes several pathogens of important crop plants belonging to

the ascomycetes and deuteromycetes[2,7,8]. However, this activity has been reported to cause chronic toxic effects on humans like cancer, reproductive damage and endocrine disruption. To avoid these side effects, the concentration of boscalid has been limited by legislation. For example the European Commission Directives 76/895/EEC, 90/642/EEC and EC/396/2005 updated in EU/600/2010, set the Maximum Residue Level (MRL) of boscalid between 1 and 10 mg/kg, depending of the cultivation considered [9,10]. The United States Environmental Protection Agency reported that boscalid leads to two primary degradation products, 2-chloronicotinic acid and 2-hydroxy-N-(4'-chlorobiphenyl-2-yl)-nicotinamide, but also to unknown by-products [11]. In the agricultural field, the elimination of pesticides results of biological, chemical and/or photochemical degradation. The study of the photochemical behavior of pollutants is thus a key element in terms of toxics formation [12,13]. The establishment of degradation pathways is also important; it gives us a better knowledge of the fate of pesticides in the environment. Previous studies were carried out on the degradation kinetics of boscalid in environmental samples. Chen *et al.* developed a simple and rapid method for the determination of boscalid in cucumber and examined its dissipation in samples collected. In their study, they deposed 0.60 and 1.48 mg/kg of boscalid in cucumber at the rates of 0.5 and 0.83 kg a.i./ha, respectively. They established that only 5 and 17% of the initial deposits were found in the cucumber six days after the last application at low and high dose, respectively [14]. Munitz *et al.* developed and validated a method for the determination of boscalid concentration and its degradation kinetics in varieties of blueberries. They deposited boscalid in blueberries at concentrations of 0.19 and 0.55 mg/kg, and noted that the remaining amounts of boscalid after 20 days were 9.7 and 7.3%, respectively. They reported that the degradation of boscalid in blueberries followed a first order kinetic rate with a half-life of about 6 days [5]. In another study, Karaka *et al.* reported the ozonation of five fungicides in grapes and concluded that boscalid was the only one not affected by ozone treatment [**Error! Bookmark not defined.**]. Lagunas-Allue *et al.* studied the TiO_2-photocatalyzed chemical degradation of boscalid in water using a mercury lamp with $\lambda = 365$ nm. Seventeen intermediates were identified and characterized through a spectra analysis. The main photoproducts were monohydroxylated and dihydroxylated boscalid [15].

The main objective of the present work was the identification of the transformation products issued from direct photolysis of boscalid in water, as it may occurs on fruit and leaves exposed to

solar irradiation. The second aim was the assessment of the potential toxicity of the resulting photoproducts. We chose a combined approach using liquid chromatography coupled with tandem mass spectrometry (LC-MS/MS) and gas chromatography coupled with multi-stage mass spectrometry ($GC\text{-}MS^n$) to cover a large range of polarities of the expected transformation products. Structural elucidation of photoproducts was carried out on the basis of collision induced dissociations experiments. Photolysis mechanisms have been proposed to rationalize the formation of these photoproducts. The potential toxicities of boscalid and its phototransformation products were estimated by an *in silico* QSAR (Quantitative Structure-Activity Relationship) approach. The software TEST, a tool for estimating toxicity developed by the U.S. Environmental Protection Agency, was used to predict mutagenicity, developmental toxicity, lethal oral doses in rats and lethal doses for aquatic organisms. Finally, the identified photoproducts were searched in a real sample of grape leaves for which boscalid was detected at 4 mg Kg^{-1} in routine analysis.

2. Materials and methods

2.1. Chemicals and reagents

Boscalid (99% purity) was purchased from Sigma Aldrich (St Quentin Fallavier, France). The chemical structure of boscalid is displayed in figure 1. Chromatographic grade solvents (99.99% purity), methylene chloride (DCM), acetonitrile (ACN) and formic acid (FA), were also purchased from Sigma Aldrich. Considering the poor solubility of boscalid in water (4.64 mg L^{-1} at 25 °C), a standard solution of boscalid at 100 mg L^{-1} was prepared in ACN [16]. ACN does not absorb light in the UV range (0% at 200 nm) so it is not excited during irradiation [17]. This solution was then used to prepare working solutions in water at 5.0 mg L^{-1} (ACN constitutes 5% of the final solution). This concentration was used for structural investigations on photoproducts as tandem and multi stage CID (Collision Induced Dissociation) experiments require quite large amounts of sample. Solutions at 0.5 mg L^{-1} were used for kinetic measurements. All solutions were degased using nitrogen bubbling for 15 minutes and sonication for 10 minutes prior to irradiation.

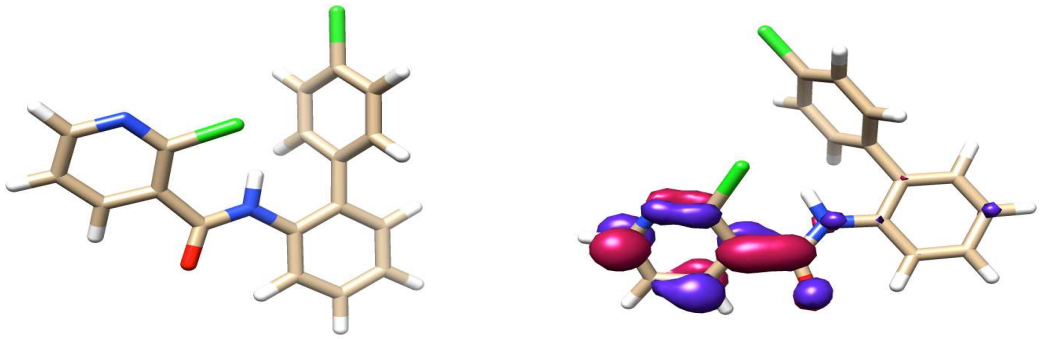

Figure 1. Chemical structure of boscalid ($C_{18}H_{11}N_2OCl_2$) and nature of the first excited state (CC2 level)

2.2. Photolysis experiments

Photolysis experiments were carried out in a self-made reactor equipped with a high-pressure mercury lamp (HPL-N 125W/542 E27 SC; Phillips, Ivry-sur-Seine, France) delivering radiation at wavelengths ranging from 200 nm to 650 nm. According to manufacturer data, the incident radiation flux was 6200 lm. The reactor consists in six quartz tubes of 120 mL disposed in a circle around the lamp and immerged into a sonicator (AL04- 12, Advantage-Lab, Switzerland) filled with deionized water. During experiments, the reactor was regularly cooled by ice addition to avoid uncontrolled heating of the irradiated solutions and to maintain a constant temperature of 25 ± 3 °C. For each experiment, 30 mL of a solution of boscalid (see above) were used.

2.3. Sample preparation

For GC-MS analysis, 6 mL of solution were taken from the quartz tube after photolysis and transferred into a separating funnel. 6 mL of methylene chloride were added to the solution which was then shaken and left to settle for ten minutes. The organic phase was collected and dried under a gentle nitrogen stream; the dry residue was dissolved into 200 µL of DCM. For LC-Q-TOF analysis, 100 µL of solution were directly taken from the quartz tube and diluted with 100 µL of ACN with 0.1% FA.

2.4. GC-MS operating conditions

Analysis were carried out on a Varian 450GC gas chromatograph equipped with a CP8400 autosampler and coupled with a VARIAN 240MS ion trap mass spectrometer operated in the

internal ionization mode. A 60 meter-long “VF-Xms” capillary column (VARIAN) with an internal diameter of 0.25 mm and a film thickness of 0.25 µm was used. For all analysis, 2 µl of solution were injected automatically in the splitless mode at a rate of 50 µL s^{-1}. The injector temperature was set to 280 °C and high purity helium (99.999 %) was used as carrier gas at a constant flow of 1.4 mL min^{-1}. The column oven temperature was programmed from an initial temperature of 50 °C held during 1 min, increased to 300 °C at 6°C/min, then increased at 15 °C/min to a final temperature of 320 °C, which was held for 3 min, for a total analysis duration of 47 minutes. The manifold, the ion-trap electrodes and the transfer line temperatures were respectively held at 100 °C, 200 °C and 280 °C. The mass spectrometer was calibrated with the ions resulting from electron ionization (EI) of perfluorotributylamine. Chemical ionization (CI) experiments were performed using methanol as the reagent. Spectra were recorded using the automatic gain control (AGC) function with target values fixed at 20.000 and 5.000 for electron ionization and chemical ionization (CI), respectively. The filament emission current was set at 10 µA in EI and 50 µA in CI. The electron multiplier voltage was automatically optimized at 2200 V for a gain value of 105. Full scan mass spectra were acquired recording ions from m/z 50 to m/z 500 at a frequency of 3 spectra s^{-1}. In multiple stage mass spectrometry (MS^n) experiments, precursor ions were stored with a Paul stability parameter (qz) of 0.30 and fragmented by collision induced dissociation with activation energies ranging from 0.30 V to 0.80 V in the resonant excitation mode.

2.5. LC-MS operating conditions

LC-MS/MS analysis were performed on a 2690 liquid chromatography module coupled with a QTOF Premier mass spectrometer (quadruple time-of-flight mass spectrometer) equipped with a Z-spray electrospray ionization (ESI) source (Waters Technologies, Saint Quentin en Yvelines, France). The analytical column used was an Atlantis T3 3µm C18 2.1 x 150 mm (Waters, France). The HPLC solvents were ACN with 0.1% FA (A) and water with 0.1% FA (B). The following program of linear gradient was applied: 45% of A for 5.0 min and 45-90% of A from 5.1 to 10.0 min. The column was reconditioned with 45% of A from 10.1 to 30.0 min. 10 µL were injected with a mobile phase flow of 0.3 mL min^{-1}. Three acquisition modes were used to characterize each compound (i) full scan in V mode; (ii) MS/MS of precursor ion and (iii) full scan in W mode for high resolution. Ions were recorded in the positive mode on the 50 - 750 m/z

range. The ESI cone and capillary voltages were set at 35 V and 3 kV, respectively. Extraction cone and ion guide voltages were set at 2.5 V and 3.2 V, respectively. Source and desolvation temperatures were fixed at 120 °C and 450 °C, respectively. Nebulization and desolvation were performed using nitrogen gas. The cone and desolvation gas flows were 80 L h^{-1} and 800 L h^{-1}, respectively. For CID experiments, argon was used as collision gas with a flow of 0.28 mL min^{-1} corresponding to a pressure of 410^{-3} mBar. Collision energies were varied from 2 to 30 eV for each compound in order to obtain the main characteristic ions. For accurate mass measurements, analyses were carried out in W-mode using an independent reference spray via the "Lockspray" interface to ensure accuracy. A sulfadimethoxine solution was used as the lock mass at a flow rate of 10 µL min^{-1}; the ion used for m/z correction was m/z 311.0814. Accurate masses and elemental compositions were determined with the MassLynx software.

2.5. Quantum chemistry calculations

Geometry optimizations were performed at the DFT/B3LYP-D3 level, including the new implementation of dispersion corrections [18] in the TURBOMOLE 6.4 package [19]. The minima were characterized by vibrational frequency calculations. All the calculations have been carried out with the polarized valence-triple-zeta TZVPP basis set. The most energetically stable conformation of the molecule presents two stabilizing interactions, i.e. C=O…H and N-H…Cl (figure 1). In addition, a favorable π-interaction occurs between one Cl atom and the cycle. This stable structure was used for the calculation of the electronic excited states by both the CC2 coupled cluster model as an approximation to the coupled cluster singles and doubles (CCSD) equations [20]. This method is considered as an accurate tool for the investigation of the excited states of molecules containing chromophore [21].

2.6. Computer aided toxicity prediction

Toxicity Estimation Software Tool (T.E.S.T.) is an Environmental Protection Agency online available computerized predictive system with Quantitative Structure Activity Relationships (QSAR) mathematical models [22]. T.E.S.T. has a variety of toxicity endpoints used to predict chemical toxicity values from their physical properties such as molecular structure. T.E.S.T.

model uses a simple linear function of molecular descriptors such as the octanol-water partition coefficient, molecular weight or the number of benzene rings (see equation 1).

$$Toxicity = ax_1+bx_2+c \qquad (1)$$

x_1 and x_2 are independent descriptor variables and a, b and c are fitted parameters. Models for assessing toxicity solely from molecular structure are based on information-rich structural descriptors that quantify transport, bulk, and electronic attributes of a chemical structure. Besides molecular weight, the QSAR model employs size-corrected E-values for quantification of molecular bulk. The size-corrected E-values are computed from a rescaled count of valence electrons. Electrotopological state values (E-values), as numerical quantifiers of molecular structure, encode information about the electron content (valence, sigma, pi and lone-pair), topology, and environment of an atom or a group of atoms, in a molecule [23]. The predicted toxicity is estimated by taking an average of the predicted toxicities from the above QSAR methods, provided the predictions are within the respective applicability domains.

3. Results and Discussion

3.1. Kinetics data

A series of experiments was carried out with 12 irradiation times ranging from 0 to 150 minutes: 0, 5, 10, 15, 20, 30, 40, 50, 60, 90, 120 and 150 minutes. All the irradiated solutions were analyzed by GC-MS and LC-MS. After 150 minutes of irradiation 10% of the initial amount of boscalid was still detected. Three photoproducts were detected by GC-MS (see Table 1) and six photoproducts were detected by LC-MS (see Table 2); the compound referred as **3** was observed by both techniques. The relative abundances of photoproducts vary greatly depending on the irradiation time. All degradation products were detected in the boscalid solution irradiated for 40 minutes so that this solution was retained to perform CID experiments on boscalid and its photoproducts. Most of photoproducts are formed after only 5 minutes of irradiation. Photoproducts abundances reach maximum values for irradiation times between 20 and 60 minutes and decrease to trace amounts after 100 minutes of irradiation.

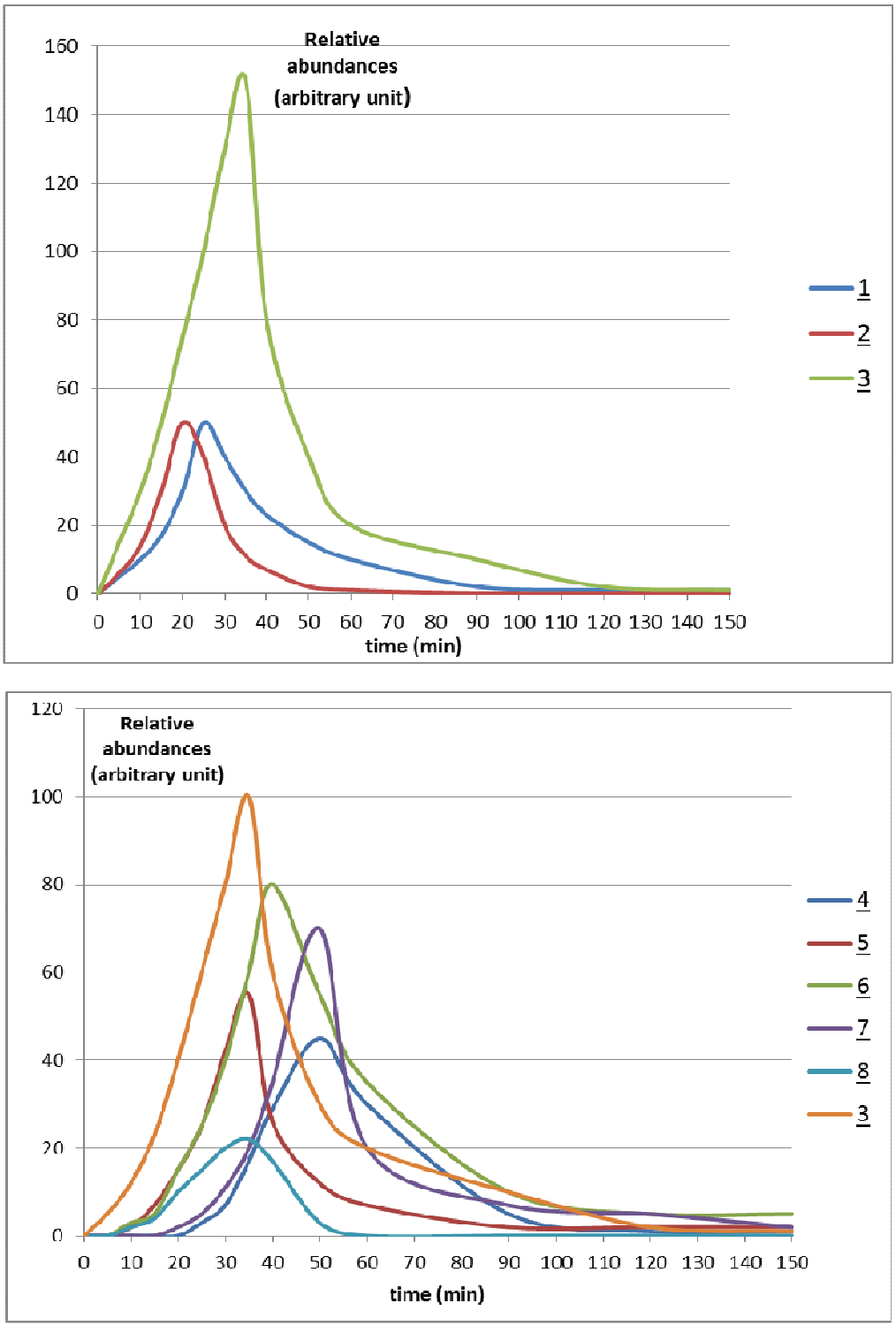

Figure 2. Relative abundances of photoproducts as a function of irradiation time – estimation based on the total ionic current in GC-MS (top) and in LC-MS (bottom)

Table 1. Molecular weight, retention time, chemical structure and main MS^n transitions recorded in GC-MS with CI and EI ionization modes for photolysis products of boscalid

Compound number	Retention time (min)	Elemental composition and molecular weight	Main transitions in CI-MS^n (m/z) [a]	Loss of neutral or radical associated with each transition	Main transitions in EI-MS^n (m/z) [a]	Loss of neutral or radical associated with each transition	Suggested structure
1	31	$C_{12}H_{10}NCl$ 203	204 → 187 187 → 161	Δ 17 (NH_3) Δ 26 (C_2H_2)	203 → 168 203 → 167 167 → 141 141 → 115	Δ 35 ($Cl^{\cdot}$) Δ 36 (HCl) Δ 26 ($^{\cdot}CN$) Δ 26 (C_2H_2)	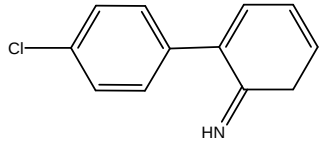
2	32.7	$C_{12}H_8NO_2Cl$ 233	234 → 216 234 → 217 217 → 189 189 → 161	Δ 18 (H_2O) Δ 17 (NH_3) Δ 28 (CO) Δ 28 (CO)	233 → 198 233 → 151 151 → 123	Δ 35 ($Cl^{\cdot}$) Δ 82 Δ 28 (CO)	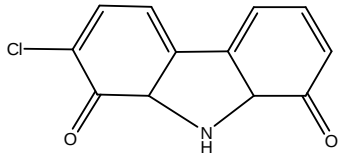
3	46.5	$C_{18}H_9N_2Cl_2$ 324	325 → 289 289 → 253	Δ 36 (HCl) Δ 36 (HCl)	324 → 289 289 → 253 324 → 288	Δ 35 ($Cl^{\cdot}$) Δ 36 (HCl) Δ 36 (HCl)	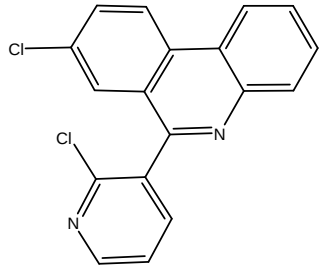

Table 2. Molecular weight, elemental composition, retention time, chemical structure and main CID mass spectra obtained in LC-MS for boscalid and its transformation products

Compound Number	Retention time (min)	Relative intensity[a]	Elemental composition of M (m/z of MH^+)[b]	Error (mDa)	DBE[c]	CID main transitions of MH^+ ions (m/z)[b]	Losses of neutral or radical associated with each transition	Suggested structure
4	1.87	10.2	$C_{18}H_{11}N_2OCl$ 307.0640	0.2	14	307 → 289 307 → 271 307 → 264	Δ 18 (H_2O) Δ 36 (HCl) Δ 43 (NHCO)	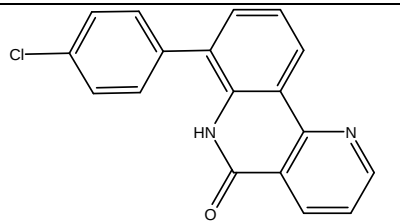
5	3.76	8.0	$C_{18}H_{13}N_2O_2Cl$ 325.0750	0.6	13	325 → 307 307 → 272 325 → 289 289 → 271	Δ 18 (H_2O) Δ 35 ($Cl^·$) Δ 36 (HCl) Δ 18 (H_2O)	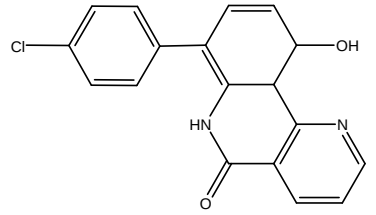 or 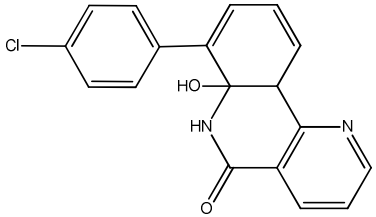

6	4.95	3.0	$C_{18}H_{13}N_2O_2Cl$ 325.0737	0.7	13	325 → 307 307 → 289 325 → 122	Δ 18 (H_2O) Δ 18 (H_2O) Δ 203 ($C_{12}H_{10}NCl$)	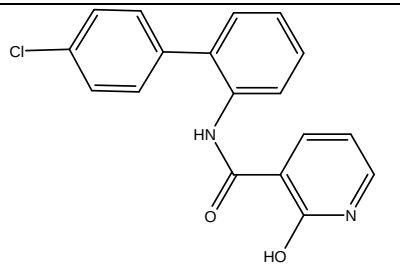
Boscalid	7.95		$C_{18}H_{12}N_2OCl_2$ 343.0396	0.1	13	343 → 307 307 → 272 307 → 271 307 → 289 343 → 140	Δ 36 (HCl) Δ 35 (Cl^-) Δ 36 (HCl) Δ 18 (H_2O) Δ 203 ($C_{12}H_{10}NCl$)	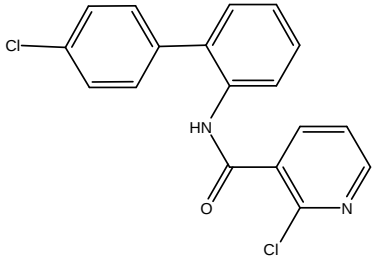
3	8.99	17.5	$C_{18}H_{10}N_2Cl_2$ 325.0306	0.7	14	325 → 289 289 → 253 325 → 212	Δ 36 (HCl) Δ 36 (HCl) Δ 113 (C_5H_4NCl)	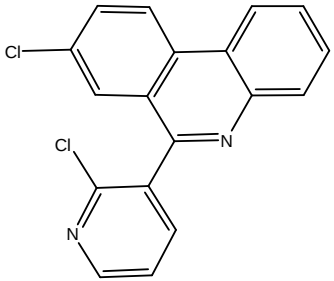
7	8.99	9.8	$C_{18}H_{11}N_2OCl$ 307.0652	0.9	14	307 → 289 307 → 272 307 → 271	Δ 18 (H_2O) Δ 35 (Cl^-) Δ 36 (HCl)	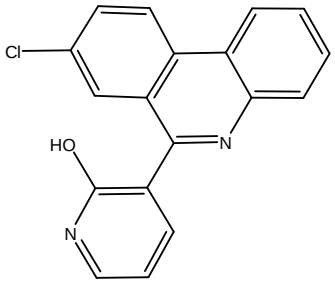

8	9.54	9.0	$C_{18}H_{12}N_2OCl_2$ 343.0409	0.4	13	343 → 307 307 → 272 307 → 271 343 → 230 343 → 140	Δ 36 (HCl) Δ 35 ($Cl^{\cdot}$) Δ 36 (HCl) Δ 113 (C_5H_4NCl) Δ 203 ($C_{12}H_{10}NCl$)	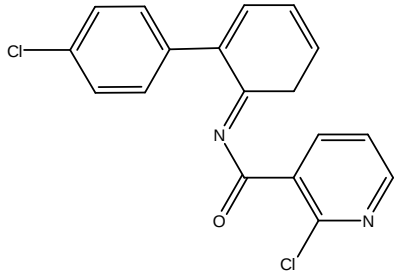

3.2. Characterization of the photoproducts of boscalid

Molecular weights (MW) of the photoproducts were easily determined. In GC-MS coupling, the heavier ion obtained in each CI mass spectrum was assumed to correspond to the protonated molecule MH^+. The molecular weight of each photoproduct was confirmed by the presence of the molecular ion $M^{+\cdot}$ in the corresponding EI mass spectrum. In LC-MS coupling, the molecular weights of the photoproducts were determined by the presence of two peaks separated by 22 u.m.a., corresponding to the protonated molecule MH^+ and to the cation sodium adduct $[M+Na]^+$. The number of chlorine atoms remaining in each photoproduct structure was easily determined on the basis of isotopic distributions [24]. For LC-MS experiments, high resolution measurements allowed to establish the elemental composition of photoproducts (Table 2).

Boscalid includes different sites that can be exited under irradiation. Quantum chemistry calculations indicate that the first excited state of the molecule corresponds to a triplet spin state with an excitation in the pyridine ring (figure 1). Consequently, the double bonds in the pyridine ring were taken as the most favorable ionization sites of boscalid. Electron removal from the pyridine ring leads to a radical cation whose three mesomeric structures, referred as A, B, and C, are displayed in figure 3. Figure 1 shows that ionization of the secondary amine can also be considered (structure D). Like in electron ionization mass spectrometry, we considered that the reactivity induced by the radical should be greater than that induced by the charge [25,26], the latter being furthermore stabilized by surrounding water molecules in the present experiment. When possible, the formation of cyclic compounds was preferred over that of their noncyclic analogues for thermodynamic reasons. First, cyclization mechanisms suggested in figure 3 involve a five or six-membered transition state and thus require low activation energy. Second, cyclization reduces the number of degrees of freedom and thus the entropy of the molecule, leading to a stable final state [27].

Table 1 presents the main CID transitions obtained in CI and EI for the three photoproducts detected by GC-MS. Compound **1** (MW=203) is detected at 31 minutes. According to the nitrogen rule and the detection of two isotopomeric molecular ions, **1** includes one chlorine atom and one nitrogen atom.

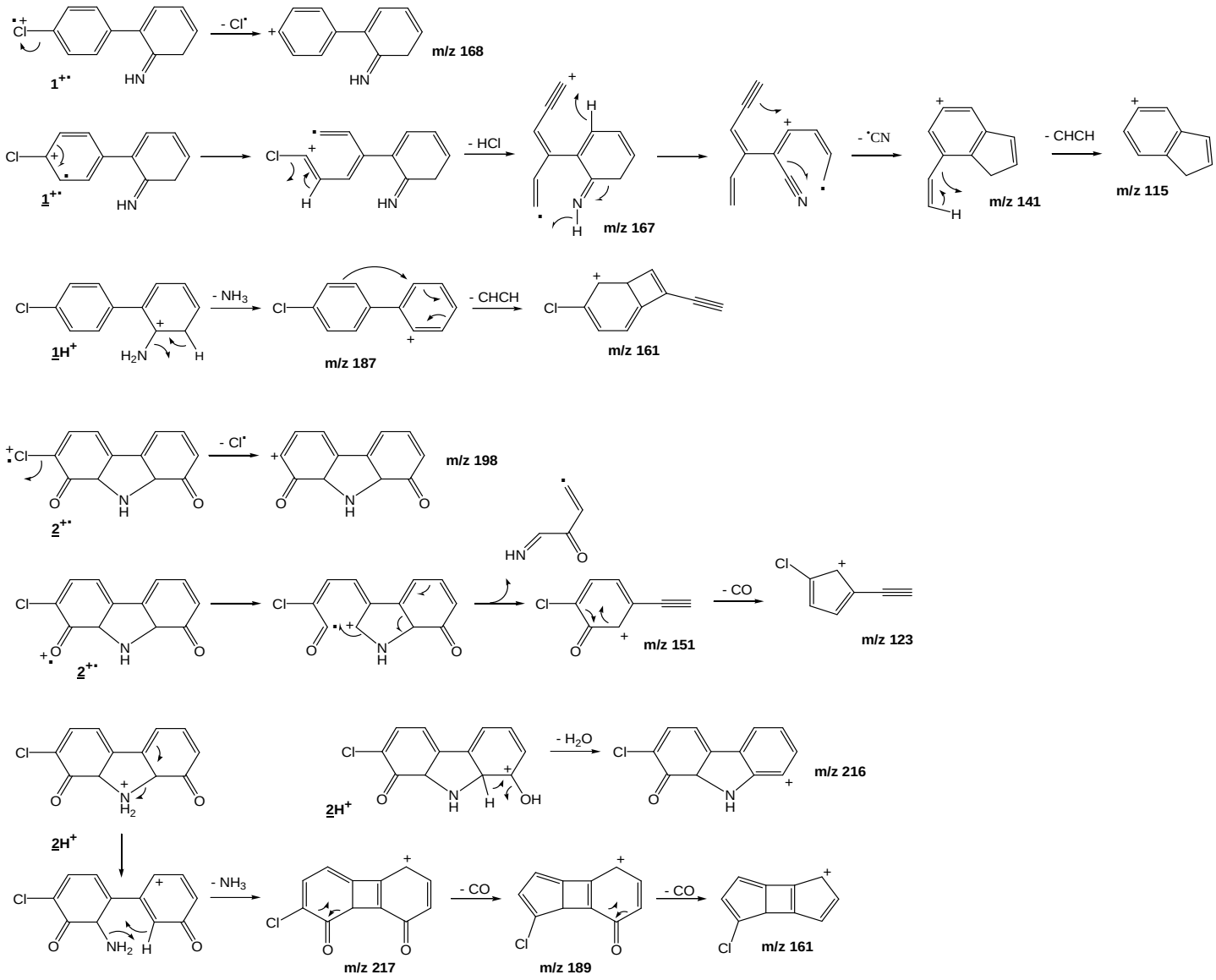

Figure 4. EI-MS^n and CI-MS^n dissociation pathways proposed for compounds **1** and **2**

The dissociation pathways proposed to explain the CID transitions observed in EI-MS^n and CI-MS^n are given in figure 4. In CI, the protonated molecule **1H**$^+$ first eliminates NH_3 (m/z 204 → m/z 187), then C_2H_2 (m/z 187 → m/z 161). Two likely structures may correspond to these transitions: 4-chlorophenyl aniline and 4-chlorophenyl cyclohexa-2,4-dienimine. The first one would correspond to a lower final state but MS^4 transitions from the molecular ion **1**$^{+\cdot}$ in EI (m/z

203 → m/z 167 (- HCl) → m/z 141 (- C_2H_2) → m/z 115 (- ˙CN)) are in agreement with the structure of 4-chlorophenyl cyclohexa-2,4-dienimine (see figure 4) but not with that of 4-chlorophenyl aniline, from which no mechanism was found to rationalize two consecutive eliminations of 26 a.m.u. The formation of **1** has been rationalized considering the addition of a water molecule on the photoionized pyridine ring of boscalid (structure B in figure 3), followed by hydrogen transfer through a seven center-transition state to provide a fully delocalized carbocation. Simultaneous eliminations of carbon monoxide and ionized 2-chloro, 3-hydroxypyridine finally lead to **1**.

Compound **2** (MW = 233) was detected in GC-MS at 32.7 minutes. **2** includes one chlorine atom and one nitrogen atom; transitions corresponding to eliminations of 28 a.m.u. in multistage collisional experiments suggest the presence of carbonyl and/or hydroxy groups in the structure of **2**. Many structures have been postulated for compound **2**, corresponding either to $C_{12}H_8NO_2Cl$ or $C_{13}H_{12}NOCl$ formula. The chemical structure proposed for **2** in Table was the only one corresponding to the CID transitions recorded in both EI and CI ionization modes. In CI-MS^2, the transitions m/z 234 → m/z 216 and m/z 234 → m/z 217 were logically attributed to water and ammonia eliminations from $\mathbf{2H^+}$, respectively. Consecutive eliminations of 28 a.m.u. from the ion at m/z 217 were attributed to CO losses as ethylene elimination from aromatic rings seems very unlikely. In EI-MS^2, the consecutive eliminations of the 2-iminocyclobutanone radical and carbon monoxide from the molecular ion $\mathbf{2}^{+\cdot}$ lead to the ions at m/z 151 and m/z 123 (figure 4). Formation of **2** under irradiation was assumed to occur from the mesomeric form of ionized boscalid referred as A in figure 3. A mechanism based on the elimination of (2-chloropyridin-3(4H)-ylidene)methanone from structure A (see left hand of figure 3) has been suggested for the formation of **2**. Addition of a water molecule on the resulting carbocation, followed by proton elimination, leads to a structure from which dehydrogenation of the alcohol function provides the structure referred as A1 in figure 3. Oxidation of a secondary alcohol to a ketone through H_2 elimination in water is known to be an easy process [28]. Photoionization of A1, followed by a mechanism close to that described above may lead to **2**. This mechanism is supported by the detection at trace level of a compound weighting 217 a.m.u. at 31.5 minutes in GC-MS which could correspond to A1.

The compound **3** (MW = 324) is detected at 46.5 min in GC-MS. According to the nitrogen rule and the detection of three isotopomeric molecular ions, the structure of **3** includes two nitrogen atoms and two chlorine atoms. Its molecular weight corresponds to that of boscalid minus 18 a.m.u., suggesting water elimination from the later. A product with the same molecular weight was detected in LC-MS coupling at 8.99 minutes (Table 2) and was assumed to correspond to **3**. In GC-MS, CID transitions in EI and CI ionization modes correspond to eliminations of $Cl^{\cdot}$ and HCl from $\mathbf{3}^{+\cdot}$ and $\mathbf{3H}^{+}$. Chlorine losses are uninformative but HCl eliminations are in good agreement with a cyclized structure, as depicted in figure 5. In LC-MS coupling, the elimination of chloropyridine (113 a.m.u.) from $\mathbf{3H}^{+}$, leading to the ion at m/z 212, greatly helped in the structure identification: it shows that the chloropyridine part of the molecule was not affected by irradiation in the formation of **3**. The formation of **3** can be rationalized from the radical cation C (see figure 3, top of the right side) in which the lone electron is partially localized on the oxygen atom. C may abstract $H^{\cdot}$ from the solvent to give a more stable ion with an even number of electrons. The following loss of H_2O and the subsequent cyclization provide an additional six-center ring in the resulting cation. Proton elimination from the latter provided the fully conjugated structure suggested for **3**.

High resolution measurements showed that the formula of compound **7** ($C_{18}H_{11}N_2OCl$) corresponds to that of **3** ($C_{18}H_{10}N_2Cl_2$) with a hydroxyl group instead of a chlorine atom. Both compounds elute at the same retention time (8.99 minutes) suggesting close structures. **7** was postulated to result from $Cl^{\cdot}$ elimination followed by hydroxyl addition on **3** under irradiation. Kinetics data are in good agreement with this hypothesis: figure 2 shows that **7** appears after **3** and that its relative abundance reaches a maximum as that of **3** sharply decreases. CID transitions from the pseudo molecular ion $\mathbf{7H}^{+}$ correspond to H_2O, $Cl^{\cdot}$ and HCl losses. The corresponding dissociation pathways are given figure 5.

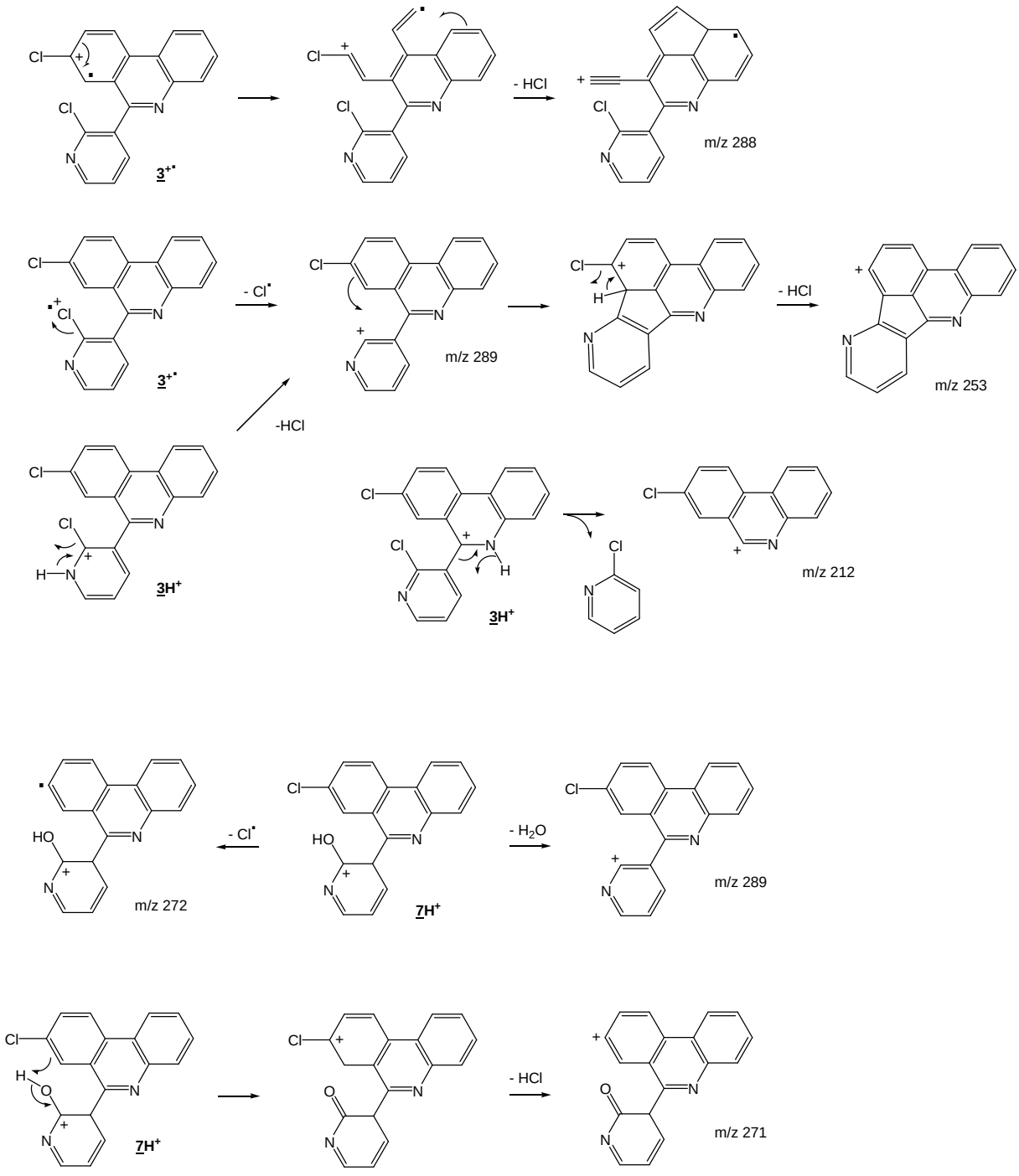

Figure 5. Dissociation pathways proposed for **3**$^{+\cdot}$, **3H**$^{+}$ and **7H**$^{+}$ ions

Compounds **5** and **6** have the same elemental composition $C_{18}H_{13}N_2O_2Cl$ and simultaneously appear after 10 minutes of irradiation. They result from chlorine elimination from boscalid followed by oxidation. $Cl^{\cdot}$ elimination is easily rationalized from the mesomeric form B in figure 3. The resulting cation may directly react with a water molecule to provide the structure referred as B1 in figure 3 or cyclize to provide a more stable structure including an additional six-center ring. In the second case, the addition of a water molecule followed by proton elimination may lead to 3 isomers referred as B2, B3 and B4 in figure 3. CID transitions from the pseudomolecular ion $\mathbf{6H}^+$ allowed to establish that **6** corresponds to the structure B1. First, the transition m/z 325 → m/z 122 (also observed in the boscalid spectrum) corresponds to p-chlorophenyl-2 aniline elimination (see figure 6); it demonstrates that this part of the structure was not affected by irradiation. Secondly, the two consecutive water eliminations (m/z 325 → m/z 307 → m/z 289) from $\mathbf{6H}^+$ imply that the hydroxy function is in ortho position on the pyridine group. The structure **6** has been reported in a previous study devoted to photocatalytic degradation of boscalid [16]. CID transitions from $\mathbf{5H}^+$ correspond to H_2O, $Cl^{\cdot}$ and HCl eliminations (see table 2); they can be rationalized on the basis on dissociation pathways analogous to those presented above and are not sufficiently informative to establish the chemical structure of **5**. The elemental composition of **4** ($C_{18}H_{11}N_2OCl$) suggests that it results from the elimination of a water molecule from **5** or **6**. Kinetics data (figure 2) show a good correlation between the formation of **4** and the disappearance of **5** in good agreement with the first hypothesis. Furthermore, B3 and B4 are the only structures from which water can be easily eliminated to lead to two structures weighting 306 a.m.u. (see figure 3, bottom of the middle part). In CID, the pseudo molecular ion $\mathbf{4H}^+$ eliminates H_2O, HCl and HNCO. A mechanism of isocyanic acid (HNCO) elimination from $\mathbf{4H}^+$ in mass spectrometry is proposed in figure 6 to rationalize the structure postulated for **4**. As depicted in figure 3, both structures B3 and B4 may correspond to **5**.

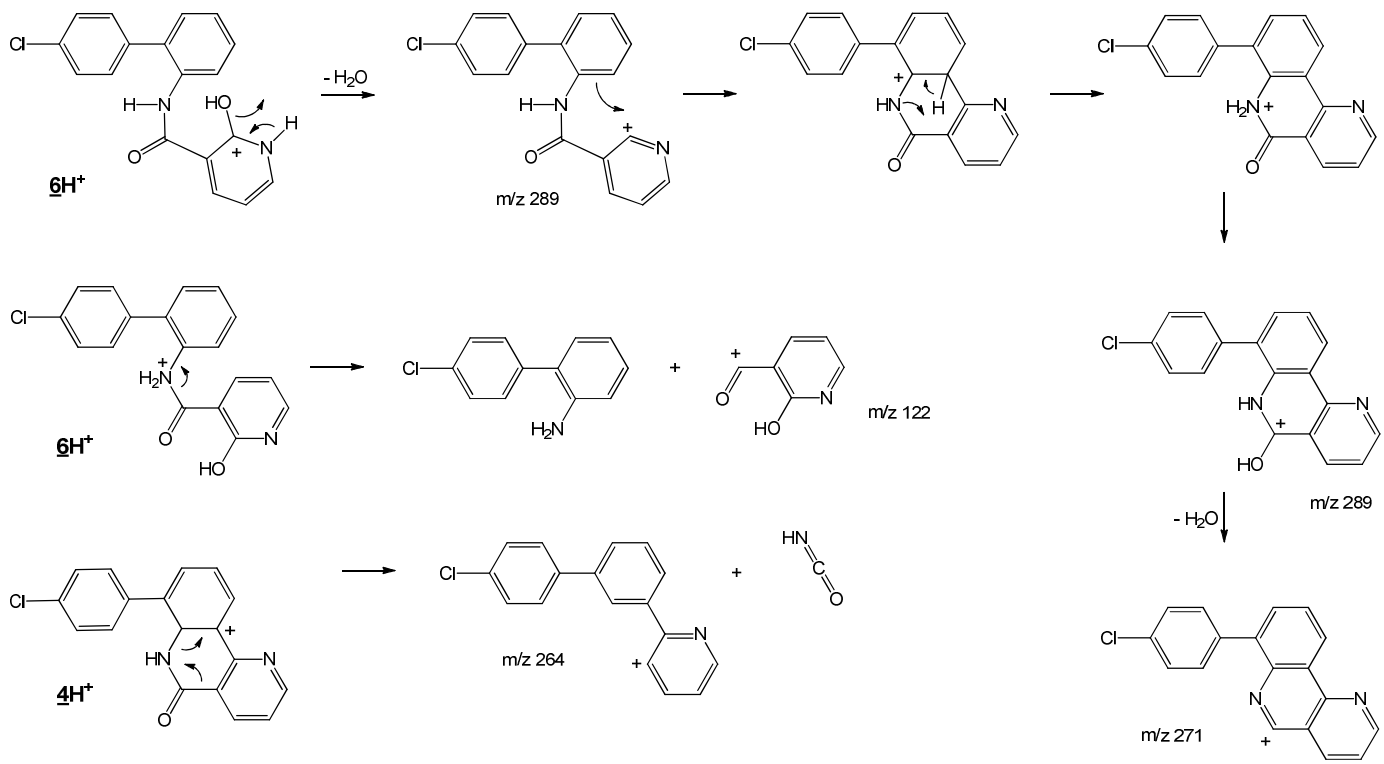

Figure 6. Dissociation pathways proposed for **6H**$^+$ and **4H**$^+$ ions

The elemental composition of compound **8** shows that **8** is an isomer of boscalid. The formation of the ion at m/z 140, also observed for boscalid, analogous to that of m/z 122 for **6** (see figure 6) allowed to conclude that the chloroaniline part of the initial structure was kept intact. CID dissociation pathways are suggested in figure 7 for the ion **8H**$^+$. The simplest mechanism of isomerization of boscalid into **8** implies photoionization of the secondary amine (structure D in figure 3) followed by hydrogen transfer through a four-center transition state and neutralization of the radical cation by capture of an aqueous electron issued from ionization of boscalid (right hand).

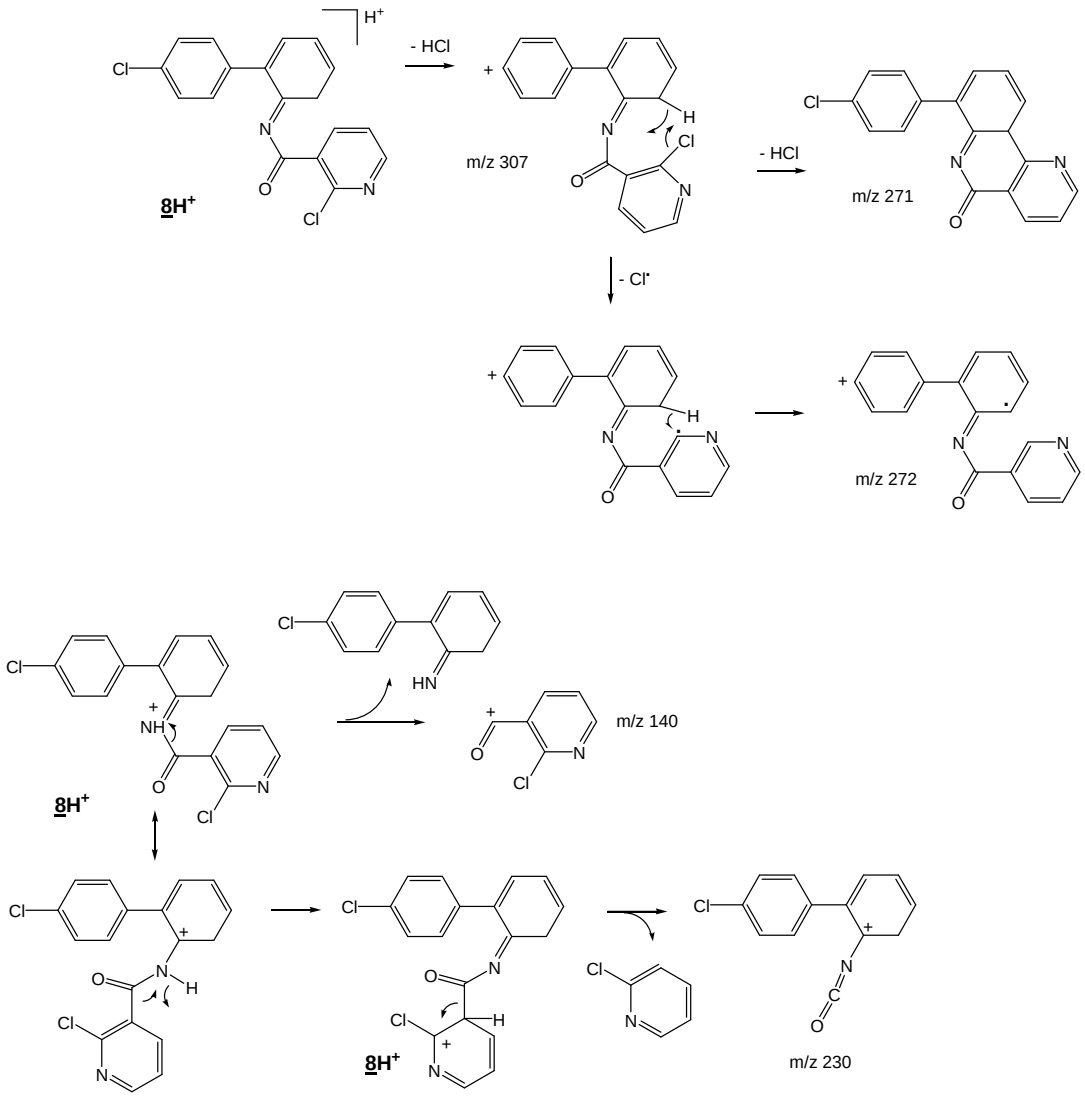

Figure 7. Dissociation pathways proposed for **8H**$^+$ ions.

3.3. Toxicity prediction

In order to evaluate the toxicity of boscalid and its photodegradation products, a toxicity simulation using *in silico* tools was performed. We were mainly interested in the oral rat LD50, the developmental toxicity and the mutagenicity results. Boscalid is classified by the US Environmental Protection Agency as "suggestive evidence of carcinogenicity, but not sufficient to assess human carcinogenic potential" [11]. According to the literature, in acute studies in rats, boscalid had an estimated oral LD50 > 5000 mg/kg [29]. The obtained values through our toxicity

estimation software are between 1006 and 4576 mg/kg for boscalid and its photoproducts **2**, **3**, **4**, **6**, **7** and **8** indicating a low toxicity (figure 8). As shown in figure 8, some of the photodegradation products are slightly more toxic than the parent compound. Compound **5**, for which two structures were postulated, seems to be of moderate toxicity according to Hodge and Sterner classification (values around 100 mg/kg). This effect can be explained by the fact that boscalid induce biochemical effects in mammals consisting in increased liver enzymes (alanine aminotransferase, gamma-glutamyl transferase) and induced thyroid adenomas but the observed responses are considered adaptive and reversible [30]. Besides, the fungicide and its photodegradation products were all shown to cause developmental toxicity at the exception of compound **3**. The reproductive toxicities reported in the literature concerning the boscalid are delayed ossification in rabbits and rats in the presence of maternal toxicity at limit dose [17]. According to the mutagenicity simulation test, boscalid and its photoproducts **1**, **4**, **5**, **6** and **7** are mutagenic. These results are interesting as no data has been reported concerning mutagenicity of boscalid and its degradates. Those predictive values indicate that boscalid and its photoproducts would be of concern as they may cause damages to human and wildlife. This finding suggests that *in vivo* and *in vitro* assays should be achieved in order to assess the real biological effect of those compounds as well as the critical doses.

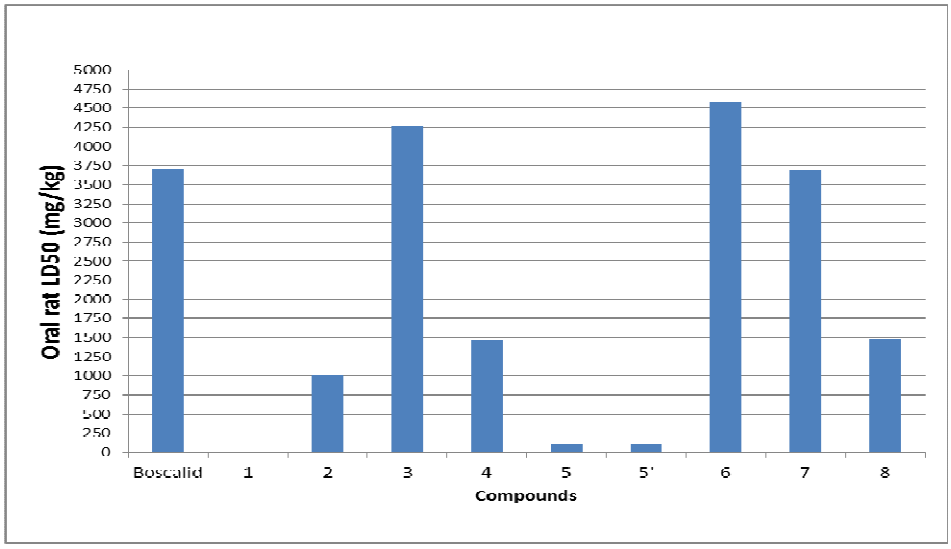

Figure 8. Oral rat LD50 (mg/kg) for boscalid and its photodegradation products predicted using the toxicity estimation software T.E.S.T.*

*Toxicity Estimation Software Tool (version 4.1) ©2012 U.S. Environmental Protection Agency

3.4. Real sample analysis

As we were studying the photoproducts of boscalid, this fungicide was detected at 4 mg Kg^{-1} in a grape leaves sample during routine analysis at the LAPPO (*Laboratoire d'Analyse des Pesticides et des Polluants Organiques*) in Beyrut. The QuEChERS sample preparation process had been applied before LC-MS analysis [30]. Analysis of the real sample was carried out on a 2690 liquid chromatography module coupled with a MS-6410 triple quadrupole (TQ) mass spectrometer (Agilent Technologies, Les Ulis, France). Chromatographic conditions were the same as those described for structural elucidation. The TQ was operated in the Multiple Reaction Monitoring (MRM) mode using the transitions reported in Table 2 (see the Results and Discussion part), with collision energies ranging from 5 to 20 V. Photoproducts **3**, **4** and **5** were unambiguously detected. In the lack of internal standards for these compounds, their concentrations in grape leaves were roughly estimated based on that of boscalid at 0.4 mg Kg^{-1} for **3** and at 0.2 mg Kg^{-1} for **4** and **5**.

4. Conclusion

Eight photoproducts of boscalid were characterized by GC-MS and/or LC-MS. With the exception of compound **6**, the structures proposed for photoproducts on the basis of mass spectra interpretation have not been reported in previous studies. Our results are very different of those reported by Lagunas-Allue *et al.* for photocatalytic degradation of boscalid using TiO_2. In their study, the catalyst induced the formation of $OH^{\cdot}$ radicals that reacted with boscalid to provide mainly mono- and di-hydroxylated products [**Error! Bookmark not defined.**]. In the present work, the lack of catalyst, and thus that of $OH^{\cdot}$ radicals, tended to favor the formation of cyclized photoproducts. The chemical structures and kinetics data permitted to suggest photo transformation pathways. *In silico* toxicity predictions showed that two photoproducts are potentially more toxic than the parent compound considering oral rat LD50 while five photoproducts may induce mutagenic toxicity. With the exception of compound **3**, all photoproducts may potentially induce developmental toxicity.

References

[1] WHO, *Public Health Impact of Pesticides Used in Agriculture*, Geneva, **1990**.

[2] European Commission Health and Consumer Protection General Directorate - Safety of the food chain. Boscalid, **2008**.

[3] M. E. Poulsen, M. Wenneker, J. Withagen, H. B. Christensen. *Crop Prot.* **2012,** 35, 5.

[4] A. Bonnechère, V. Hanot, R. Jolie, M. Hendrickx, C. Bragard, T. Bedoret, J. V. Loco. *Food Control*. **2012**, 25, 397.

[5] S. M. Munitz, S. L. Resnik, M. I. Montti. *Food Chem.* **2013,** 136, 1399.

[6] H. Karaca, S. S. Walse, J. L. Smilanick. *Postharvest Biol. Tech.* **2012**, 64, 154.

[7] H. W. Dehne, H. B. Deising, U. Gisi, K. H. Kuck, P. E. Russell, H. Lyr. Modern fungicides and antifungal compounds VI. *16th International Reinhards Burn Symposium.* **2010**, 10.

[8] T. Veloukas, M. Leroch, M. Hahn, G. S. Karaoglanidis. *Plant Dis.* **2011**, 95, 1302.

[8] European Commission. EU/600/2010. *Journal Officiel de l'Union Européenne* **2010**, 174, 18.

[9] European Commission. 90/642/EEC. *Journal Officiel de l'Union Européenne* **1990,** 350, 70.

[10] United States Environmental Protection Agency (Ed.: Office of Prevention Pesticides and Toxic substances). Boscalid. **2003**, 85.

[11] W. Schwack, B. Bourgeois, F. Walker. *Chemosphere.* **1995**, 31, 4033.

[12] T. Katagi. *Rev. Environ. Contam. T.*, **2004**, 182, 1.

[13] M. F. Chen, J. W. Hang, H. P. Chien. *J. Food Drug Anal.* **2007**, 15, 174.

[14] L. Lagunas-Allue, M. T. Martínez-Soria, J. Sanz-Asensio, A. Salvador, C. Ferronato, J. M. Chovelon. *Appl. Catal. B* **2010**, 98, 122.

[15] European Commission Health and Consumer Protection General Directorate. Ed. Chain safety of the food. Boscalid. **2008**, 3919.

[16] M. Ashley. ROMIL technical report. *www.romil.com* **2006**, Cambridge GB-CB5 9QT.

[17] S. Grimme, J. Antony, S. Ehrlich, H. Krieg. *J. Chem. Phys.* **2010**, 132, 154104.

[18] TURBOMOLE V6.4. A development of the University of Karlsruhe and the Forschungszentrum of Karlsruhe GmbH, *available from www.turbomole.com.* **2012**.

[19] C. Hättig, F. Weigend. *J. Chem. Phys.* **2000**, 113, 5154.

[20] R. Send, V. R. I. Kaila, D. Sundholm. *J. Chem. Theory Comput.* **2011**, 7, 2473.

[21] USEPA. Final contaminant candidate list 3 chemicals: Identifying the universe. U.S. Environmental Protection Agency. *Available from: http://www.epa.gov/safewater /ccl /ccl3.html#chemical 2009.*

[22] L. H. Hall, B. Mohney, L. B. Kier. *J. Chem. Inf. Comput. Sci.* **1991**, 31, 76.

[23] S. Bouchonnet. Introduction to GC-MS Coupling, CRC Press, Boca Raton – Florida, USA, **2013**.

[24] H. Budzickiewicz, C. Djerassi, D. H. Williams, Mass Spectrometry of Organic Compounds, 1st ed., Holden-Day, Inc., San Francisco, USA, **1967.**

[25] F. W. McLafferty. Interpretation of Mass Spectra. 3rd ed., Mill valley, California, USA, **1980**.

[26] A. Kinani, A. Rifai, S. Bourcier, F. Jaber, S. Bouchonnet. *J. Mass. Spectrom.* **2013**, 48, 983.

[27] P. Laszlo. Organic reactions simplicity and logic. 1rst edition, Wiley and Son, Chichester, UK, **1995**.

[28] Public Release Summary on Evaluation of the new active BOSCALID in the product FILAN FUNGICIDE Australian Pesticides and Veterinary Medicines Authority April. *http://www.apvma.gov.au/registration/assessment/docs/prs_ boscalid.pdf*. (accessed 22.05.13), **2004**.

[29] A. A. Elskus. Toxicity, sublethal effects, and potential modes of action of select fungicides on freshwater fish and invertebrates: U.S. Geological Survey Open-File Report 2012. *http://pubs.usgs.gov/of/2012/1213/*. **2012**, 1213, 42.

[30] P. Payá, M. Anastassiades, D. Mack, I. Sigalova, B. Tasdelen, J. Oliva, A. Barba. *Anal. Bioanal. Chem.* **2007**, 389, 1697.

VI-3. Conclusion

Caractérisation structurale

Huit photoproduits du boscalid ont été détectés : cinq seulement par LC/MS, deux par GC/MS uniquement et un par les deux techniques. Deux photoproduits ont conservé les deux atomes de chlore ; les autres photoproduits contiennent un seul atome de chlore. Des calculs de chimie théorique ont montré que les doubles liaisons du cycle pyridine constituent les sites d'ionisation les plus favorables. L'arrachement d'un électron conduit à quatre formes mésomères d'un ion dystonique. Les photoproduits résultent de réactions de ces structures avec l'eau. L'irradiation du boscalid fournit en particulier un isomère de ce dernier, deux structures au sein desquelles un hydroxyle a remplacé un atome de chlore ainsi que des composé tri- et tétra cycliques.

Aspects cinétiques

La cinétique de l'apparition et de la disparition des produits de dégradation du boscalid en fonction du temps d'irradiation a été étudiée sur 150 minutes. Le boscalid et ses produits de transformation sont sous forme de traces près 100 min d'irradiation.

Toxicité prédictive

L'estimation à l'aide d'outils *in silico* de la toxicité des photoproduits a montré que deux d'entre eux sont légèrement plus toxiques que la molécule mère concernant la LD50 chez le rat et que cinq d'entre eux sont potentiellement mutagènes. A l'exception du composé 3, les photoproduits peuvent induire des retards de développement.

VI-4. Analyse d'un échantillon réel

Dans les études précédentes, les expériences de transformation de pesticides sous irradiation UV-visible ont été faites au laboratoire loin des conditions naturelles et en absence des matières organiques présentes dans les matrices réelles. Pour valider la démarche expérimentale utilisée, nous avons analysé un échantillon de feuilles de vigne pour lequel du boscalid avait été détecté à 4 mg L^{-1} lors d'une analyse de routine au LAPPO-Liban. La méthode d'extraction « QuECHERs », validée au LAPPO pour l'extraction des composés organiques en matrices biologiques a été utilisée préalablement à l'analyse par LC-MS.

L'analyse de cet échantillon a été réalisée sur une chromatographie en phase liquide (2610-Agilent Technologies) couplée à un spectromètre de masse triple quadripolaire (MS 6410-Agilent Technologies). Une méthode *Multiple Reaction Monitoring* (MRM) a été développée en ESI en mode positif pour détecter les photoproduits sur la base des transitions établies au DCMR présentées dans le tableau VI-1.

Un mélange eau/0.1% acide formique (A) et méthanol/0.1% acide formique (B) a été utilisé comme phase mobile. Une colonne analytique Agilent C18 3 µm C18 2.1 x 150 mm a été utilisée pour la séparation. La séparation débute avec 45% de B, proportion qui augmente à 90% en 35 min. La proportion de 90% de B est conservée pendant 11,5 min puis ramenée à 45% en 0,1 min. Cette dernière proportion est conservée 9,4 min pour une durée totale de méthode de 56 min. Les paramètres de source ESI sont les suivants : température de l'azote (gaz de nébulisation) à 350 °C, débit de gaz à 9 L min^{-1} et tension de 4000 V sur le capillaire.

Les photoproduits 3, 4 et 5 (voir ci-dessus tableau 2 - article) ont pu ainsi être détectés sans ambiguïté. La figure VI-1 (a et b) montrent les pics des courants ioniques des trois transitions identifiés pour le boscalid et du produit 5, respectivement.

Tableau VI-1. Méthode de MRM utilisée pour détecter les photoproduits du boscalid

Precursor Ion	*Prod Ion*	*Dwell time*	*Fragmenter (V)*	*CID (V)*	*Polarity*
343	307	50	130	5	Positive
343	272	50	130	15	Positive
343	271	50	130	15	Positive
307	289	50	130	5	Positive
307	264	50	130	15	Positive
307	212	50	130	15	Positive
325	307	50	130	5	Positive
325	272	50	130	5	Positive
325	271	50	130	5	Positive
325	289	50	130	10	Positive
325	264	50	130	20	Positive
325	212	50	130	25	Positive
325	288	50	130	20	Positive
325	253	50	130	10	Positive

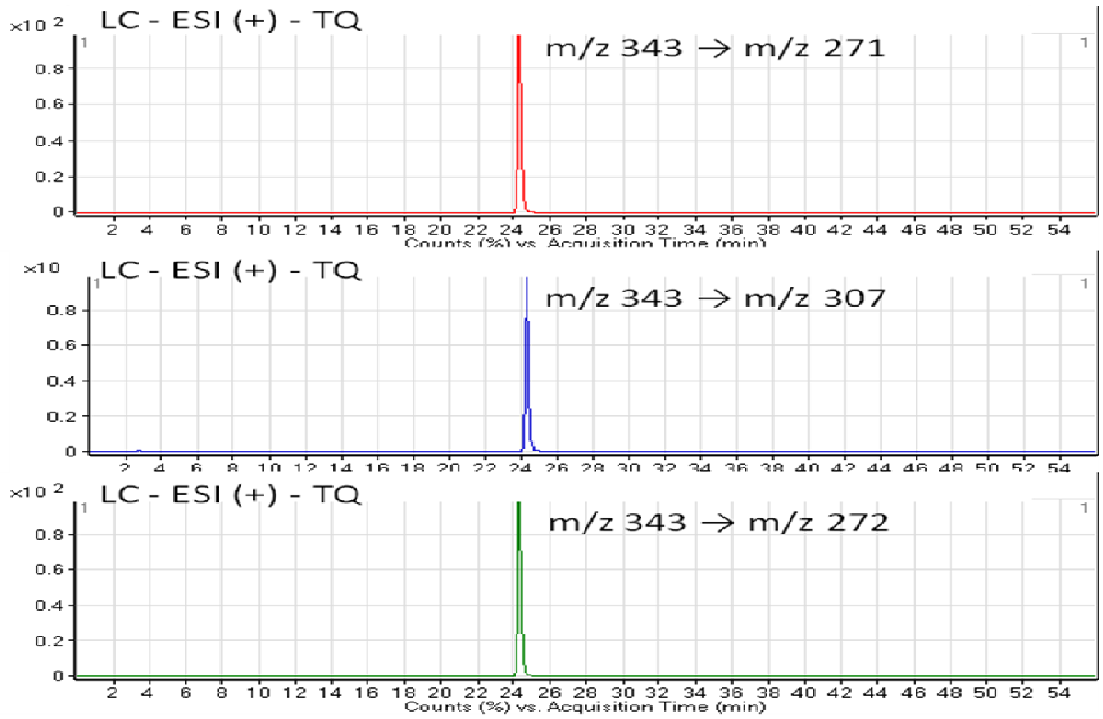

a

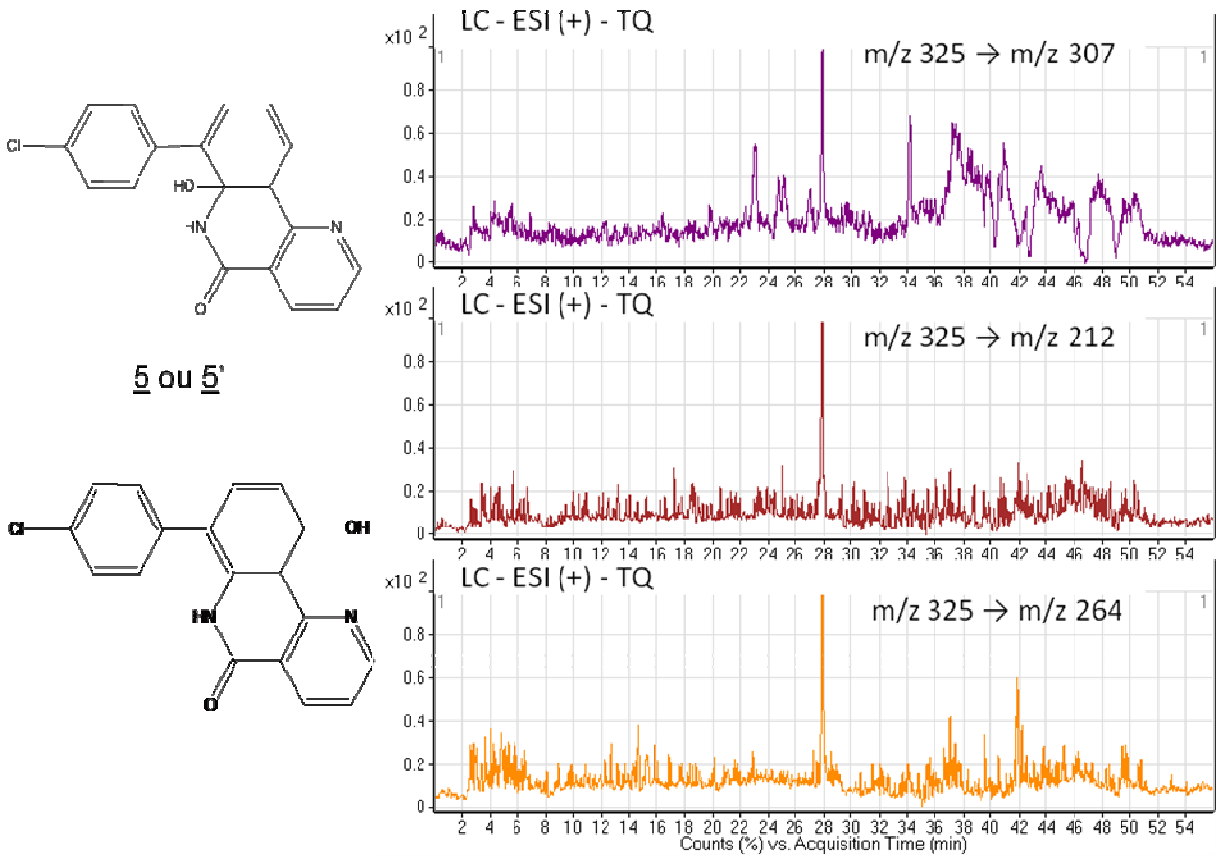

b

Figure VI-1. a- Courant ionique des transitions spécifiques du boscalid. b- Courant ionique des transitions spécifiques du photo-produit 5 avec les structures proposées.

Conclusion générale et perspectives

Les pesticides connus par leurs toxicités aigue et chronique sur les divers constituants de la biosphère (sol, eau et air) et par suite sur l'être humain, sont parfois persistants dans l'environnement et dans certains matrices alimentaires. Les règlements internationaux sont strictes sur l'usage et sur les résidus de pesticides dans les divers matrices alimentaires et imposent des Limites Maximales de Résidus (LMR) à ne pas dépasser. La surveillance de ces LMR nécessite le développement des méthodes analytiques sensibles et efficaces pour l'extraction et l'analyse de résidus des pesticides qui appartiennent à des familles chimiques différentes.

La chromatographie gazeuse ou liquide couplée à des détecteurs par spectrométrie de masse est la technique analytique la mieux adaptée pour cet objectif, elle permet la séparation et la purification des plusieurs dizaines des molécules actives de pesticides aboutissant ainsi à une analyse quantitative fiable et robuste. Également, la GC/MS ou la LC/MS simple ou tandem sont utilisées afin d'identifier les produits de dégradation de pesticides par l'irradiation solaire sur les matrices réelles. En effet, la plupart des études de dégradation des pesticides sont focalisées sur l'élimination de ces molécules de l'environnement par la méthode la plus rapide soit en ajoutant des catalyseurs (sel, enzyme etc..), soit par effet photon.

Les travaux de recherche de cette thèse ont porté sur la photodégradation de fongicides sous irradiation UV-visible. Il s'agissait d'établir si ces fongicides étaient susceptibles de se dégrader sous irradiation solaire, lorsqu'ils sont nébulisés sur les plantes (sur la vigne en particulier). Les travaux de thèse ont débuté par l'étude de la photodégradation d'un herbicide organochloré, le métolachlore, dans l'eau. Cette étude m'a permis d'assimiler la stratégie analytique utilisée au DCMR pour caractériser les structures de photoproduits.

Trois fongicides ont ensuite été choisis sur les critères suivants : molécules nébulisées sur les cultures et utilisées au Liban donc susceptibles d'être retrouvées dans des échantillons de contrôle de routine. Ces molécules sont la procymidone (composé organochloré), le pyriméthanil (anilinopyrimidine) et le boscalid (carboxamide); elles sont reconnues comme perturbateurs endocriniens.

La recherche de molécules inconnues imposait l'utilisation d'une méthode d'extraction non sélective. L'extraction liquide-liquide a été utilisée préalablement à l'analyse des solutions par GC/MS en raison de la nécessité de transférer les analytes dans un solvant organique. Après plusieurs tests portant sur les répétabilités et les rendements d'extraction en SPE, la préparation d'échantillon a été réduite au minimum pour les solutions analysées par LC/MS : simple ajout de méthanol à la solution aqueuse irradiée. Les solutions des pesticides irradiées ont été analysées par GC/MS^n et $LC\text{-}MS^2$ pour couvrir une large gamme de polarités.

Les fongicides retenus pour cette étude se dégradent sous l'irradiation UV mais ne se minéralisent pas. Les résultats obtenus montrent qu'il convient de parler de « photo transformation » plutôt que de photolyse. La stratégie d'élucidation structurale des produits de dégradation des pesticides étudiés a été basée sur l'étude des mécanismes de fragmentation sous différentes énergies de collision des ions moléculaires et pseudo-moléculaires des pesticides formés selon différents modes d'ionisation : ionisation électronique et ionisation chimique en $GC\text{-}MS^n$, ionisation par électronébulisation en LC-Q-TOF. Des études cinétiques ont permis de corréler l'apparition de certains photoproduits à la disparition d'autres et ainsi de déterminer des structures intermédiaires. La rémanence des photoproduits après irradiation a également fiat l'objet d'études, en particulier pour le métolachlore.

Les molécules de fongicides étudiées présentent plusieurs sites susceptibles de perdre un électron lors de l'excitation par irradiation UV-visible. Des calculs de chimie quantique ont permis de déterminer la répartition de la densité électronique de la molécule et ainsi d'établir le ou les sites préférentiels d'ionisation.

La stratégie utilisée pour l'élucidation structurale des produits de dégradation s'est avérée pertinente, la plupart des structures chimiques des produits formés ayant été élucidées sans ambiguïté. Des mécanismes de photolyse ont pu ainsi être proposés. Dans l'eau les réactions dominantes sont l'addition d'une ou deux fonctions hydroxy ainsi que la formation de cycles à cinq et six atomes.

Les structures de certains composés demeurent des hypothèses plausibles mais elles ne sont pas démontrées. La Disposition de produits marqués permettrait d'être plus catégorique. De plus, les mécanismes proposés sont plausibles mais non démontrés et ils peuvent s'avérer complexes et surtout très difficiles à prévoir.

La toxicité des photoproduits identifiés a été estimée à l'aide du programme de calcul de toxicité prédictive T.E.S.T. Ces estimations *in silico* ont montré que les photo-produits du métolachlore et de la procymidone ne présentaient pas de mutagénicité. Cependant, tous les sous produits de ces deux pesticides auraient des effets toxiques sur le développement du fœtus avant la naissance et sur la taille de l'animal après la naissance. L'estimation de la dose létale LD50 chez le rat des produits de dégradations observés par LC-MS a montré que neuf photo-produits du métolachlore et trois photo-produits de la procymidone seraient plus toxiques que les molécules mères (composés hydroxylés en particulier) en accord avec des données de la littérature. Les résultats obtenus ne sont que des estimations visant à orienter les tests des biologistes. Pour être recevables, ils doivent être comparés à des résultats de la littérature (tests in vitro et/ou in vivo). Ils ne considèrent pas les effets agonistes et antagonistes.

Suite à ces études, nous avons analysé un échantillon de feuilles de vigne dans lequel 4 mg/L de boscalid avaient été détectés lors d'analyses de routine au LAPPO- Liban. Nous avons détecté trois produits de dégradation du boscalid identifiés dans les solutions de standards irradiées en laboratoire. Ces résultats illustrent la pertinence de la stratégie utilisée : la modélisation en laboratoire de la photo transformation sous rayonnement UV-visible, bien que très éloignée des conditions naturelles d'irradiation des pesticides (absence de matière organique en particulier) permet d'établir les structures des principaux photoproduits et ainsi de programmer des méthodes pour une détection spécifique et sensible en matrices environnementales.

La continuité de notre étude sera par la proposition des méthodes d'analyse des pesticides avec leurs photo-produits en LC-MS dans les méthodes MRM utilisées au LAPPO. Ces méthodes aident pour valider le modèle sur un nombre conséquent d'échantillons. Puis, il faut prendre en considération la quantité de fongicide photo-transformé dans l'interprétation des résultats.

Pour les produits rémanent, il faut les synthétiser en disposant un standard de dosage en matrice. Puis, il faut réaliser des tests *in vitro* à partir de ce photoproduit pour confronter les résultats à ceux issus des tests *in silico.*

De plus, on doit étudier l'influence de l'irradiation solaire sur les adjuvants dans les pesticides commerciaux et si ces additifs se réagissent avec les molécules mères ainsi que avec les photo produits de ces polluants. De plus, il faut estimer la réaction des pesticides utilisés dans la commerces avec les constituants des matrices réelles (ex. feuilles des arbres ou des plantes, les peaux des fruits et des légumes etc..) et la migration de ces pesticides à l'intérieur de ces matrices. Proposer des mécanismes réactionnels qui expliquent ces phénomènes et identifier les structures de ces composés.

Travaux associés

Fragmentation reactions of phenoxide anions: deprotonated Dinoterb and related structures

Ahmad Rifai, Sophie Bourcier, Delphine Arquier, Yannick Charvet, Farouk Jaberc and Guy Bouchoux

J. Mass. Spectrom. 2011, 46, 1079–1088

Abstract

Dinoterb (6-t-butyl-2,4-dinitrophenol), 1, Dinoseb (6-secbutyl-2,4-dinitrophenol), 2, TBP (2-t-butylphenol), 3, and DNP (2,4- dinitrophenol), 4, have been analyzed by electrospray ionization in the negative mode (ESI-N) - tandem mass spectrometry. Nominal laboratory collision energy was varied from zero to 60 eV during the experiments. Apparent fragmentation energies were estimated from a parametric fitting of the collision efficiency curves. In parallel, fragmentation mechanisms of the deprotonated molecules $[M-H]^-$ were explored using quantum chemistry modeling at the B3LYP/6-31 + G(d,p) level. A major fragmentation of the $[M-H]^-$ ions of Dinoterb and Dinoseb is elimination of an alcohol molecule. This reaction is shown to involve one oxygen atom originating from a nitro group rather than the phenoxide moiety. Eliminations of NO, CH_4 and $CH_2=C(CH_3)_2$, i.e. reactions involving significant rearrangements, constitute the major part of the other fragmentation pathways observed from $[3-H]^-$ and $[4-H]^-$ ions.

Keywords: herbicides; tandem mass spectrometry; negative ions; ESI; DFT; quantum chemistry computations; fragmentation mechanisms

INTRODUCTION

Detection and quantitation of pesticide multiresidues by mass spectrometry, coupled with GC or LC separation methods, have been extensively reviewed in the recent years.[1–9] However, elucidation of the corresponding mass spectra and examination of the role of activation conditions in MS/MS experiments have not been always considered.

In the course of a general study of the fragmentation mechanisms of ionized pesticides, we examined the mass spectra of Dinoterb (6-t-butyl-2,4-dinitrophenol), 1 and Dinoseb (6-secbutyl-2,4-dinitrophenol), 2. Two structuraly related substituted phenols, 2-t-butylphenol (TBP), 3 and

2,4-dinitrophenol (DNP), 4 were also investigated (Scheme 1). Obviously, due to the presence of a phenol function, characterization of these molecules by mass spectrometry was expected to be easier using negative ionization mode (ESI-N). Indeed, determination of phenolic pesticides using egative electrospray ionization, ESI, or atmospheric pressure chemical ionization, APCI, was reported earlier.[10,11] In the present study, molecules M= 1–4 were examined using ESI and tandem mass spectrometry experiments. Surprisingly, contrasting and specific fragmentation routes have been observed from the four corresponding $[M-H]^-$ ions. In order to understand these peculiarities, we have explored the structural and energetic aspects of these fragmentations by quantum chemistry computations using density functional theory on several model ions.

EXPERIMENTAL AND COMPUTATIONAL SECTION

Chemicals, acetic acid, ammonium acetate and HPLC grade solvents were all purchased from Sigma Aldrich (Saint Quentin Fallavier, France) and used as received. Solutions of each compound at 10_2M were prepared in methanol. Buffer solutions (10 mM) were prepared by dissolving 0.07 g of ammonium acetate in 100 mL of water and adding an appropriate volume

of a 10mM acetic acid solution to obtain a pH of ca. 4.6. These solutions were diluted at 10^{-5}M in a mixture of buffer solution/ CH3CN (50:50) mixture for acquisition in the negative-ion mode.
Mass spectra were collected with a triple quadrupole (TQ) mass spectrometer Thermo-Electron TSQ Quantum (Orsay University). Solutions were infused into the electrospray ionization source with a syringe pump at an infusion rate of 10 $mL.min^{-1}$. Two acquisition modes were used to characterize each compound (1) full scan mode, and, (2) MS/MS of several selected ions in order to study decomposition pathways. The capillary voltage was set to -3.5 kV negative-ion mode at a temperature of 270 °C. Nitrogen was used as both nebulizing and desolvatation gas. High resolution and precise mass measurements were carried out with a Q-TOF Premier instrument equipped with a Z-spray electrospray source (Waters, Saint Quentin-en-Yvelines, France) using W-mode.
Phosphoric acid was used in mixture to pesticide as internal calibrant. Precise masses and elemental compositions were obtained using the software MassLynx. The ion used for the mass correction was m/z 292.9229. Ion signals were optimized by adjusting the source parameters as follows: cone voltage = 20 V, capillary voltage =-3.2 kV, extraction cone voltage = 2 V, ion

guide voltage of 2.4 V. Source and désolvatation temperatures were set at 80 _C and 250 _C, respectively.

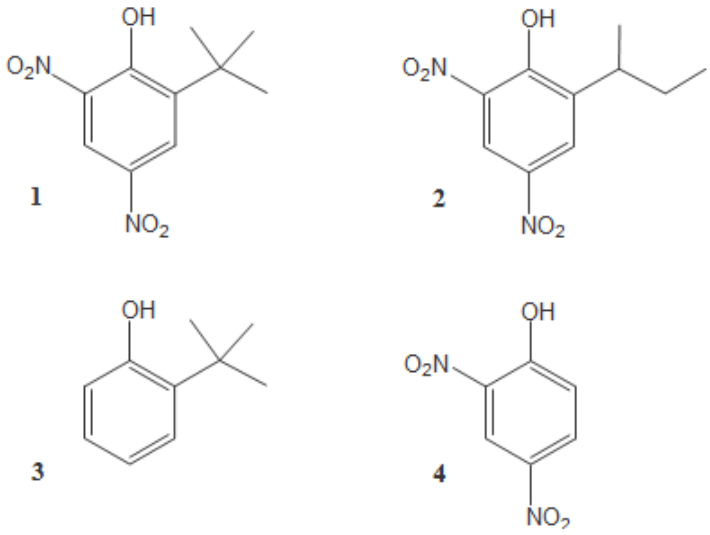

Scheme 1. Chemical structures of the studied compounds.

The MS/MS decomposition of ions of interest was studied in the TQ instrument as a function of the collision energy in the laboratory frame whose nominal value, Elab, was typically varied in the 0–60 eV range by steps of 1–2 eV. The results are presented as breakdown graphs showing the abundances of the various fragment ions as a function of the centre of mass energy on Figs. 1–5. The conversion of E_{lab} into centre of mass relative energies, E_{cm}, has been done using the usual formula (Eqn 1):

$$E_{cm} = E_{lab}\, m_n / (m_n + m_i) \qquad (1)$$

where m_n and m_i represent the masses of the neutral target and the projectile ion, respectively. Argon was used as collision gas. Breakdown graphs were obtained by reporting relative abundances of each ion, I_i, as a function of E_{cm}. In order to gain some quantitative information on the appearance thresholds of the fragment ions, each Ii versus E_{cm} curve has been fitted with a parametric sigmoid function (Eqn 2).

$$I_i = a + b/[1 + \exp\{(c - E_{cm})/d\}] \qquad (2)$$

According to this relationship, the half population of ion i ($I_i = a + b/2$) corresponds to $E_{cm1/2} = c$ and the baseline intercept of the tangent of the sigmoid curve passing by the half population

point (I_i = a) is equal to E_{cm0} = c – 2 d. The four parameters a–d were determined using a least square regression analysis procedure (Igor Pro 5.0 program, WaveMetrics). The resulting

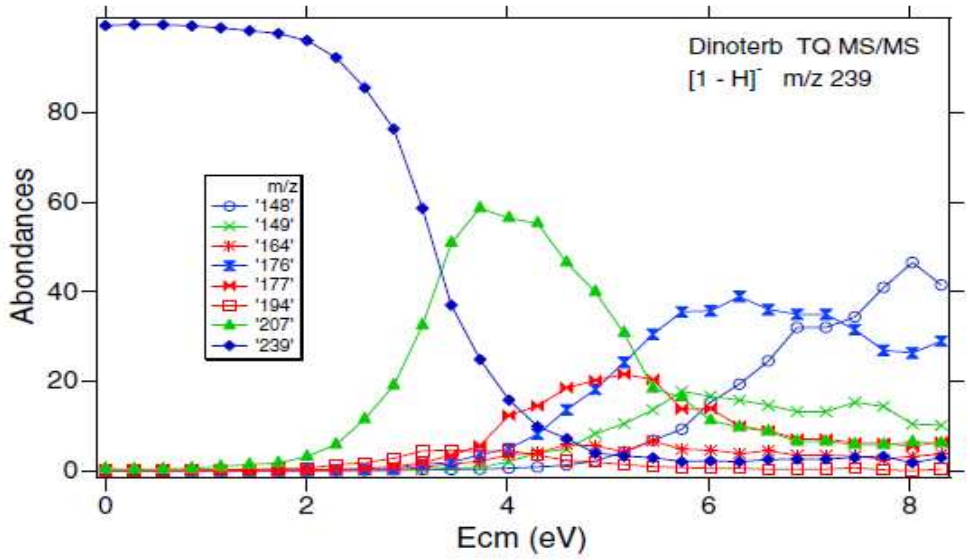

Figure 1. Breakdown graph associated with the decomposition of [**1**-H]⁻ (**1**=Dinoterb) *(m/z* 239).

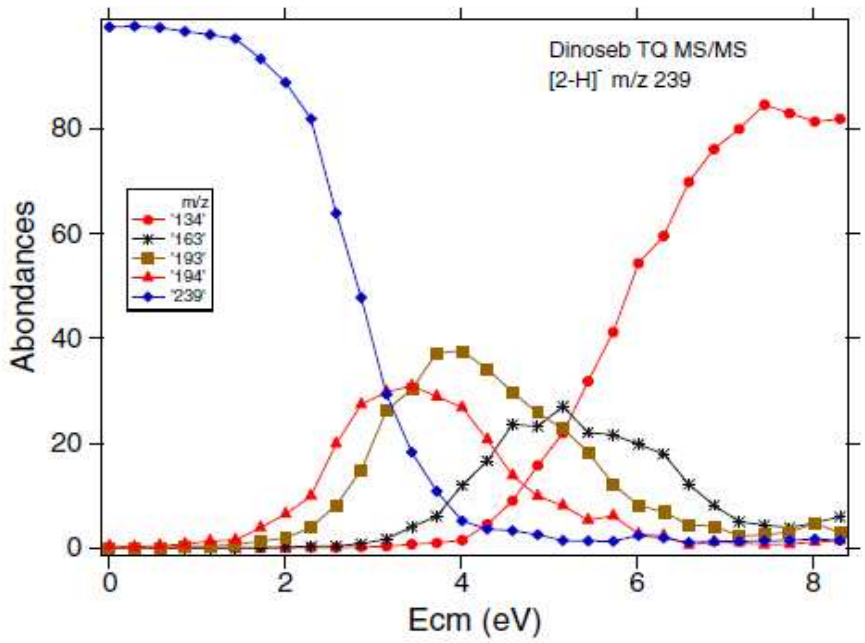

Figure 2. Breakdown graph associated with the decomposition of [**2**-H]⁻ (**2**=Dinoseb) *(m/z* 239).

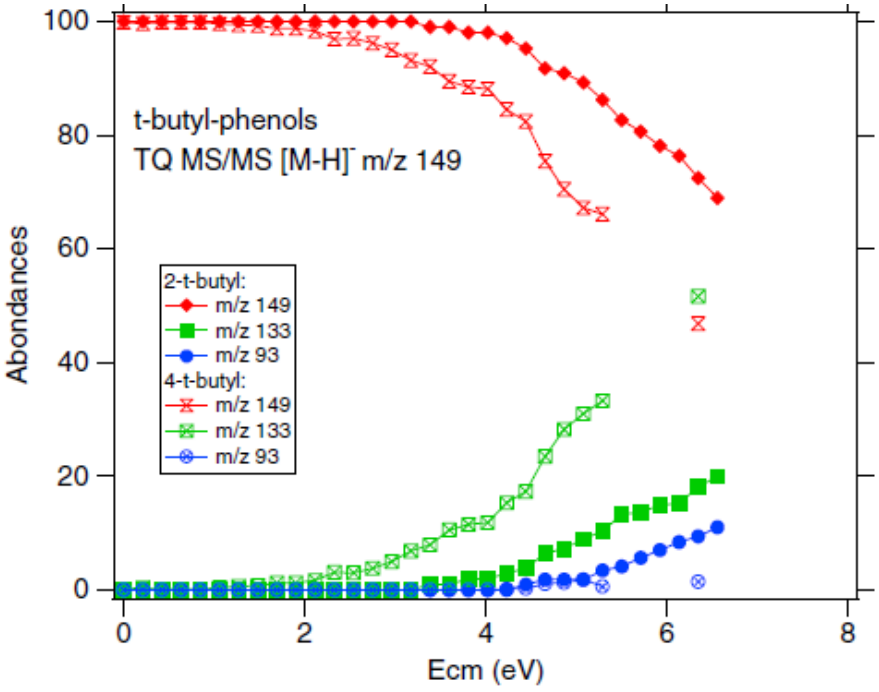

Figure 3. Breakdown graph associated with the decomposition of [**3**-H]$^-$ and [**3**'-H]$^-$ (**3**=2-t-butyl-phenol, **3**'=4-t-butyl-phenols) *(m/z* 149).

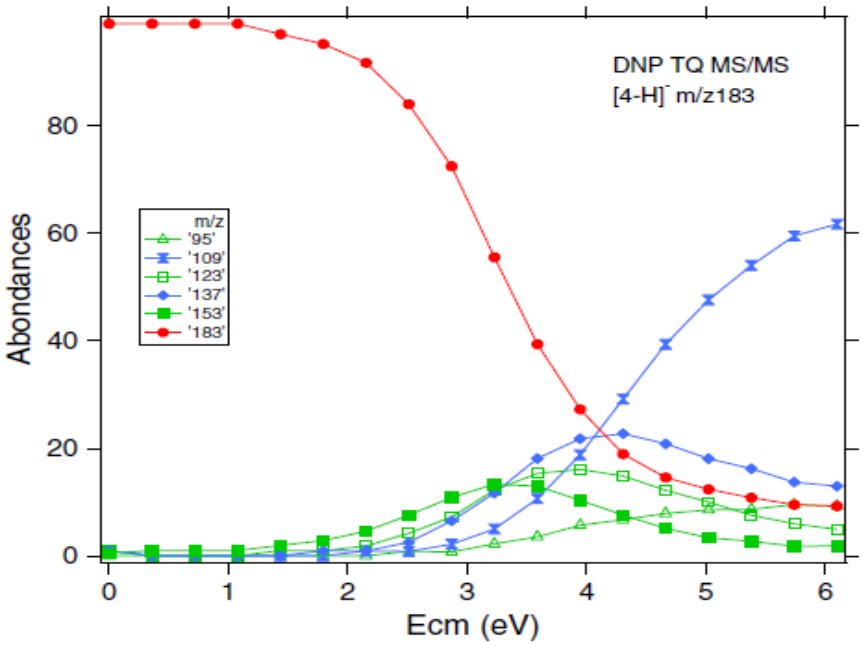

Figure 4. Breakdown graph associated with the decomposition of [**4**-H]$^-$ (**4**=2,4-dinitrophenol) *(m/z* 183).

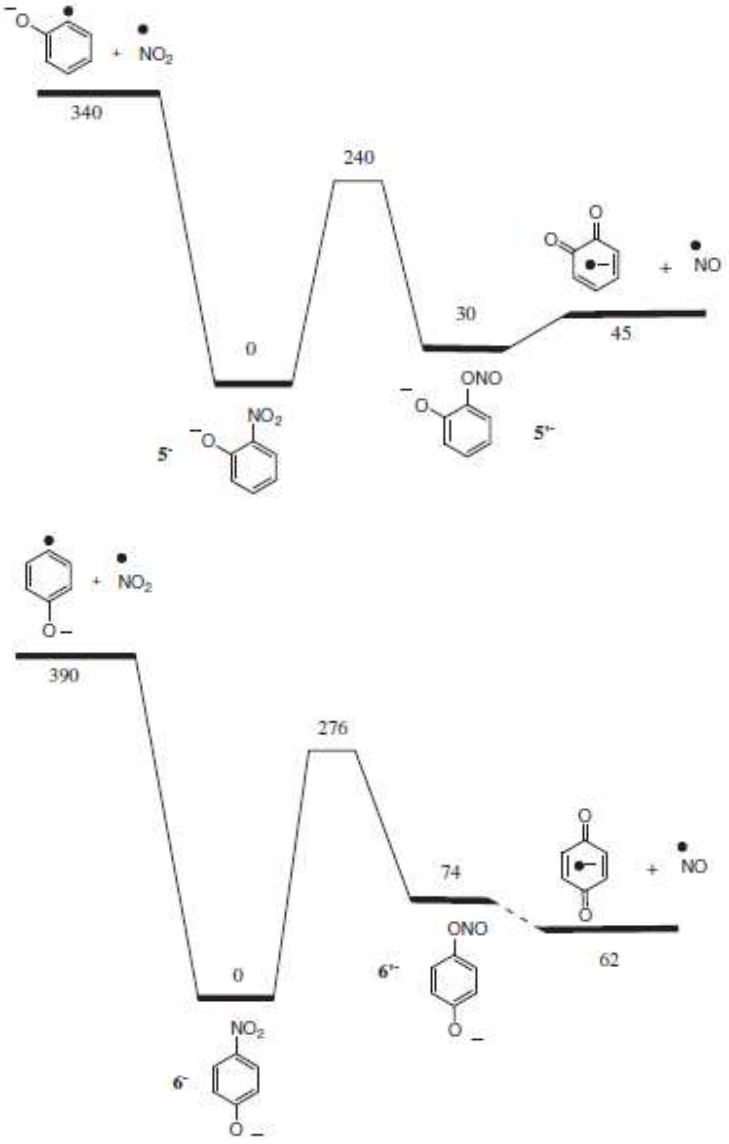

Figure 5. H°_{298} (kJ.mol^{-1}) profiles for the eliminations of $^{\bullet}NO$ or $^{\bullet}NO_2$ from *ortho* and *para* nitro-phenoxide ions.

Table 1. Apparent threshold energie E_{cm0} (in eV) for the considered systems[a]

Precursor ion	Fragment ion (*m/z*)	Attribution	E_{cm0}
[**1**-H]$^-$ (*m/z* 239)	207	$-CH_3OH$	2.5
	177	$-CH_3OH-NO$	3.3
	176	$-CH_3OH-OCH_3$	4.0
	149	$-CH_3OH-NO-CO$	4.1
	148	$-CH_3OH-OCH_3-CO$	5.3
[**1**-H-CH_3OH]$^-$ (*m/z* 207)	177	$-NO$	1.7
	176	$-CH_3O$	2.3
	149	$-NO-CO$	2.6
	148	$-CH_3O-CO$	3.6
[**2**-H]$^-$ (*m/z* 239)	194	$-CH_3NO$	2.0
	193	$-C_2H_5OH/-NO_2$	2.4
	163	$-C_2H_5OH/-NO_2-NO$	3.5
	134	$-NO_2-NO-C_2H_5$	4.7
[**2**-H-C_2H_5OH]$^-$ (*m/z* 193)	163	$-NO$	1.6
	135	$-NO-CO$	1.9
	134	$-NO-C_2H_5$	2.7
[**3**-H]$^-$ (*m/z* 149)	133	$-CH_4$	4.0 (3.4)[b]
	93	$-CH_2C(CH_3)_2$	4.9
[**4**-H]$^-$ (*m/z* 183)	153	$-NO$	1.8
	137	$-NO_2$	2.6
	123	$-NO-NO$	2.3
	109	$-NO-NO_2$	3.4

a) As deduced from a sigmoid fitting (see text), ±0.1 eV. b) into parentheses, 4-t-butylphenol.

E_{cm0} values are reported in Table 1. It should be underlined that these E_{cm0} energies should be considered only as phenomenological quantities and do not represent true critical energies. Accordingly, a complete treatment of the experimental breakdown graphs in order to derive correct threshold energies would include a modeling of the fragmentation kinetics and considerations of the conversion of collision energies (including a calibration of the E_{lab} scale) to internal energies.[12–14] Molecular orbital calculations have been conducted using the GAUSSIAN03 suite of programs[15,16] within the density functional theory. Geometries were optimised at the B3LYP/6-31 + G(d,p) level of theory, and unscaled vibrational frequencies calculated at this level were used to calculate vibrational contribution to enthalpy at 0 K and 298 K. Transition structures have been characterized by the occurrence of one negative eigen value in the force constant matrix.

EXPERIMENTAL RESULTS

Dinoterb, 1

The ESI-N mass spectrum of Dinoterb shows essentially two peaks at m/z 239 and m/z 207. Exact mass measurement shows that the former peak corresponds to $[1\text{-H}]^-$ ($C_{10}H_{11}N_2O_5$) ions and the latter to $[1\text{-H-CH}_3\text{OH}]^-$ ($C_9H_7N_2O_4$). The fragmentation pattern of deprotonated Dinoterb, $[1\text{-H}]^-$, as deduced from the breakdown graphs of $[1\text{-H}]^-$ (m/z 239, Fig. 1) and [1-H-CH3OH]$^-$ (m/z 207) ions, is summarized in Scheme 2. The major process is the loss of a methanol molecule from$[1\text{-H}]^-$ leading to m/z 207 ions. This fragmentation is followed by a competitive elimination of $^{\cdot}$NO or $^{\cdot}OCH_3$ radicals to produce m/z 177 and m/z 176 ions which in turn may eliminate a CO molecule thus giving rise to m/z 149 and m/z 148 ions. $^{\cdot}$NO loss from m/z 207 ions is energetically favoured over $^{\cdot}OCH_3$ loss by ~0.6 eV (Table 1). Interestingly enough, a small amount of ions m/z 194 ([1-H-CH3NO]$^-$) and m/z 164 ([1-H-CH3NO $^{\cdot}$NO]$^-$) are produced from $[1\text{-H}]^-$ (Fig. 1).

As observed from Fig. 1, total ion current in the m/z 239 MS/MS mass spectrum corresponds essentially to m/z 207, 176 and 148 ions in the E_{cm} range 0–8 eV. Detection and quantitation of Dinoterb by multiple reactions monitoring (MRM) is consequently expected to be easier using the m/z 239 → m/z 207, m/z 239 → m/z 176 and m/z 239 → m/z 148 transitions. Fig. 1 also shows that the maximum sensitivity for using m/z 207, 176 and 148 ions in MRM experiments corresponds to centre of mass collision energies E_{cm} equal to 4, 6 and 8 eV, respectively.

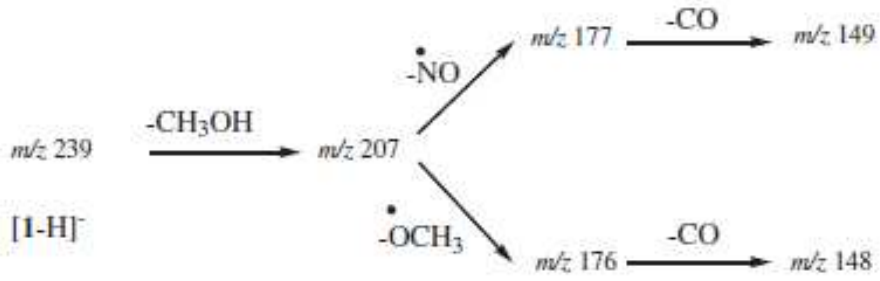

Scheme 2. Decomposition pathways of [**1**-H]$^-$ ions of Dinoterb (**1**, m/z 239) evidenced by MS/MS experiments.

Dinoseb, 2

In the ESI-N conditions, the mass spectrum of Dinoseb presents significant signals at m/z 239, $[2\text{-H}]^-$, m/z 194 and m/z 193. Exact mass measurement shows that m/z 193 ions from the ion source mainly (~95%) correspond to the composition $C_8H_5N_2O_4$, i.e. to $[2\text{-H-}C_2H_5OH]^-$ ions. The remaining ~5% of the m/z 193 signal is attributable to [2-H-NO_2]- ions (i.e. $C_{10}H_{11}NO_3$). In the ESI source, m/z 194 ions are essentially originating from the CH3NO loss from the $[2\text{-H}]^-$ pseudo-molecular ions. Approximately 10% of the m/z 194 signal should be, however, due to the 13 C and 15 N isotopic contributions of the m/z 193 ions. Two other, minor, peaks are observed in the ESI-N mass spectrum of Dinoseb: m/z 209 and m/z 207 which may be attributed to $[2\text{-H-NO}]^-$ and $[2\text{-H-}CH_3OH]^-$ ions.

The MS/MS spectrum of $[2\text{-H}]^-$ presents also peaks at m/z 193 and m/z 194. These products correspond to the lowest energy processes (Fig. 2, Table 1). Beside these signals, peaks at m/z 163 and m/z 134 (but also minor signals at m/z 209 and 162) are also observed. As seen from examination of Fig. 2, the maximum sensitivity in MRM analysis of Dinoseb is expected to occur near 4 eV for transitions m/z 239 → m/z 194 or 193, 5 eV for m/z 239 → m/z 163 and 8 eV for m/z 239 → m/z 134.

Although the MS/MS spectra of m/z 193 and m/z 194 ions should be considered with care since the parent signal consists in a mixture of ions of different elemental composition several observations are of interest. The MS/MS spectrum of m/z 193 ions shows signals corresponding to m/z 163 (major) and 162 (minor) ions and, at higher collision energy, to m/z 134. A small peak at m/z 135 probably associated with a CO loss from m/z 163 is also observed. The MS/MS spectrum of m/z 194 ions shows essentially a peak at m/z 135 pointing to the elimination of C2H5NO. A small amount of m/z 164 ions is detected at low collision energy; this signal rapidly disappears to the benefit of m/z 135 when the collision energy increases. This may be taken as evidence that loss of C_2H_5NO may result from successive eliminations of NO and C_2H_5. Considering these results, a possible fragmentation pathway is proposed in Scheme 3.

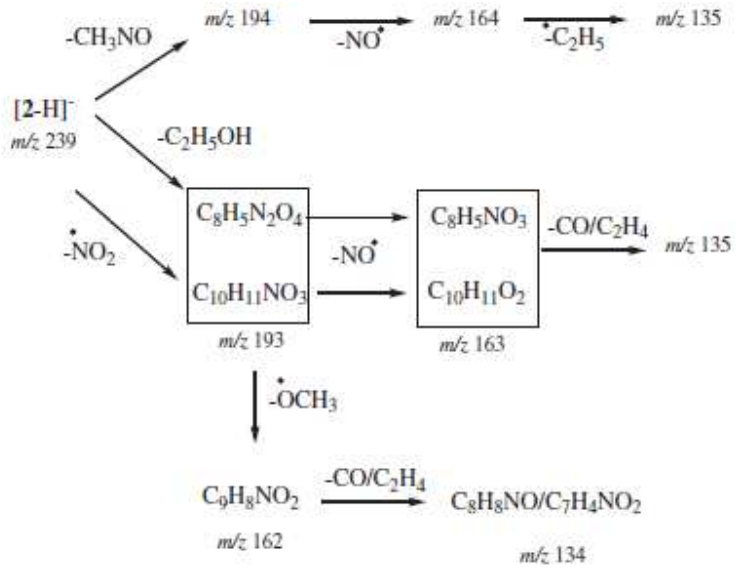

Scheme 3. Decomposition pathways of [**2**-H]⁻ ions of Dinoseb (**2**, m/z 239) evidenced by MS/MS experiments.

2-t-butylphenol, 3

The ESI-N mass spectrum of 2-t-butylphenol, 3 presents only one peak corresponding to the pseudo molecular ions $[3\text{-H}]^-$ (m/z 149). The MS/MS spectrum of these ions presents two peaks at m/z 133 and m/z 93 corresponding to competitive losses of 16 and 56 mass units which may be attributed to elimination of methane and 2-methylpropene, respectively (Scheme 4). Methane loss from alkyl phenoxide ions, and particularly [3-H]-, has been previously evidenced under comparable mass spectrometry conditions (collision energy Elab = 35 eV); by contrast, alkene loss has not been reported before[17]. The breakdown graph presented in Fig. 3 shows that the methane elimination is the process of lowest energy. A difference in centre of mass collision energy, E_{cm0}, of ca. 1 eV is observed between the two dissociation routes.

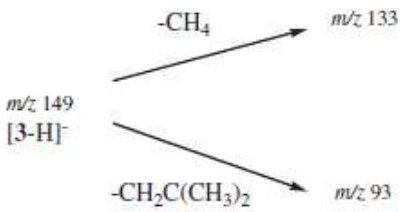

Scheme 4. Decomposition pathways of [**3**-H]⁻ ions of 2-terbutylphenol (**3**, m/z 149) evidenced by MS/MS experiments.

Examination of the isomeric phenoxide ion derived from 4-t-butylphenol, 3', has been done for comparison. The collision efficiency curves for m/z 149 and m/z 133 ions are also presented in Fig. 3. It is noteworthy that m/z 93 ions are only detected at trace level showing a negligible efficiency of the 2-methylpropene elimination for the para isomer. A second interesting observation is that the apparent threshold formethane loss is reduced by ca. 0.6 eV for the 4-t-butylphenol.

The ESI-N mass spectrumof 2,4-dinitrophenol, 4 exhibits only the m/z 183 peak corresponding to the pseudo molecular ions $[4\text{-H}]^-$. Upon collision activation, these ions undergo significant decompositions (Scheme 5 and Fig. 4). The lowest energy route leads to m/z 153 ions by ˙NO loss. A second elimination of ˙NO follows and produces m/z 123 ions which in turnmay dissociate by elimination of a CO molecule. Beside these successive dissociations, a competitive route is associated with the elimination of the ˙NO2 group from the $[4\text{-H}]^-$ ions and a subsequent elimination of CO leading to m/z 137 and m/z 109 ions. It should be emphasized that, despite a higher energy requirement, these latter processes rapidly produce the most abundant fragment ions (see Fig. 4).

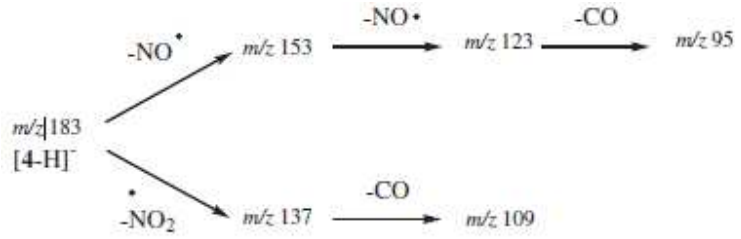

Scheme 5. Decomposition pathways of [**4**-H]⁻ ions of 2, 4-dinitrophenol (**4**, m/z 183) evidenced by MS/MS experiments.

MODELING OF THE FRAGMENTATION REACTIONS AND DISCUSSION

What is remarkable is the contrasting behaviour of the four phenoxide ions $[\text{M-H}]^-$ (M = 1–4). While the reactivity of $[3\text{-H}]^-$ and $[4\text{-H}]^-$ phenoxide ions seems to be located on the substituents (either the alkyl or nitro groups), $[1\text{-H}]^-$ and $[2\text{-H}]^-$ ions mainly dissociate by elimination of an alcoholmolecule, a process necessarily involving interaction between the alkyl group and an oxygen containing moiety. To shed light on these mechanistic peculiarities, we have performed computational modeling of several key processes (Table 2).

Table 2. Total (Hartree) and relative ($kJmol^{-1}$) $H°_0$ and $H°_{298}$ related to fragmentations of $[4\text{-H}]^-$ (B3LYP/6-31+G(d,p) calculations)

Species	$H°_0$		$H°_{298}$	
	total	relative	total	relative
para-nitro-phenoxide, $\mathbf{6}^-$	−511.387496	0	−511.378902	0
para-nitrite-phenoxide, $\mathbf{6'}^-$	−511.359307	74	−511.350021	76
TS-*para*-nitro-nitrite, $\mathbf{6/6'}^-$	−511.282416	276	−511.273729	276
ortho-nitro-phenoxide, $\mathbf{5}^-$	−511.369920	0	−511.361169	0
ortho-nitrite-phenoxide, $\mathbf{5'}^-$	−511.358383	30	−511.349214	31
TS-*ortho*-nitro-nitrite, $\mathbf{5/5'}^-$	−511.279695	237	−511.270967	237
$[\mathbf{4\text{-H}}]^-$	−715.904067	0	−715.892843	0
$\mathbf{4a}^-$	−715.883600	54	−715.871670	56
$\mathbf{4b}^-$	−715.900318	10	−715.888668	11
$\mathbf{4c}^-$	−510.684641		−510.675285	
$\mathbf{4f}^-$	−510.682511		−510.673106	
$\mathbf{4d}^-$	−510.694205		−510.685390	
$\mathbf{4e}^-$	−510.712209		−510.703577	
$\mathbf{4g}^-$	−585.992022		−585.982402	
$\mathbf{4h}^-$	−585.997315		−585.987741	
$\mathbf{4i}^-$	−456.105089		−456.097019	
$^{\cdot}\mathbf{NO}$	−129.890966		−129.887661	
$^{\cdot}\mathbf{NO_2}$	−205.075105		−205.071225	
$\mathbf{4c}^- + {}^{\cdot}\mathbf{NO_2}$	−715.759746	379	−715.74651	384
$\mathbf{4f}^- + {}^{\cdot}\mathbf{NO_2}$	−715.757616	384	−715.744331	390
$\mathbf{4d}^- + {}^{\cdot}\mathbf{NO_2}$	−715.76931	354	−715.756615	358
$\mathbf{4e}^- + {}^{\cdot}\mathbf{NO_2}$	−715.787314	306	−715.774802	310
$\mathbf{4g}^- + {}^{\cdot}\mathbf{NO}$	−715.882988	56	−715.870063	60
$\mathbf{4h}^- + {}^{\cdot}\mathbf{NO}$	−715.888281	42	−715.875402	46
$\mathbf{4i}^- + 2\ {}^{\cdot}\mathbf{NO}$	−715.887021	45	−715.872341	54

˙NO and ˙NO2 losses from nitro phenoxide ions

Eliminations of ˙NO2 and ˙NO are common processes in the chemistry of nitroaromatic compounds. The latter reaction is generally interpreted by the occurrence of a nitro-nitrite isomerisation as already established for positively charged or neutral systems.[18,19]

A critical energy of ~110 kJmol_1 has been calculated for the nitrobenzene!phenylnitrite isomerisation for both the neutrals[19] and the radical cations.[18] Moreover, the nitro-nitrite isomerisation is predicted to be the energy determining step toward ˙NO loss in both cases.[18,19] To the best of our knowledge, no information is available on a similar reaction on even-electrons negative ions. We have consequently examined theoretically the nitro-nitrite

isomerisation process on the simplest models of ortho- and para-nitro (5^- and 6^-) and nitrite phenoxides ions, $5'^{\cdot}$ and $6'^{\cdot}$. At the B3LYP/6-31 +G(d,p) level, it turns out that the transition structure of the isomerisation reactions is situated 240 and 276 $kJmol^{-1}$ above the phenyl nitrite form for the ortho- and para - nitrophenoxides, respectively (Table 2 and Fig. 5).

Another interesting finding is that the phenyl nitrite forms are less stable than the nitro isomers, a situation comparable to neutral nitrobenzene, but opposite to that observed for positive ions where the nitrite structure is 150 $kJmol^{-1}$ more stable than its nitro form.[18] Finally, the highest stability of the nitro phenoxide ion with respect to its nitrite analogue, particularly pronounced for the para isomer, should be mentioned. Considering the above results, possible pathways associated with the eliminations of ˙NO or ˙NO2 radicals from the deprotonated molecular ions $[4\text{-H}]^-$ may be proposed, as summarized in Scheme 6.

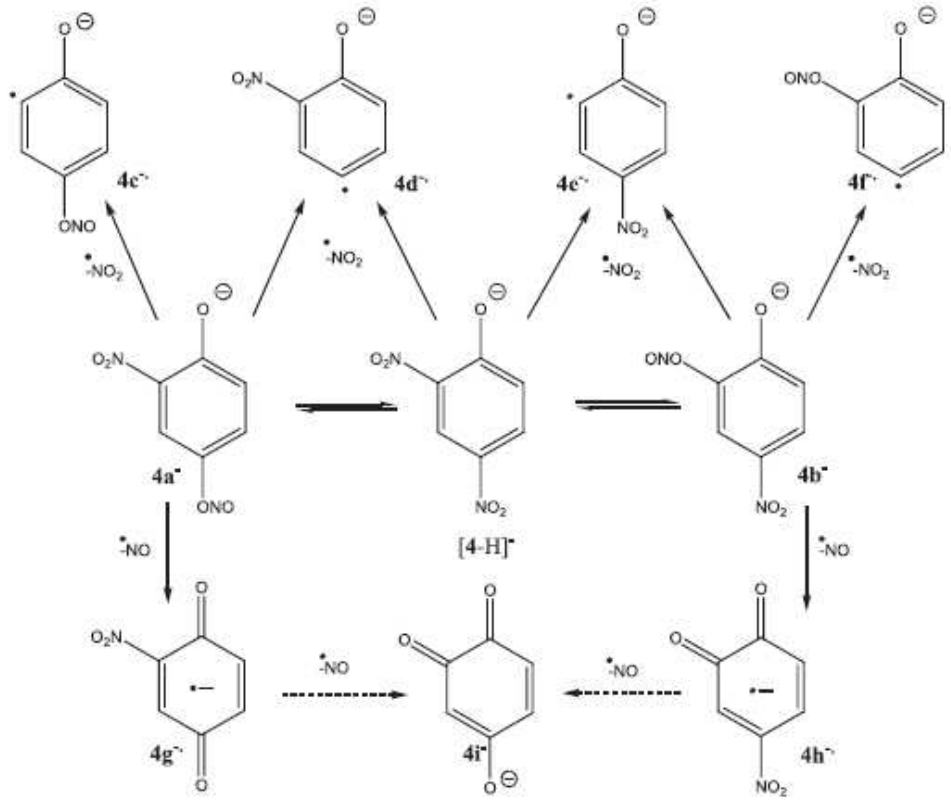

Scheme 6. Pathways associated with the eliminations of ˙NO or ˙NO_2 radicals from $[4\text{-H}]^-$ ions of 2, 4-dinitrophenol.

The general 0 K enthalpy diagrams associated with the various structures displayed in Scheme 6 are presented in Fig. 6. It appears clearly that the ˙NO losses, leading to ions $4g^{-\cdot}$ or $4h^{-\cdot}$ are the lowest energy processes. Starting from $[4\text{-H}]^-$, the energy determining steps of these rearrangement are the nitronitrite isomerisations $[4\text{-H}]^- \rightarrow 4a^-$ and $[4\text{-H}]^- \rightarrow 4b^{-\cdot}$ The simple dissociation reactions $[4\text{-H}]^- \rightarrow 4d^{-\cdot} + {}^{\cdot}NO_2$ and $[4\text{-H}]^- \rightarrow 4\ e^{-\cdot} + {}^{\cdot}NO2$ need approximately 65 $kJmol^{-1}$ more energy to occur. This seems to be reflected by experiments since the apparent threshold for ˙NO loss is approximately 0.8 eV above that of the $^{\cdot}NO_2$ elimination.

Finally, the double ˙NO eliminations, $[4\text{-H}]^- \rightarrow 4a^- \rightarrow 4g^{-\cdot} + {}^{\cdot}NO \rightarrow 4i^- + 2\,{}^{\cdot}NO$ and $[4\text{-H}]^- \rightarrow 4b^- \rightarrow 4h^{-\cdot} + {}^{\cdot}NO \rightarrow 4i^- + 2\ {}^{\cdot}NO$ are limited by the nitro-nitrite isomerisation barriers attached to ions 4g_. and 4h_. which are probably close to 300 $kJmol^{-1}$ and could compete with the NO or NO_2 losses, as experimentally observed.

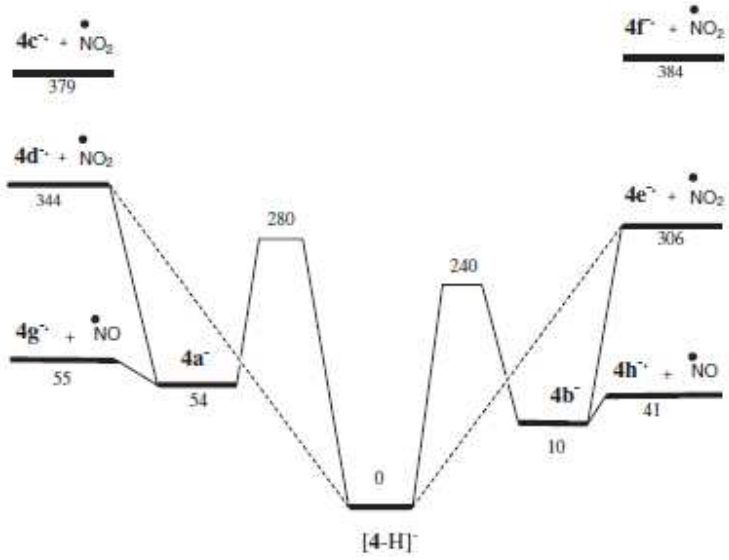

Figure 6. H°_{298} (kJ.mol^{-1}) profiles for the eliminations of ˙NO or $^{\cdot}NO_2$ from $[4\text{-H}]^-$ (**4**=2,4-dinitrophenol).

Methane and methylpropene eliminations from t-butyl phenoxide ions [3-H]- and [3'-H]$^-$

Elimination of CH4 and $CH_2{=}C(CH_3)_2$ from t-butyl phenoxide ions $[3\text{-H}]^-$ and $[3'\text{-H}]^-$ (3: 2-t-butyl phenol and 3': 4-t-butyl phenol) are high energy processes as indicated by their high Ecm0 values (3.4 to 4.9 eV, i.e. 330 to 470 $kJmol^{-1}$). Computed endothermicities at 0 K are, however, rather small: from 4 to 54 $kJmol^{-1}$ (Table 3).

Table 3. Total (Hartree) and relative (kJmol^{-1}) $H°_0$ and $H°_{298}$ related to fragmentations of $[3\text{-H}]^-$ (B3LYP/6-31+G(d,p) calculations)

Species	$H°_0$		$H°_{298}$	
	total	relative	total	relative
$[3\text{-H}]^-$	−463.997092	0	−463.985651	0
3a	−306.045616		−306.039193	
$\mathbf{3a}^{\cdot-}$	−306.165022		−306.158734	
3b	−424.038893		−424.028494	
$\mathbf{3b}^{\cdot-}$	−424.082149		−424.071425	
$\mathbf{3c}^-$	−306.838767		−306.832545	
$\mathbf{3d}^-$	−423.507995		−423.498069	
$\mathbf{3e}^-$	−463.979951	45	−463.968510	45
$\mathbf{3f}^-$	−306.774905		−306.768579	
$^{\cdot}CH_3$	−39.817522		−39.813527	
$^-CH_3$	−39.818688		−39.814805	
CH_4	−40.481360		x−40.477548	
$^{\cdot}C(CH_3)_3$	−157.700349		−157.693074	
$^-C(CH_3)_3$	−157.693549		−157.039193	
$CH_2{=}C(CH_3)_2$	−157.137779		−157.131502	
$\mathbf{3a}+{}^-C(CH_3)_3$	−463.739165	677	−463.726272	681
$\mathbf{3a}^{\cdot-}+{}^{\cdot}C(CH_3)_3$	−463.865371	346	−463.851808	351
$\mathbf{3c}^-+CH_2{=}C(CH_3)_2$	−463.976546	54	−463.964047	57
$\mathbf{3f}^-+CH_2{=}C(CH_3)_2$	−463.912684	222	−463.900081	225
$\mathbf{3b}+{}^-CH_3$	−463.857581	366	−463.843299	374
$\mathbf{3b}^{\cdot-}+{}^{\cdot}CH_3$	−463.899671	256	−463.884952	264
$\mathbf{3d}^-+CH_4$	−463.989355	20	−463.975617	26
$[\mathbf{3'}\text{-H}]^-$	−463.994660	6	−463.982940	7
$\mathbf{3'a}^{\cdot-}$	−306.163748		−306.157052	
$\mathbf{3'b}^{\cdot-}$	−424.085830		−424.074888	
$\mathbf{3'd}^-$	−423.511647		−423.501701	
$\mathbf{3'a}^{\cdot-}+{}^{\cdot}C(CH_3)_3$	−463.864097	349	−463.850126	356
$\mathbf{3'b}^{\cdot-}+{}^{\cdot}CH_3$	−463.903352	246	−463.888415	
$\mathbf{3'd}^-+CH_4$	−463.993007	11	−463.979249	

Large critical energies are consequently associated to these two fragmentations. In fact, these two elimination reactions involve two major events: a C–C bond cleavage and a hydrogen transfer from a position with respect to the broken C–C bond. This kind of reaction may be formally decomposed into a two steps process where the hydrogen exchange is assumed during the C–C bond elongation, inside ion-neutral complex intermediates, as depicted in Scheme 7.[20–25] Starting from $[3\text{-H}]^-$ ions, the two homolytic C–C bond cleavages leading to $3a^{-\cdot}$ + t-butyl radical $3b^{-\cdot}$+methyl radical, need approximately 350 and 250 kJmol^{-1}, respectively, while the corresponding heterolytic process (i.e. $[3\text{-H}]^- \rightarrow$3a + t-butyl anion and $[3\text{-H}]^- \rightarrow$ 3b+methyl anion) are, by far, more energy demanding (Table 3). Scheme 7 consequently presents only radical-anion/radical complexes as ion/neutral intermediates.

As also presented in Scheme 7 in the case of $[3\text{-H}]^-$ ions, a second mechanism involving a 1,5-proton migration on the phenoxide oxygen, leading to intermediate $3e^-$, may be also devised for the methyl-2-propene elimination. The energetics of these fragmentation processes are illustrated by Fig. 7.

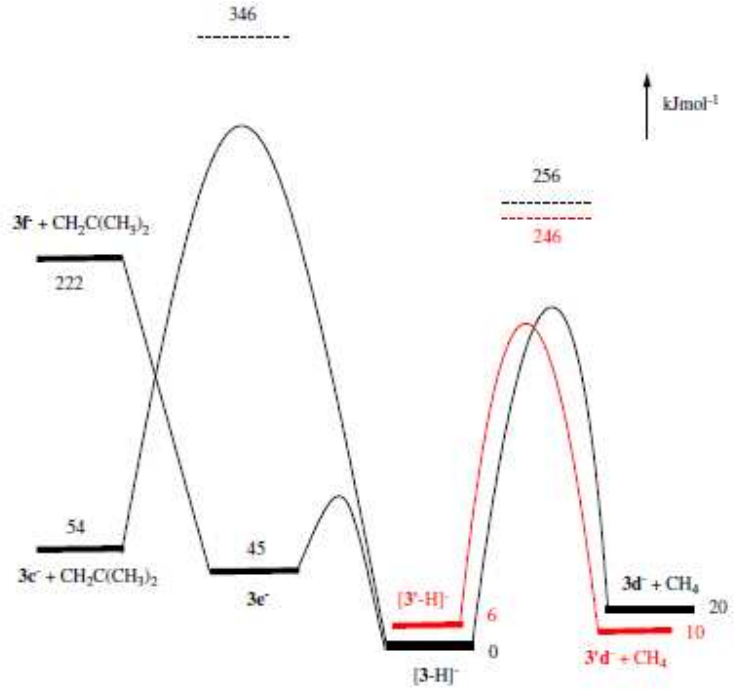

Figure 7. $H°_{298}$ (kJ.mol^{-1}) profiles for the eliminations of CH_4 or $CH_2C(CH_3)_2$ from $[3\text{-H}]^-$ and $[3'\text{-H}]^-$ (**3**=2-t-butyl-phenol, **3'**=4-t-butyl-phenols).

The first observation which may be drawn from examination of Table 3 and Fig. 7 is that comparable homolytic C-C bond energies are associated with methyl or t-butyl radical formation from both $[3\text{-H}]^-$ and $[3'\text{-H}]^-$ ions. Since the relative energies of the corresponding C-C bond elongation products should represent maximum values for the critical energies of the alkene/alkane elimination processes, comparable critical energies are expected for $[3\text{-H}]^-$ and $[3'\text{-H}]^-$ ions. Experimental observations are not in agreement with this expectation since it is observed that only $[3\text{-H}]^-$ leads to significant methyl propene elimination. We thus conclude that the passage through intermediate $3e^-$ is the energetically preferred pathway for the CH2 = $C(CH_3)_2$ elimination as presented in Fig. 7.

Concerning the methane loss, it has been experimentally observed that this fragmentation process is less energy demanding than the CH2 = $C(CH_3)_2$ elimination. This is in line with the fact that the maximum values for the corresponding critical energies leading to $[3\text{-H-CH4}]^-$ and $[3'\text{-H-CH4}]^-$ are ~100 $kJmol^{-1}$ below that of the $[3\text{-H-CH}_2 = C(CH_3)_2]^-$ ions (Fig. 7). Moreover, the fact that the lowest apparent threshold energy Ecm0 (Table 1) is observed

for 3 is in agreement with a lower homolytic CAr-$C(CH_3)_3$ bond dissociation energy from $[3\text{-H}]^-$ (Table 3, Fig. 7). Finally, the lower Ecm0 observed for the CH_4 loss with respect to $CH_2 = C(CH_3)_2$ elimination from $[3\text{-H}]^-$ (Table 1) may be accounted for by a critical energy slightly below the energy level corresponding to $3f^- + CH_2 = C(CH_3)_2$ (Scheme 7, Fig. 7).

Alcohol eliminations from alkyl nitro phenoxide ions $[1\text{-H}]^-$ and $[2\text{-H}]^-$

The two preceding paragraphs show that nitro and alkyl phenoxide ions, separately, eliminate $^{\cdot}NO$ or $^{\cdot}NO_2$ substituents and alkane or alkene molecules. By contrast, when these substituents are gathered on the same molecule, the previous reactions are replaced by methanol and ethanol eliminations from $[1\text{-H}]^-$ and $[2\text{-H}]^-$, respectively. This suggests that a new, more favourable, route is opened by the simultaneous presence of the alkyl and nitro groups. The simplest explanation that may be proposed is that the eliminated alcohol contains part of the alkyl group and one oxygen atom originating from a nitro function. Indeed, the formation of an alcohol molecule containing the phenoxide oxygen may be excluded since this reaction is not occurring from $[3\text{-H}]^-$. Rather, the observed fragmentations of $[3\text{-H}]^-$ are alkane and alkene eliminations. Since these processes are associated with Ecm0 close to 4 eV, this means that the phenoxide oxygen participation would need at least this energy. This seems to be hardly compatible with the Ecm0 of ~2.5–2.0 eV associated with the methanol and ethanol eliminations from $[1\text{-H}]^-$ and $[2\text{-H}]^-$.

We have examined by quantum chemistry computation two possible reaction paths involving the participation of either the ortho (o) or the para (p) nitro group to the methanol elimination induced by a t-butyl group. These two models are described in Schemes 8 and 9, and the corresponding computed energies are reported in Table 4.

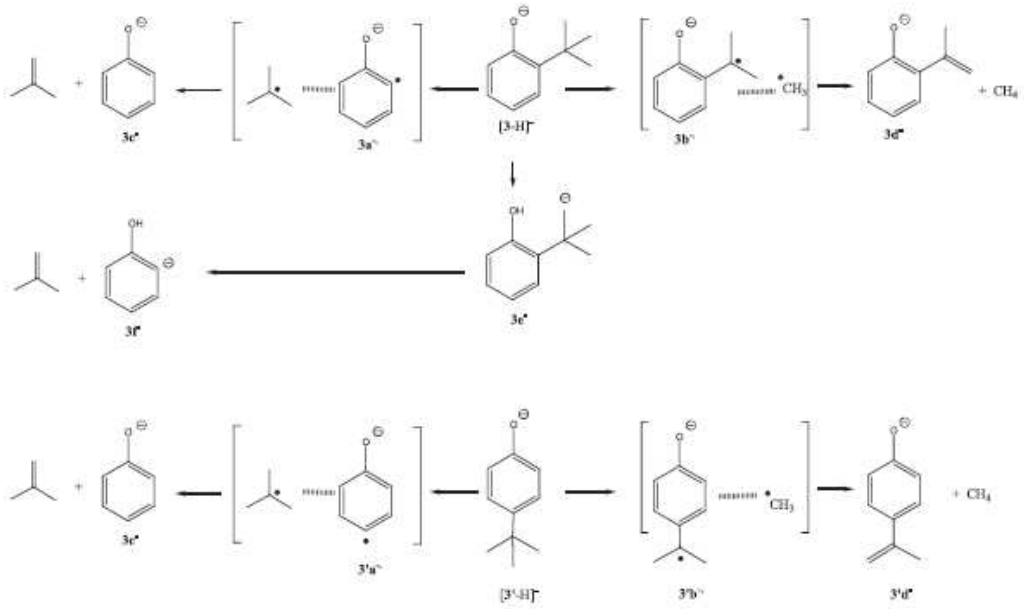

Scheme 7. Elimination pathways of $CH_2=C(CH_3)_2$ from $[\mathbf{3}\text{-H}]^-$ ions of 2-terbutylphenol and from $[\mathbf{3'}\text{-H}]^-$ ions of 4-terbutylphenol (**3** and **3'**, m/z 149).

Table 4. Total (Hartree) and relative ($kJmol^{-1}$) H°_0 and H°_{298} related to fragmentations of $[\mathbf{1}\text{-H}]^-$ (B3LYP/6-31+G(d,p) calculations)

Species	H°_0		H°_{298}	
	total	relative	total	relative
1o⁻-a⁻	−668.525362	0	−668.512196	0
1o⁻-b⁻	−668.442322	218.02	−668.427097	223.4
1o⁻-c⁻	−668.452117	192.3	−668.436625	198.4
1o-d	−553.409357		−553.396613	
1o-e⁻	−552.829912		−552.818305	
1p-a⁻	−668.543840	0	−668.529890	0
1p-b⁻	−668.511992	83.6	−668.497147	86
1p-c⁻	−668.456519	229.2	−668.440901	233.6
1p-d	−552.757704		−552.745501	
1p-e⁻	−552.845800		−552.834107	
$^-OCH_3$⁻	−115.080573		−115.076720	
CH_3OH^-	−115.683636		−115.679360	
1o-d + $^-OCH_3$	−668.48993	93.0	−668.473333	102.0
1o-e⁻ + CH_3OH	−668.513548	31.0	−668.497665	38.1
1p-d + $^-OCH_3$	−668.460786	218.0	−668.444791	223.4
1p-e⁻ + CH_3OH	−668.529436	37.8	−668.513467	43.11

In the ortho model, the methyl cation migration is relayed by the negatively charged oxygen of the phenoxide ion. In the para model, the ortho carbon C(3) serves as first methyl cation acceptor. In both models, a N-methoxy derivative results (1o-c$^-$ and 1p-c$^-$, Schemes 8 and 9, respectively). These structures may in turn form high energy CH_3O^-/neutral complexes where a

proton exchange readily occurs to give phenoxides ions 1o-e$^-$ and 1p-e$^-$. It appears from examination of Table 4 that both pathways need the passage via intermediates of comparable energies (~220 kJmol^{-1}, Table 4). Thus, the two mechanisms are probably operative from deprotonated Dinoterb and Dinoseb, 1 and 2. A general mechanistic scheme explaining the alcohol losses from [1-H]$^-$ and [2-H]$^-$ is presented in Scheme 10. Loss of a NO$^{\cdot}$ radical from the m/z 207, [1-H-CH_3OH]$^-$, or m/z 193, [2-H-C_2H_5OH]$^-$, ions may occur either by direct C–N bond cleavage or after a nitro-nitrite isomerisation. Only this latter process is reported in Scheme 10 since it leads to a quinonic radical-anion which is expected to easily eliminate a CO molecule.

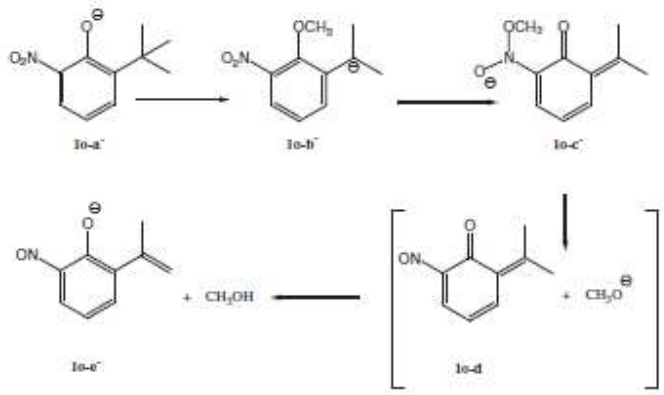

Scheme 8. Model of alcohol elimination from [**1o**-H]$^-$ ions of ortho nitro-tbutylphenol.

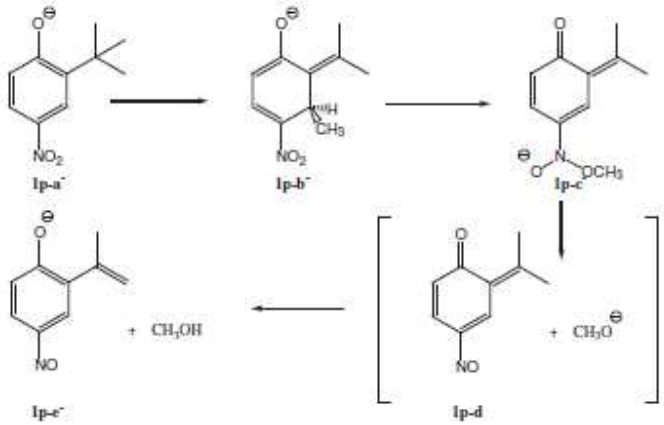

Scheme 9. Model of alcohol elimination from [**1p**-H]$^-$ ions of para nitro-tbutylphenol.

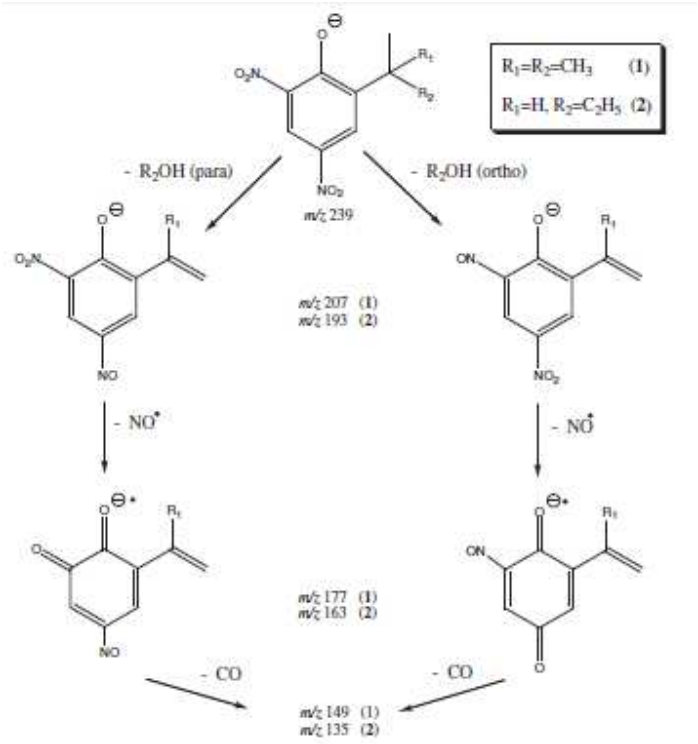

Scheme 10. Model of alcohol elimination from [**1**-H]$^-$ and [**2**-H]$^-$ ions of Dinoterb and Dinoseb respectively.

Further fragmentations from alkyl nitro phenoxide ions [2-H]$^-$

Dinoseb phenoxide ions, [2-H]$^-$, present particularly rich fragmentation pattern as summarized in Scheme 3. Beside formation of m/z 193 ions by elimination of a C_2H_5OH molecule presented above, it remains to interpret formation of the second component of m/z 193 ions, corresponding to the $C_{10}H_{11}NO_3$ formula, and the loss of CH_3NO molecule leading to m/z 194 ions. Several speculative proposals are given in Scheme 11. Elimination of $NO_2^{\cdot}$ may obviously occur from either positions 2 and 4 of the initial structure or isomeric forms of [2-H]$^-$ ions such as, for example, those suggested to intervene during ethanol elimination in Schemes 8 and 9. In order to understand the further losses of $NO^{\cdot}$ and $^{\cdot}OCH_3$ we propose that both pathways are operative. A possible mechanism involving elimination of the nitro group from position 4 is summarized in Scheme 11. The direct elimination of NO2$^{\cdot}$ from the initial form of [2-H]$^-$ ions leads to m/z 193 ions able to eliminate a $NO^{\cdot}$ radical after a nitro-nitrite isomerisation. A second possibility of

NO2˙ elimination is suggested to occur from an isomeric form of [2-H]- resulting from a methyl migration (a structure analogous to 1o-c' in Scheme 8).

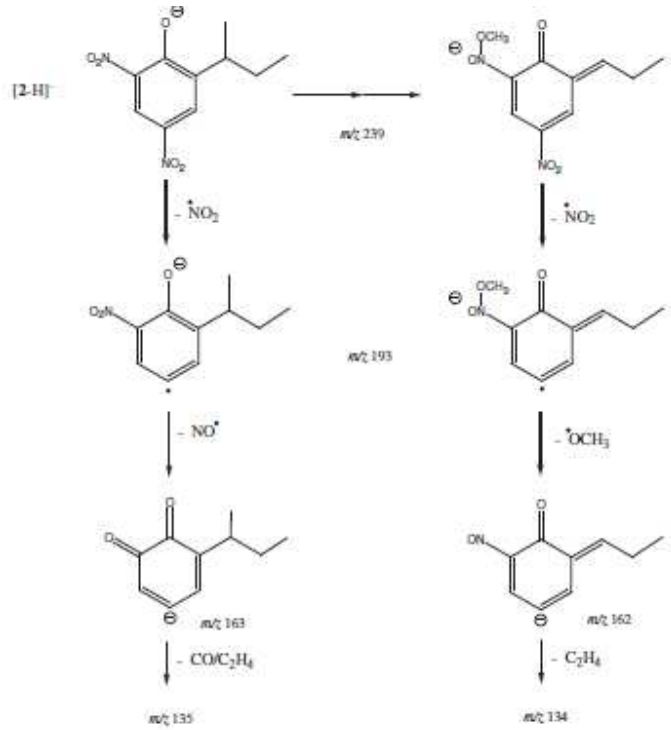

Scheme 11. Decomposition pathways of m/z 193 ions of Dinoseb.

The formed m/z 193 ions are able to eliminate ˙OCH3 thus producing m/z 162 ions. The extensive formation of m/z 134 ions at high collision energies from [2-H]_ ions is explained here by a C2H4 elimination (rather than CO which, however, remains a possibility) from intermediate m/z 162 ions, probably by a 1,2- elimination process.

CONCLUSION

In summary, the present work provides experimental data on the fragmentations energetics and mechanisms of [M-H]- ions of two pesticides, Dinoterb, 1, and Dinoseb, 2, and of three phenol derivatives containing structural similarities, 2-t-butyl phenol, 3, 4-t-butyl phenol, 3', and 2,4-dinitrophenol, 4. Extensive, variable collision energy tandem mass spectrometry allows information on the fragmentation pattern and on the conditions of MRM analysis, particularly for 1 and 2. Fragmentation mechanisms of the corresponding phenoxide ions are shown to be very different from each precursor molecules. Alkyl substituted phenoxide ions eliminate alkane and

alkene molecules by fragmentation reactions involving ion/neutral complexes. 2,4-Dinitrophenoxide ions reactivity is dominated by eliminations of NO2 and NO radicals, details on the nitro-nitrite isomerisation process preceding NO loss are given by quantum chemistry computations (B3LYP/6-31 + G(d,p)level). For 1 and 2, interactions between alkyl and nitro functional groups open new reaction routes, in particular an alcohol loss. Again, quantum chemistry computations at the B3LYP/6-31 +G(d,p) level provide several clues helping us to propose mechanistic schemes.

REFERENCES

[1] D.B. Barr, L. L. Needham. Analytical methods for biological monitoring of exposure to pesticides: a review. *J. Chromatogr., B: Anal. Technol. Biomed. Life Sci.* **2002**, 778(1–2), 5–29.

[2] W.L. Budde. Analytical mass spectrometry of herbicides. *Mass Spectrom. Rev.* **2004**, 23(1), 1–24.

[3] Y. Pico, C. Blasco, G. Font. Environmental and food applications of LC-tandem mass spectrometry in pesticide-residue analysis: An overview. *Mass Spectrom. Rev.* **2004**, 23(1), 45–85.

[4] Y. Pico, G. Font, M. J. Ruiz, M. Fernandez. Control of pesticide residues by liquid chromatography-mass spectrometry to ensure food safety. *Mass Spectrom. Rev.* **2006**, 25(6), 917–960.

[5] M. Kuster, M. L. de Alda, D. Barcelo. Analysis of pesticides in water by liquid chromatography-tandem mass spectrometric techniques. *Mass Spectrom. Rev.* **2006**, 25(6), 900–916.

[6] W.M.A. Niessen, P. Manini, R. Andreoli. Matrix effects in quantitative pesticide analysis using liquid chromatography-mass spectrometry. *Mass Spectrom. Rev.* **2006**, 25(6), 881–899.

[7] S. Lacorte, A. R. Fernandez-Albaz. Time of flight mass spectrometry applied to the liquid chromatographic analysis of pesticides in water and food. *Mass Spectrom. Rev.* **2006**, 25(6), 866–880.

[8] L. Alder, K. Greulich, G. Kempe, B. Vieth. Residue analysis of 500 high priority pesticides: Better by GC-MS or LC-MS/MS? *Mass Spectrom. Rev.* **2006**, 25(6), 838–865.

[9] W. M. A. Niessen. Group-specific fragmentation of pesticides and related compounds in liquid chromatography-tandem mass spectrometry. *J. Chromatogr. A* **2010**, 1217(25), 4061–4070.

[10] J. Y. Hu, T. Aizawa, Y. Magara. Analysis of pesticides in water with liquid chromatography atmospheric pressure chemical ionization mass spectrometry. *Water Res.* **1999**, 33(2), 417–425.

[11] X. B. Song, W. L. Budde. Determination of chlorinated acid herbicides and related compounds in water by capillary electrophoresiselectrospray negative ion mass spectrometry. *J. Chromatogr. A* **1998**, 829(1–2), 327–340.

[12] P.M. Mayer, C. Poon. The mechanisms of collisional activation of ions in mass spectrometry. *Mass Spectrom. Rev.* **2009**, 28(4), 608–639.

[13] P. B. Armentrout, K. M. Ervin, M. T. Rodgers. Statistical Rate Theory and Kinetic Energy-Resolved Ion Chemistry: Theory and Applications. *J. Phys. Chem. A* **2008**, 112(41), 10071–10085.

[14] S. Narancic, A. Bach, P. Chen. Simple fitting of energy-resolved reactive cross sections in threshold collision-induced dissociation (T-CID) experiments. *J. Phys. Chem. A* **2007**, 111(30), 7006–7013.

[15] M. J. Frisch, G. W. Trucks, H. B. Schlegel, G. E. Scuseria, M. A. Robb, J. R. Cheeseman, J. A. Montgomery, T. Vreven, Jr, K. N. Kudin, J. C. Burant, J. M. Millam, S. S. Iyengar, J. Tomasi, V. Barone, B. Mennucci, M. Cossi, G. Scalmani, N. Rega, G. A. Petersson, H. Nakatsuji, M. Hada, M. Ehara, K. Toyota, R. Fukuda, J. Hasegawa, M. Ishida, T.

Nakajima, Y. Honda, O. Kitao, H. Nakai, M. Klene, X. Li, J. E. Knox, H. P. Hratchian, J. B. Cross, C. Adamo, J. Jaramillo, R. Gomperts, R. E. Stratmann, O. Yazyev, A. J. Austin, R. Cammi, C. Pomelli, J. W. Ochterski, P. Y. Ayala, K. Morokuma, G. A. Voth, P. Salvador, J. J. Dannenberg, V. G. Zakrzewski, S. Dapprich, A. D. Daniels, M. C. Strain, O. Farkas, D. K. Malick, A. D. Rabuck, K. Raghavachari, J. B. Foresman, J. V. Ortiz, Q. Cui, A. G. Baboul, S. Clifford, J. Cioslowski, B. B. Stefanov, G. Liu, A. Liashenko, P. Piskorz, I. Komaromi, R. L. Martin, D. J. Fox, T. Keith, M. A. Al-Laham, C. Y. Peng, A. Nanayakkara, M. Challacombe, P. M. W. Gill, B. Johnson, W. Chen, M. W. Wong, C. Gonzalez, J. A. Pople, *Gaussian 03*, R.B., Pittsburgh PA, **2003**.

[16] M. J. Frisch, G. W. Trucks, H. B. Schlegel, G. E. Scuseria, M. A. Robb, J. R. Cheeseman, V. G. Zakrzewski, J. A. Montgomery, Jr, R. E. Stratmann, J. C. Burant, S. Dapprich, J. M. Millam, A. D. Daniels, K. N. Kudin, M. C. Strain, O. Farkas, J. Tomasi, V. Barone, M. Cossi, R. Cammi, B. Mennucci, C. Pomelli, C. Adamo, S. Clifford, J. Ochterski, G. A. Petersson, P. Y. Ayala, Q. Cui, K. Morokuma, D. K. Malick, A. D. Rabuck, K. Raghavachari, J. B. Foresman, J. Cioslowski, J. V. Ortiz, B. B. Stefanov, G. Liu, A. Liashenko, P. Piskorz, I. Komaromi, R. Gomperts, R. L. Martin, D. J. Fox, T. Keith, M. A. Al-Laham, C. Y. Peng, A. Nanayakkara, C. Gonzalez, M. Challacombe, P. M. W. Gill, B. Johnson, W. Chen, M. W. Wong, J. L. Andres, C. Gonzalez, M. Head-Gordon, E. S. Replogle, J. A. Pople, *Gaussian 98*, R.A.I., Pittsburgh PA, **1998**.

[17] L. Bajpai, M. Varshney, C. N. Seubert, S. M. Stevens, J. V. Johnson, R. A. Yost, D. M. Dennis. Mass spectral fragmentation of the intravenous anesthetic propofol and structurally related phenols. *J. Am. Soc. Mass Spectrom.* **2005**, 16(6), 814–824.

[18] M. Polasek, F. Turecek, P. Gerbaux, R. Flammang. Nitrobenzene isomers. *J. Phys. Chem. A* **2001**, 105(6), 995–1010.

[19] T. Glenewinkel-Meyer, F. F. Crim. The isomerization of nitrobenzene to phenylnitrite. *J. Mol. Struc.: Theochem.* **1995**, 337(3), 209–224.

[20] C. E. Hudson, D. J. McAdoo. Methane loss from $(CH_3)(3)O^+$: an asynchronous, concerted 1,2-alkane elimination. *Int. J. Mass Spectrom.* **2006**, 248(3), 103–107.

[21] W. Tumas, R. F. Foster, J. I. Brauman. Mechanistic studies of gasphase negative-ion unimolecular decomposition - Alkoxide anions. *J. Am. Chem. Soc.* **1988**, 110(9), 2714–2722.

[22] W. Tumas, R. F. Foster, M. J. Pellerite, J. I. Brauman. A Stepwise mechanism for gas-phase unimolecular ions decomposition - Isotope effects in the fragmentation of tert-Butoxide anion. *J. Am. Chem. Soc.* **1987**, 109(4), 961–970.

[23] D. J. McAdoo, T. H. Morton. Gas-phase analogs of cage effects. *Acc. Chem. Res.* **1993**, 26(6), 295–302.

[24] P. Longevialle. Ion-neutral complexes in the unimolecular reactivity of organic cations in the gas-phase. *Mass Spectrom. Rev.* **1992**, 11(3), 157–192.

[25] R. D. Bowen. Ion-neutral complexes. *Acc. Chem. Res.* **1991**, 24(12), 364–371.

Structures and dissociation mechanisms of protonated and electron ionized methamidophos

Ahmad Rifai, Sophie Bourcier, Farouk Jaber, Guy Bouchoux

International Journal of Mass Spectrometry 339– 340 (2013) 7– 15

abstract

Methamidophos, **1**, is examined by tandem mass spectrometry (Q-TOF) under electrospray ionization in the positive ion mode (ESI-P). Variable collision energy MS–MS mass spectra of protonated methamidophos, $\mathbf{1H}^+$, reveal that CH_2O, CH_3SH, CH_3OH and NH_3 losses occur with comparable threshold energies. Fragmentations leading to m/z 125, 112, 110, 94, 79 and m/z 64 ions are explained by combinations of 1,2- elimination reactions and isomerizations via 1,3-proton migrations as supported by B3LYP/6-31+G(d) calculations. The behavior of electron ionized methamidophos, $\mathbf{1}^{\bullet+}$, particularly its fragmentations by losses of $^{\bullet}SCH_3$ and CH_2S, is also explored at the B3LYP/6-31+G(d) level. G4MP2 calculation shows that protonation of **1** occurs preferentially at the oxygen atom of the P O group with a corresponding proton affinity equal to PA(**1**) = 897 kJ mol^{-1}. Calculated G4MP2 ionization energy and heat of formation of methamidophos are IE(**1**) = 8.77 eV and $\Delta_f H^{\circ}_{298}$(**1**) = −626 kJ mol^{-1}.

1. Introduction

Methamidophos (O,S-dimethyl phosphoramidothioate), **1**, (Scheme 1), is a representative chemical in a series of widely used systemic organophosphorus (OP) insecticides. This molecule was introduced in agriculture to avoid insects damaging on fruits and vegetables in the 1970s [1,2]. This OP compound presents a high toxicity for human and mammalians since it inhibits the action of acetylcholinesterase by phosphorylation in nerve cells. As a consequence, chronic and neurotoxic effects on developing organisms, even at low level of exposure, were reported [3–7]. In this context it may be recalled that a number of chemical weapon agents are also OP derivatives. Furthermore, methamidophos, **1**, is the major metabolite of its N-acetylated derivative (Acephate, O,S dimethyl N-acetylphosphoramidothioate), another extensively used pesticide.

Polar OP pesticides such as methamidophos, **1**, may be extracted from environmental matrix and analyzed using liquid chromatography (LC) coupled with mass spectrometry (MS). In recent years, single stage mass spectrometry and, mainly, tandem mass spectrometry (MS/MS), associated with high pressure ionization sources (mainly electrospray ionization, ESI) are increasingly used for analyzing pesticide residues including methamidophos, **1** [8–17]. In addition, selected or multiple reaction monitoring (SRM or MRM) are often used to specifically detect and to quantify with high accuracy and sensitivity the pesticides of interest. To perform SRM or MRM determination of a target compound, knowledge of the m/z values and optimal collision energy conditions for the quantification transitions are obviously essential. The goal of the present study is to provide support for a rational use of SRM and MRM techniques. For this purpose, methamidophos, **1**, was studied using a tandem quadrupole-time of flight (Q-TOF) mass spectrometer equipped with a ESI source working in the positive ion mode (ESI-P). Fragmentations of the protonated molecules $[MH]^+$ were examined at variable collision energy and MS/MS experiments were performed to ascertain the most significant fragmentation transitions. Fragmentation reaction mechanisms and energetic diagrams were proposed on the basis of quantum chemistry calculations using density functional theory.

2. Experimental and theoretical section

HPLC-grade solvents (99.9%), formic acid and methamidophos standards (98% purity) were supplied by Sigma–Aldrich (Saint Quentin Fallavier, France) and used as received. Individual pesticide stock solutions (1000 mg L^{-1}) were prepared in acetonitrile and stored at −20 °C in the dark. Dilutions have been made in a H_2O/CH_3CN (50:50) mixture acidified with formic acid (0.1%) for acquisition in the positive-ion mode. Solutions were infused into the electrospray ionization source with a syringe pump at an infusion rate of 10 µL min^{-1}. Mass spectra were collected with a Waters Q-TOF Premier instrument equipped with a Z-spray electrospray source. Instrument parameters were as follows, cone voltage: from 10 to 60 V in order to optimize intensity of selected ion, capillary voltage: 3.2 kV, extraction cone voltage: 2 V, ion guide voltage: 2.4 V, source and desolvatation temperatures were set at 80 ◦C and 250 ◦C, respectively. Nitrogen was used as both the nebulizing (10 L h^{-1}) and desolvatation gas (150 L h^{-1}). Argon

was used as collision gas at a flow rate of 0.28 (mL min^{-1}) corresponding to a pressure of ca. 4×10^{-3} mBar.

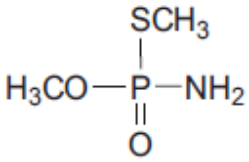

1

Scheme 1. Chemical formula of methamidophos, **1**.

Two acquisition modes were used to characterize the molecule of interest: (i) full scan mode, and (ii) MS/MS of several selected ions in order to study their decomposition pathways. The MS/MS fragmentations of MH^+ ions were studied in more details as a function of the collision energy in the laboratory frame whose nominal value, E_{lab}, was varied in the 0–60 eV range by steps of 2 eV. The results are presented as a breakdown graph showing the abundances of the various fragment ions as a function of the center of mass energy on Fig. 1. The conversion of Elab into center of mass relative energies, Ecm, has been done using the usual formula (Eq. (1)):

$$E_{cm} = E_{lab}\, m_n / m_n + m_i \qquad (1)$$

where mn and mi represent the masses of the neutral target and the projectile ion, respectively. Using argon as collision gas, Eq. (1) reduces to $E_{cm} = 0.22\ E_{lab}$ for protonated methamidophos ions. As proposed earlier in order to gain quantitative information on the

appearance thresholds of the fragment ions [17], representative curves of the ion relative abundances, I_i, vs. E_{cm} have been fitted with a parametric sigmoid function (Eq. (2)).

$$I_i = a+b\ [1+\exp\{(c - E_{cm})/d\}] \quad (2)$$

According to this relationship, the half population of ion i ($I_i = a + b/2$) corresponds to $E_{cm1/2} = c$ and the baseline intercept of the tangent of the sigmoid curve passing by the half population point ($I_i = a$) is equal to $E_{cm0} = c - 2d$. This latter parameter can be considered as a

phenomenological quantity related to the threshold energy of the considered ion [17]. The four parameters a–d were determined using a least square regression analysis procedure (Igor Pro 5.0 program, WaveMetrics).

Molecular orbital calculations have been conducted using the GAUSSIAN03 and GAUSSIAN09 suites of programs [18]. Geometries were optimized at the B3LYP/6-31+G(d) level of theory and unscaled vibrational frequencies calculated at this level were used to calculate vibrational contribution to enthalpy at 0 K and 298 K. Transition structures have been characterized by the occurrence of one negative eigenvalue in the force constant matrix. In order to obtain more reliable relative energies, single point energy calculations have been done at the B3LYP/6-311+G(3df,2p) level on the B3LYP/6-31+G(d) geometry. Several calculations were done using the composite G4MP2 method [19b] in order to obtain accurate proton affinity and heats of formation values. Accordingly, this level of theory has been demonstrated to provide accuracy better than 5 kJ mol^{-1} on $\Delta_f H^\circ$, PA and IE included in test sets of up to 454 energies [19a]. Theoretical heat of formation at 0 K was obtained from the computed atomization energies of the individual species combined with the experimental gas phase 0 K heats of formation of the constituent atoms [20]. The $\Delta_f H^\circ_0$ of H, C, N, O, P and S gaseous atoms were taken as 216.035, 711.2, 470.8, 246.8, 315.6 and 274.7 kJ mol^{-1}, respectively. Temperature correction to enthalpy, $H^\circ 298 - H^\circ 0$, is obtained using the theoretical correction calculated for the species of interest and the experimental contribution for the constituent elements, i.e. for these latter: 8.468, 1.050, 8.669, 8.680, 5.360 and 4.410 kJ mol^{-1} for H2(g), C(s), N_2(g), O_2(g), P(solid) and S(solid), respectively [21]. Adiabatic ionization energy (IE) is calculated as the difference in total atomization energies at zero K of the cation and the corresponding neutral at their respective optimized geometries. Proton affinity (PA(X)), defined as the enthalpy of the reaction $XH^+ \rightarrow X + H+$, is obtained from the total atomization enthalpies at 298 K, $H^\circ 298$, of both the neutral and protonated species and calculated from: $PA(X) = H^\circ_{298}(X) - H^\circ_{298}(XH+) + 6.2$ kJ mol^{-1}, where the latter term is the enthalpy of the proton at 298 K [22].

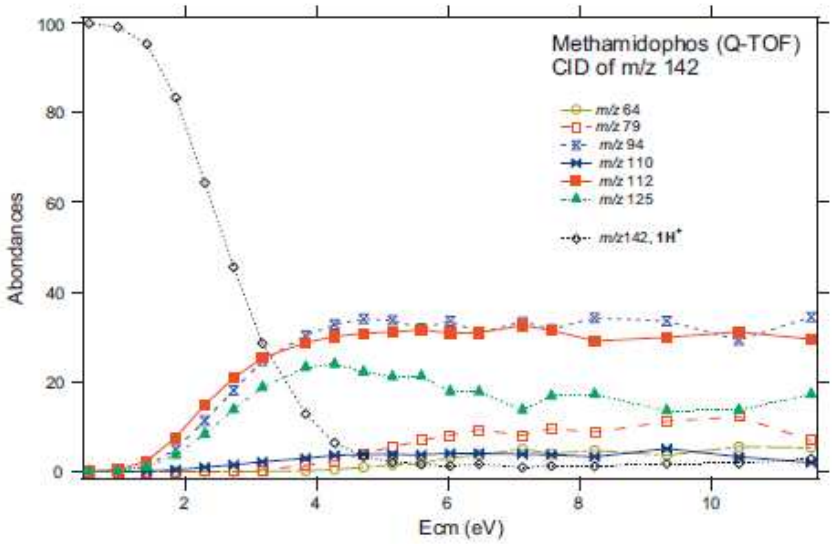

Fig. 1. Breakdown graph of $\mathbf{1H}^+$ (*m/z* 142) ions originating from protonation of methamidophos (ESI-P ion source) as a function of the center of mass collision energy (E_{cm}).

3. Results and discussion

3.1. ESI-P mass spectrometry results

The ESI-P full scan mass spectrum of methamidophos, **1**, presents an intense peak corresponding to pseudo-molecular $\mathbf{1H}^+$ ions at m/z 142. Selection of this precursor ion in MS/MS experiments leads to a first generation of fragment ions at m/z 94, 110, 112 and 125. These ions are originating from the losses of CH_3SH, CH_3OH, CH_2O and NH_3 from $\mathbf{1H}^+$ ions, respectively. Increasing the collision energy, small amount of m/z 64 and m/z 79 ions begins to appear. MS/MS experiments on m/z 125 ions show essentially formation of m/z 79 ions by loss of CH_2S. Similarly, upon collision, m/z 112 ions lead mainly to m/z 94 by water loss, but small signals are also detected at m/z 95 (ammonia loss) and m/z 64 (CH_3SH loss) at high collision energy. Finally, collision induced dissociation of m/z 94 ions indicates that these species may eliminate CH_2O to produce m/z 64 ions and m/z 110. These experimental observations are summarized in Scheme 2.

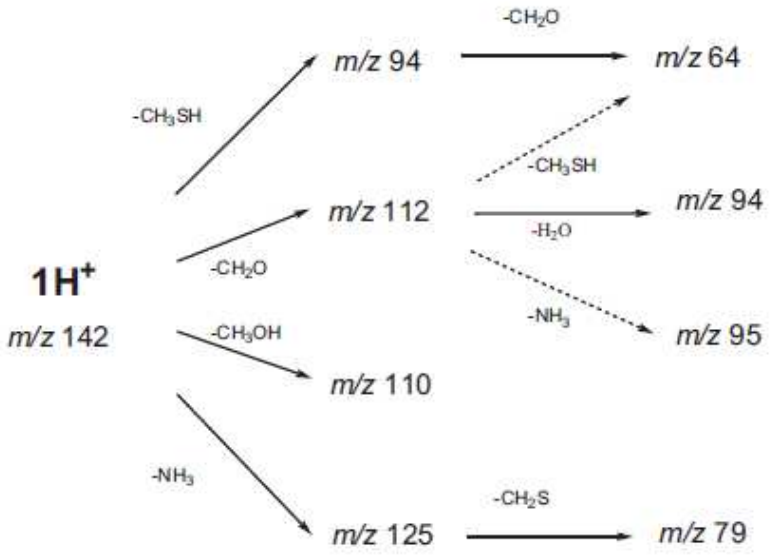

Scheme 2. Major dissociation routes of protonated methamidophos **1H**$^+$.

The breakdown graph of m/z 142 ions presented in Fig. 1 clearly suggests that fragmentations of **1H**+ ions leading to m/z 112, m/z 94 and m/z 125 need comparable critical energies. Indeed, the sigmoid fitting procedure described in Section 2 allows determining apparent threshold energies Ecm0 equal to 1.3, 1.6 and 1.7 eV (with standard deviations of ~0.1 eV), respectively for ions m/z 112, m/z 94 and m/z 125. Although of lower abundance, ions m/z 110 are associated with Ecm0 of 1.7 ± 0.1 eV, close to that of ions m/z 94 and m/z 125. As expected, formation of secondary ions m/z 79 and 64 are more energy demanding, this is reflected by the corresponding Ecm0 values which are equal to 3.7 ± 0.1 and 4.5 ± 0.2 eV, respectively.

Detection and quantitation of methamidophos by using the MRM mode has been performed mainly using transitions m/z 142 → m/z 94 [8,10,13–16], m/z 142 → m/z 112 [8,14] and m/z 142 → m/z 125 [10] in the 15–20 eV laboratory collision energy. Our results perfectly confirm the validity of these previous choices. It may be moreover underlined that the two former transitions are not significantly influenced by the collision energy value in the range of 4–12 eV in center of mass collision energy (i.e. 18–55 eV in the laboratory frame using argon as collision gas) and are thus of larger reliability.

3.2. Structures of protonated methamidophos, **1H**$^+$

Protonation of methamidophos, **1**, may occur on the four basic sites surrounding the central phosphorus atom. Quantum chemistry computations indicate that protonation is thermochemically most favorable at the oxygen of the PO group. The second basic site in order of decreasing basicity is the amino group, its H°_{298} value is situated 40 kJ mol^{-1} above the PO protonated form (B3LYP/6-311+G(3df,2p)//B3LYP/6-31G+(d) calculations, see Table S1 of Supporting Information). Protonation on the SCH_3 or OCH_3 groups lead to protonated structures significantly higher in energy since their corresponding H◦298 values are 69 and 112 kJ mol^{-1}, respectively (Table S1 of Supporting Information). Fig. 2 summarizes our computational results in showing optimized structures of these various protonated forms, denoted **1Ha**$^+$ to **1Hd**$^+$ in order of decreasing stabilities. It may be observed that structures **1Hb**$^+$, **1Hc**$^+$ and **1Hd**$^+$ (N, S and O protonated forms of **1**, respectively) present elongated P. . .NH_3, P. . .$SH(OCH_3)$ and P. . .$OH(SCH_3)$ bonds and should be consequently considered as ion-neutral complexes rather than fully covalent species.

Proton affinity (PA) and gas phase basicity (GB) values of methamidophos were, until now, unknown [23]. The present study offered the opportunity to calculate these thermochemical quantities. As extensively demonstrated, in order to obtain accurate PA and GB it is essential to (i) locate the most stable conformers of neutral and protonated species and, (ii) to use a high level computational method [22]. In a first step we thus explored the conformational space of neutral and PO protonated methamidophos by varying the dihedral angles of these two species. These studies, conducted at the B3LYP/6(31+G(d) level, have been followed by computations using the composite G4MP2 method on the most stable conformers **1** and **1Ha**$^+$.

At this level of theory, proton affinity and gas-phase basicity of methamidophos are PA(methamidophos) = 896.8 kJ mol^{-1} and GB(methamidophos) = 865.9 kJ mol^{-1}. These values may be compared to experimental thermochemical data relevant to similar species where preferred protonation is expected to occur on the oxygen of a PO group. For example, PA(OP(OCH3)3) is equal to 890.6 kJmol^{-1} [23], i.e. only 6 kJmol^{-1} below PA (methamidophos). Recently, proton affinities of a set of organophosphorus weapon agents has been computed and established to lie in the range 889–915 kJ mol^{-1} [2], in line with our PA(methamidophos) value.

Heat of formation of gaseous methamidophos is also lacking from thermochemical compilations. At the G4MP2 level, this quantity is calculated to be $\Delta_f H^\circ_{298}$(methamidophos) = −626 kJ mol^{-1}.

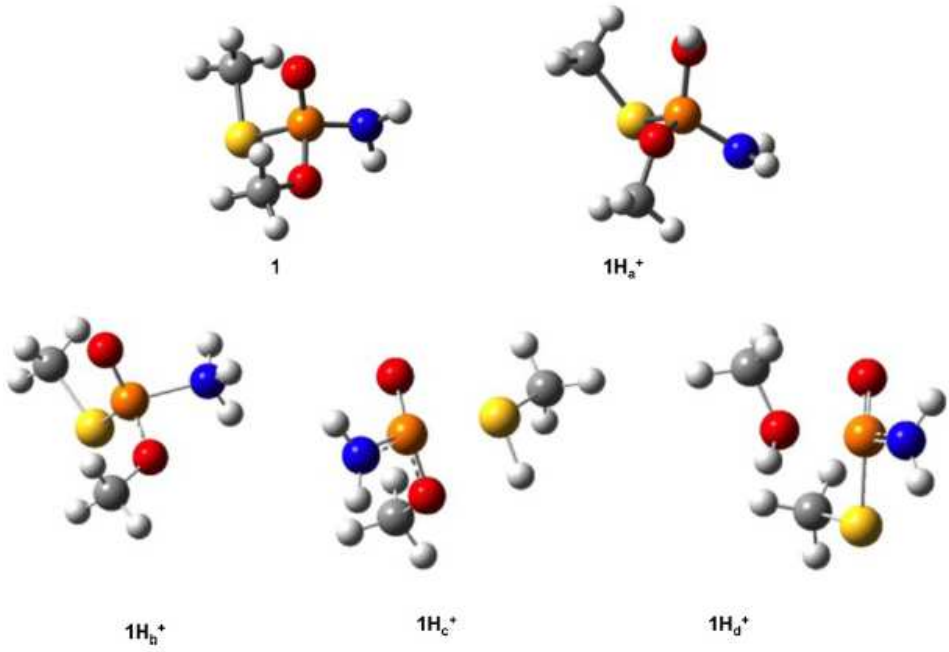

Fig. 2. Optimized structures of the most stable forms of neutral, **1**, and protonated, **1H**$^+$, methamidophos.

3.3. Fragmentation mechanisms of protonated methamidophos, **1H**$^+$

Considering the relative energies of the various protonated forms of methamidophos, there is no doubt that the population of **1H**$^+$ ions produced in the ESI source and thermally relaxed before entering the collision region is dominated by the P OH+ species, **1Ha**$^+$ (Fig. 2). Starting from this structure, fragmentation reactions of protonated methamidophos were examined using quantum chemistry calculations conducted at the B3LYP/6- 311+G(3df,2p)//B3LYP/6-31+G(d) level. The ensemble of primary fragmentations depicted in Scheme 3 was examined.

Formation of ions m/z 125, 94 and 110 can be rationalized by 1,3-proton migrations leading to the isomeric forms **1Hb**$^+$, **1Hc**$^+$ and **1Hd**$^+$ which, considering their ion-neutral complex nature established above by quantum chemistry computation, are prone to formation of ions **1B**, **1C** and **1D** by simple separation of their components leading to elimination of ammonia, methanethiol and methanol, respectively.

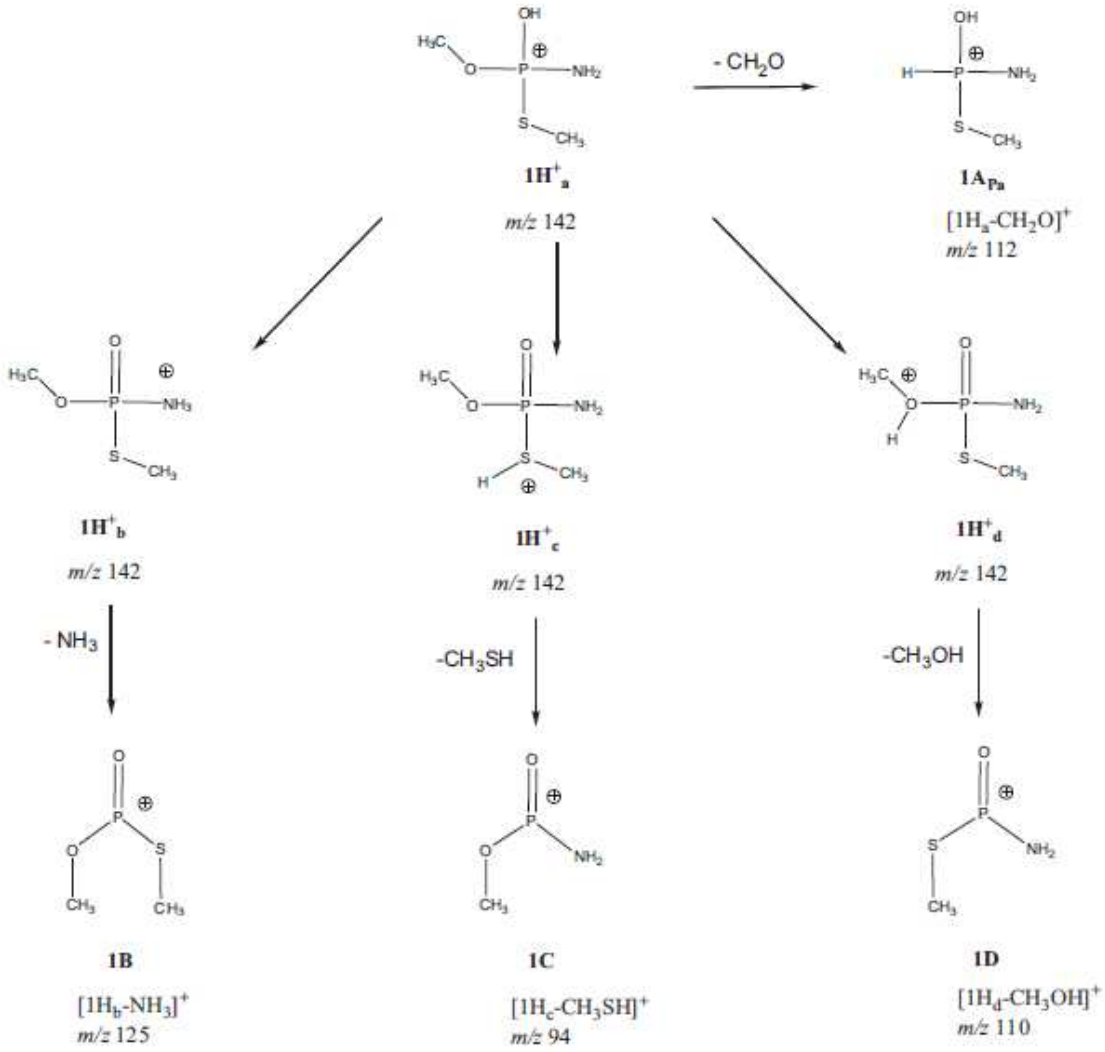

Scheme 3. Fragmentation pathways of protonated methamidophos, $\mathbf{1H^+}$.

Quantum chemistry calculations show that 1,3-proton migrations transforming $\mathbf{1Ha}^+$ into ion-neutral complexes $\mathbf{1Hb}^+$, $\mathbf{1Hc}^+$ or $\mathbf{1Hd}^+$ are associated with comparable critical energies of 140–165 kJ mol^{-1}. These isomerization barriers are situated below the energy levels corresponding to the separated component of these complexes, i.e. **1B** (m/z 125) + NH_3, **1C** (m/z 94) + CH_3SH and **1D** (m/z 110) + CH_3OH fragments (Fig. 3). Consequently, the energy requirements for formation of ions m/z 125, 94 and 110 is expected to be equal to the reaction endothermicities, i.e. 199, 194 and 210 kJ mol^{-1}, respectively. This result is in correct agreement with experimental observation presented in Fig. 1. Indeed, ions m/z 125, m/z 94 and m/z 110 present very similar apparent thresholds energies E_{cm0}, close to 1.7 eV.

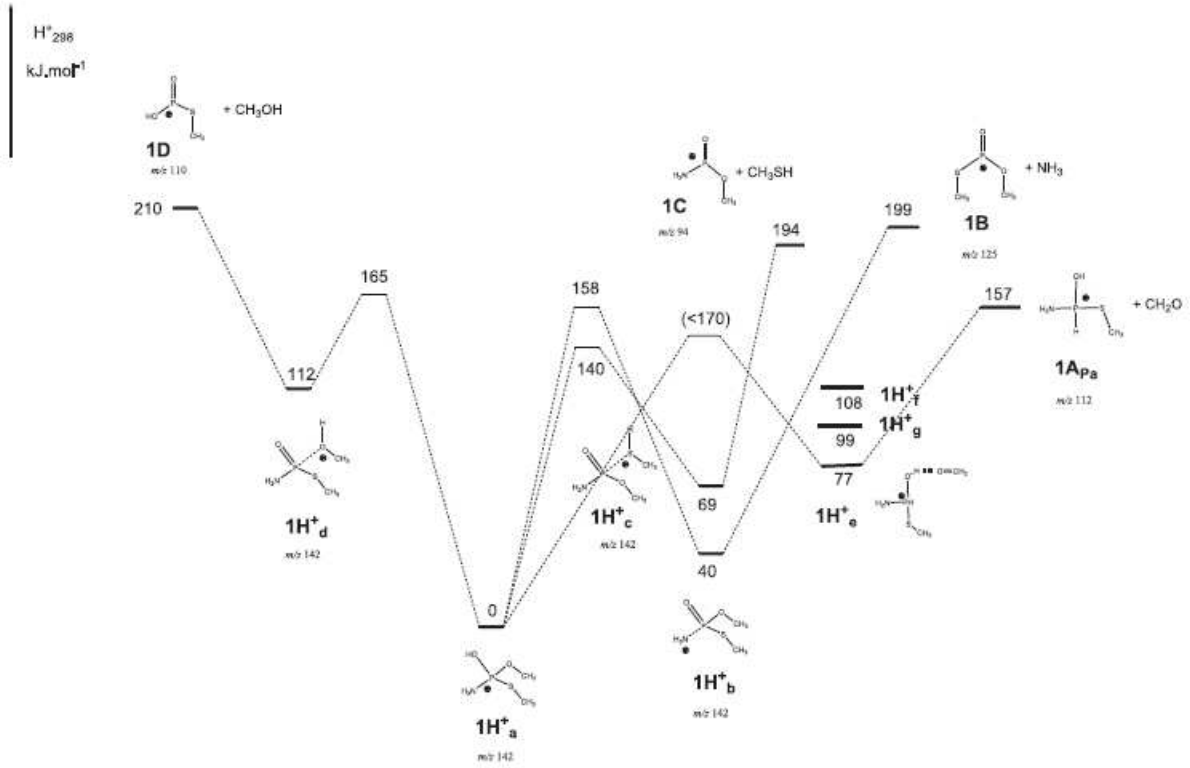

Fig. 3. $H°_{298}$ diagram associated with fragmentations of protonated methamidophos **1H**$^+$ (B3LYP/6-311+G(3df,2p)//B3LYP/6-31+G(d) calculations).

Formation of ions m/z 112, [**1H**$^+$-CH2O], may be explained by formal 1,2-elimination reaction from **1Ha**$^+$, **1Hb**$^+$ and **1Hc**$^+$ but also by mechanisms involving 1,4 proton transfers and leading to structures where the proton is located on N, O or S rather than on the phosphorus atom. B3LYP/6-311+G(3df,2p)//B3LYP/6-31+G(d) computations show that structure **1APa**, corresponding to a 1,2- elimination process from **1Ha**$^+$, is the most stable [**1H**$^+$-CH2O] species whereas the two next forms, in increasing H◦298, i.e. **1AN** and **1AS** which would result from an initial 1,4 proton transfers, are situated ca. 30–40 kJ mol^{-1} above **1APa** (Scheme 4, and see also Table S1 in Supporting information). Experiment demonstrates that ions m/z 112 possess an apparent threshold energy Ecm0 lower than that of ions m/z 125, m/z 94 and m/z 110 by ca. 0.3 eV (see Fig. 1 and related comments). In view of the computed relative energies of the possible fragment ions [**1H**$^+$-CH_2O] presented in Scheme 4 and the results obtained for ions m/z 125, m/z 94 and m/z 110, the only possible structure for m/z 112 ions is consequently **1APa** Moreover, the Ecm0 values suggest that the energy determining step for reaction **1Ha**$^+$ → **1APa** + CH2O is

lower than that leading to ions m/z 125, m/z 94 and m/z 110, by ca. 30 kJ mol^{-1} thus in the ~170 kJ mol^{-1} region.

We were not able to locate a transition structure for a direct, concerted, 1,2-elimination reaction **1Ha**$^{+}$→ **1APa**+CH_2O. Rather, all tentative converged on the formation of ion neutral complexes [**1APa**. . .CH_2O], the most stable of which, **1He**+ being situated only 77 kJ mol^{-1} above **1Ha**$^{+}$. Complex **1He**$^{+}$ is characterized by a strong CH_2O. . .HO-PH(SCH_3)(NH_2)$^{+}$ hydrogen bond which provide a stabilization of 80 kJ mol−1 with respect to its separated components. By comparison, species such as CH_2O. . .HP(OH)(SCH_3)(NH_2)$^{+}$, **1Hf**+, or CH_2O. . .HNH-PH(SCH_3)(OH)$^{+}$, **1Hg**$^{+}$, which were also identified (see Supporting Information) are stabilized by only 49 and 58 kJ mol^{-1}, respectively.

The three secondary fragmentations 94 → m/z 64, m/z 125 → m/z 79 and 112 → m/z 94 (Scheme 2) have been also examined by quantum chemistry calculations. Interestingly enough, the corresponding fragments ions m/z 64, 79 and 94 may present two tautomeric forms **a** and **b** (Scheme 5). According to B3LYP/6-311+G(3df,2p)//B3LYP/6-31+G(d) calculations, the most stable form corresponds to the pseudo-allylic conjugated structure **a**.

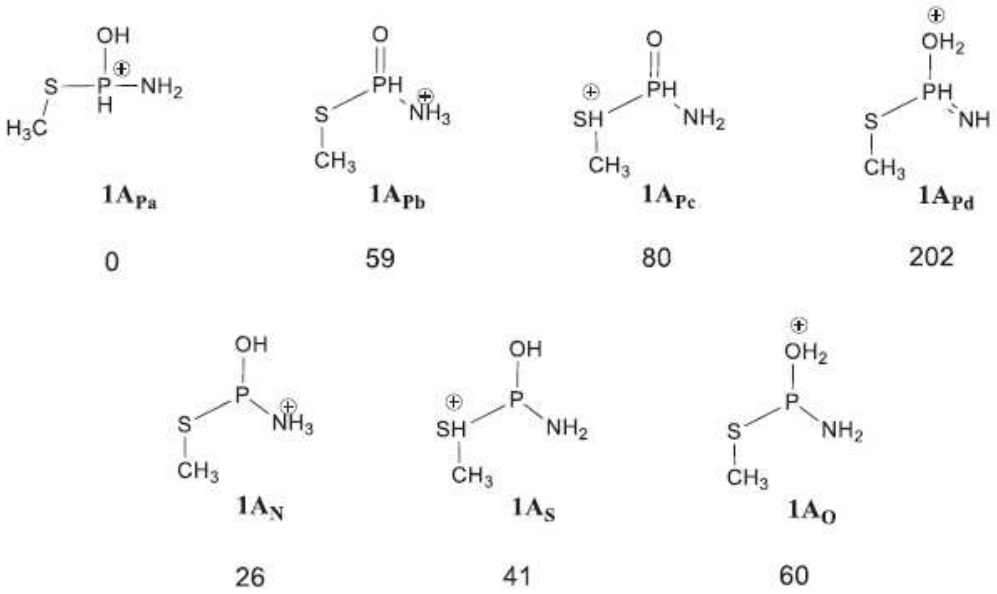

Scheme 4. Calculated B3LYP/6-311+G(3df,2p)//B3LYP/6-31+G(d) relative ΔH°_{298} (kJ mol^{-1}) of various possible structures of *m/z* 112, [**1H**$^{+}$ – CH_2O], ions.

	a	b
m/z 64 X=NH_2, Y=O	0	125
m/z 79 X=OCH_3, Y=O	0	120
m/z 94 X=SCH_3, Y=NH	0	170
m/z 95 X=SCH_3, Y=O	0	115

Scheme 5. Calculated B3LYP/6-311+G(3df,2p)//B3LYP/6-31+G(d) relative $\Delta H°_{298}$ (kJ mol^{-1}) of tautomeric *m/z* 64, 79, 94 and 95 ions.

Fragmentations m/z 94 → m/z 64 and m/z 125 → m/z 79 may be interpreted by 1,2-elimination reactions associated with CH2O and CH2S losses, respectively and leading to fragment ions of type **b**. Conversely, formation of ions of type a may result from a combination of 1,4-H migration and P O or P S bond elongations as summarized in Scheme 6. According to the calculation, formation of ions m/z 64 and m/z 79 from protonated methamidophos needs energies higher than ~300 kJ mol^{-1} (the energy levels of the fragmentation products with respect to **1Ha**$^+$). This is consistent with the apparent threshold energies, E_{cm0}, of 4.5 and 3.7 eV determined for these ions.

The major fragmentation reaction of m/z 112 ions is elimination of a water molecule to give m/z 64 fragment ions. Starting from its most stable structure, **1APa**, m/z 112 ion may support a 1,2-proton shift giving rise to the isomeric form **1AO** able to form by water loss m/z 64 ion of type a. Another possible pathway is a 1,3-proton migration producing structure **1APd** able to eliminate H_2O by simple bond elongation thus leading to m/z 64 ion of type **b** (Scheme 6). It may be finally noted that the marginal formation of ions m/z 64 and m/z 95 from m/z 112 may be similarly rationalized.

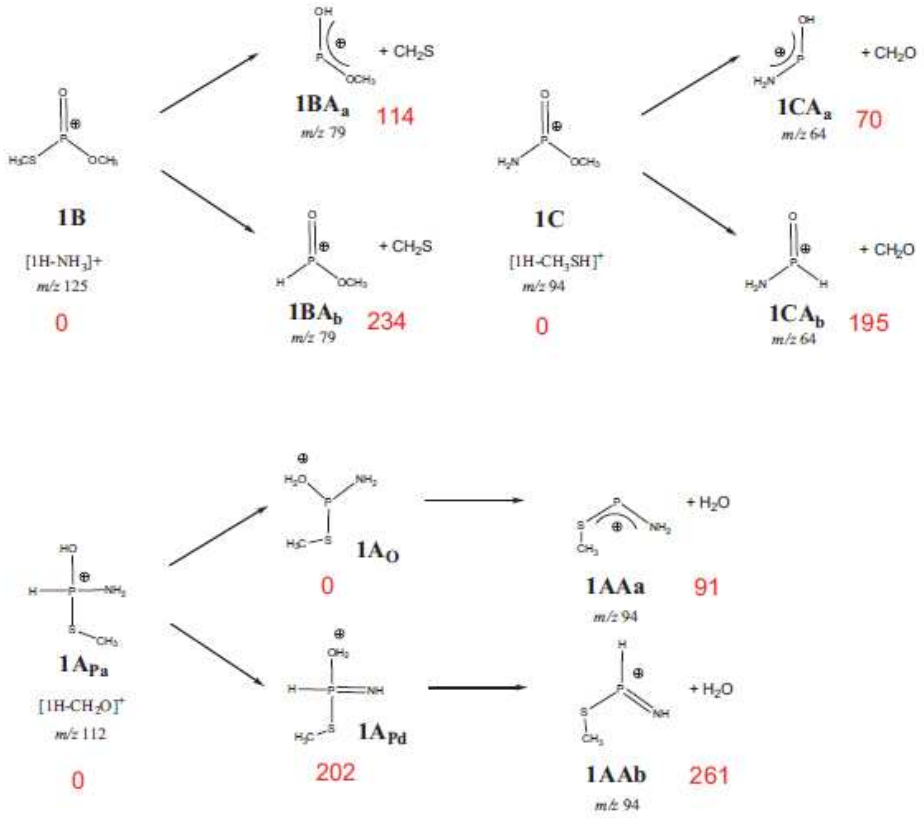

Scheme 6. Fragmentation pathways of *m/z* 125, 94 and 112 ions (in red, calculated B3LYP/6-31+G(d) ΔH°_{298} values, in kJ mol^{-1}). (For interpretation of the references to colour in this scheme, the reader is referred to the web version of this article.)

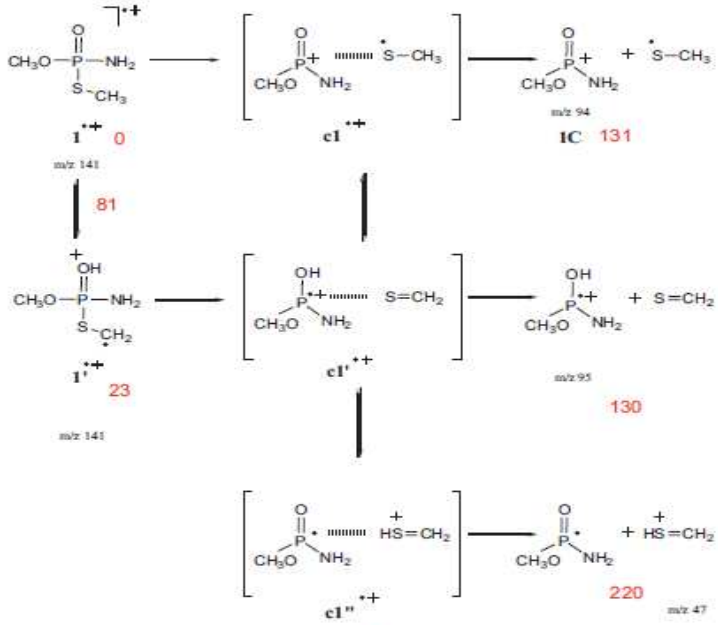

Scheme 7. Fragmentation pathways of electron ionized methamidophos **1**$^{\bullet+}$ (in red, calculated B3LYP/6-31+G(d) ΔH°_{298} values, in kJ mol^{-1}). (For interpretation of the references to colour in this scheme, the reader is referred to the web version of this article.)

3.4. Fragmentation mechanisms of electron ionized methamidophos, **1**•+

Methamidophos is a sufficiently volatile substance to be studied by electron ionization or chemical ionization mass spectrometry. Indeed a number of previous pesticide residue analysis used GC–MS or GC–MS–MS experimental apparatus [24–28]. The electron ionization mass spectrum of methamidophos is dominated by peaks at m/z 141 (molecular ions $\mathbf{1}^{\bullet+}$, rel. ab. 40%), m/z 95 (rel. ab. 60%), m/z 94 (rel. ab.100%) and m/z 47 (rel. ab. 45%) [23,28,29]. Less intense signals appear at m/z 64, m/z 78, m/z 79, m/z 80, m/z 110, m/z 111 and m/z 125. Since some of these fragment ions may correspond to those observed under ESI-P ionization conditions, it was of interest to investigate the major fragmentation pathways of electron ionized methamidophos, $\mathbf{1}^{\bullet+}$. Scheme 7 summarizes the mechanistic routes proposed to explain formation of ions m/z 95, m/z 94 and m/z 47 and explored by quantum chemistry calculations at the B3LYP/6-31+G(d) level. In addition, we have computed ionization energy of methamidophos and heat of formation of its molecular cation $\mathbf{1}^{\bullet+}$ at the G4MP2 level. These theoretical values are equal to IE(methamidophos) = 8.77 eV and $\Delta_f H^\circ_{298}(\mathbf{1}^{\bullet+})$ = 222 kJ mol^{-1}, respectively.

Direct P. . .S bond cleavage from $\mathbf{1}^{\bullet+}$ may obviously explain formation of ions m/z 94 of structure **1C** as suggested in a previous report by Terlouw and coworkers mainly devoted to ions m/z 78 from acephate and methamidophos [29]. In the same study, the authors suggested that ions m/z 95 are of structure P O(CH3O)(NH2)$^{\bullet+}$ and may be generated from rearranged ions $\mathbf{1'}^{\bullet+}$ (Scheme 7). We fully confirm these expectations since $\mathbf{1}^{\bullet+}$ and **1'**•+ are predicted to be of comparable enthalpies and separated

by a critical energy barrier lower than the dissociation products (81 kJ mol^{-1}, Scheme 6, B3LYP/6-31+G(d) computations). Furthermore we observe that the two fragmentations leading to m/z 94 and m/z 95 ions are associated with identical reaction enthalpies (of ~130 kJ mol^{-1}, Scheme 7) in agreement with the comparable intensities of the corresponding signals in the electron ionization mass spectrum of methamidophos.

To rationalize the competitive formation of CH_2SH^+, m/z 47, ions beside m/z 94 and m/z 95, it may be suggested that proton exchange is allowed to occur inside ion-neutral complexes $\mathbf{c1'}^{\bullet+}$ and

c1"•+ before separation of the corresponding fragments as described in Scheme 6. In the same vein, hydrogen atom exchange **c1**$^{\bullet+}$ → **c1**'$^{\bullet+}$ cannot be excluded from the general fragmentation process leading to m/z 94 and m/z 95, as indicated in Scheme 7.

4. Conclusion

In the present study we examined the behavior of methamidophos, **1**, by mass spectrometry under electrospray ionization in the positive ion mode and electron ionization. Quantum chemistry calculations at the B3LYP/6-31+G(d) and G4MP2 levels were used to interpret the energetic and mechanistic aspects of the mass spectrometry data.

The MS–MS mass spectra of protonated methamidophos, **1H**$^{+}$, obtained at various collision energies up to 60 eV in the laboratory frame, reveal facile fragmentations by CH_2O, CH_3SH, CH_3OH and NH_3 losses, giving rise to m/z 112, m/z 94, m/z 110 and m/z 125 ions, respectively with comparable threshold energies. Calculation shows that protonation of **1** occurs preferentially at the oxygen atom of the P O group with a corresponding proton affinity equal to 897 kJ mol^{-1}. Formation of m/z 112 ions, of structure $HP(SCH_3)(OH)(NH_2)^{+}$, **1APa**, is explained by a 1,2-elimination reaction involving the passage trough ion-neutral complexes. Isomerizations via 1,3-proton migrations precede eliminations of NH3, CH3SH and CH3OH leading to m/z 125, m/z 94 and m/z 110 ions, respectively. Secondary fragmentations leading to minor ions m/z 79 (m/z 125 –CH_2S), m/z 64 (m/z 112 – CH_3SH) and m/z 94 (m/z 112 – CH_2O), are also explained by the occurrence of 1,2-elimination or(and) 1,3-proton migration reactions. Finally, the behavior of electron ionized methamidophos, **1**$^{\bullet+}$, particularly its fragmentations by losses of •SCH_3 and CH_2S, is also enlightened by quantum chemistry calculation.

Acknowledgments

A.R. acknowledges Ecole Polytechnique (Ecole Doctorale) and Dr. Stéphane Bouchonnet for financial and academic supports during the preparation of this study.

Appendix A. Supplementary data

Supplementary data associated with this article can be found, in the online version, at http://dx.doi.org/10.1016/j.ijms.2013.02.003.

References

[1] J.H. Yen, K.H. Lin, Y.S. Wang, Potential of the insecticides acephate and methamidophos to contaminate groundwater, Ecotoxicology and Environmental Safety 45 (2000) 79–86.

[2] A.J. Midey, T.M. Miller, A.A. Viggiano, Survey of ion energetic properties of chemical weapons agent (CWA) breakdown products using G3MP2 theory, International Journal of Mass Spectrometry 315 (2012) 1–7.

[3] M.C. Wang, Y.H. Liu, Q. Wang, M. Gong, X.M. Hua, Y.J. Pang, S. Hu, Y.H. Yang, Impacts of methamidophos on the biochemical, catabolic, and genetic characteristics of soil microbial communities, Soil Biology and Biochemistry 40 (2008) 778–788.

[4] M.M. Hurley, A. Balboa, G.H. Lushington, J. Guo, Interactions of organophosphorus and related compounds with cholinesterases, a theoretical study, Chemico-Biological Interactions 157–158 (2005) 321–325.

[5] A.T. Farag, A.H. Radwan, M.H. Eweidah, R.H. ElMazoudy, A. ElSebae, Evaluation of male-mediated reproductive toxic effects of methamidophos in the mouse, Andrologia 44 (2012) 116–124.

[6] J.D. Yang, J. Cao, X.W. Sun, Z.J. Feng, D.F. Hao, X.J. Zhao, C.H. Sun, Effects of long term exposure to low levels of organophosphorous pesticides and their mixture on altered antioxidative defense mechanisms and lipid peroxidation in rat liver, Cell and Biochemical Function 30 (2012) 122–128.

[7] S.C. Joshi, P. Sharma, Male reproductive toxicity of organophosphorous compounds: a review, Toxicological and Environmental Chemistry 93 (2011) 1486–1507.

[8] S.W.C. Chung, B.T.P. Chan, Validation and use of a fast sample preparation method and liquid chromatography–tandem mass spectrometry in analysis of ultra-trace levels of 98 organophosphorus pesticide and carbamate residues in a total diet study involving diversified food types, Journal of Chromatography A 1217 (2010) 4815–4824.

[9] M. Radisic, S. Grujic, T. Vasilevic, M. Lausevic, Determination of selected pesticides in fruit juices by matrix solid-phase dispersion and liquid chromatography–tandem mass spectrometry, Food Chemistry 113 (2009) 712–719.

[10] C. Ferrer, M.J. Martínez-Bueno, A. Lozano, A.R. Fernández-Alba, Pesticide residue analysis of fruit juices by LC–MS/MS direct injection. One year pilot survey, Talanta 83 (2011) 1552–1561.

[11] Y. Pico, C. Blasco, G. Font, Environmental and food applications of LC–tandem mass spectrometry in pesticide residue analysis: an overview, Mass Spectrometry Review 23 (2004) 45–85.

[12] S.J. Lehotay, K.A. Son, H. Kwon, U. Koesukwiwat, W. Fu, K. Mastovska, E. Hoh, N. Leepipatpiboon, Comparison of QuEChERS sample preparation methods for the analysis of pesticide residues in fruits and vegetables, Journal of Chromatography A 1217 (2010) 2548–2560.

[13] T. Hayama, H. Yoshida, K. Todoroki, H. Nohta, M. Yamaguchi, Determination of polar organoposphorous pesticides in water samples by hydrophilic interaction liquid chromatography with tandem mass spectrometry, Rapid Communication in Mass Spectrometry 22 (2008) 2203–2210.

[14] M. Hiemstra, A. de Kok, Comprehensive multi-residue method for the target analysis of pesticides in crops using liquid chromatography–tandem mass spectrometry, Journal of Chromatography A 1154 (2007) 3–25.

[15] (a) H.G.J. Mol, R.C.J. van Dam, O.M. Steijger, Determination of polar organophosphorous pesticides in vegetables and fruits using liquid chromatography with tandem mass spectrometry: selection of extraction solvent, Journal of Chromatography A 1015 (2003) 119–127;

(b) B.A. Ingelse, R.C.J. van Dam, R.J. Vreeken, H.G.J. Mol, O.M. Steijger, Determination of polar organophosphorous pesticides in aquous samples by direct injection using liquid

chromatography–tandem mass spectrometry, Journal of Chromatography A 918 (2001) 67–78.

[16] S.N. Sinha, M.V.V. Rao, K. Vasudev, M. Odetokun, A liquid chromatography mass spectrometry-based method to measure organophosphorous insecticide, herbicide and non-organophosphorous pesticide in grape and apple samples, Food Control 25 (2012) 636–646.

[17] A. Rifai, S. Bourcier, D. Arquier, Y. Charvet, F. Jaber, G. Bouchoux, Fragmentation reactions of phenoxide anions: deprotonated Dinoterb and related structures, Journal of Mass Spectrometry 46 (2011) 1079.

[18] (a) M.J. Frisch, G.W. Trucks, H.B. Schlegel, G.E. Scuseria, M.A. Robb, J.R. Cheeseman, J.A. Montgomery, T. Vreven Jr., K.N. Kudin, J.C. Burant, J.M. Millam, S.S. Iyengar, J. Tomasi, V. Barone, B. Mennucci, M. Cossi, G. Scalmani, N. Rega, G.A. Petersson, H. Nakatsuji, M. Hada, M. Ehara, K. Toyota, R. Fukuda, J. Hasegawa, M. Ishida, T. Nakajima, Y. Honda, O. Kitao, H. Nakai, M. Klene, X. Li, J.E. Knox, H.P. Hratchian, J.B. Cross, C. Adamo, J. Jaramillo, R. Gomperts, R.E. Stratmann, O. Yazyev, A.J. Austin, R. Cammi, C. Pomelli, J.W. Ochterski, P.Y. Ayala, K. Morokuma, G.A. Voth, P. Salvador, J.J. Dannenberg, V.G. Zakrzewski, S. Dapprich, A.D. Daniels, M.C. Strain, O. Farkas, D.K. Malick, A.D. Rabuck, K. Raghavachari, J.B. Foresman, J.V. Ortiz, Q. Cui, A.G. Baboul, S. Clifford, J. Cioslowski, B.B. Stefanov, G. Liu, A. Liashenko, P. Piskorz, I. Komaromi, R.L. Martin, D.J. Fox, T. Keith, M.A. Al-Laham, C.Y. Peng, A. Nanayakkara, M. Challacombe, P.M.W. Gill, B. Johnson, W. Chen, M.W. Wong, C. Gonzalez, J.A. Pople, Gaussian 03, Revision B.03, Gaussian, Inc., Pittsburgh, PA, 2003;

(b) M.J. Frisch, G.W. Trucks, H.B. Schlegel, G.E. Scuseria, M.A. Robb, J.R. Cheeseman, G. Scalmani, V. Barone, B. Mennucci, G.A. Petersson, H. Nakatsuji, M. Caricato, X. Li, H.P. Hratchian, A.F. Izmaylov, J. Bloino, G. Zheng, J.L. Sonnenberg, M. Hada, M. Ehara, K. Toyota, R. Fukuda, J. Hasegawa, M. Ishida, T. Nakajima, Y. Honda, O. Kitao, H. Nakai, T. Vreven, J.A. Montgomery Jr., J.E. Peralta, F. Ogliaro, M. Bearpark, J.J. Heyd, E. Brothers, K.N. Kudin, V.N. Staroverov, T. Keith, R. Kobayashi, J. Normand, K.

Raghavachari, A. Rendell, J.C. Burant, S.S. Iyengar, J. Tomasi, M. Cossi, N. Rega, J.M. Millam, M. Klene, J.E. Knox, J.B. Cross, V. Bakken, C. Adamo, J. Jaramillo, R. Gomperts, R.E. Stratmann, O. Yazyev, A.J. Austin, R. Cammi, C. Pomelli, J.W. Ochterski, R.L. Martin, K. Morokuma, V.G. Zakrzewski, G.A. Voth, P. Salvador, J.J. Dannenberg, S. Dapprich, A.D. Daniels, O. Farkas, J.B. Foresman, J.V. Ortiz, J. Cioslowski, D.J. Fox, Gaussian 09, Revision B.01, Gaussian, Inc., Wallingford, CT, 2010.

[19] (a) L.A. Curtiss, P.C. Redfern, K. Raghavachari, Gaussian-4 theory, Journal of Chemical Physics 126 (2007) 084108;

(b) L.A. Curtiss, P.C. Redfern, K. Raghavachari, Gaussian-4 theory using reduced order perturbation theory, Journal of Chemical Physics 127 (2007) 124105.

[20] A. Nicolaides, A. Rauk, M.N. Glukhostsev, L. Radom, Heats of formation from G2, G2(MP2), and G2(MP2, SVP) total energies, Journal of Physical Chemistry 100 (1996) 17460–17464.

[21] J.D. Cox, D.D. Wagman, V.A. Medvedev, CODATA Key Values for Thermodynamics, Hemisphere Publishing Corp., New York, 1989.

[22] G. Bouchoux, Gas-phase basicities of polyfunctional molecules. Part 1. Theory and methods, Mass Spectrometry Review 26 (2007) 775–835.

[23] E.P. Hunter, S.G. Lias, Standard reference database no. 69, in: P.J. Linstrom, W.G. Mallard (Eds.), NIST Chemistry Webbook, National Institute of Standards Technology, Gaithersburg, MD, 2012, p. 20899, June http://webbook.nist.gov

[24] A. Agüera, M. Contreras, J. Crespo, A.R. Fernández-Alba, Multiresidue method for the analysis of multiclass pesticides in agricultural products by gas chromatography–tandem mass spectrometry, Analyst 127 (2002) 347–354.

[25] A.D. St-Amand, L. Girard, Determination of acephate and its degradation product methamidophos in soil and water by solid-phase extraction (SPE) and GC–MS, International Journal of Environmental and Analytical Chemistry 84 (2004) 739–748.

[26] A. Kotonia Chrissi, S. Liapis Konstadinos, N. Ziogas Vasilios, Determination of residues of 14 insecticides and metabolites in grapes and peaches by gas chromatography–mass spectrometry, Fresenius Environmental Bulletin 16 (2007) 223–226.

[27] J.L. Fernandez Moreno, A. Garrido Frenich, P. Plaza Bolanos, J.L. Martinez Vidal, Multiresidue method for the analysis of more than 140 pesticides residues in fruits and vegetable by gas chromatography coupled to triple quadrupole mass spectrometry, Journal of Mass Spectrometry 43 (2008) 1235–1254.

[28] N. Adachi, H. Kinoshita, M. Nishigushi, M. Takahashi, H. Ouchi, T. Minami, K. Matsui, T. Yamamura, H. Motomura, N. Ohtsu, S. Yoshida, S. Hishida, Simultaneous analysis of acephate and methamidophos in human serum by improved extraction and GC–MS, Forensic Toxicology 26 (2008) 76–79.

[29] L.N. Heydorn, C.Y. Wong, R. Srivinas, J.K. Terlouw, The isobaric ions CH3OPO•+ and CH3OPNH2+ and their neutral counterparts: a tandem mass spectrometry and CBS-QB3 computational study, International Journal of Mass Spectrometry 225 (2003) 11–23

Résumé

Les pesticides appartiennent à la grande famille des polluants organiques. Ils sont destinés à lutter contre les parasites des cultures au sens large.La diffusion des pesticides dans la nature engendre une pollution des différents compartiments de la biosphère (eau, sol et atmosphère) et peut induire des effets toxiques aigus sur les êtres vivants de la biomasse terrestre et aquatique. Il est aujourd'hui démontré que certains pesticides sont des perturbateurs endocriniens et présentent en particulier des effets cancérogènes et mutagènes chez l'être humain. Les pesticides peuvent subir différents processus de transformation dans le cycle biologique naturel (biodégradation, volatilisation, irradiation solaire…) ou suite aux traitements appliqués dans les filières de potabilisation des eaux naturelles et dans les stations de retraitement des eaux usées. La présence de produits de dégradation de pesticides dans notre environnement est d'autant plus alarmante que leurs structures et leurs toxicités potentielles demeurent généralement inconnues. Des molécules qui appartiennent à deux familles de pesticides ont été choisies pour cette étude : les herbicides, représentés par le metholachlore, et les fongicides, représentés par la procymidone, le pyrimethanil et le boscalid. Le premier volet de la thèse a porté sur le développement d'une stratégie analytique permettant de caractériser les structures de composés issus de la dégradation par photolyse de ces pesticides. Le deuxième volet a porté sur l'estimation de la toxicité des produits de dégradation à l'aide d'une base de test *in silico*. L'identification des produits de dégradation a été réalisée grâce à deux techniques d'analyses complémentaires : la chromatographie en phase gazeuse couplée à un spectromètre de masse "multi étapes" (GC-MSn) et la chromatographie en phase liquide couplée à un spectromètre de masse en tandem (LC-MS/MS). L'estimation de la toxicité des produits de dégradation a été réalisée grâce au programme T.E.S.T. QSAR récemment développés pour tenter de prévoir la toxicité des molécules. La stratégie d'élucidation structurale des produits de dégradation des pesticides étudiés est basée sur l'étude des mécanismes de fragmentation des molécules mères des produits de dégradation. La masse molaire des molécules mères a été précisée par l'identification des masses sur charge (m/z) des ions pseudo moléculaires obtenus à l'aide des différentes modes d'ionisations en spectrométrie de masse : ionisation électronique (EI) et ionisation chimique (CI) en GC-MS et ionisation par électronébulisation (ESI) en LC-MS. La stratégie utilisée pour l'élucidation structurale des produits de dégradation est avérée très efficace, la plupart des structures chimiques des produits formés ayant été élucidées. Une étude cinétique a été réalisée pour visualiser l'apparition et la disparition des produits de dégradation durant la photolyse et pour donner une idée sur le taux de disparition de la molécule mère pour chaque pesticide. Les résultats de photolyse ont montré que le méthalochlore, le procymidone et le boscalid ont été dégradés sous irradiation après un certain temps en libérant des produits de dégradation avec des structures proches ou différentes des molécules mères. Tandis que le pyrimethanil a présenté une grande stabilité pendant 8 heurs d'irradiation (quantité restante après irradiation est de 60%) et a donné des produits de dégradation avec des quantités modérées. Concernant l'estimation de la toxicité, la plupart des produits de dégradation identifiés présentent des toxicités équivalentes ou plus importantes que celles des molécules d'origine. Les méthodes chimiques d'analyses utilisées et l'estimation de toxicités des produits de dégradations identifiés sont avérées complémentaires et indispensables pour mettre en évidence la présence d'autres produits polluants toxiques qui émergent dans l'environnement sans vrai contrôle.

Mots-clés: fongicides, spectrometrie de masse, photodégradation,approche mécanistique, teste detoxicité *in silico*

Abstract

Pesticides belong to the large family of organic pollutants. In general, they are intended to fight against crop pests. Distribution of pesticides in nature creates pollution in DIFFERENT compartments of the biosphere (water, soil and air) and can induce acute toxic effects on human beings of the terrestrial and aquatic living biomass. It is now shown that some pesticides are endocrine disruptors and are particularly carcinogenic and mutagenic effects in humans. Pesticides can undergo various processes of transformation in the natural life cycle (biodegradation, volatilization, solar radiation ...) or following applied in the sectors of natural water purification and treatment stations sewage treatment. The presence of degradation products of pesticides in our environment is even more alarming that their structures and potential toxicities generally unknown. Molecules belonging to two families of pesticides were selected for this study: herbicides, represented by metolachlor, and fungicides represented by procymidone, pyrimethanil and boscalid. The first part of the thesis focused on the development of an analytical strategy to characterize the structures of compounds from degradation by photolysis of pesticides. The second part focused on estimating the toxicity of degradation products using a test database in silico. Identification of degradation products was achieved through two complementary analysis techniques: the gas chromatography coupled to a mass spectrometer "multi-stage" (GC-MSn) and liquid chromatography coupled to a tandem mass spectrometer (LC-MS/MS). The estimation of the toxicity of the degradation products was performed using the TEST program QSAR recently developed to try to predict the toxicity of molecules. The strategy of the structural elucidation of degradation products of pesticides studied is based on studying of the mechanisms of fragmentation of parent molecules of the degradation products. The molar mass of parent molecules was clarified by the identification of mass-to-charge (m /z) of the pseudo molecular ions obtained using different modes of ionization in mass spectrometry: electronic ionization (EI) and chemical ionization (CI) in GC-MS and electrospray ionization (ESI) in LC-MS. The strategy used for the structural elucidation of degradation products has been very effective; most of the chemical structures of the products formed have been elucidated. A kinetic study was performed to visualize the appearance and disappearance of degradation products during the photolysis and gave us an idea of the rate of disappearance of the parent compound for each pesticide. The results showed that the photolysis méthalochlore, procymidone and boscalid were degraded under UV light after a while releasing degradation products with structures close or different from the parent molecules. While, pyrimethanil presented a high stability during 8 hours of irradiation (remaining amount after irradiation is 60%) and gave degradation products with moderate amounts. Regarding the estimation of the toxicity, most identified degradation products are equivalent or greater than those of the original molecules toxicities. The chemical analysis methods used and the estimated toxicities of the identified degradation products are proven complementary and indispensable for highlighting the presence of other toxic pollutants that emerge in the real environment without control.

Keywords: Fungicides, Mass spectrometry, Photodegradation, mechanistical approach, toxicity test *in silico*